國立成功大學
太空與電漿科學研究所
碩士論文

National Cheng Kung University
Institute of Space and Plasma Sciences
Master Thesis

微小型托克馬克環向磁場之建置
Development of the toroidal field in a mini tokamak

研究生 **(Author) :** 陳俊宇 **Jun-Yu Chen**
指導教授 **(Advisor) :** 張博宇 **Dr. Po-Yu Chang**
中華民國一百一十一年五月 **May, 2022**

國立成功大學
碩士論文

微小型托克馬克環向磁場之建置

Development of the toroidal field in a mini tokamak

研究生：陳俊宇

本論文業經審查及口試合格特此證明

論文考試委員：張存續

向克強

張博宇

指導教授：張博宇

單位主管：電漿所 所長 河森榮一郎

（單位主管是否簽章授權由各院、系（所、學位學程）自訂）

中 華 民 國 111 年 5 月 25 日

摘要

本論文主要進行的工作是建置一個僅有環向磁場的教學用微小型托克馬克，並且利用單極蘭摩爾探針去驗證電漿是否約束住電漿。現在組建完成的微小型托克馬克包含幾個物件，分別為圓柱狀的真空腔、交流電源供應器、環型磁場線圈、脈衝形成網路、單極蘭摩爾探針。圓柱狀真空腔的材質為玻璃管，玻璃管直徑為 30 cm 高度為 45 cm。點燃電漿之前會先在真空腔內部通入氬氣並將壓力維持在 10^{-1} torr，由交流電源供應器提供振幅~ 1-kV 頻率為 20 kHz 交流電壓，通過真空腔上的電子饋通來產生電漿。此外，環型線圈是由 8 組 AWG-8 導線製成，每組環型線圈的高為 400 mm，寬為 250 mm 的矩形，並且環型線圈作用是用於產生環向磁場。脈衝形成網路系統包含了如下幾個物件，分別為觸發盒、脈衝產生器、火花間隙開關、四階脈衝形成網路。觸發盒是用於觸發脈衝產生器，產生-8.0 ±0.4 kV 的負高電壓，用來觸發火花間隙開關。最終當火花間隙開關運作時，四階脈衝形成網路會釋放出脈衝電流，用於驅動環型磁場線圈。經由放電電流測試，當四階脈衝形成網路的充電電壓為 500 V 時，釋放出的平均脈衝電流大小為 760 ±80 A，電流寬度為 0.9218±0.0004 ms，當此電流驅動環型磁場線圈時，並在距離微小型托克馬克中心處 2.5 cm 的地方會產生 448±5 G 的磁場。在未來我們會將四階脈衝形成網路的充電電壓提供到 1 kV 時，預期可以產生平均~ 1.4 kA 的脈衝電流來驅動環型磁場線圈，在距離微小型托克馬克中心 2.5 cm 處時產生 876 G 的磁場，供給 2.45 GHz 的微波，可以透過電子迴旋共振加熱(electron-cyclotron resonance heating (ECH))的方式加熱電漿。最後，我們使用單極蘭摩爾探針去量測電漿特性，在單極蘭摩爾探針上施加 0～50V 的電壓，我們發現沒有環向磁場時，量測到來自電漿的電流大小為 4.25~4.89 uA，當有環向磁場產生時，量測到來自電漿的電流大小為 0.93~1.61 uA，這顯示了環向磁場約束了電漿，使得更多的電子撞擊單極蘭摩爾探針，造成來自電漿的電流下降，也就是說電漿被環向磁場約束住。關鍵字:托克馬克、磁侷限核融合、蘭牟爾探針、環向磁場、脈衝形

成網路。

Abstract

In this thesis, we built a mini Tokamak with toroidal magnetic field only. A single Langmuir probe was used to verify that the plasma was confined by the toroidal magnetic field. To date, the mini Tokamak consists of a cylindrical vacuum chamber, an AC high-voltage power supply, a set of toroidal magnetic field coils, a pulsed-forming network (PFN), and a single Langmuir probe. The cylindrical vacuum chamber is made of a quartz tube. The diameter of the chamber is 30 cm and the height is 45 cm. The chamber is filled with Ar with a pressure of 10^{-1} torr. To generate the plasma, the AC high-voltage power supply with a ~ 1-kV AC voltage, and a frequency of 20 kHz is used to provide the AC voltage through an electrical feedthrough. Further, 8 rectangular toroidal field coils made of AWG-8 wires with a width of 250 mm and a height of 400 mm are used to generate the toroidal magnetic field. Furthermore, the PFN system is used to provide the pulsed current to drive the toroidal magnetic field coils. The PFN system includes a trigger box, a pulse generator, a spark-gap switch, and the four-stage PFN. The trigger box is used to trigger the pulse generator. The pulse generator generated the pulse with a peak voltage of -8.0±0.4 kV to trigger the spark-gap switch. When the spark-gap switch is activated, the pulse current is delivered to the toroidal field coils. From the discharge test, the four-stage PFN charged to 500 V provided an average current of 760±80 A with a width of 0.9218±0.0004 ms. In other words, a pulse magnetic field of 448±5 Gauss at r = 2.5 cm was generated. In the future, we will charge the PFN to 1 kV and generate the pulsed current of ~ 1.4 kA for toroidal magnetic field coils. Then, the expected toroidal magnetic field will be 876 G at r $\approx$ 2.5 cm. Therefore, with 2.45-Ghz microwave, electron-cyclotron resonance heating (ECH) can be used for heating the plasma. Finally, the single Langmuir probe with a bias voltage of 0~50 V was used to measure the plasma characteristics. We found that the current flowing into the probe was 4.25~4.89 uA and 0.93~1.61 A without and with toroidal magnetic field, respectively. It indicated that the toroidal magnetic field confined the plasma and more electrons hitting the single Langmuir probe so that the current was reduced. In other words, the plasma was confined by the toroidal magnetic field.

Keyword: Tokamak、Magnetic confinement fusion (MCF)、Langmuir probe、Toroidal magnetic field、Pulse-forming network.

致謝

很幸運能夠就讀成大電漿所,在這裡遇到很多很厲害的人,促使自己一直進步。很感謝能夠加入博宇老師的實驗室,很幸運可以得到老師的幫助,謝謝老師這一路以來的指導與幫助,每當在實驗上遇到問題時,老師總是不吝於分享解決問題的想法與方法,使得實驗可以順利的完成,在做人處事方面,謝謝老師的身教與言教讓我學習很多。謝謝實驗室的大家,實驗室的每個人都是不吝於分享所學,在遇到問題時也都會互相幫忙,每天都有說不完的話題,很喜歡這樣的氣氛,很幸運可以遇到你們。謝謝所辦的大家,一直麻煩你們處理很多事情,謝謝你們的幫忙。謝謝求學路上幫助過我的每一個人。

最後想謝謝我的家人,一直以來你們辛苦了,抱歉讓你們一直擔心,有你們一路上的支持,才可以順利完成學業。對我來說這一路走來不容易,辛苦了。

Contents

List of Figures

1. Introduction

In this thesis, we are building the toroidal field coil of a mini tokamak for teaching demonstration. We will introduce the basic theory of the tokamak system in this chapter. We are introducing nuclear fusion energy in section 1.1, including two main approaches: Magnetic confinement fusion (MCF) and Inertial confinement fusion (ICF). Finally, the goal of this thesis will be introduced in section 1.2.

1.1 Nuclear fusion

Fusion is the energy source of stars. The simplest case is like the sun in Figure 1.1 [1]. The sun is composed of hydrogen (~75 % of the total mass) and helium (~ 25 % of the total mass). The temperature of the sun surface is 5800 K. When it is closer to the core of the sun, the temperature is higher. At the region of the core of the sun, both the temperature and the pressure are very high. Gas becomes plasma. Hydrogen atoms loss their electrons. Thus, hydrogen atoms become hydrogen ions, i.e., protons. The high-speed protons collide with each others, fuse together, and thus generate energy. Energetic particles try to escape from the sun. However, the sun's mass is huge and has huge gravity. Therefore, the gravity confines all particles in the sun and maintain the high temperature and high-pressure condition in the sun so that fusion can keep happening.

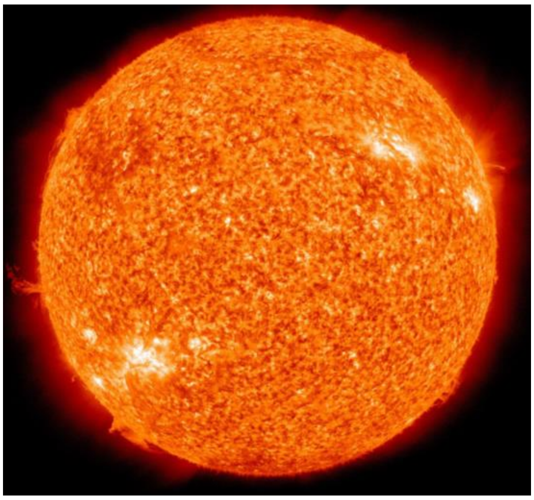

Figure 1.1: The photo of sun [1].

The easiest fusion reaction that can be achieved on earth is shown in Figure 1.2 [2]. The fusion of a deuterium nucleus and a tritium nucleus results to a helium nucleus (3.5 MeV) and a neutron (14.1 MeV).

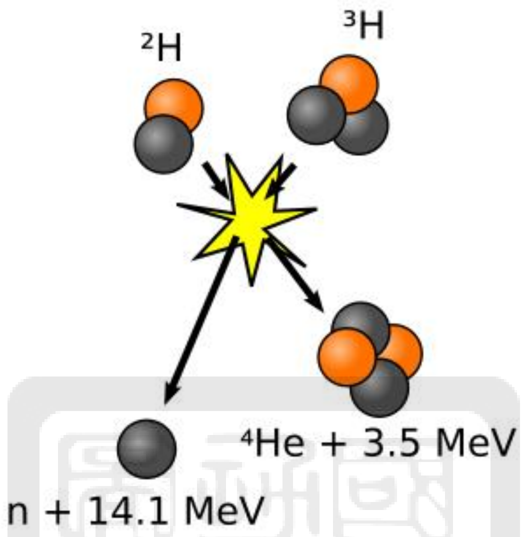

Figure 1.2: The easiest fusion process [2].

Figure 1.3 [3] shows the reactivity of different fusion reactions. The y axis is the reactivity of fusion reactions, σ is the reaction cross-section, ν is the velocity of reaction nuclei. The x-axis is the temperature of two reaction nuclei. We can see the D-T reaction rate (blue line) peaks at ~70 keV or 800 million kelvin. The temperature of the peak is the lowest compared to those of other fusion reactions. Most importantly, the reactivity is about two orders higher than those of the rest reactions. So, the D-T rate fusion fuel is the most easily.

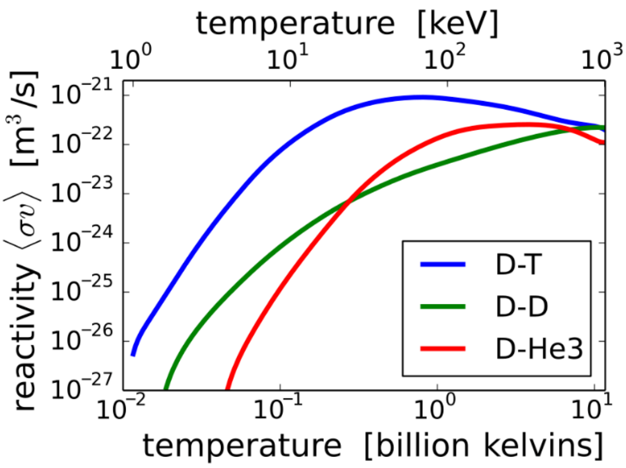

Figure 1.3: The easiest fusion process [3].

1.1.1 Magnetic confinement fusion (MCF)

The basic principle of MCF is using a magnetic field to confine the hot plasma. Due to the Lorentz forces, charged particles gyro around magnetic field lines. Therefore, charged particles in the plasma will move along magnetic field lines as shown in Figure 1.4 [4]. As a result, as long as magnetic field lines do not cross the chamber, the hot plasma can be maintained at thermonuclear temperatures without touching the chamber wall.

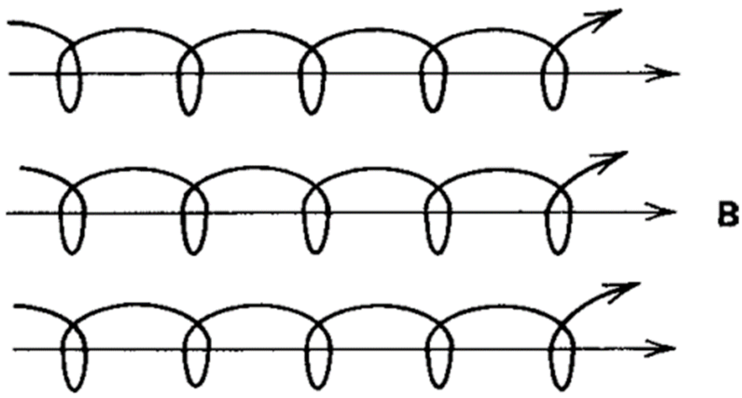

Figure 1.4: The motion of charge particle of plasma [4].

A tokamak is one of the MCF devices as shown in Figure 1.5 [5]. To heat the plasma reaching the required temperature, people use a solenoid at the center to drive the plasma current. The plasma current heats the plasma via ohmic heating first. Afterward, plasma can be heated by using electron cyclotron resonance heating (ECH), ion cyclotron resonance heating (ICRH), neutral beam injection, etc. Finally, temperature ~ 10 keV is generated in Tokamak. On the other hand, the tokamak uses magnetic fields to confine the plasma. There are toroidal magnetic field provided by the toroidal coil in the poloidal direction. Furthermore, there are poloidal magnetic field provided by the plasma current in the toroidal direction. As a result, twisted magnetic field lines confine plasma in a donut shape plasma chamber. Therefore, the hot plasma does not cool down via touching the chamber wall. So, the tokamak is a good device for fusion.

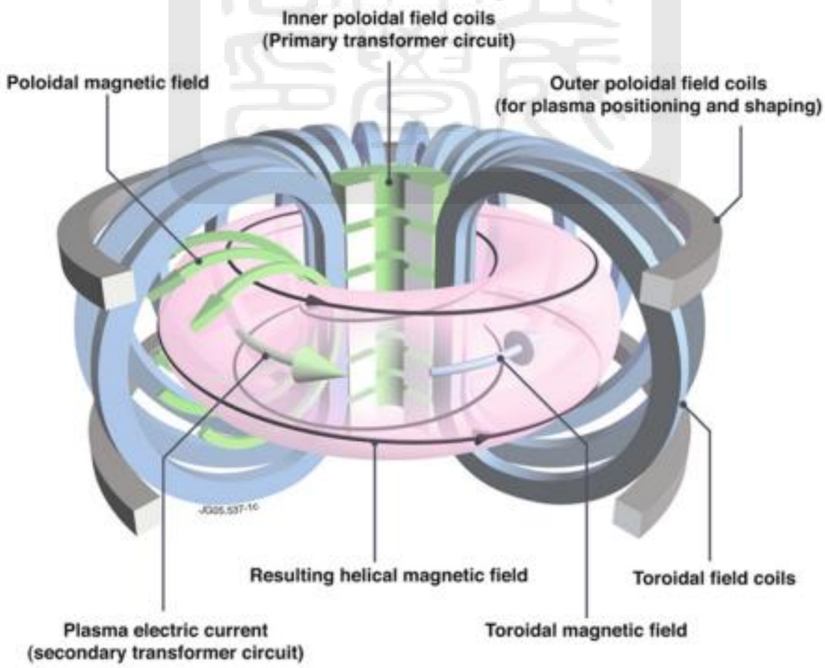

Figure 1.5: The device of tokamak [5].

1.1.2 Inertial confinement fusion (ICF)

The Inertial confinement fusion (ICF) is the other branch to achieve the fusion. The basic principle of ICF is to compress a target to a small volume reaching high temperature and high density via adiabatic compression. If the temperature is high enough, a fusion reaction can occur. The target eventually explodes due to the high internal pressure. However, it takes some time for material to escape from the target due to its inertial. In other words, material is confined by its own inertial. Generally, a giant laser is used to deliver the compression energy. The process of the ICF implosion is shown in Figure 1.6 [6]. The blue arrows are laser beams that heat the outer layer of the spherical capsule. The orange arrows represent the ablation of the heated outer surface. Therefore, the reaction force (purple arrows) from the ablation compresses the capsule. The compression occurs rapidly so that it's an adiabatic compression. The compressed core is heated due to the adiabatic compression reaching a temperature of ~5 keV and initiates the fusion reaction. Finally, a burn wave supported by the nuclear fusion reaction at the compressed core burn out the target before it explodes.

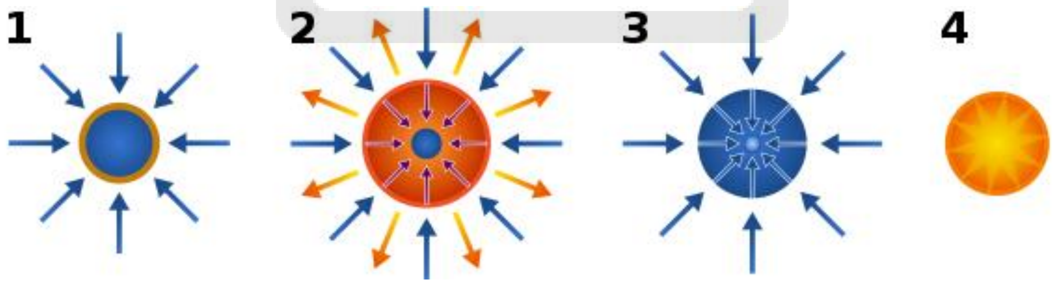

Figure 1.6: The Inertial confinement fusion [6].

1.2 The goal of the thesis

We would like to build a mini tokamak as a demonstration in class. In particular, a spherical tokamak is being built. A spherical tokamak is a type of tokamak where the plasma shape is almost spherical and is more compact than conventional ones.

Therefore, a higher magnetic field in the plasma is possible so that plasma with higher pressure can be contained. Figure 1.7 is the spherical tokamak made by Tokamak Energy, Ltd as an example [7]. We would like to build the mini tokamak in couple of years.

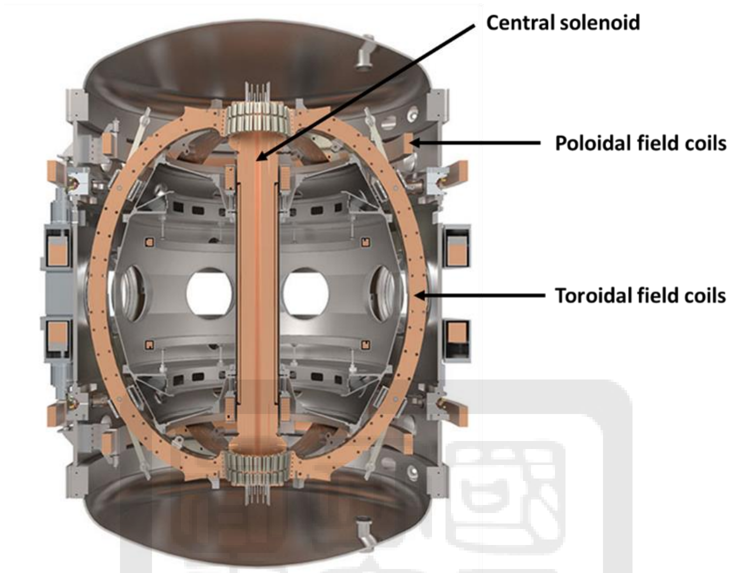

Figure 1.7: The spherical tokamak [7].

Figure 1.8 is the design of our tokamak. Eventually, we will have (1) Toroidal field coil to generate toroidal magnetic field; (2) Vertical field coil to shape the plasma; (3) Microwave injection to heat the plasma via electron cyclotron heating; (4) Central solenoid to generate the plasma current for providing the poloidal field. In this thesis, we focus on building the vacuum chamber system introduced in chapter 2; the Pulse-forming-network system, which is used to drive the toroidal magnetic field coils, is given in chapter 3; the toroidal magnetic field coils system and the generated magnetic field is shown in chapter 4; and finally, we use the single Langmuir probe to measure that the plasma to verify whether the plasma is confined by the toroidal magnetic field or not.

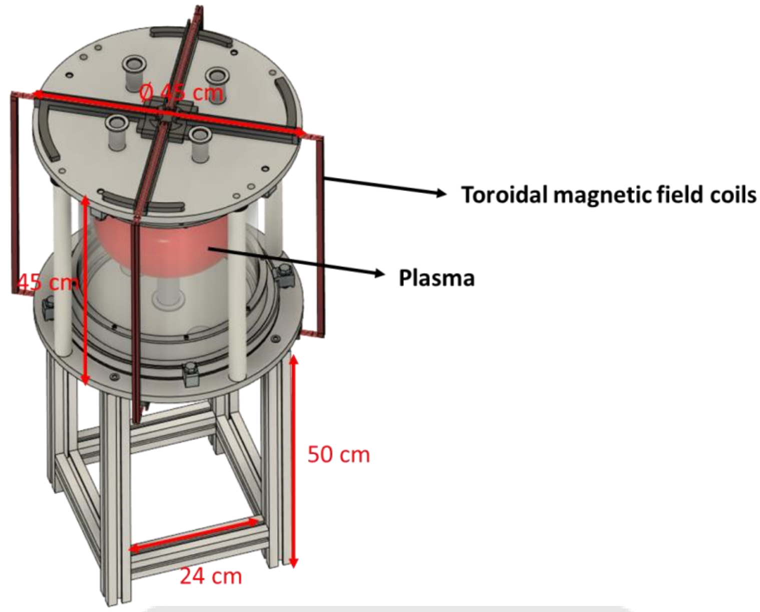

Figure 1.8: The spherical tokamak system.

2.Vacuum system and plasma generator

We will introduce all subsystems and we built for the spherical tokamak. The whole system includes: (1) the vacuum system introduced in section 2.1; (2) the gas injection system introduced in section 2.2; (3) the AC discharge system given in section 2.3; (4) the summary in section 2.4; (5) the PFN system given in chapter 3; (6) the toroidal magnetic field system shown in chapter 4; (7) the plasma measuring in chapter 5.

2.1 Vacuum system

Figure 2.1 (a) is the vacuum chamber for the spherical tokamak. Figure 2.1 (b) is the photo of the vacuum chamber. The vacuum chamber is a quartz tube sandwiched between the top and the bottom metal plates. The KF 40 tube is use for inserting the toroidal magnetic field coils. The four stands are use to support the the top plate and the bottom plate. Both diameters of the top plate and the bottom plate are 45 cm. The top plate has four KF 25 flanges. Details of the use of each KF 25 flange will be described later. The bottom plate has two KF 50 flanges. Details of the use of each KF 50 flange will also be described later. The distance between the top plate and the bottom plate is 45 cm. Finally, the support of the vacuum chamber is made of four 50-cm TF4040 aluminum extrusions and four 24-cm TF4040 aluminum extrusions. The structure of spherical tokamak is shown in Appendix A 2.1.

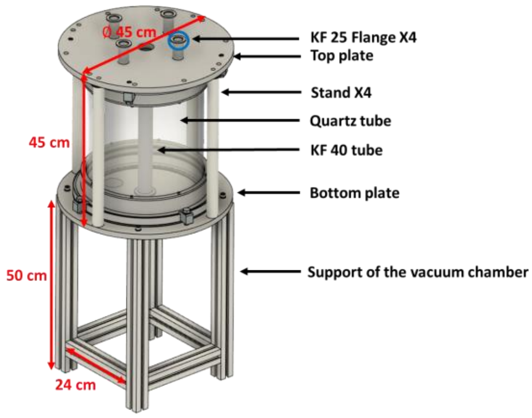

(a)

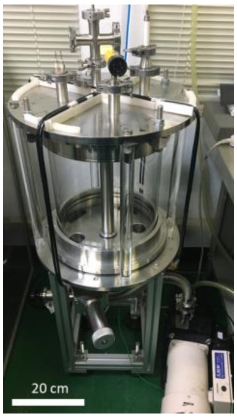

(b)

Figure 2.1: (a) The spherical tokamak. (b) The photo of spherical tokamak.

Figure 2.2 (a) is the top plate of vacuum chamber the vacuum chamber. The use of four KF40 flange is described in the following:

(1) To insert the single Langmuir probe system. The detail will introduce in chapter 5.

(2) To connect the pressure gauge, worker bee model CVG 101 GA-01.

(3) It is connected to a KF-25 cross tube. The KF 25 cross tube has another three open flanges. One is connected to a blind flange. The second one is connected to the gas injection system. The last one is connected to the relief valve for venting the chamber if necessary.

(4) An electrode connected to the AC discharge system is inserted through here.

Figure 2.2 (b) is the bottom plate of the vacuum chamber. There are two KF 50 flange. One is connected to the pump system. The other one is connected to a blind flange and is not used.

(a) (b)

Figure 2.2: (a) The top plate of the vacuum chamber. (b) The bottom plate of vacuum chamber.

Figure 2.3 is the cross section of the vacuum chamber. The red square are locations of O-rings. We use O-rings at the top and at the bottom to construct the vacuum side. The parameters of the O-rings are shown in Table 2.1. The 4290 O-rings are used to separte the vacuum side and the atmospheric side. The 4300 O-rings are used to make sure that the quartz tube is up right and does not touch the metal flanges.

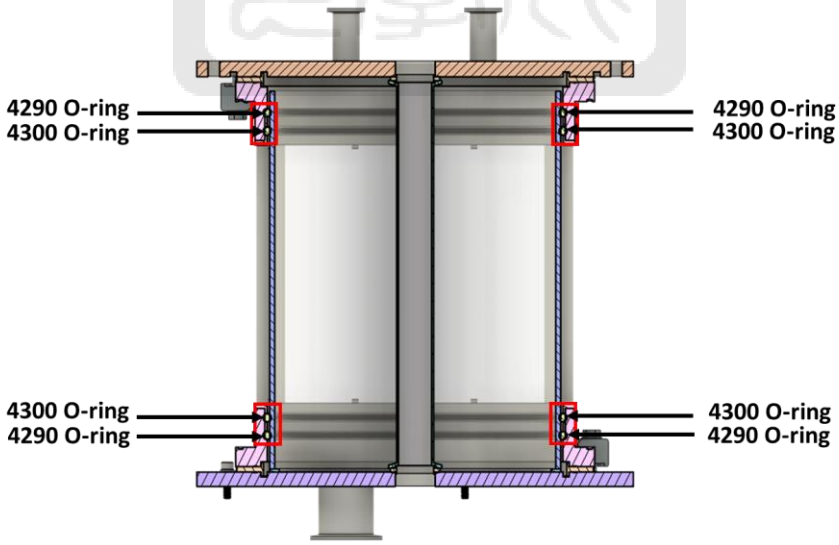

Figure 2.3: The sectional view of spherical tokamak.

Table 2.1: The parameters of O-rings.

O-ring specification	I.D. (mm)	O.D. (mm)	Thickness (mm)
4290	290	298	4
4300	300	308	4

On the bottom plate of Figure 2.4 has the pump system of the spherical tokamak. At the bottom plate,a gate value is connected to one of the KF50 flange. Then, it is connected to KF25 Tee tube through a KF50-KF25 adapter one end of the Tee tube is connected to the vacuum pump (Model No. AETFL64PH004) through the KF25 vacuum below. The other end is connected to a KF25 venting value. The gate valve is used to separate the chamber side from the pump. We close the gate valve when the experiment is finished to keep the chamber at high vacuum condition. To pump down the pressure, the gate value is open and the air is pumped out through the direction indicated in purple arrows. To vent the pump and the bellow and keep the chamber in vacuum condition, we close the gate value and open the relief value. Therfore, the bellow is vent by the air flow indicated by the yellow arrows.

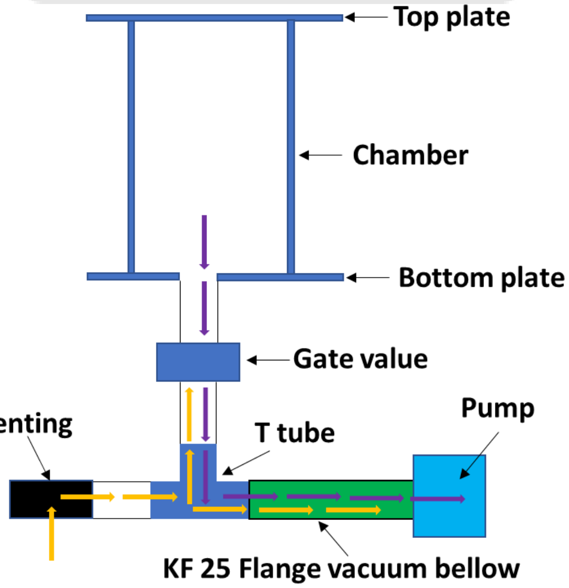

Figure 2.4: The pump system of the spherical tokamak.

2.2 Gas injection system

Figure 2.5 shows the setup of the gas injection system at the top plate. The purple line is the gas tube which is a 1/4 inch PU tube. The cross tube is using KF 25 flange. The red arrows is the airflow of argon into the vacuum chamber. The green arrows is indicated the airflow of air when venting value (1) open.

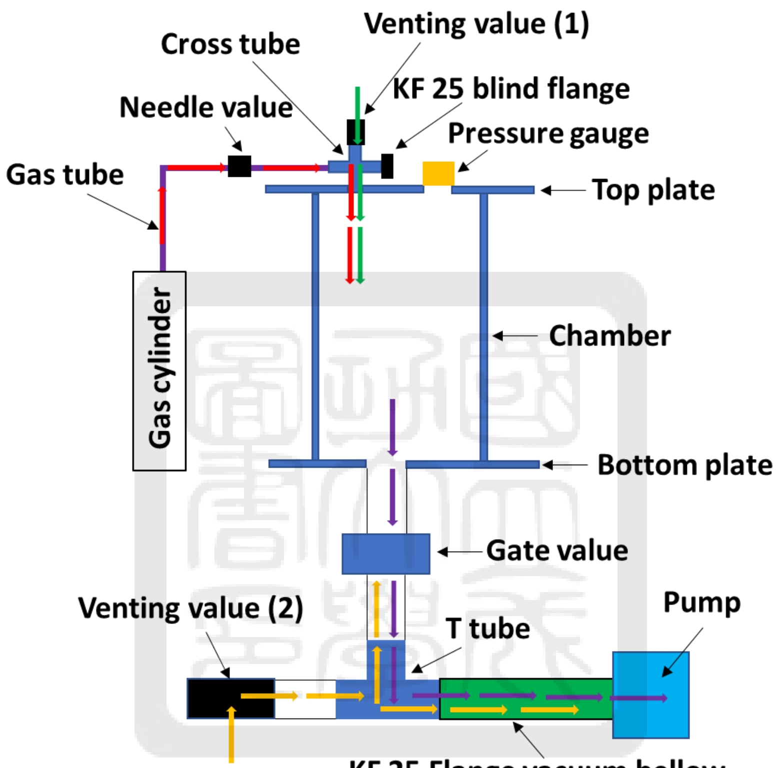

Figure 2.5: The setup of gas injection system.

We would like to produce Argon plasma. Therefore, we replace the air in the chamber with Argon. To way we do is to pump down the pressure to 10^{-3} torr. Then, we vent the chamber with Argon back to 10^{-1} torr. Therefore, the percentage of the residual gas is 1%. Then, we pump down the chamber to 10^{-3} torr and vent the chamber with Argon back to 10^{-1} torr again. Then, the percentage of the residual gas is 0.01% assuming the pumping speeds of different air molecules are the same. We repeated the process three times in total. Finally, we can have a 10^{-1} torr vacuum with the percentage of the Argon equals to 0.0001%. The process of gas injection shown in Appendix A 2.2.

2.3 AC discharge system

The AC discharge system is used to generate plasma as shown in Figure 2.6. The AC discharge system consists of a DC power supply and a pulse generator as shown in Figure 2.7 and Figure 2.8, respectively. The power is provided by the DC power supply. Then, the pulse generator converts the DC power to AC power. The connections are shown in Figure 2.6. The top plate and the bottom plate are grounded. Then, the ground line of the pulse generator is connected to the top plate. The output line of the pulse generator is inserted into the chamber through an insulating feed through. To provide the AC power for igniting the plasma, we first provide a 15-V DC voltage with a current up to 1A from the DC power supply to the pulse generator. Then, the pulse generator will convert the DC voltage to a 20 kHz AC voltage with amplitude ~ 1 kV. Finally, if the chamber is filled with 10^{-1} torr of Argon, the plasma is ignited as shown in Figure 2.8.

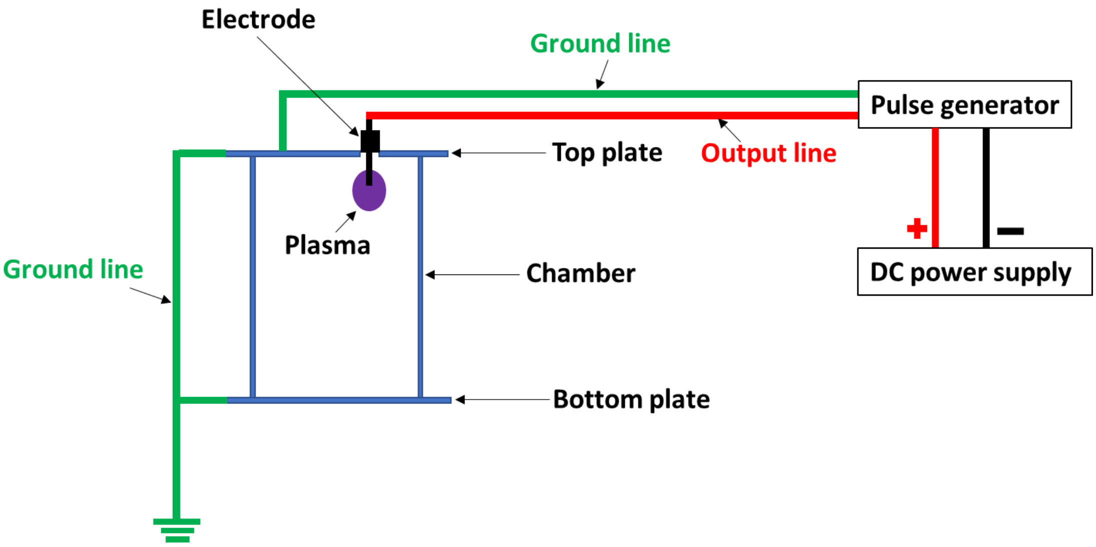

Figure 2.6: The setup of AC discharge system.

Figure 2.7: The DC power supply and pulse generator.

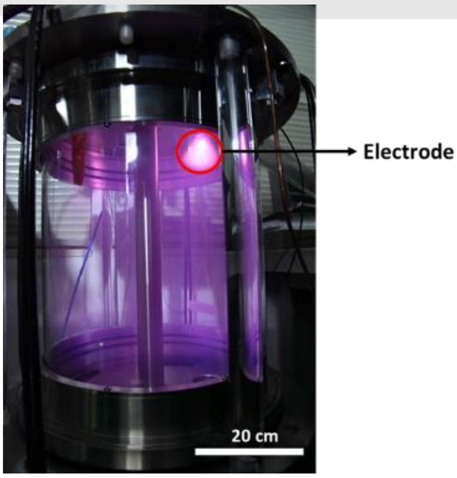

Figure 2.8: The visible light photo of plasma.

2.4 Summary

A cylindrical vacuum chamber made of a quartz tube was built. The diameter and the height of the chamber is 30 cm and 45 cm, respectively. The chamber is filled with Ar with a pressure of 10^{-1} torr. When a ~1 kV AC voltage with a 20 kHz is applied to the electrode in the chamber, the plasma can be ignited.

3. Pulse-forming-network system

In order to generate the high-pulse current for the toroidal coil to generate the toroidal magnetic field, we built the pulse-forming-network system (PFN system). Firstly, the structure of the PFN system will be introduced in section 3.1. Next, the spark-gap switch, which is used to control the PFN, will be introduced in section 3.2. Section 3.3 introduces the trigger box. It is used to control the pulse generator. In section 3.4, the pulse generator, which is used to trigger the spark-gap switch, is described. In section 3.5, the discharge testing results of the PFN will be given. Finally, the summary will be provided in section 3.6.

3.1 The structure of the PFN system

The whole structure of the PFN system is shown in Figure 3.1. It includes several components: the trigger box, the pulse generator, the spark-gap switch, and the PFN. The power supply is HF-Z103-20AC made by Chyng Hong Electronic CO, LTD. The power supply was used to charge capacitors in the PFN. The current monitor was used to measure the PFN discharge current. The high-voltage probes, Tektronix P6015A, were used to measure the voltage of capacitors in the PFN and the voltage of the trigger pin of the spark-gap switch. Finally, we used the oscilloscope, Tektronix DPO2024B, to record signals from the current monitor and high voltage probes.

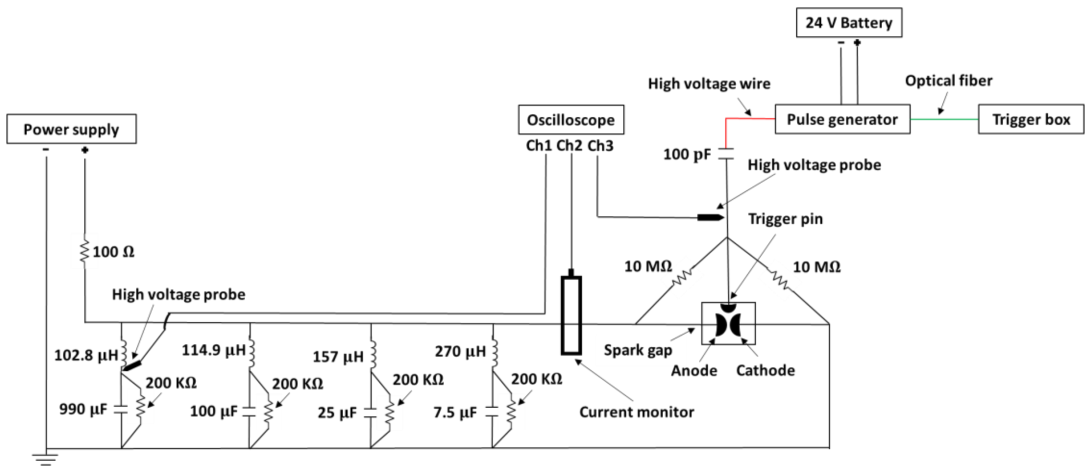

Figure 3.1: The PFN system.

3.2 The spark-gap switch

The red box in Figure 3.2 is the spark-gap switch. It was made by the former student Mei-Feng Huang [8]. It is used to control the discharge of the PFN. When the trigger pin receives a -8-kV pulse from the pulse generator, a spark will occur between the anode and the cathode. Therefore, the gap between the anode and the cathode becomes shorted.

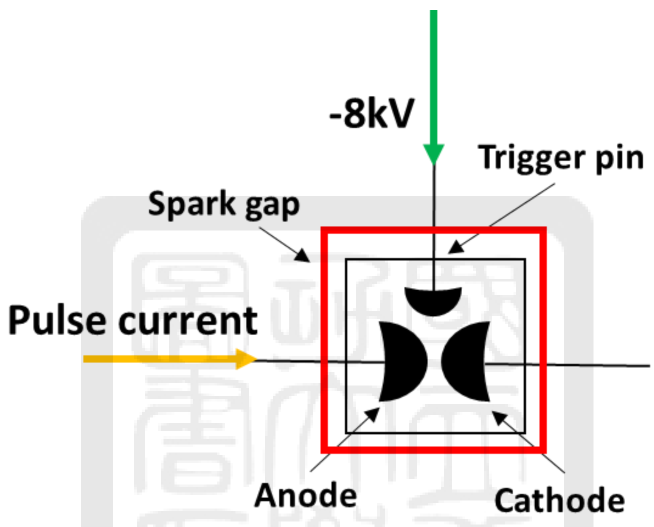

Figure 3.2: The spark-gap switch.

Two M8 cap nuts are used as the anode and cathode in the spark-gap switch. On the other hand, the M3 cap nut is used as the trigger pin. The material of the spark-gap switch case is acrylic as shown in Figure 3.3(a). The length of the spark gap switch is 11 cm and the diameter is 6 cm as shown in Figure 3.3(b).

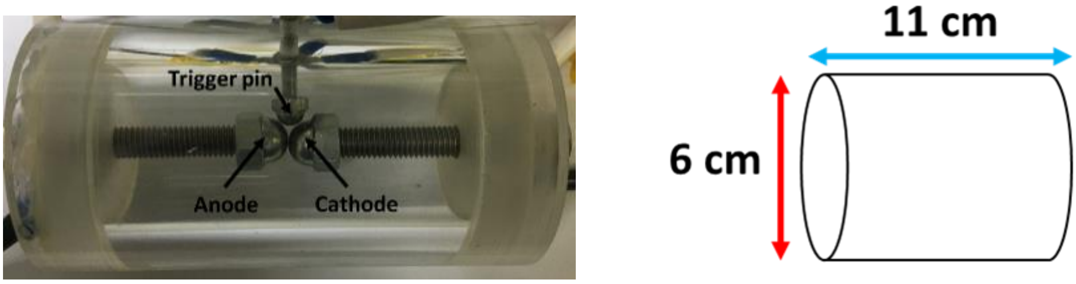

(a) (b)

Figure 3.3: (a) The spark-gap switch. (b) The scale of spark-gap switch.

We use the Paschen's curve to predict in what voltage condition the breakdown will occur. Therefore, based on the Paschen's curve, we adjust the gap distances of the spark-gap switch, including the gap between the anode and the cathode (d_1 in Figure 3.4), the gap between the trigger pin and the anode (d_2 in Figure 3.4), and the gap between the trigger pin and the cathode (d_3 in Figure 3.4). In our design, the gap between the anode and the cathode can hold at least 500 V when the filled gas is air. As shown in Figure 3.4, the gap distance d_1 is 1 mm and both d_2 and d_3 are approximately 3 mm.

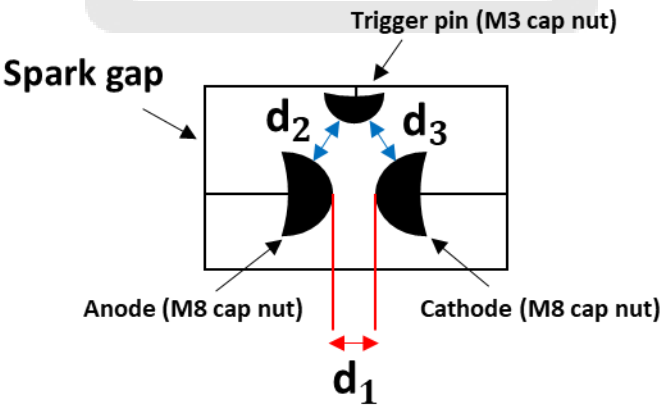

Figure 3.4: Gap distances of the spark-gap switch.

3.3 The trigger box

In order to trigger the pulse generator and provide a -8-kV pulse, we use the trigger box to send out an optical triggering signal to the pulse generator. The trigger box contains three components as shown in Figure 3.5. The first one is a switch box. The second one is a signal generator. The last one is a 5-V charger.

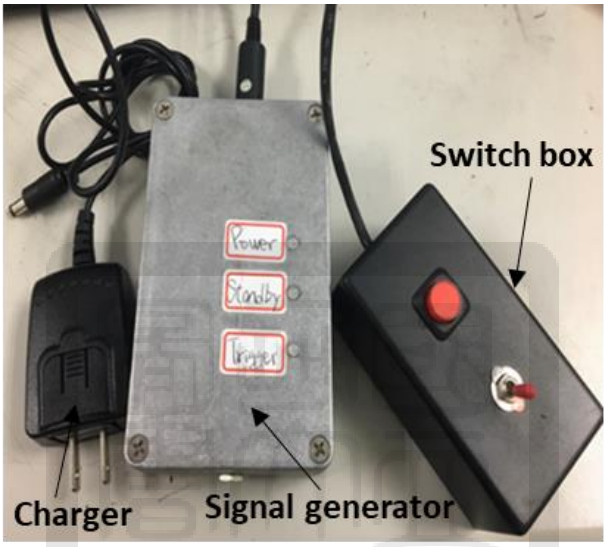

Figure 3.5: The trigger box.

The switch box is used to control the signal generator, and the 5-V charger is used to power the signal generator. The power light is ON when the signal generator is powered. The signal generator has three modes: the "Pre-standby" mode, the "Standby" mode and the "Trigger" mode. Figure 3.6 is the flow chart of the trigger box. When the signal generator is powered, it enters the "Pre-standby" mode. Only when the toggle switch is changed from OFF state (0 in logical state) to ON state (1 in logical state), the signal generator can enter the "Standby" mode, and the standby light becomes ON. It means the signal generator is ready to send out the triggering signal. If the button of the trigger box is pressed (1 in logical state) in the "Standby" mode, a 4-V square pulse with a width of 0.3 ms is generated in the signal generator. The 4-V square pulse is then converted to an optical signal and sent out by an optical fiber transmitter. The trigger light is ON during the 0.3-ms peroid. Afterward, the signal generator goes back to the "Pre-standby" mode. Both the "Standby" and the trigger LEDs become OFF. Figure 3.7 is the circuit of the trigger box [9]. The layout of the signal generator and the source code of the Arduino is given in Appendix A 3.1. Figure 3.8 is the electrical output signal from the trigger box. A 4-V square pulse with a width of 0.3 ms was generated. Then, the optical fiber transmitter (HFBR-1528Z) converts the electrical signal to the optical signal. Finally, the optical signal is sent to the pulse generator via a optical fiber.

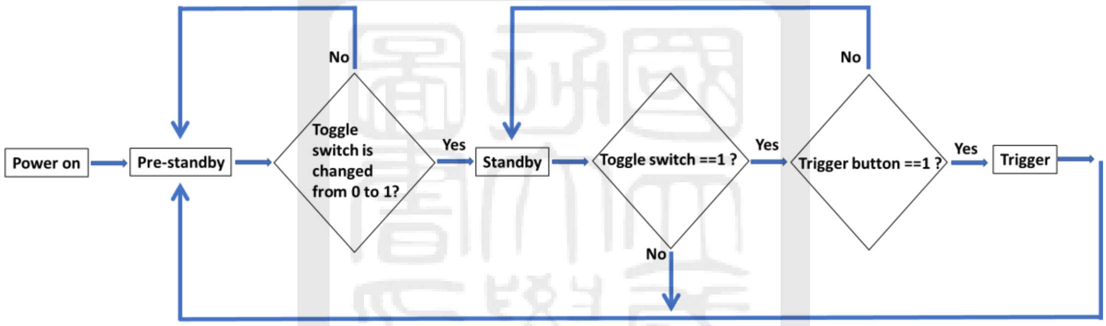

Figure 3.6: The chart of the trigger box.

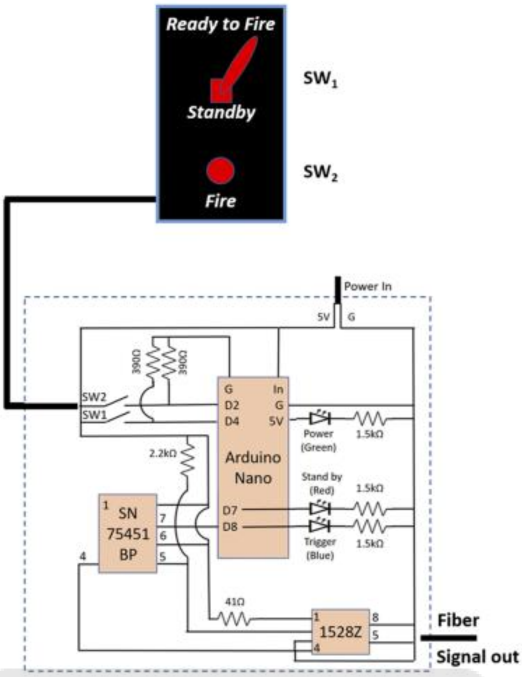

Figure 3.7: The circuit of the trigger box.

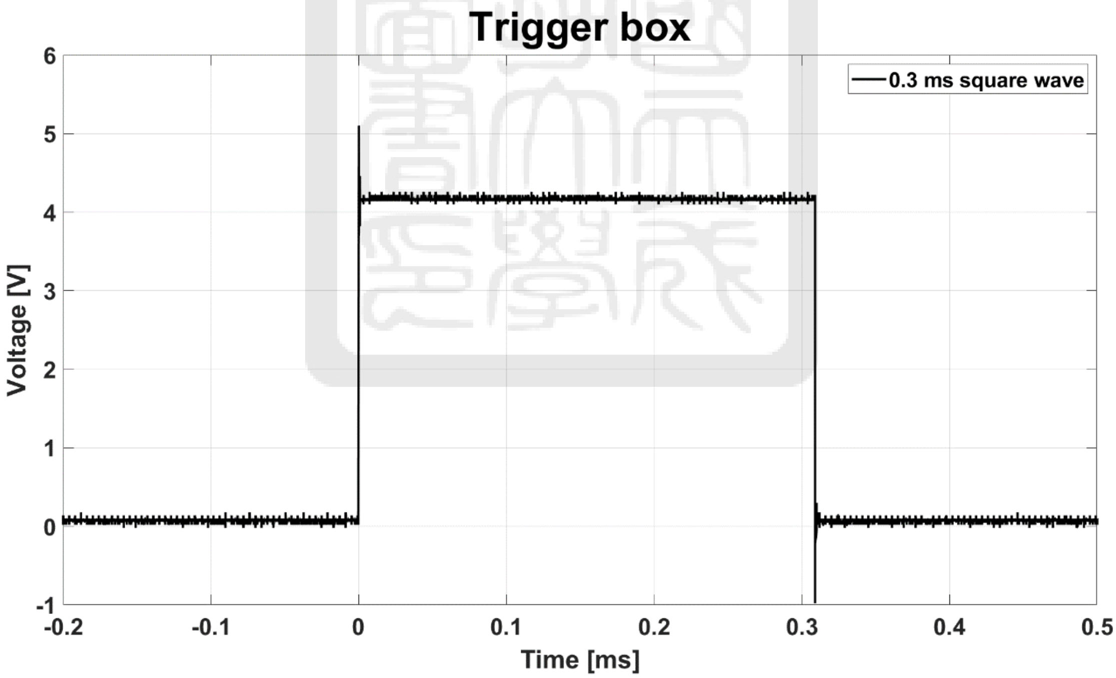

Figure 3.8: The electrical output signal of the trigger box.

3.4 The pulse generator

The pulse generator is used to trigger the spark-gap switch. When the pulse generator receives the optical square pulse with a width of 0.3 ms from the signal generator, the pulse generator will generate a high-voltage pulse of -8 kV. Figure 3.9 is the photo of the pulse generator.

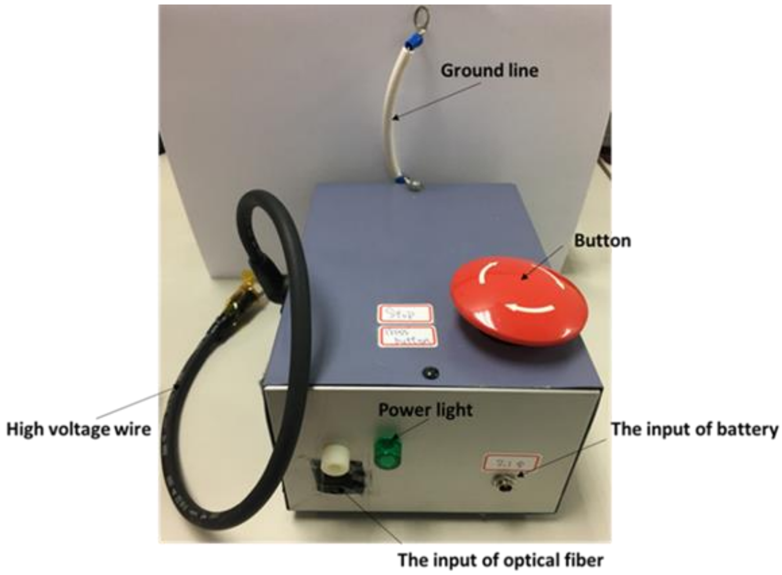

Figure 3.9: The pulse generator.

The fiber is used for delivering the optical signal from the trigger box to the pulse generator. In other words, the trigger box is isolated from the pulse generator. Therefore, the electromagnetic pulse (EMP) noise does not propagete from the pulse generator back to the trigger box. The pulse generator is powered by a 24-V battery. In Figure 3.9, the red button is the power switch of the pulse generator. When the button is pressed, no power is supplied to the pulse generator. Contrarily, when the button is pulled up, the pulse generator is powered. Then, the green light lights out indicating the power is ON. The high-voltage wire is used to deliver the -8-kV signal to the spark-gap switch. Finally, the pulse generator should be grounded using the ground wire.

Figure 3.10 is the circuit of the pulse generator. The pulse generator produces the high voltage using the Ignition coil (Hitachi C6R-500S 12V). The energy is first stored in the primary coil of the Ignition coil when the current flows through the primary coil. Then, the secondary coil generates the high voltage output when the IGBT is suddenly open.

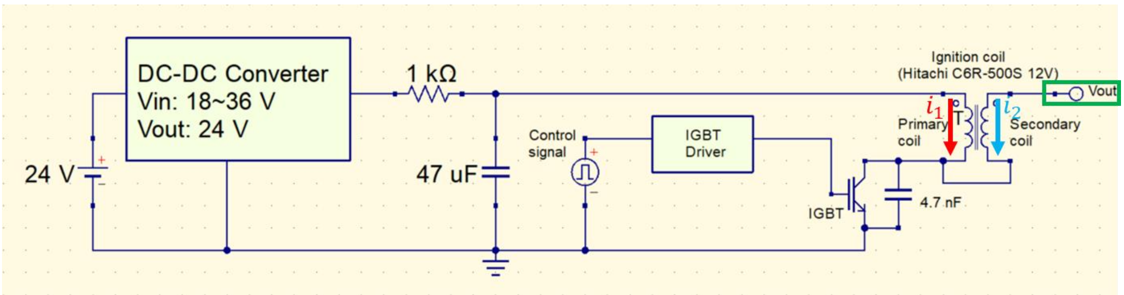

Figure 3.10: The circuit of pulse generator.

The IGBT is controlled by the trigger box. When the trigger box sent out a square pulse so that the IGBT is turned on, the energy in the 47-uF capacitor starts being delivered to the Ignition coil. In Figure 3.11, we can see the voltage of the 47-uF capacitor drops approximately 4 V in 0.3 ms. The energy is delivered to the Ignition coil during this period. When the signal from the trigger box becomes zero, the IGBT is turned off, i.e. discharge current from the 47-uF capacitor stops since current does not go through the IGBT any more. When the current i_1 in Figure 3.10 drops to zero in a short period of time, the high voltage $V_{out} = \mathrm{M}\frac{\mathrm{di_2}}{\mathrm{dt}}$ is generated where M is the mutual inductance of the ignition coil and dt is determined by the switch-off time of the IGBT. Figure 3.12 is the output of the pulse generator. The output voltage is -8.0$\pm$ 0.4 kV, with a rise time of $\mathrm{t_{rise}}= \mathrm{t_{0.9}} - \mathrm{t_{0.1}}$= 0.04 ms.

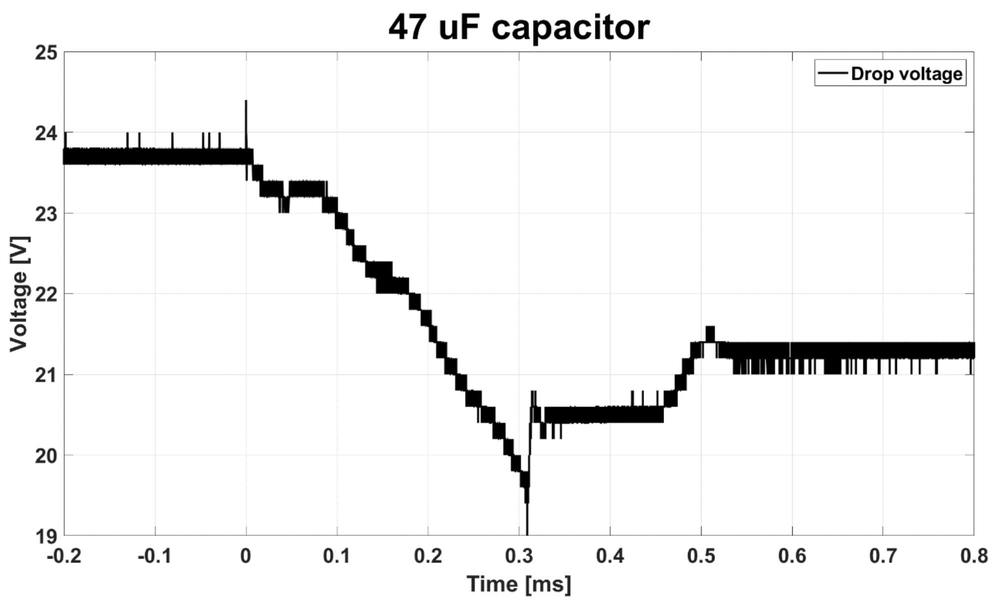

Figure 3.11: The output of pulse generator.

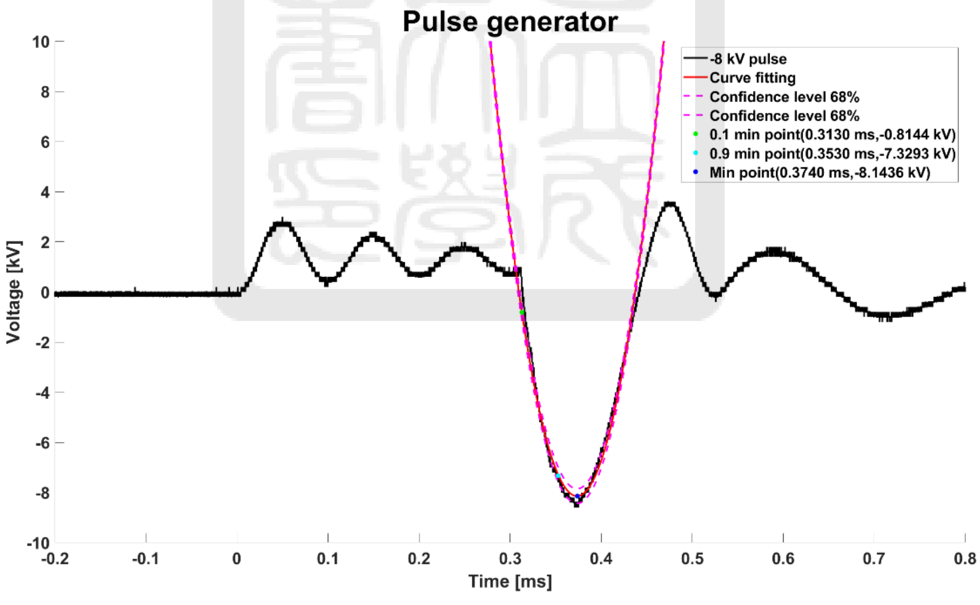

Figure 3.12: The output of pulse generator.

Figure 3.13 is the voltage data of the trigger box, the 47-uF capacitor, and pulse generator. The black line is the trigger box signal. The blue line is the voltage of the 47-uF capacitor. The red line is the pulse generator output. When the trigger box voltage is pulled up, the voltage of the 47-uF capacitor begins to drop. After 0.3 ms, the trigger box signal is pulled down, and the -8 kV output single is generated by the pulse generator.

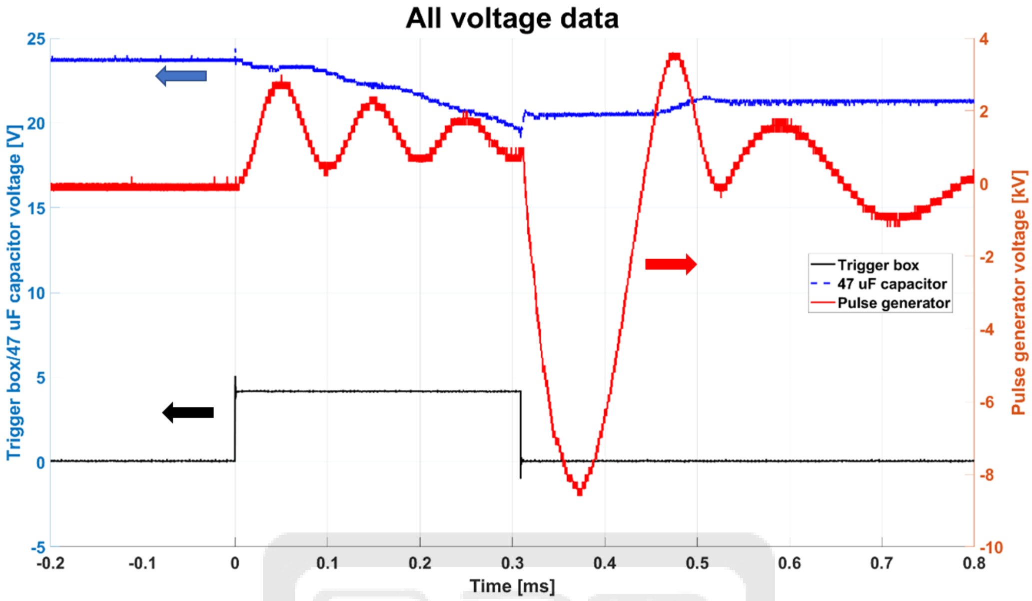

Figure 3.13: The process of pulse generator output.

3.5 The PFN

In order to provide the trapezoidal current to the load, "toroidal coil", we use the PFN as shown in Figure 3.14. The PFN consists of many capacitors and inductors. The energy is stored in capacitors. Then, the PFN releases the energy through a spark gap switch or hydrogen thyratron. When the energy in each stage of the PFN is released, each stage of the PFN behaves as a LC oscillation. Finally, the output of the PFN is the sum of the output from each stage.

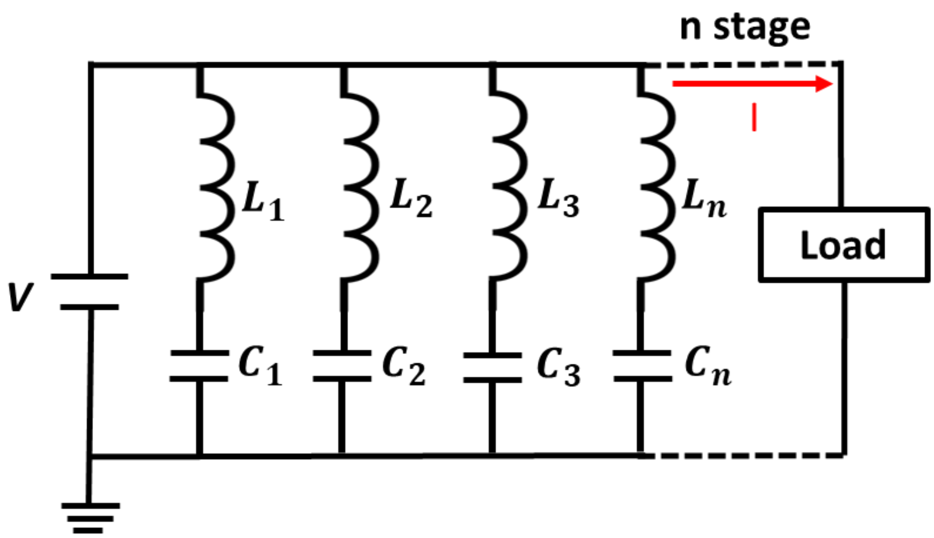

Figure 3.14: The nth-stage PFN.

3.5.1 Design of the PFN

We use the theory of Fourier series analysis to determine capacitances and inductances of the PFN. It is because Fourier series can be used to create any periodic waves as shown in Eq (3-1). The function $\mathrm{f}(t)$ represents the wave we want to generate, a_0 is a constant of, a_n is the constant of each cosine term, b_n is the constant of each sinusoidal term, and τ is the half period of the foundamental frequency.

$$\mathrm{f}(t) = \frac{a_0}{2} + \sum_{\mathrm{n}=1}^{\infty} a_n \cos\frac{n\pi t}{\tau} + b_n \sin\frac{n\pi t}{\tau} \ . \tag{3-1}$$

We would like to generate a trapezoidal current to drive the tororidal coil. Therefore, the current waveform $i(t)$ of PFN is an odd function. As shown in Eq (3-2), only the sinusoidal terms of the Fourier series remain. The constant of each sinusoidal term can be obtained by Eq (3-3). The normalized current waveform $i(t)$ we want is the trapezoidal wave given in Eq (3-4). The width of the trapezoidal wave is τ. The rise time and the falling time is a$\cdot\tau$. Substituting Eq (3-4) into Eq (3-3), we can obtain the constant of each sinusoidal term given in Eq (3-5). Then, Eq (3-5) will be used to determine the capacitance and the inductance of each stage of the PFN.

$$i(t) = \sum_{\mathrm{n}=1}^{\infty} b_n \sin\frac{n\pi t}{\tau}, \tag{3-2}$$

$$b_n = \frac{2}{\tau}\int_0^{\tau} i(t) \sin\frac{n\pi t}{\tau} dt, \tag{3-3}$$

$$\begin{cases} i(t) = \frac{t}{a\tau}, & 0 \le t \le a\tau \\ i(t) = 1, & a\tau \le t \le \tau - a \\ i(t) = \frac{\tau - t}{a\tau}, & \tau - a\tau \le t \le \tau \end{cases}, \tag{3-4}$$

$$b_n = \frac{4}{n\pi}\frac{\sin n\pi a}{n\pi a}, \text{ where } n = 1,3,5\ldots \quad . \tag{3-5}$$

Equation (3-6) is the current flow of a PFN, where V is the charged voltage of capacitors, I is the output current of the PFN, C_n is the capacitance of each PFN stage, L_n is inductance of each PFN stage. It represents that the current from the PFN is the sum of the current from each stage. The circuit of each stage is a simple LC oscillation, i.e, $i_n(t) = \frac{V}{I}\sqrt{\frac{C_n}{L_n}}\sin\frac{t}{\sqrt{L_n C_n}}$. Comparing Eq (3-2) to Eq (3-6), we can obtain Eq (3-7), and thus Eq (3-8). Equation (3-8) is the formula we use to determine the capacitance and inductance in each stage of the PFN. Finally, we substituce the Eq (3-5) into Eq (3-8) and get the capacitance and inductance of each stage of the PFN.

$$i(t) = \sum_{\mathrm{n}=1}^{\infty} i_n(t) = \sum_{\mathrm{n}=1}^{\infty} \frac{V}{I}\sqrt{\frac{C_n}{L_n}} \sin\frac{t}{\sqrt{L_n C_n}}. \tag{3-6}$$

$$b_n = \frac{V}{I}\sqrt{\frac{C_n}{L_n}} \;, \; \frac{n\pi t}{\tau} = \frac{t}{\sqrt{L_n C_n}}. \tag{3-7}$$

$$L_n = \frac{V\tau}{In\pi b_n} \ , \ C_n = \frac{I\tau b_n}{Vn\pi} . \tag{3-8}$$

Initially, we wanted to use a five-stage PFN charged to 1 kV, i.e, V = 1kV in Eq (3-8), to generate the 2.5-kA trapezoidal current with a width of 1 ms, i.e, i = 2.5 kA , τ = 1ms. Both the rise time and the fall time are 0.1 ms. Therefore, b_n are calculated and listed in Table 3.1. The theoretical inductance and capacitance of each PFN stage are also shown in Table 3.1.

Table 3.1: Five-stage PFN parameters.

	Stage 1	Stage 2	Stage 3	Stage 4	Stage 5
bn	1.25	0.36	0.16	0.06	0.01
Inductance	101.66 μH	116.47 μH	157 μH	271.46 μH	910.49 μH
Capacitance	997.65 μF	96.75 μF	25.84 μF	7.62 μF	1.37 μF

Although the designed PFN is charged to 1 kV, we only have a 500-V power supply. Therefore we only study the PFN charged to 500 V for generating a current of 1.25 kA. On the other hand, we built the inductors ourself. It will use too many wires to make the 910-μH inductor in stage 5. Therefore, we dropped the 5th stage of the PFN. In order to verify if the PFN with only 4 stage is enough, we did the simulation of discharge from both four-stage PFN and five-stage PFN. The simulation result is given in Figure 3.15. Figure 3.15 shows the comparison between the four-stage PFN in red, the five-stage PFN in black, and the trapezoidal current we want in the blue-dashed line. The parameters we used in the simulation is given in Table 3.2 where capacitances and inductances are what we actually can get on the shelf. We calculated the root mean square of the difference between four-stage PFN and the trapezoidal current. The number is 0.033. And calculated the root mean square of the difference between five-stage PFN and the trapezoidal current. The number is 0.031. Using the five-stage PFN only improves the rms for 6%, which is not significant. Therefore, we decided using only the four-stage PFN.

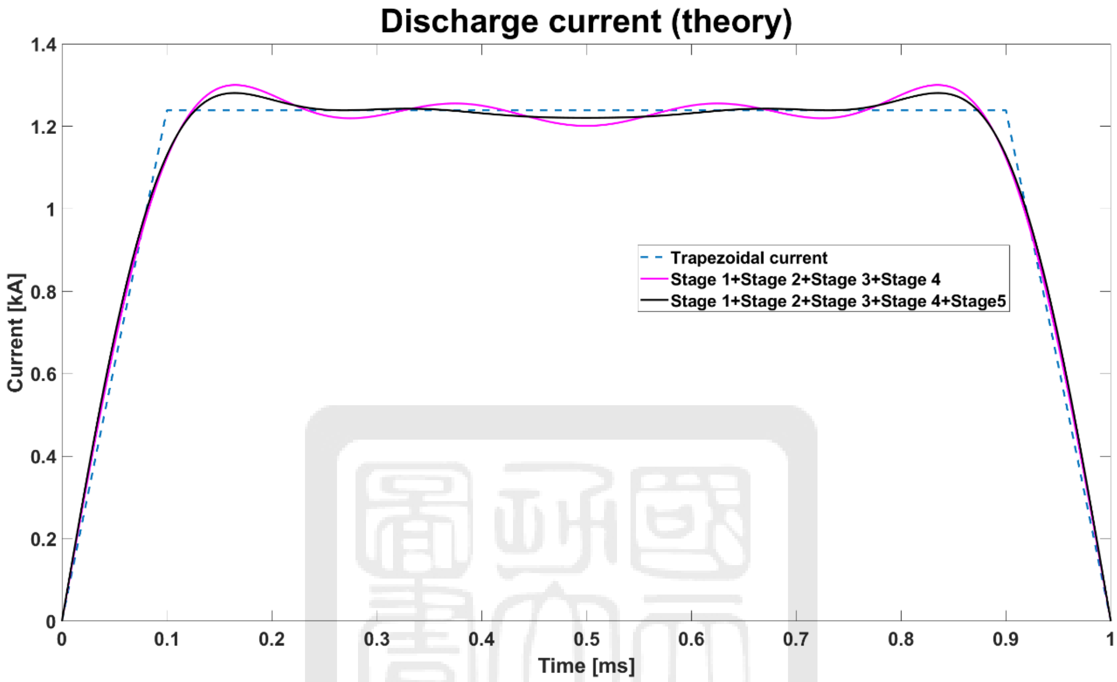

Figure 3.15: The PFN theory discharge current.

We use wires to wrap around Polyvinyl chloride (PVC) tubes to make inductors. The closest inductance we can obtain from making the inductors are shown in Table 3.2. The closest capacitance we can obtain from the capacitor vendor are also shown in Table 3.2. The detail process of determing the number of turns is shown in Figure 3.16.

(1) Step 1: Use the theory of the Fourier series to obtain the expected inductance.

(2) Step 2: They are the same numbers from Table 3.1. Ignore the decimals of the expected inductance.

(3) Step 3:The theoretical inductance of a solenoid and the corresponding parameters. The inductance L in step 2 is used. The parameter μ_0 is permeability of vacuum. The ℓ is length of the inductor. In our design, it is 10 cm. The parameter A is the cross-sectional area of

the inductor. In our design, a half-inch (4 分管) is used and A is $9.07\ \text{cm}^2$.

(4) Step 4: The correction factor. We previously found that the measured inductance is 10% higher than the theoretical value. For example, if we want an inductance of 50 uH, we use 45.4 uH to do the calculation in step 3.

(5) Step 5: For a given inductance, we can obtain the square of turns and thus the number of turns we need to make the inductor.

(6) Step 6: We measured the inductance of the inductors we built and compared to the expected value.

Table 3.2: Four-stage PFN parameters.

	Stage 1	Stage 2	Stage 3	Stage 4
bn	1.25	0.36	0.16	0.06
Inductance	102.8 μH	114.9 μH	157 μH	270 μH
Capacitance	990 μF	100 μF	25 μF	7.5 μF

Step 1: The expected inductance

	Inductance
Stage 1	101.66 µH
Stage 2	116.47 µH
Stage 3	157 µH
Stage 4	271.46 µH

Step 2: To ignore the decimals

	Inductance
Stage 1	101 µH
Stage 2	116 µH
Stage 3	157 µH
Stage 4	271 µH

Step 3: Formula of inductor

$$L = \frac{\mu_0 N^2 A}{\ell}$$

$L =$ inductance

$\mu_0 = 1.26 \times 10^{-6}\,\mathrm{H/m}$

$\ell =$ length of inductor

$A =$ Cross-sectional area

Step 4: Correction factor

$$\frac{50\ \mathrm{uH\ (measure)}}{45.4\ \mathrm{uH\ (calculation)}} \approx 1.1$$

Step 5: Obtain N

	N^2	N
Stage 1	8.07×10^3	89.8
Stage 2	9.25×10^3	96.2
Stage 3	1.25×10^4	112
Stage 4	2.15×10^4	147

Step 6: To compare inductance value

	Inductance (expected)	Inductance (measure)	Difference(%)
Stage 1	101 µH	102.8 µH	1.8 %
Stage 2	116 µH	114.9 µH	-1.1 %
Stage 3	157 µH	157 µH	0.0 %
Stage 4	271 µH	270 µH	-1.0 %

Figure 3.16: The process of determing the number of turns of the solenoid.

Finally, Figure 3.17 is the schematic diagram of the four-stage PFN, including the spark-gap switch and the load "toroidal coil". The spark-gap switch is used to control the four-stage PFN. When the spark-gap switch is activated, the current will be delivered to the load "toroidal coil".

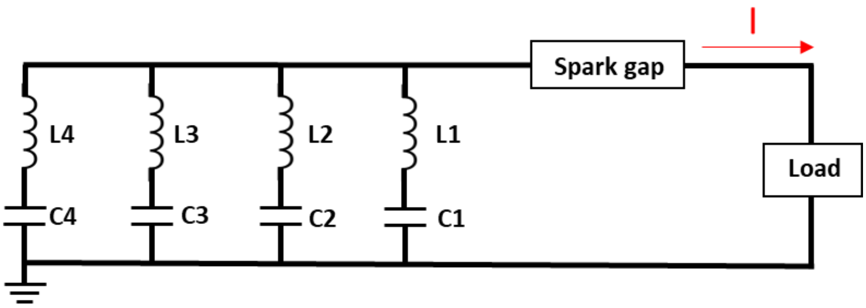

Figure 3.17: Four-stage PFN schematic diagram.

The calculated results of each stage of PFN are shown in Figure 3.18. Notice that the impedance of the load is ignored. In Figure 3.18, the trapezoidal current we want is the blue-dashed line. The red line is the output only from the first-stage of the PFN. The bule line is the superposition of outputs from the first-stage and the second-stage of the PFN. The green line is the superposition of outputs from the first-stage, the second-stage, and the third-stage of the PFN. The purple line is calculated output of the whole PFN. A trapezoidal current with a root mean square of the difference between the trapezoidal current equals to 0.031 is expected.

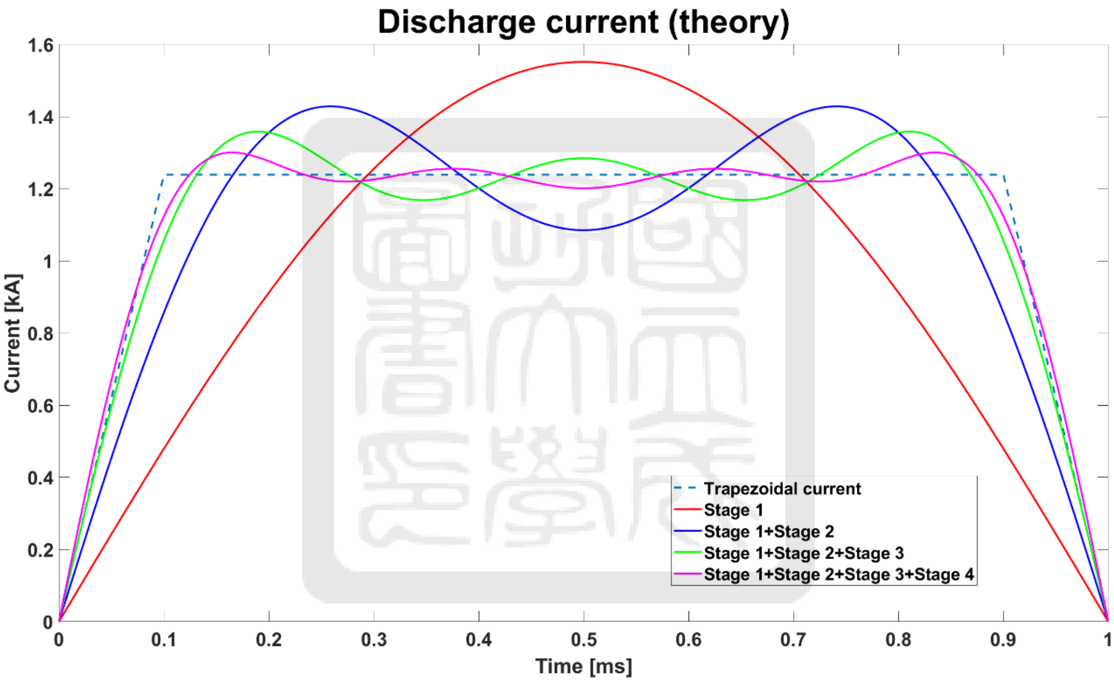

Figure 3.18: The result of each stage PFN.

3.5.2 The results of the PFN discharge test

In order to get the resistance and inductance of the whole PFN system, we conducted discharge tests of each stage of the PFN alone. Then, we used the curve fitting process to fit to the discharge current. Finally, we obtained resistance and inductance information from the curve fitting results.

3.5.2.1 The 1st PFN stage

Figure 3.19 is the discharge test circuit of the 1st PFN stage. In Figure 3.19, channel one (Ch1) measured the voltage of the 990-uF capacitor in the 1st PFN stage. Channel two (Ch2) measured the discharge current. Channel three (Ch3) measured the triggering voltage from the pulse generator.

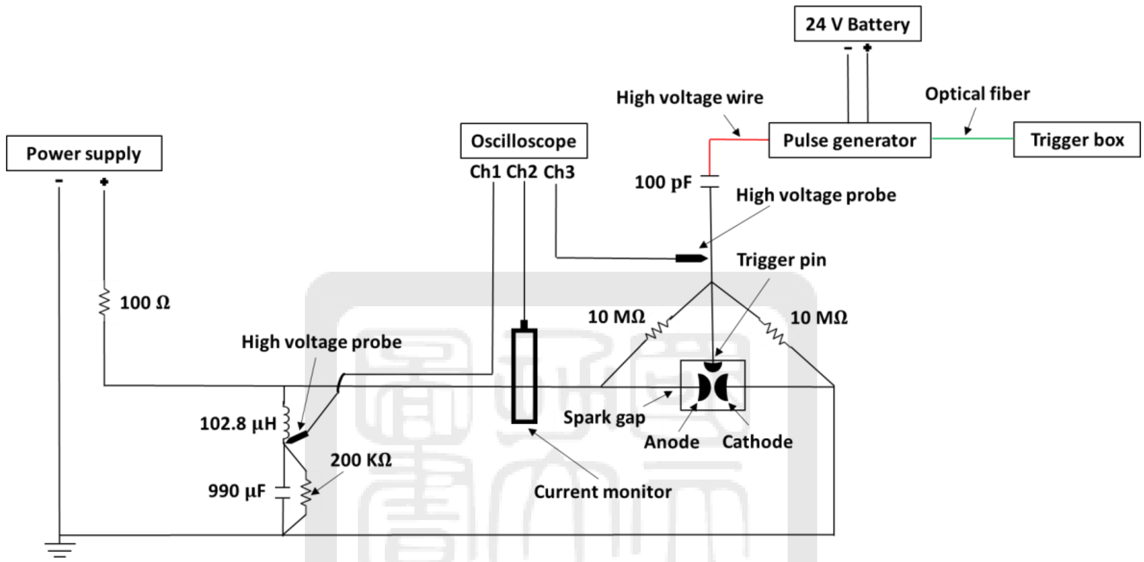

Figure 3.19: The circuit of the 1st PFN stage discharge test.

Figure 3.20 is the discharge current test result of the 1st PFN stage. In Figure 3.20, the blue line is the discharge current and the red line is the curve-fitting result. We repeated the experiment ten times. We only show one result as an example. Rest of data are given in Appendix A 3.2.

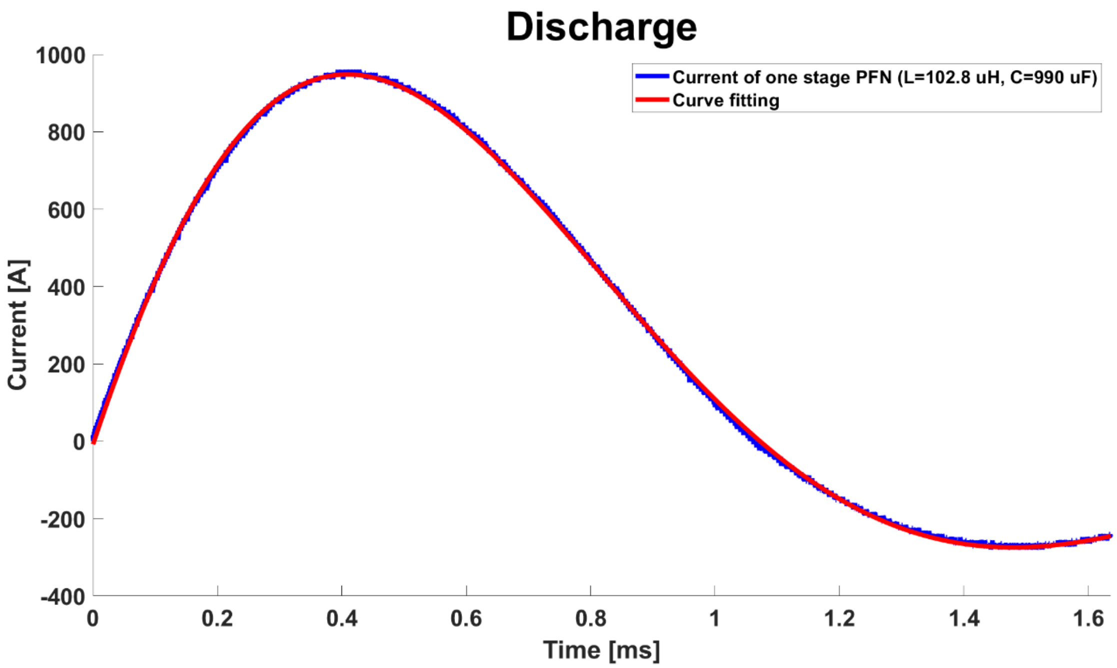

Figure 3.20: The result of the 1st PFN stage discharge test.

We use Eq (3-9) to fit to each discharge current of the 1st PFN stage. Parameters "a" , "α" , "φ" , "w_d" are fitting coefficients. Then, we can obtain the inductance and the corresponding standard deviation of the inductance of the 1st PFN stage using Eq (3-9) ~ Eq (3-14).

$$i(t) = \text{a*exp[-}\alpha * (t+\varphi)] * \sin[w_d * (t+\varphi)]\,, \tag{3-9}$$

$$w_d = \sqrt{{w_0}^2 - \alpha^2}\,, \tag{3-10}$$

$$w_0 = \frac{1}{\sqrt{LC}}\,, \tag{3-11}$$

$$\frac{1}{LC} = {w_d}^2 + \alpha^2\,, \tag{3-12}$$

$$L = \frac{1}{C}\frac{1}{{w_d}^2 - \alpha^2} \,, \tag{3-13}$$

$$\sigma_L = \sqrt{(\frac{\partial L}{\partial w_d}\sigma_{w_d})^2 + (\frac{\partial L}{\partial \alpha}\sigma_\alpha)^2} \quad . \tag{3-14}$$

Using Eq (3-15) and Eq (3-16) we can obtain the resistance of the 1st PFN stage and the corresponding standard deviation.

$$R = 2L\alpha \,, \tag{3-15}$$

$$\sigma_R = \sqrt{(\frac{\partial R}{\partial L}\sigma_L)^2 + (\frac{\partial R}{\partial \alpha}\sigma_\alpha)^2} \quad . \tag{3-16}$$

Table 3.3 is our results from the curve fitting of the 1st PFN stage discharge current. The inductance and the resistance is $132 \pm 4\ \mu$H and $0.28 \pm 0.01\ \Omega$, respectively.

Table 3.3: The curve fitting results of 1st PFN stage.

Data point	Data 1	Data 2	Data 3	Data 4	Data 5
Inductance (uH)	139	132	135	125	129
Resistance (Ω)	0.32	0.28	0.29	0.27	0.29

Data point	Data 6	Data 7	Data 8	Data 9	Data 10	Avg	Std
Inductance (uH)	132	133	136	126	133	132	4
Resistance (Ω)	0.28	0.28	0.30	0.26	0.28	0.28	0.01

3.5.2.2 The 2nd PFN stage

Figure 3.21 is the discharge test circuit of the 2nd PFN stage. The experimential setup was similar to that used to test the 1st PFN stage. The only difference was the capacitor and the inductor were replaced by those for the 2nd PFN stage, ie, L=114.9 μH, and C= 100 μF.

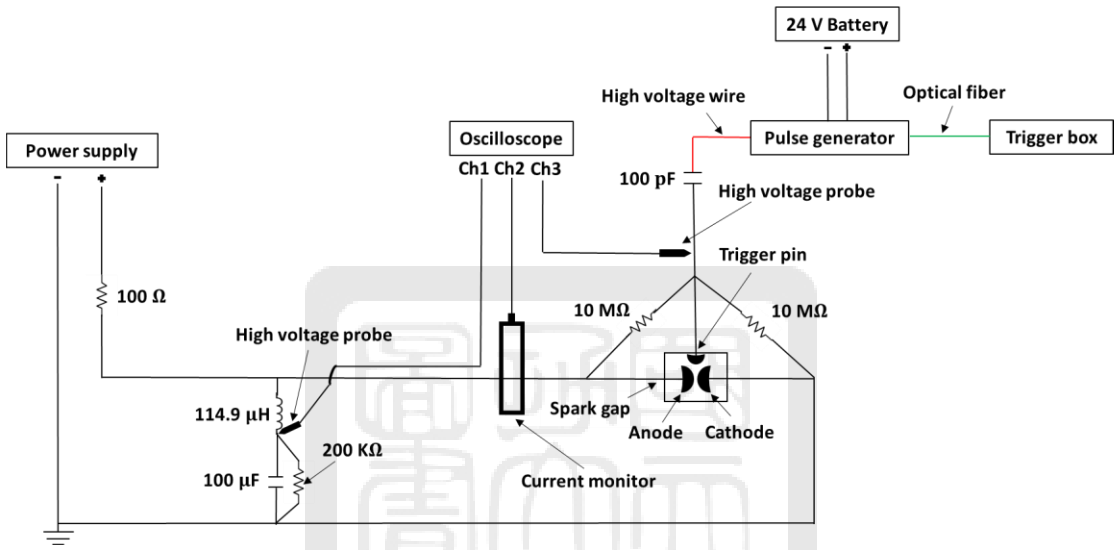

Figure 3.21: The circuit of the 2nd PFN stage discharge test.

Figure 3.22 is the discharge current test result of the 2nd PFN stage. In Figure 3.22, the blue line is the discharge current and the red line is the curve-fitting reault. We repeated the experiment ten times. We only show one of the results as an example. Rest of data are given in Appendix A 3.3.

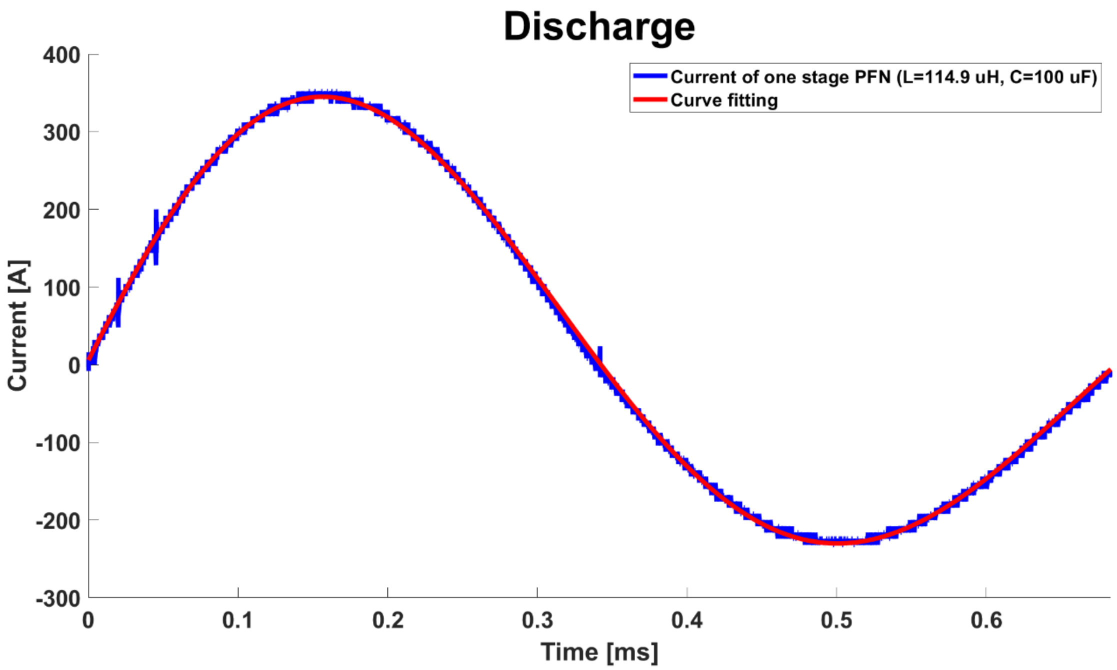

Figure 3.22: The result of 2nd PFN stage discharge test.

The curve fitting process used in the 1st PFN stage testing was used. The fitted resistance and inductance of the 2nd stage PFN is listed in Table 3.4. The inductance and the resistance of the 2nd PFN stage is L = 123 $\pm$ 0.4 μH and R= 0.32 $\pm$ 0.02 Ω, respectively.

Table 3.4: The curve fitting result of the 2nd PFN stage.

Data point	Data 1	Data 2	Data 3	Data 4	Data 5
Inductance (uH)	122	123	123	123	123
Resistance (Ω)	0.28	0.32	0.33	0.35	0.35

Data point	Data 6	Data 7	Data 8	Data 9	Data 10	Avg	Std
Inductance (uH)	122	122	123	123	123	123	0.4
Resistance (Ω)	0.30	0.31	0.33	0.33	0.35	0.32	0.02

3.5.2.3 The 3rd PFN stage

Figure 3.23 is the discharge test circuit of the 3rd PFN stage. The experimential setup was similar to that used to test the 1st PFN stage. The only difference was the capacitor and the inductor were replaced by those for the 3rd PFN stage, ie, L=157 μH, and C= 25 μF.

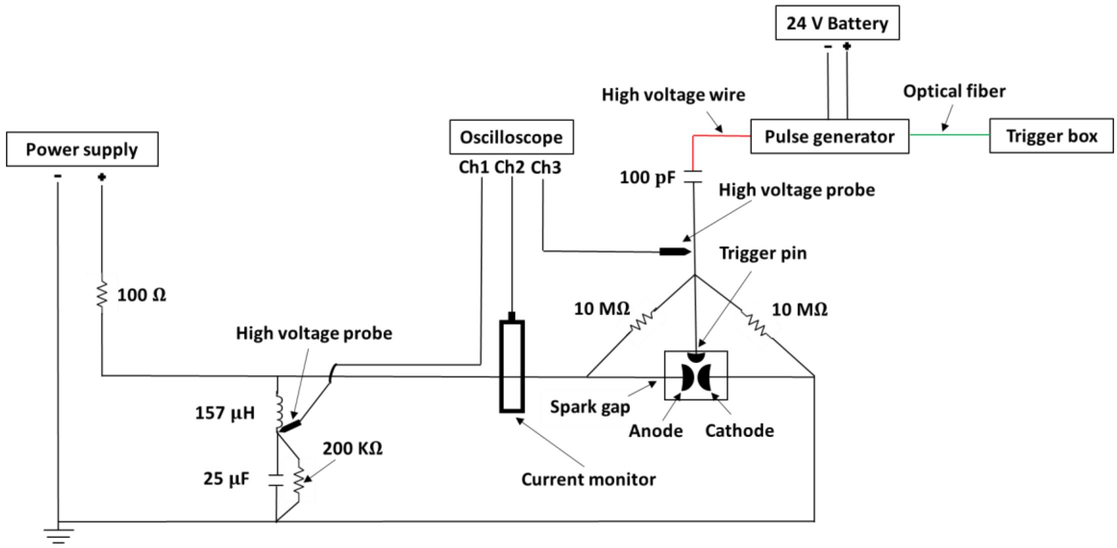

Figure 3.23: The circuit of the 3rd PFN stage discharge test.

Figure 3.24 is the discharge current test result of the 3rd PFN stage. In Figure 3.24, the blue line is the discharge current and the red line is the curve-fitting result. We repeated the experiment ten times. We only show one of the results as an example. Rest of data are given in Appendix A 3.4.

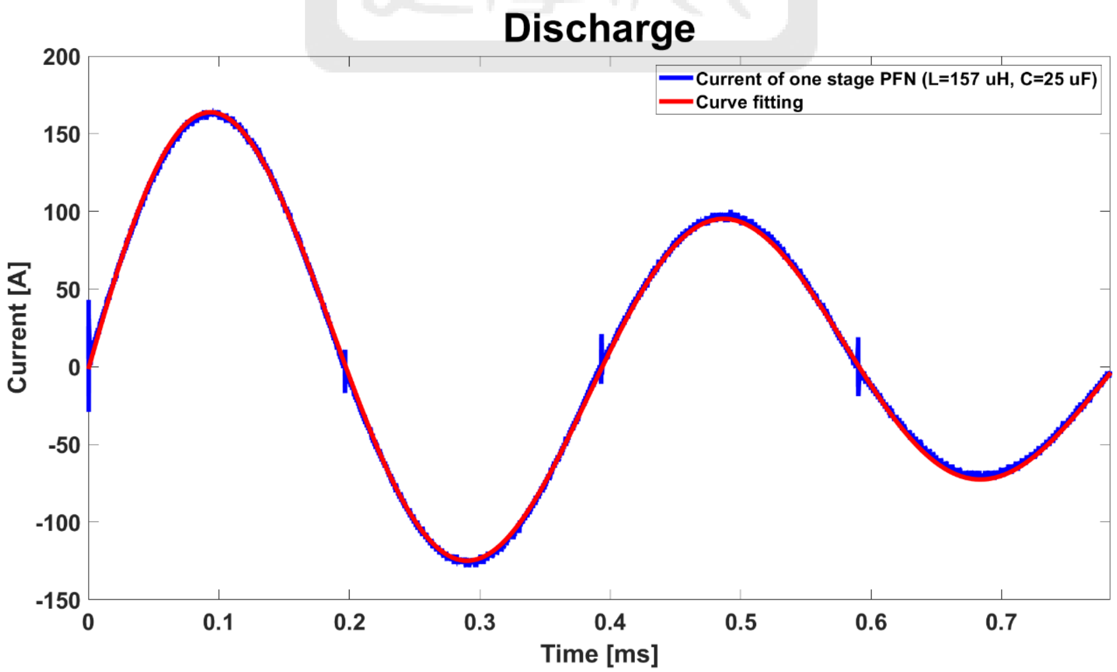

Figure 3.24: The result of the 3rd PFN stage discharge test.

The curve fitting process used in the 1st PFN stage testing was used. The fitted resistance and inductance of the 3rd stage PFN is listed in Table 3.5. The inductance and the resistance of the 3rd PFN stage is L = 158 $\pm$ 1 μH and R= 0.43 $\pm$ 0.01 Ω, respectively.

Table 3.5: The curve fitting result of the 3rd PFN stage.

Data point	Data 1	Data 2	Data 3	Data 4	Data 5
Inductance(uH)	158	158	158	158	158
Resistance(Ω)	0.43	0.43	0.41	0.43	0.43

Data point	Data 6	Data 7	Data 8	Data 9	Data 10	Avg	Std
Inductance(uH)	159	158	158	161	158	158	1
Resistance(Ω)	0.44	0.44	0.43	0.44	0.42	0.43	0.01

3.5.2.4 The 4th PFN stage

Figure 3.25 is the discharge test circuit of the 4th PFN stage. The experimential setup was similar to that used to test the 1st PFN stage. The only difference was the capacitor and the inductor were replaced by those for the 4th PFN stage, ie, L=270 μH, and C= 7.5 μF.

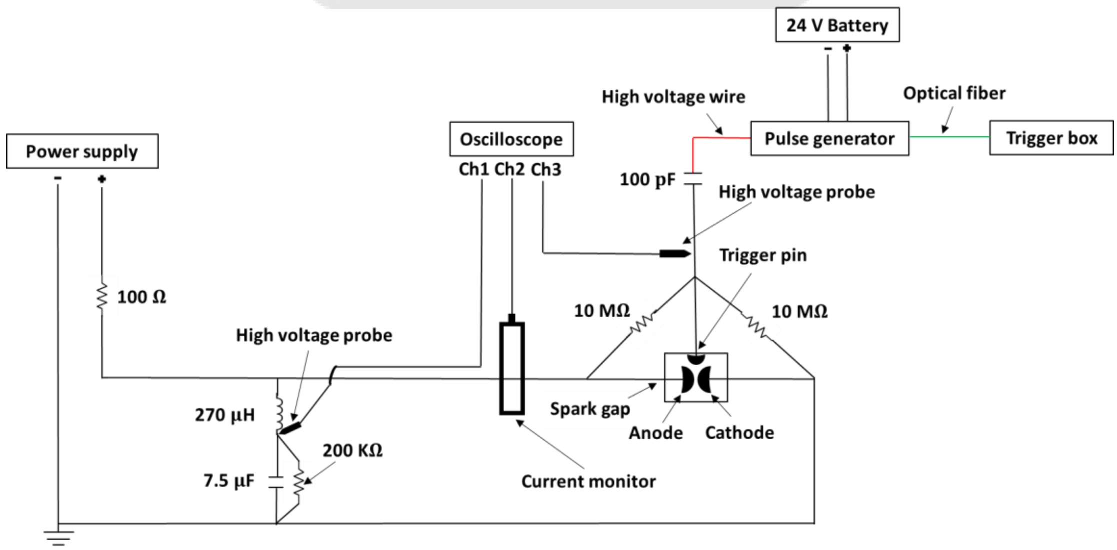

Figure 3.25: The circuit of the 4th PFN stage discharge test.

Figure 3.26 is the discharge current test result of the 4th PFN stage. In Figure 3.26, the blue line is the discharge current and the red line is the curve fitting. We repeated the experiment ten times. We only show one of the results as an example. Rest of data are given in Appendix A 3.5.

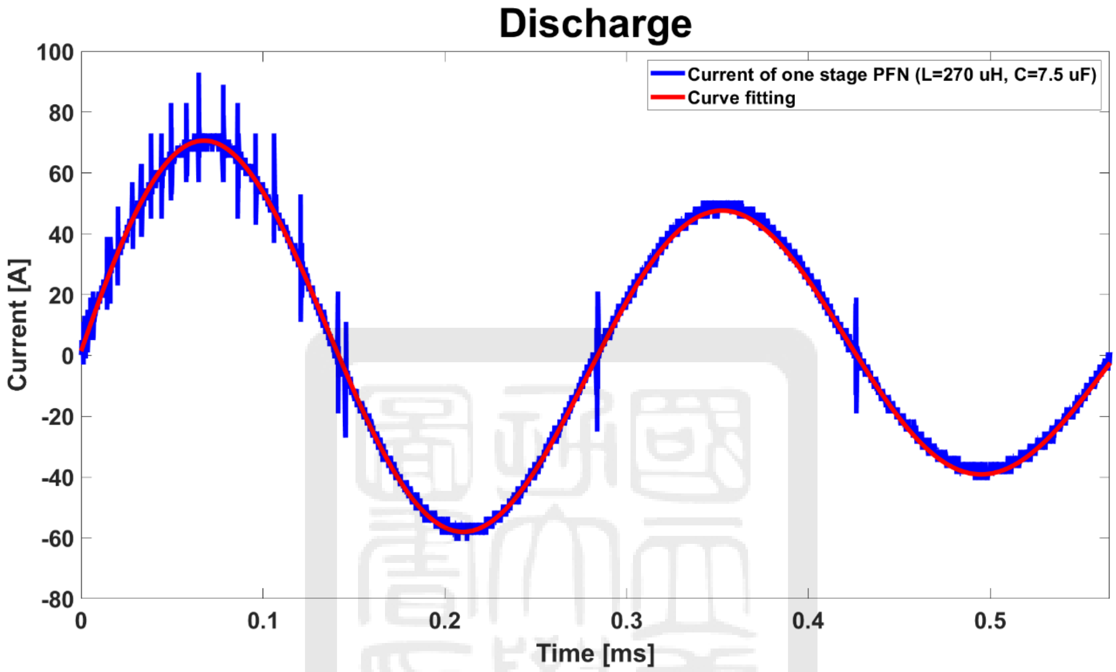

Figure 3.26: The result of the 4th PFN stage discharge test.

The curve fitting process used in the 1st PFN stage testing was used. The fitted resistance and inductance of the 4th stage PFN is listed in Table 3.6. The inductance and resistance of the 4th PFN stage is L = 277 $\pm$ 7 μH and R= 0.73 $\pm$ 0.03 Ω, respectively.

Table 3.6: The curve fitting result of the 4th PFN stage.

Data point	Data 1	Data 2	Data 3	Data 4	Data 5
Inductance(uH)	275	274	274	274	275
Resistance(Ω)	0.76	0.75	0.69	0.74	0.74

Data point	Data 6	Data 7	Data 8	Data 9	Data 10	Avg	Std
Inductance(uH)	274	274	274	297	274	277	7
Resistance(Ω)	0.68	0.74	0.69	0.79	0.69	0.73	0.03

Figure 3.27 shows fitted curves from all PFN stages. The red line is the curve-fitting result of the 1st PFN stage. The bule line is the curve fitting result of the 2nd PFN stage. The green line is a the curve-fitting result of the 3rd PFN stage. The purple line is the curve fitting result of the 4th PFN stage. Table 3.7 summerizes measured results of each PFN stage.

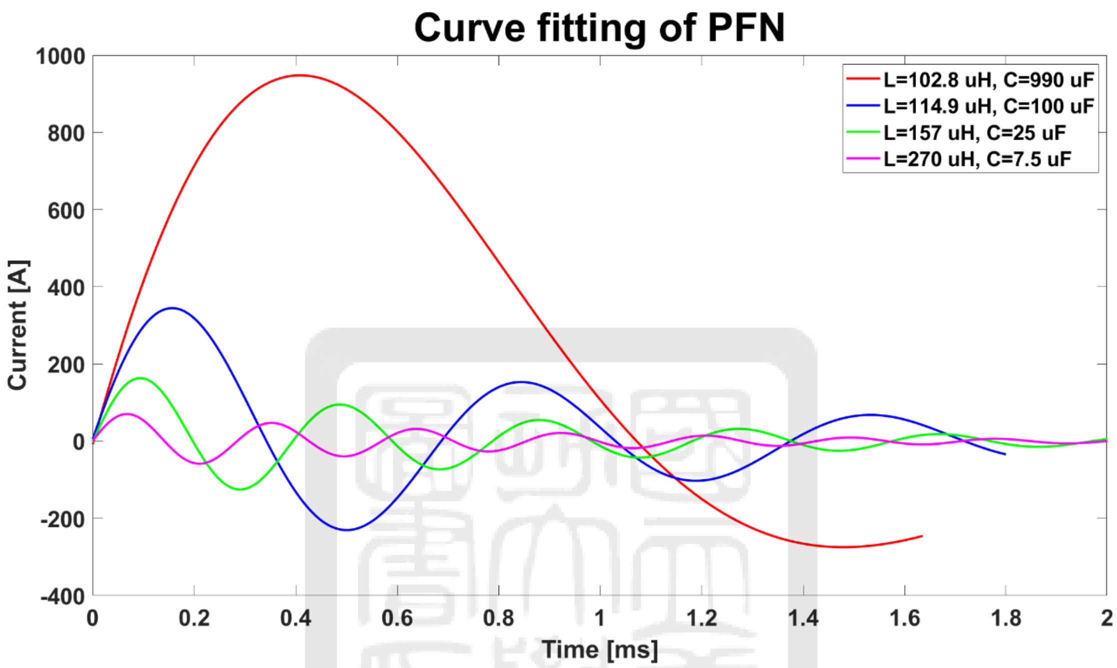

Figure 3.27: The fitted curves from each PFN stage.

Table 3.7:The measured results of each PFN stage.

	Stage 1	Stage 2	Stage 3	Stage 4
Inductance	132±4 μH	123±0.4 μH	158±1 μH	277±7 uH
Resistance	0.28±0.01 Ω	0.32±0.02 Ω	0.43±0.01 Ω	0.73±0.03 Ω

3.6 The result of PFN discharge test

Figure 3.28 is the discharge test result of the whole PFN.We repeated the experiment ten times. We only show one of the results as an example. Rest of data are shown in Appedix A 3.6 The bule line is the data of the total discharge test. The red line is the curve-fitting result to represent the average current within 1 ms. The two purple dotted line are one standard deviation away from the fitted curve obtain from the curve fitting. The function of the curve fitting to represent the average current is given in Eq (3-17), which is a supergaussion with a power of c. The parameters "a" , "b" , "c" , "d" are fitting coefficients. The fitted parameter "a" represent the averaged current. On the other hand, the FWHM can also be obtained using Eq (3-17) and the fitted parameters. Table 3.8 shows the average current and FWHM of each data. Finally, the average current is 759±83A with a width of 0.9218± 0.0004 ms.

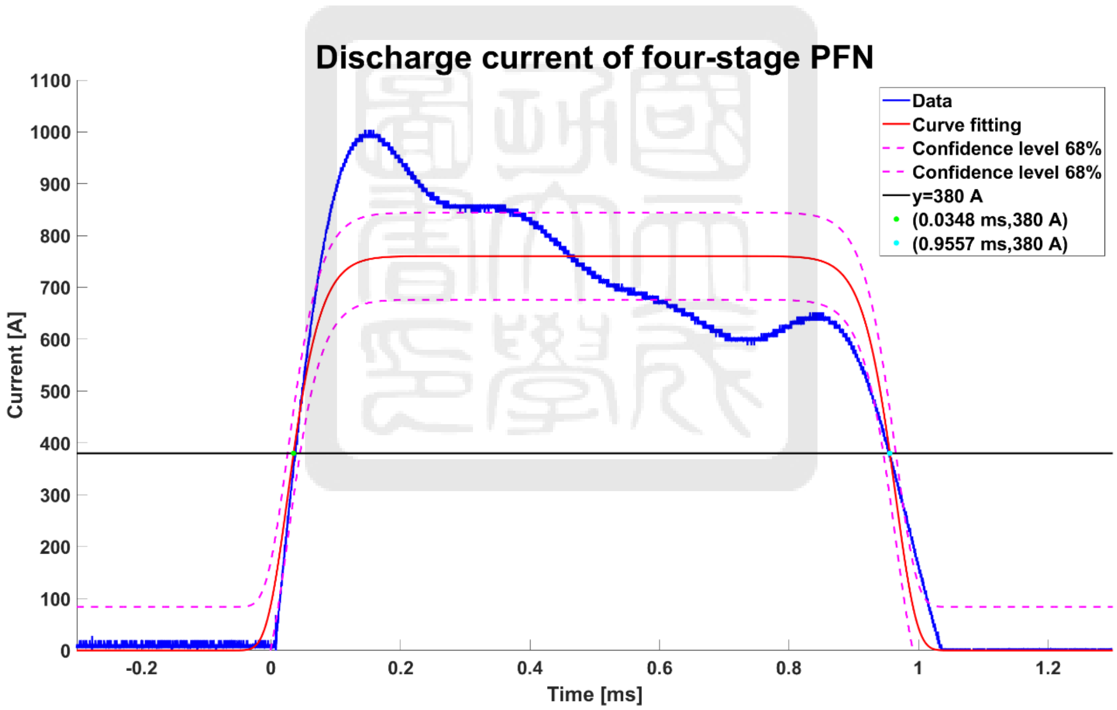

Figure 3.28: Total discharge test.

$$f(t) = a^{*}\exp\left(\frac{-|t-b|^{c}}{2d^{c}}\right). \tag{3-17}$$

Table 3.8: The average current and FWHM of each data.

	Data 1	Data 2	Data 3	Data 4	Data 5
Current	760 ± 84 A	759 ± 84 A	760 ± 84 A	759 ± 84 A	759 ± 84 A

	Data 6	Data 7	Data 8	Data 9	Data 10	Avg	Std
Current	759 ± 83 A	760 ± 83 A	759 ± 84 A	759 ± 83 A	758 ± 84 A	759A	±83A

	Data 1	Data 2	Data 3	Data 4	Data 5
FWHM (ms)	0.9209	0.9215	0.9218	0.9217	0.9221

	Data 6	Data 7	Data 8	Data 9	Data 10	Avg	Std
FWHM (ms)	0.9217	0.9219	0.9222	0.9224	0.9222	0.9218	0.0004

Figure 3.29 is the comparison of the PFN discharge test with the theoretical ones. The blue dashed line is the 1.25-kA trapezoidal current we want. The purple line is the expected discharge current of the four-stage PFN. The red line is the sum of curve fitting from each stage PFN. The bule line is the total discharge test of four-stage PFN. The green line is a SPICE simulation result using the parameters in Table 3.7. The resistance of whole system which is not included in the PFN design caused the difference between the purple line and the blue line.

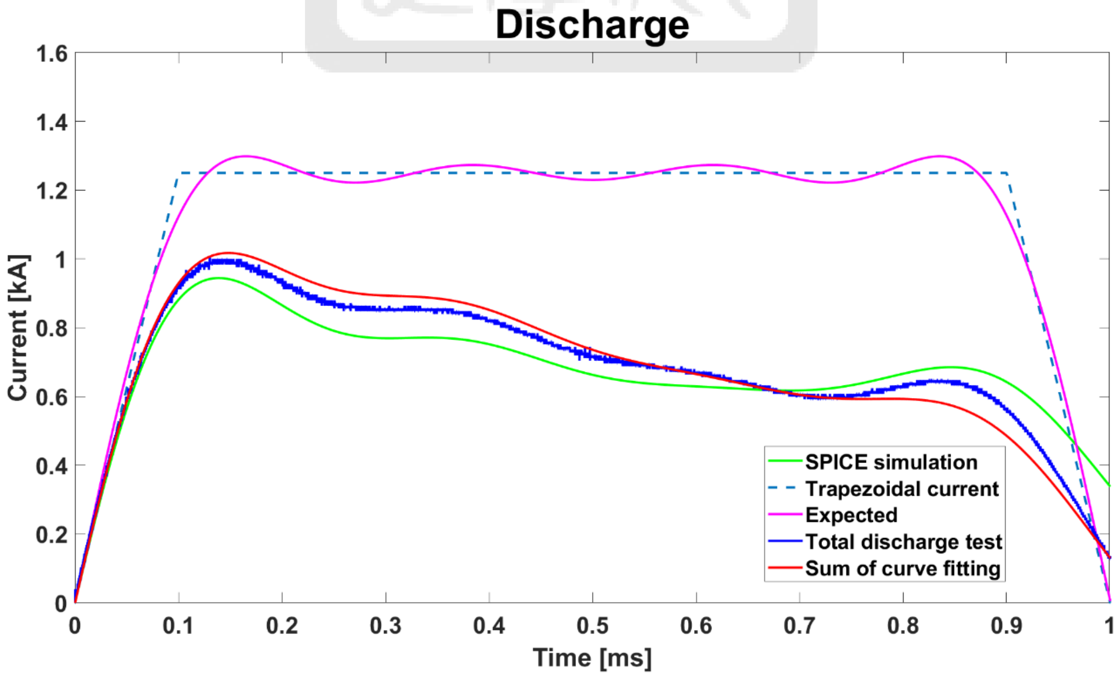

Figure 3.29: The result of PFN discharge test.

3.7 Summary

The PFN system providing the pulse current to drive the toroidal coil was built. The system includes the spark-gap switch, the trigger box, the pulse generator, and the four-stage PFN. The trigger box is used to trigger the pulse generator.The pulse generator generated a pulse with a voltage of -8.0$\pm$ 0.4 kV to trigger the spark-gap switch. We have tested each stage of the PFN individually to obtain the inductance and the resistance of each stage. Finally, the total discharge test was conducted. An average current of 759±83A with a width of 0.9218±0.0004 ms was obtained.

4. Toroidal magnetic field system

In order to confine the plasma and prevent the plasma from hitting the chamber wall, we generate the toroidal magnetic field using toroidal magnetic field coils. The structure of the toroidal magnetic field coils will be introduced in section 4.1. Supports of toroidal magnetic field coils will be introduced in section 4.2. In section 4.3, the experimental result of driving toroidal magnetic field coils using the PFN system introduced in chapter 3 will be given. Finally, summary will be provided in section 4.4.

4.1 The structure of the toroidal magnetic field coils

We built the toroidal magnetic field coils to produce the toroidal magnetic field. The pulsed current is provided by the PFN system introduced in chapter 3. The toroidal magnetic field is generated when the pulsed current is delivered to the toroidal magnetic field coils. In our design, we use four toroidal magnetic field coils. Each coil has two turns of coils as shown in Figure 4.1. In other words, eight turns of coils in total are used.

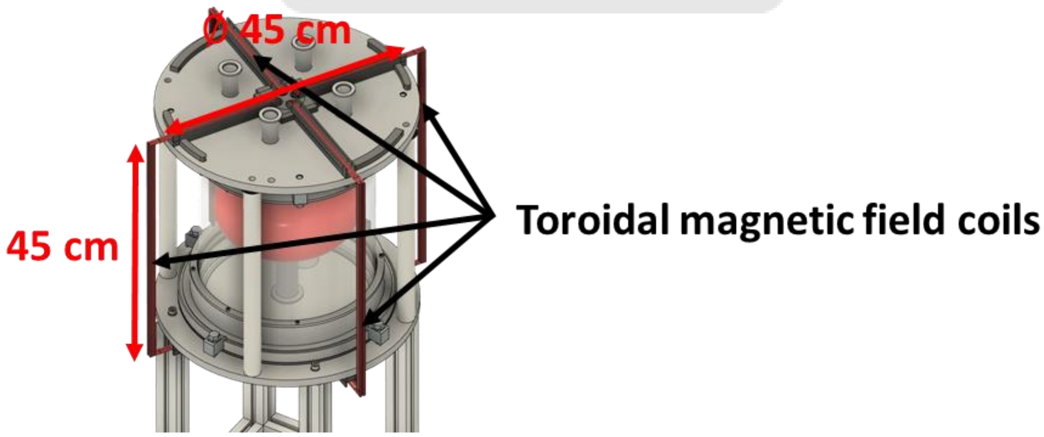

Figure 4.1: The toroidal magnetic field coils.

For each toroidal magnetic field coil, a single wire is used. We use AWG 8 wires to make the coils. Figure 4.2 shows the dimensions of each turn of the toroidal magnetic field coils. The height is 45 cm, and the width is 25 cm.

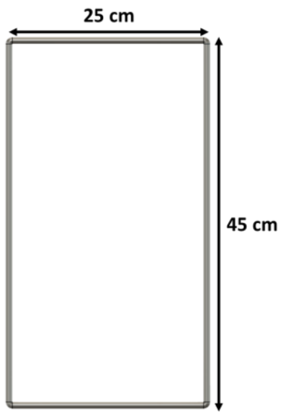

Figure 4.2: The dimensions of one turn of each toroidal magnetic field coil.

Four toroidal magnetic field coils are connected to each other using ring terminals, M8 screws, M8 gasket and M8 nuts as shown in Figure 4.3. All connections locate near the center of the bottom plate of the vacuum chamber. To prevent the arcing between the connections and the grounded vacuum chamber when discharge current goes through the wire, we use Kapton films and Kapton tapes to wrap around metal connections as shown in Figure 4.4. Finally, we can get eight turns of identical coils connected in series. Figure 4.5 is the top view of the toroidal magnetic field coils. Figure 4.6 is the bottom view of the toroidal magnetic field coils. Supports are used to guide the coils going through the center tube.

Figure 4.3: The connection of toroidal magnetic field coils.

Figure 4.4: The Kapton and Kapton Tape to wrap up the parts of metal.

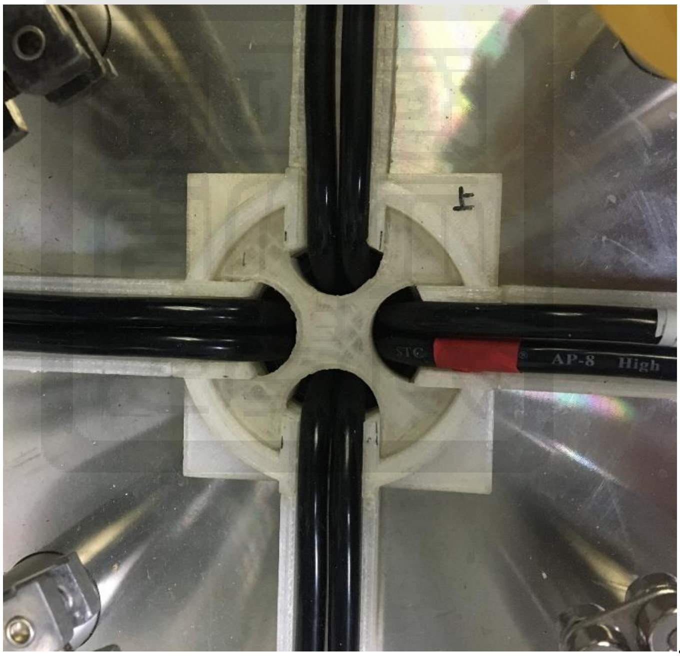

Figure 4.5: The eight turns toroidal magnetic field coils at tokamak top plate.

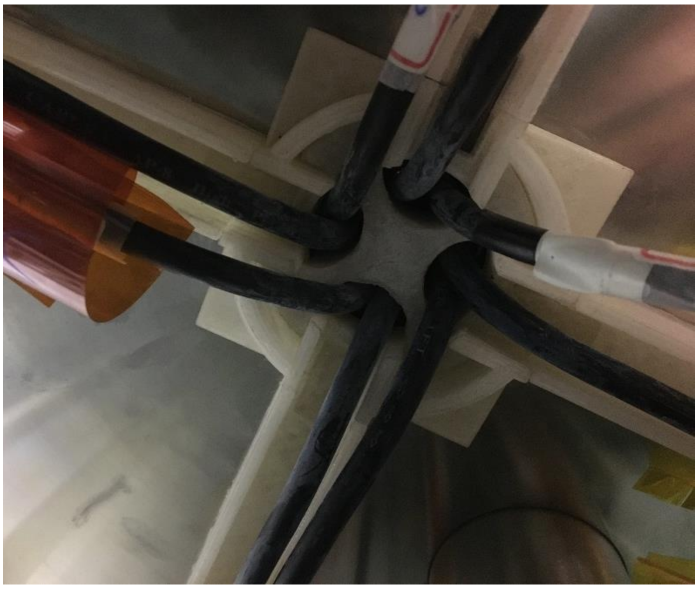

Figure 4.6: The eight turns toroidal magnetic field coils at tokamak bottom plate.

Eq (4-1) is the formula of theoretical resistance of the straight wire where R is the resistance, ρ = 1.7 x $10^{-8}\ \Omega \cdot \mathrm{m}$ is the resistivity of copper, L = 11.2 m is the total length of eight turns of toroidal magnetic field coils, and S = 8.34 x $10^{-6}\ \mathrm{m}^2$ is the cross-sectional of the AWG 8 wire. Eq (4-2) is the formula of inductance of a straight single wire, where L is the inductance, μ_0 is the permeability of vacuum, l = 11.2 m is the total length of coils, r = 1.63 mm is the radius of AWG 8 wire. The estimated resistance and inductance of the coil is given in Table 4.1. On the other hand, we measured the resistance and the inductance using a LCR meter (GWINSTEK LCR-6300). The measured result is also shown in Table 4.1. The difference between the theoretical resistance and the measured resistance is 53 %. The difference between theoretical inductance and the measured inductance is 28 %.

$$R = \rho\frac{L}{S}, \tag{4-1}$$

$$L = \frac{\mu_0 l}{2\pi}\left(\ln\frac{2l}{r} - 0.75\right). \tag{4-2}$$

Table 4.1: The parameters of eight turns toroidal magnetic field coils.

Resistance (theory)	0.022 Ω
Inductance (theory)	21.49 uH
Resistance (measured)	0.047 Ω
Inductance (measured)	29.91 uH

4.2 Supports of toroidal magnetic field coils

Supports of toroidal magnetic field coils are used to make sure coils do not move. Figure 4.7 (a) is the top view of the tokamak. Figure 4.8 (a) is the bottom view of the tokamak. Figure 4.7 (b) is the upper supports of toroidal magnetic field coils. Figure 4.8 (b) is the bottom support of toroidal magnetic field coils. The diameter of the supports is 45 cm. The supports were made by combining many pieces. The detail drawings of all pieces are given in Appendix A 4.1.

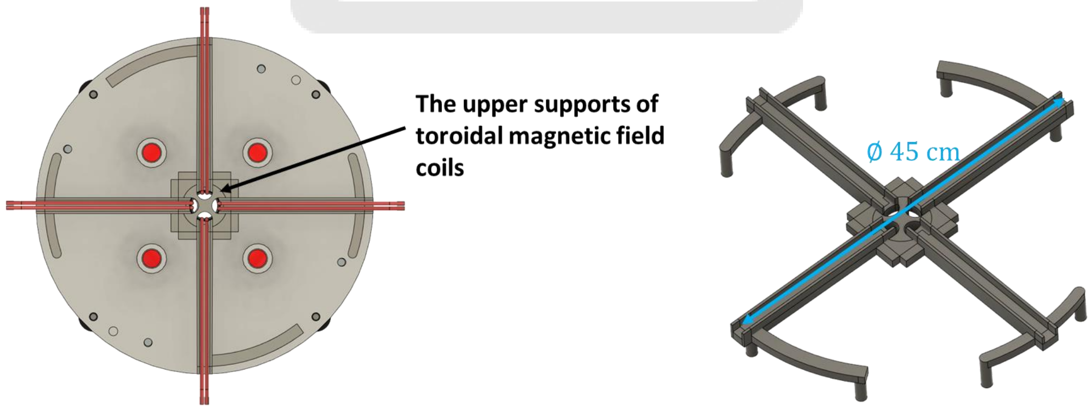

(a) (b)

Figure 4.7: (a) The top view of the tokamak. (b) The upper supports of toroidal magnetic field coils.

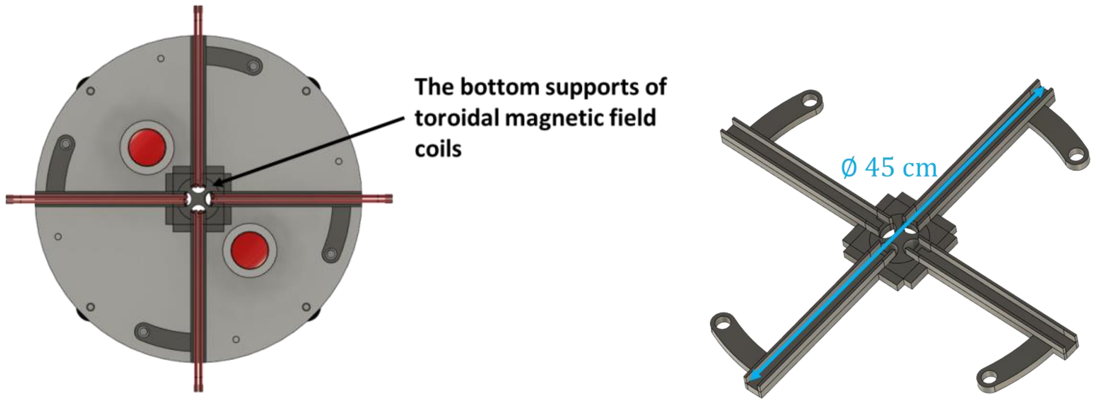

(a) (b)

Figure 4.8: (a) The bottom view of the tokamak. (b) The bottom supports of toroidal magnetic field coils.

We used the Prusa i3 3D printer to print all pieces of supports of toroidal magnetic field coils. Then, we used a fastener to connect each piece. The fasteners were also printed using the 3D printer. To make each piece, first used the software Fusion 360 to design each piece of supports. Then, we exported the STL file from Fusion 360 and import the STL file into the software Ultimaker Cura. Finally, Ultimaker Cura generated the gcode file for the Prusa i3 3D printer. Table 4.2 shows the parameters of the 3D printer. Procedure of using the 3D printer is shown in Appendix A 4.2.

Table 4.2: Parameters of the 3D printer.

Material	PLA
Layer height	0.1 mm
Wall thickness	1.2 mm
Top/ Bottom thickness	1.2 mm
Infill density	20 %
Printing temperature	200 ℃
Build plate temerature	60 ℃
Print speed	50 mm/s
Travel speed	120 mm/s

4.3 The experimental result of driving toroidal magnetic field coils using the PFN system

Figure 4.9 is one of the results of discharge current when we the toroidal magnetic field coils is driven by the PFN as the load. The blue line is the raw data of discharge current. The red line is the curve fitting for obtaining the averaged discharge current. The two purple dashed lines are region of one standard deviation of the fitted curve. We repeated the experiment ten times. The function of the curve fitting to represent the averaged current is given in Eq (4-3), which is a super gaussian with a power of c. The parameters "a", "b", "c", "d" are fitting coefficients. The fitted parameter "a" represent the averaged current. On the other hand, the FWHM can also be obtained using Eq (4-3) and the fitted parameters. Table 4.3 shows the averaged current and FWHM of each data. Finally, the averaged current is 696±56 A with a width of 0.9613± 0.0004 ms. Rest of data are given in Appendix A 4.3.

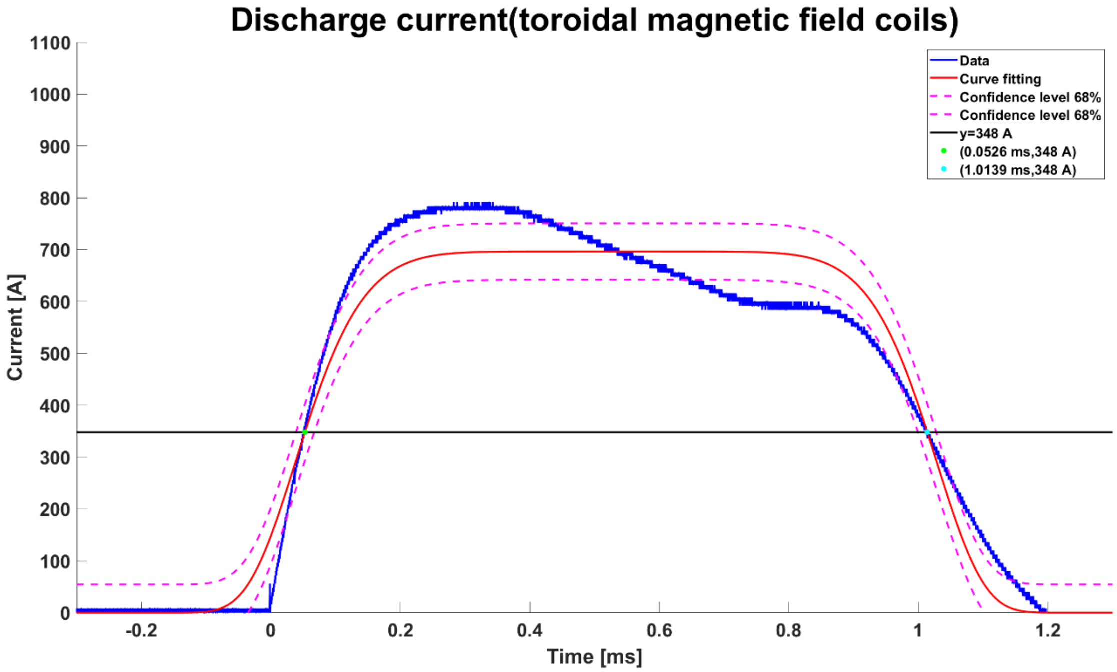

Figure 4.9: The results of discharge current add the load toroidal magnetic field coils.

$$f(t) = a^{*}\exp\left(\frac{-|t-b|^{c}}{2d^{c}}\right). \tag{4-3}$$

Table 4.3: The experiment results of discharge current with the toroidal magnetic field coils.

	Data 1	Data 2	Data 3	Data 4	Data 5
Current (A)	696 ± 54	697 ± 55	696 ± 62	699 ± 54	696 ± 67

	Data 6	Data 7	Data 8	Data 9	Data 10	Avg	Std
Current (A)	696 ± 55	696 ± 55	696 ± 55	696 ± 55	695 ± 55	696	± 56

	Data 1	Data 2	Data 3	Data 4	Data 5
FWHM (ms)	0.9613	0.9615	0.9612	0.9602	0.9617

	Data 6	Data 7	Data 8	Data 9	Data 10	Avg	Std
FWHM (ms)	0.9614	0.9614	0.9614	0.9615	0.9618	0.9613	0.0004

To compare, we have 5 lines in Figure 4.10. They are (1) the designed 1.25-kA trapezoidal current; (2) the theoretical of discharge current of four-stage PFN in purple line without a load; (3) the result of discharge current of four-stage PFN in green; (4)

the SPICE simulation result of discharge current of four-stage PFN with the toroidal magnetic field coils; (5) the measured discharge current of four-stage PFN with the toroidal magnetic field coils.

The purple line is the theoretically current of our designed four-stage PFN. Parameters in Table 3.1 in chapter 3 are used. Therefore, the purple line is closed to the designed 1.25-kA trapezoidal current. However, the green line is very different from the purple line. The amplitude of the green line is much lower than that of the purple line. Further, the green line is not symmetric with more ripples over the pulse period. There are two reason: (1) no resistance was included in the purple line. Contrarily, resistance exists in red line. Therefore, the output current becomes lower. Oscillating current from each stage also damping with time due to the resistance in wires. Therefore the current drops at the second half of the current pulse. (2) The inductance and the capacitance in green lines were determined by how inductors were mode and by the capacitor vendor. Parameters are given in Table 3.7 in chapter 3. Therefore, the frequency of the output from each stage many be slightly off from the theoretical values used in the purple line. (Table 3.2 in chapter 3). As a result, more ripples occur. To consider the effect of resistance, we can see the amplitude of green line is lower than the purple line.

The red line is SPICE simulation result of discharge current of four-stage PFN with the toroidal magnetic field coils. The value of capacitance, inductance, and resistance used in the green line in the four-stage PFN are used. The inductance and the resistance of toroidal magnetic field coils are the measured value in Table 4.1. The blue line is the experiment data of discharge current of four-stage PFN with the toroidal magnetic field coils. Additional inductance and the resistance are added to the circuit. Therefore, both the amplitude and the pulse width become lower and wider, respectively, than the green line. The averaged current of the blue line(measured discharge current) is 700±60 A with a FWHM of 0.9613± 0.0004 ms.

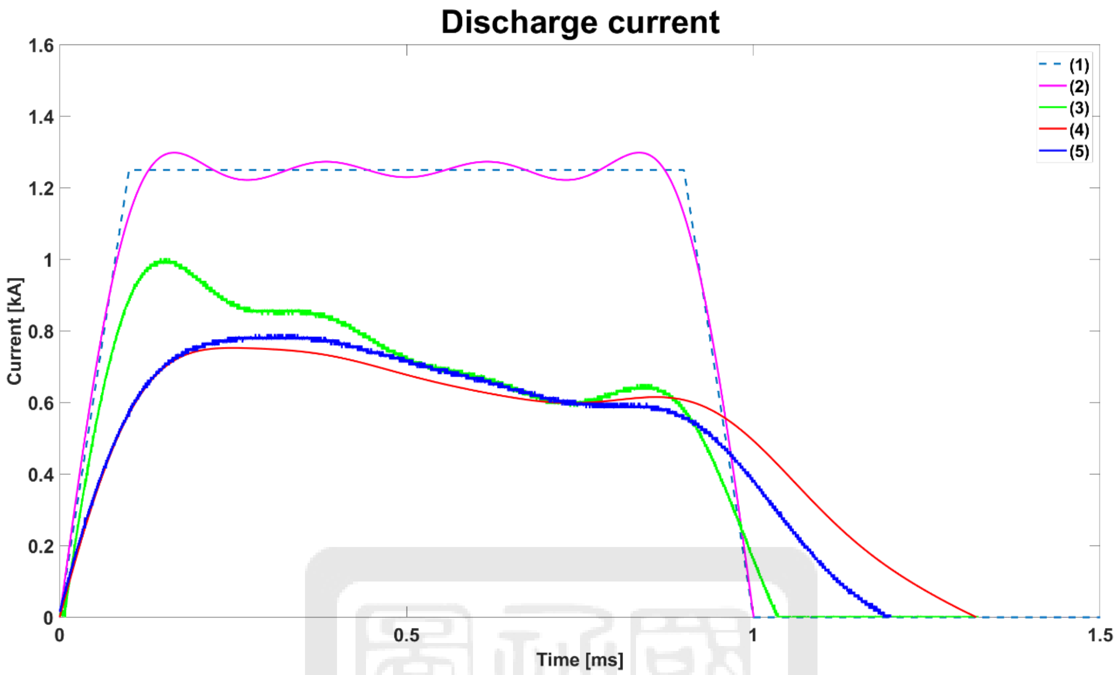

Figure 4.10: All discharge current of four-stage PFN.

To confine the plasma, we need to generate the toroidal magnetic field. At the center of the spherical tokamak, there are eight turns of coils in total. When the four-stage PFN is charged to 500 V, the averaged discharge current is ~700 A last for 1 ms in experiment. In other words, the total current at the center of the spherical tokamak is 5.6 kA. Using Eq (4-4), we estimate the toroidal magnetic field at r = 2.5 cm using the magnetic field generated by a straight wire is 448 G.

$$B = \frac{\mu_0 I}{2\pi r} . \tag{4-4}$$

In the future, we will charge the PFN to 1 kV and produce a current of ~ 1.4 kA for toroidal coil. In other words, the total current at the center of the spherical tokamak will be 11.2 kA. Thus, at r ≈ 2.5 cm, the toroidal magnetic field will be 876 G, the electron will resonate with a 2.45 GHz microwave for electron resonance heating (ECH).

4.4 Summary

The toroidal magnetic field coils were built by AWG 8 wires. Eight turns in total were used. The coils were driven by the four-stage PFN. The four-stage PFN is charged to 500 V and provides the average discharge current ~ 700 A last for ~ 1 ms to the toroidal magnetic field coils. In future, we will charge the PFN to 1 kV and generate a current of ~ 1.4 kA for toroidal coils. Therefore, the expected toroidal magnetic field is 876 G at r ≈ 2.5 cm where ECH can occur.

5. Plasma confinement

We would like to verify that the plasma is confined by the toroidal magnetic field. The single Langmuir probe is the simplest device to measure the plasma characteristic. We built a single Langmuir probe to check whether the toroidal magnetic field confined the plasma or not. In section 5.1, the theory of single Langmuir probe will be given. In section 5.2, experimental setup will be provided. In section 5.3, the experimental results will be given. In section 5.4, the summary will be given.

5.1 The theory of single Langmuir probe

The circuit of single Langmuir probe is shown in Figure 5.1. Figure 5.2 is the typical I-V curve of a single Langmuir probe. In the figure, V_B is the bias voltage of the single Langmuir probe relative to the ground. The probe current I flowing from the probe to the plasma includes the ion current I_i and the electron current I_e. When $I_i = I_e$, i.e, I = 0, it is the point of floating potential. I_{es} is the electron saturation current. I_{is} is the ion saturation current. ϕ_P is the plasma potential. The I-V curve is separated into three parts: the first part is the ion saturation region; the second part is the transition region; and the last one is electron saturation region.

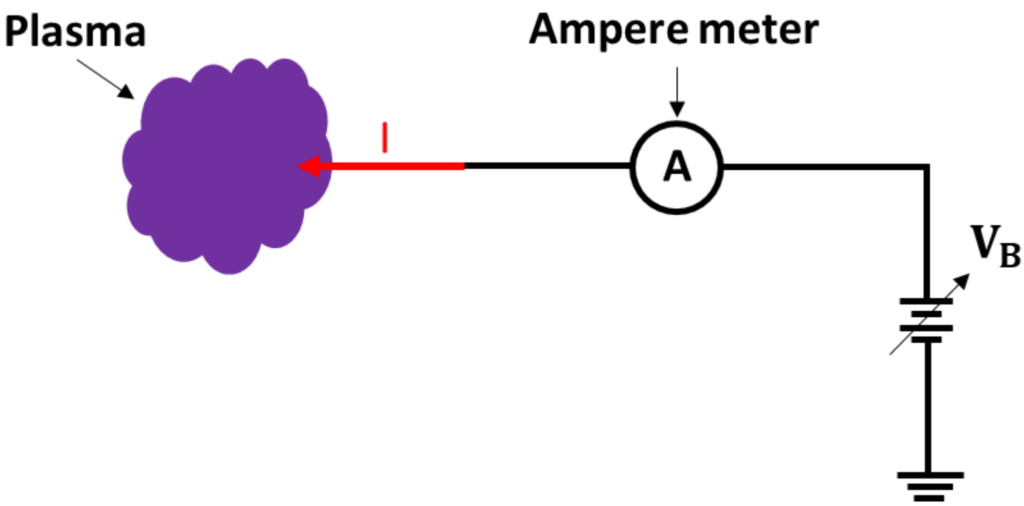

Figure 5.1: The circuit of single Langmuir probe.

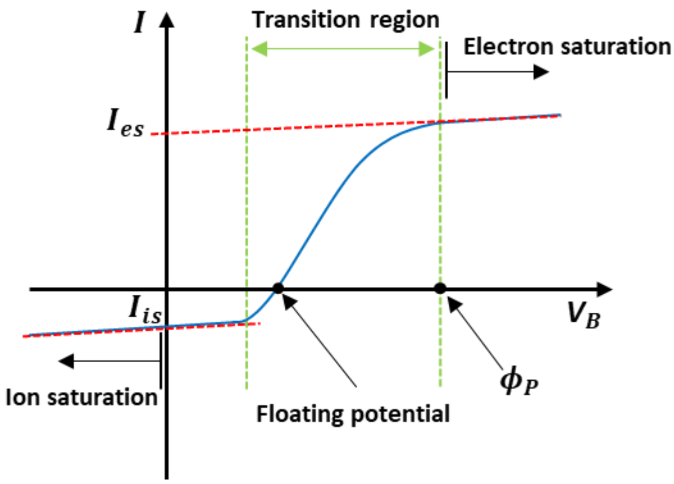

Figure 5.2: The typical single Langmuir probe I-V curve.

5.1.1 The ion saturation region

In the condition where the bias voltages $V_{\mathrm{B}} \ll \phi_{\mathrm{P}}$, all electrons are repelled. Contrarily, ions are collected by the single Langmuir probe. Therefore, the current is saturated and the ion saturation current I_{is} can be calculated by using Eq (5-1) where A_{P} is the tip surface area of the single Langmuir probe, J_{is} is the ion saturation current density, n_0 is the plasma density, e is the elementary charge, $\overline{v_{\mathrm{i}}}$ is the ion thermal speed, k is the Boltzmann constant, T_{i} is the ion temperature, and m_{i} is the mass of ion.

$$I_{\mathrm{is}} = A_{\mathrm{P}} J_{\mathrm{is}} = \frac{1}{4} n_0 \mathrm{e} A_{\mathrm{p}} \overline{v_{\mathrm{i}}}\,, \qquad \overline{v_{\mathrm{i}}} = \sqrt{\frac{8kT_{\mathrm{i}}}{\pi m_{\mathrm{i}}}}. \tag{5-1}$$

5.1.2 The electron saturation region

In the condition where the bias voltages $V_{\mathrm{B}} \geq \phi_{\mathrm{P}}$, all ions are repelled. Contrarily, electrons are collected by the single Langmuir probe. Therefore, the current is saturated and the electron saturation current I_{es} can be calculated by using Eq (5-2) where A_P is the tip surface area of the single Langmuir probe, J_{es} is the electron saturation current density, n_0 is the plasma density, e is the elementary charge, $\overline{v_e}$ is the electron thermal speed, k is the Boltzmann constant, T_e is the electron temperature, and m_e is the mass of electron.

$$I_{es} = A_p J_{es} = \frac{1}{4} n_0 e A_p \overline{v}_e \,, \quad \overline{v}_e = \sqrt{\frac{8kT_e}{\pi m_e}} \,. \tag{5-2}$$

5.1.3 The transition region

The transition region is between the ion saturation region and the electron saturation region. The bias voltage of the single Langmuir probe is $V_B < \phi_p$. Both ions and electrons are collected by the single Langmuir probe. We describe the current using Eq (5-3), Eq (5-4) and Eq (5-5). I_p is the total current from the probe to the plasma including the ion current and the electron current. I_{is} is the ion saturation current. A_p is the tip surface area of the single Langmuir probe, J_{is} is the ion saturation current density, n_0 is the plasma density, e is the elementary charge, $\overline{v_i}$ is the ion thermal speed, k is the Boltzmann constant, T_i is the ion temperature, and m_i is the mass of ion. I_e is the electron current. J_e is the electron current density, $\overline{v_e}$ is the electron thermal speed, T_e is the electron temperature, and m_e is the mass of electron. If the current of the I-V curve in the log scale, the electron temperature can be obtained by the slope in this region.

$$I_p = I_{is} + I_e \,, \tag{5-3}$$

$$I_{\mathrm{is}} = A_{\mathrm{P}} J_{\mathrm{is}} = \frac{1}{4} n_0 \mathrm{e} A_{\mathrm{p}} \bar{v}_{\mathrm{i}} , \quad \bar{v}_{\mathrm{i}} = \sqrt{\frac{8kT_{\mathrm{i}}}{\pi m_{\mathrm{i}}}} . \tag{5-4}$$

$$I_{\mathrm{e}} = A_{\mathrm{p}} J_{\mathrm{e}} = \frac{1}{4} 0.6 n_0 \mathrm{e} A_{\mathrm{p}} \exp\left(\frac{e\phi_{\mathrm{p}}}{KT_{\mathrm{e}}}\right) \bar{v}_{\mathrm{e}} , \quad \bar{v}_{\mathrm{e}} = \sqrt{\frac{8kT_{\mathrm{e}}}{\pi m_{\mathrm{e}}}} . \tag{5-5}$$

5.2 Experimental setup

Figure 5.3 is the circuit of our single Langmuir probe. In Figure 5.3, I is the probe current from the plasma flowing into the probe. Notice that it is opposite to the current defined in section 5.1. The bias voltage is definition by Eq (5-6), which includes the contribution of the battery voltage V_{battery} and IR_{scope}. The battery is used to provide the voltage of the single Langmuir probe. The 1-MΩ resistor is provided by the internal resistance of the oscilloscope. Figure 5.4 is the actual setup for providing the voltage of the single Langmuir probe. The battery in Figure 5.4 consists of six 12-V batteries (YUASA NP1.2-12) connected in series. The total voltage is 72 V. We can provide the V_{battery} from 0 V to 50 V on a single Langmuir probe by adjusting resistance of the 10 kΩ variable resistor in the voltage divider.

$$V_{\mathrm{bias}} = V_{\mathrm{battery}} + IR_{\mathrm{scope}} . \tag{5-6}$$

The structure of the single Langmuir probe is shown in Figure 5.5. The single Langmuir probe is made of a 1.5-mm wire. The single Langmuir probe is soldered to a crocodile clip. The crocodile clip is then connected to a vacuum feedthrough. The feedthrough is made of a M3 threaded rod with 15 cm in length. The rod is than mounted on a KF25 blank flange forming the feedthrough.

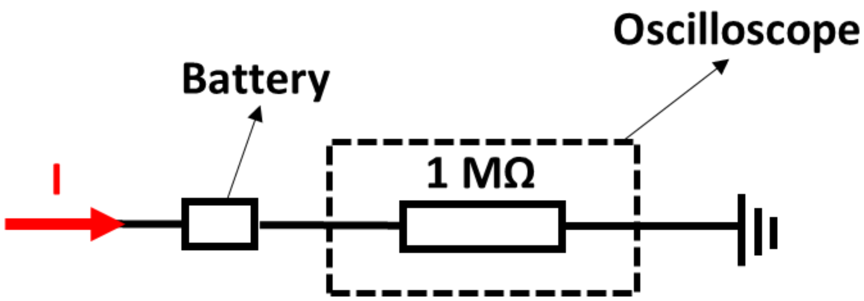

Figure 5.3: The circuit of single Langmuir probe.

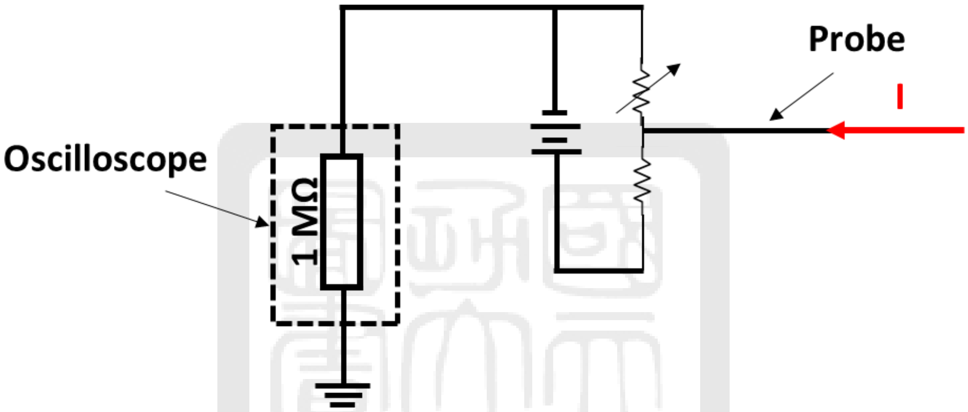

Figure 5.4: The setup of battery of single Langmuir probe.

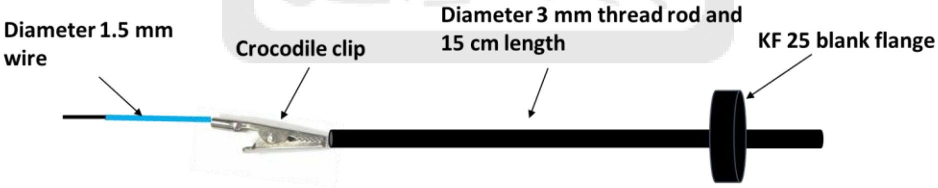

Figure 5.5: The structure of the single Langmuir probe.

In order to shield out the noise, we make the three-layer shielding around the single Langmuir probe which is shown in Figure 5.6. The most important layer is an aluminum foil which is used to shield the noise from the plasma. The aluminum foil is grounded by being connected to the KF25 blank flange by wire and aluminum tape. The inner layer Kapton is using to separate the feedthrough and the aluminum foil. The outer layer Kapton is used to separate the plasma and aluminum foil so that the plasma does not directly hit the aluminum foil. Finally, the product is shown in Figure 5.7. In figure 5.8, red circle is the single Langmuir probe in the tokamak.

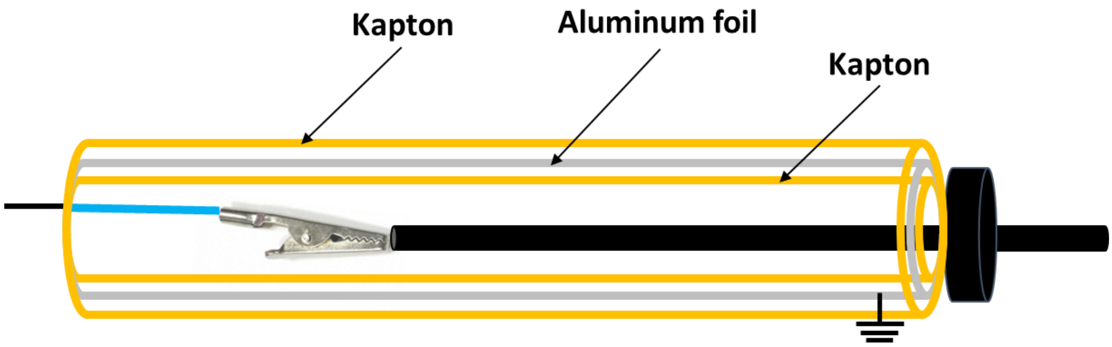

Figure 5.6: The shielding layers of a single Langmuir probe.

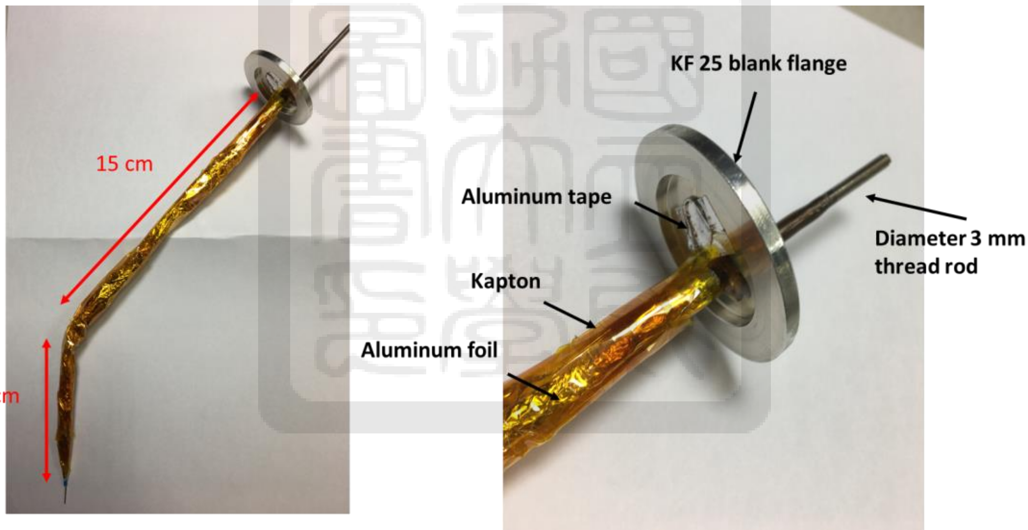

Figure 5.7: The single Langmuir probe.

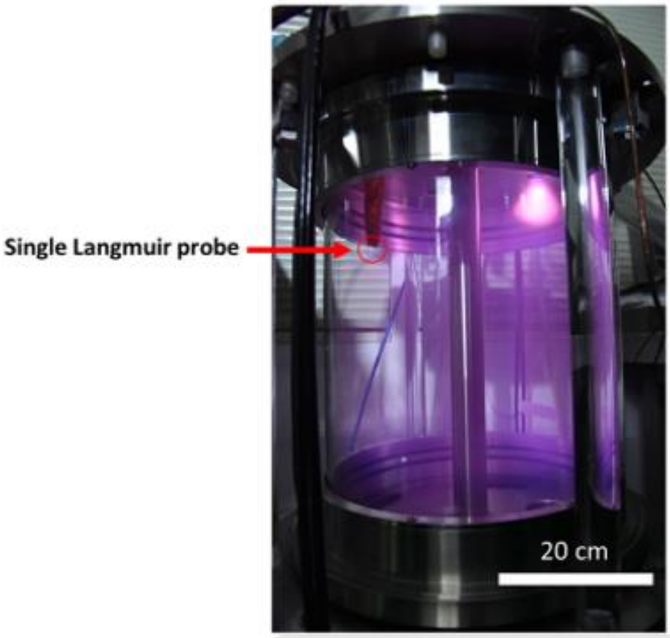

Figure 5.8: The schematic of single Langmuir probe in the tokamak.

In our goal, we would like to see whether the plasma is confined by the toroidal magnetic field or not. We measure the I-V curve around the floating potential. To adjust the bias voltage, a battery with voltage divider is used to provide the voltage in the range of 0 V~ 50 V. In general, the bias voltage is provided by a sweeping voltage. Therefore, the current flowing into the Langmuir probe with different bias voltage is obtained in a single shot. It complicates the experiments. Therefore, assuming that the plasma confinements are the same in all experiments, we can use a DC bias voltage in all experiments. Then, to obtain the I-V curve, we only need to repeat the experiments with different bias voltages. Finally, I-V curve at different time during the discharge can be obtained.

5.3 Experimental results

Here in this section, we will introduce how we analyze the raw data in section 5.3.1. In section 5.3.2, the I-V curve will be given.

5.3.1 The data analysis

In Figure 5.9 (a), it is the raw data of the discharge current of four-stage PFN. In Figure 5.9 (b), it is the raw data of current from the plasma flowing into the Langmuir probe. In this particular data, $V_{\text{battery}} = 0$ V. Nevertheless, all data with the V_{battery} from 0 V~ 50 V have the same characteristics and are provided in Appendix A 5.3 only. In section 5.3.1.1, we will introduce the process of data analysis of the discharge current of the four-stage PFN. In section 5.3.1.2, we will introduce the filter of current from the plasma.

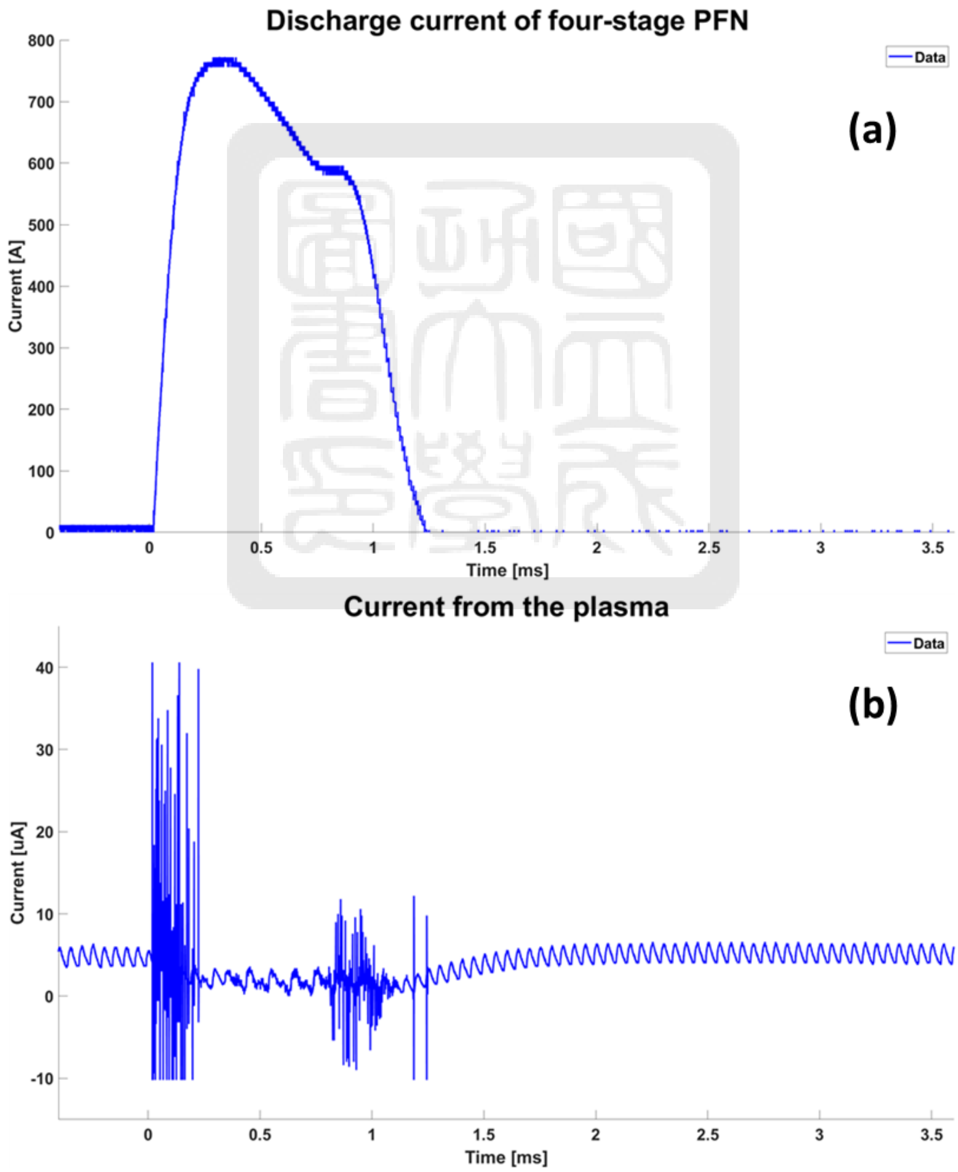

Figure 5.9: The typical raw data.

5.3.1.1 The process of data analysis of the discharge current of the four-stage PFN

Figure 5.10 is the discharge current with V_{battery} = 0 V as an example. The blue line is the raw data of the discharge current. The discharge current reaches the peak value at ~ 0.3 ms. The total discharge current pulse last for 1 ms. We would like to obtain the peak discharge current, averaged discharge current, and the FWHM of the discharge current to calculate the magnetic field. Then, we will compare the magnetic field to the current flowing into the Langmuir probe.

The red line in Figure 5.10 is the curve fitting for obtaining the peak of the discharge current of the four-stage PFN. The two purple dashed lines are region of one standard deviation of the fitted curve. The function of the curve fitting to represent the peak of the discharge current of the four-stage PFN is given in Eq (5-7). Parameter "a" , "b" , and "c" are fitting coefficients. The coefficient "a" represents the opening size and the direction of the function. The coefficient "b" represents the time that the peak of the discharge current of the four-stage PFN occurs. The coefficient "c" represents the peak of the discharge current of the four-stage PFN. The peaks of discharge currents of four-stage PFN and the times they occur in all shots are shown in Table 5.1. The averaged peak current is 766 $\pm$ 2 A, at 0.3295 $\pm$ 0.0126 ms.

$$\mathrm{f}(t) = \mathrm{a}^*(t - \mathrm{b})^2 + \mathrm{c}. \tag{5-7}$$

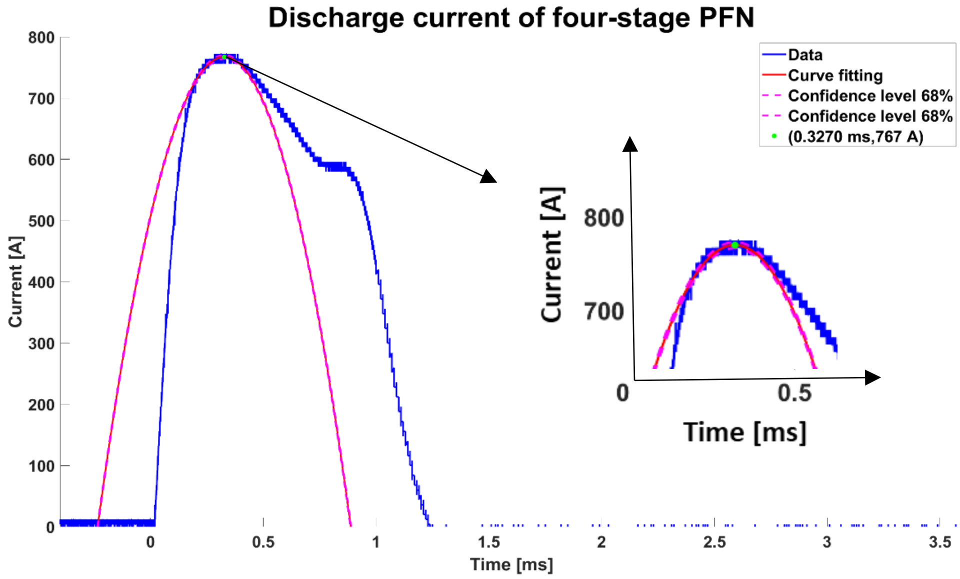

Figure 5.10: The analysis data of peak of the discharge current of four-stage PFN.

Table 5.1: The peak of the discharge current of four-stage PFN.

Battery voltage	0V	3V	6V	10V	15V	20V	25V
Peak	(0.3270 ms, 767 A)	(0.3425 ms, 769 A)	(0.3425 ms, 769 A)	(0.3380 ms, 766 A)	(0.3140 ms, 764 A)	(0.2980 ms, 762 A)	(0.3370 ms, 767 A)

Battery voltage	30V	35V	40V	45V	50V	Avg	Std
Peak	(0.3250 ms, 766 A)	(0.3240 ms, 767 A)	(0.3320 ms, 767 A)	(0.3330 ms, 768 A)	(0.3420 ms, 768 A)	(0.3295 ms, 766 A)	(±0.0126 ms, ±1.9 A)

Figure 5.11 shows the result of the averaged discharge current of the four-stage PFN using a supergaussian equation given in Eq (5-8). The V_{battery} is 0 V in this plot. Parameters "a", "b", "c", and "d" are fitting coefficients. The fitted parameter "a" represents the averaged current. On the other hand, the FWHM can also be obtained by solving the intersection between Eq (5-8) and $\mathrm{I} = \frac{\mathrm{a}}{2}$. The detail process is given in Appendix A 5.1. The values of averaged currents and the FWHMs of discharge currents of four-stage PFN in all shots are shown in Table 5.2. The averaged FWHM is 0.9667 $\pm$ 0.0002 ms. The averaged discharge current is 690 $\pm$ 40 A. The expected magnetic field at r = 2.5 cm is 880 $\pm$ 50 Gauss when the PFN is charged to 1 kV.

$$f(t) = a^{*}\exp\left(\frac{-|t-b|^{c}}{2d^{c}}\right). \tag{5-8}$$

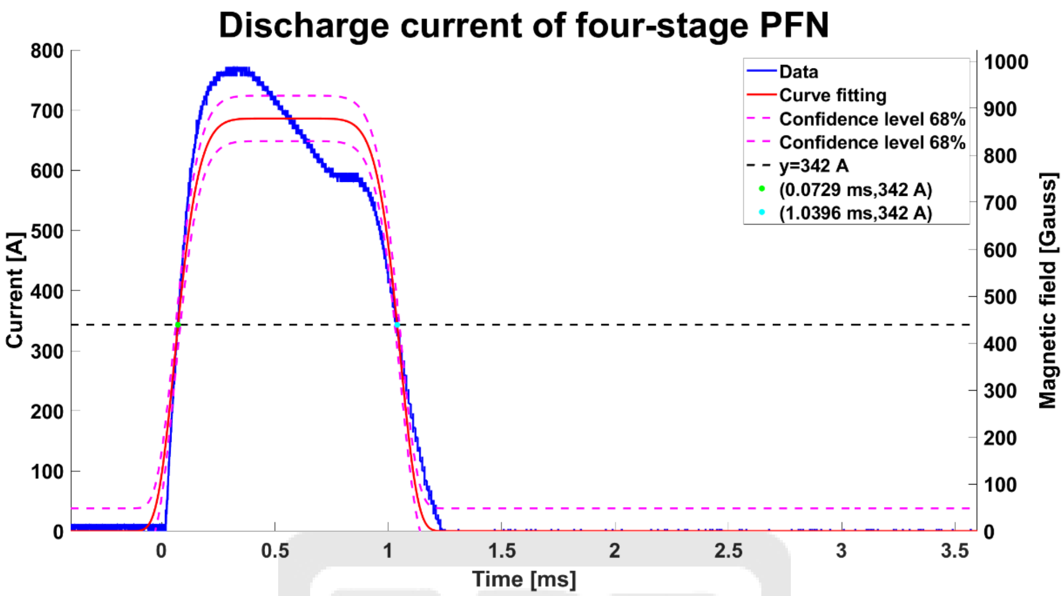

Figure 5.11: The analysis data of peak of the discharge current of four-stage PFN.

Table 5.2: The value of averaged current and FWHM of discharge current of four-stage PFN.

Battery voltage	0V	3V	6V	10V	15V	20V	25V
Current	685±38 A	687±38 A	685±39 A	685±38 A	685±39 A	685±38 A	685±39 A

Battery voltage	30V	35V	40V	45V	50V	Avg	Std
Current	685±38 A	686±38 A	685±39 A	686±39 A	686±39 A	685 A	±38 A

Battery voltage	0V	3V	6V	10V	15V	20V	25V
FWHM (ms)	0.9667	0.9655	0.9660	0.9663	0.9662	0.9661	0.9660

Battery voltage	30V	35V	40V	45V	50V	Avg	Std
FWHM (ms)	0.9663	0.9660	0.9663	0.9658	0.9661	0.9661	±0.0002

5.3.1.2 The process of the data analysis of current from the plasma flowing into the Langmuir probe

Figure 5.13 shows the current from the plasma flowing into the Langmuir probe with $V_{\mathrm{battery}} = 0$ V as an example. Huge high frequency noise occurs. Therefore, we would like to filter it out.

Figure 5.12 is the detail of the process filtering.

(1) Step 1: Load data of current from the plasma.

(2) Step 2: Use the Fourier Transform to convert the data of current from the plasma from the time domain to the frequency domain.

(3) Step 3: Use the supergaussian function as the low-pass filter to remove the high-frequency noise.

(4) Step 4: Use the inverse Fourier Transform to convert the data of current from the plasma from the frequency domain back to the time domain.

(5) Step 5: Obtain the filtered data.

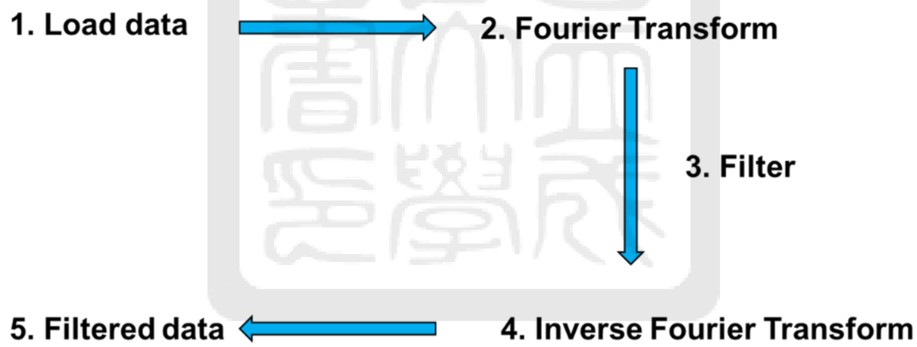

Figure 5.12: The process of filter.

Figure 5.13 to figure 5.17 is the processed data in each step. Figure 5.13 is the raw data of the current from the plasma where data is in the time domain. The noise is indicated by red squares in figure 5.13. We want to remove it. The next step is using the Fourier Transform to convert the data of current from the plasma from the time domain to the frequency domain as shown in Figure 5.14. We can see the peak noise is at -20 kHz and 20 kHz in the frequency domain. The next step is to choose the filter as shown in the red dashed line in Figure 5.15 and remove the peak noise at -20 kHz and 20 kHz.

We choose the supergaussian filter in Eq (5-9). The order is 30 and the cut-off frequency is ±15 kHz. The result of the filtered data in the frequency domain is shown in Figure 5.16. The peak noise of -20 kHz and 20 kHz are removed by the supergaussian filter. Finally, we use the inverse Fourier Transform to convert the data of the current from the plasma from the frequency domain back to the time domain. Figure 5.17 is the result of the filtered data in the time domain.

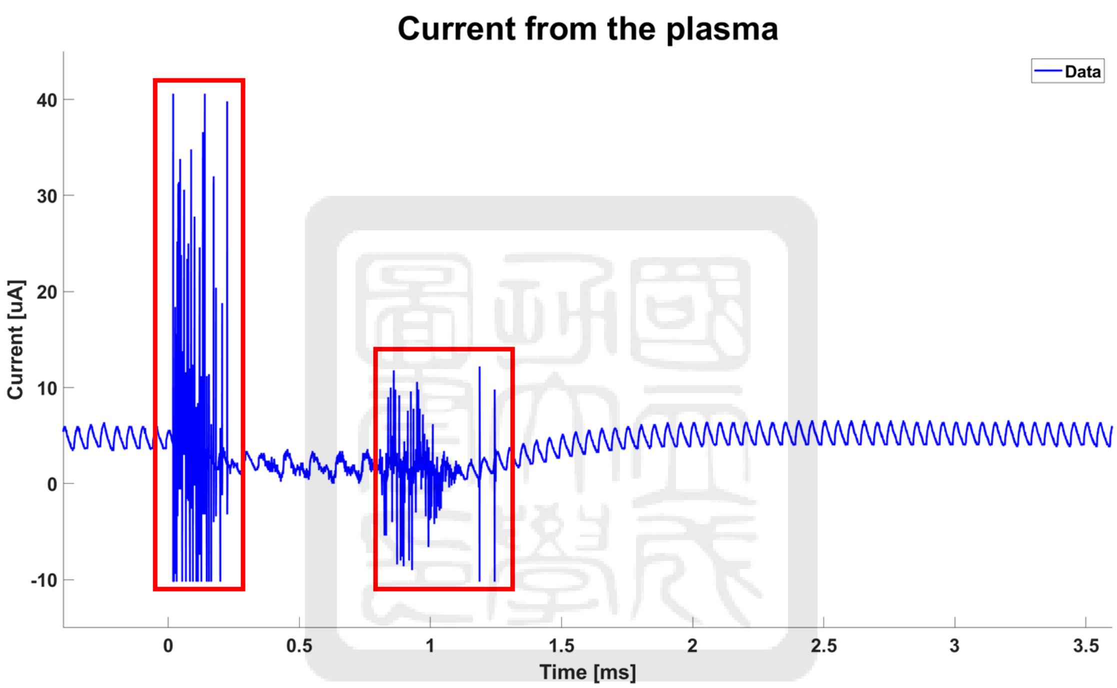

Figure 5.13: The data of current from the plasma (time domain).

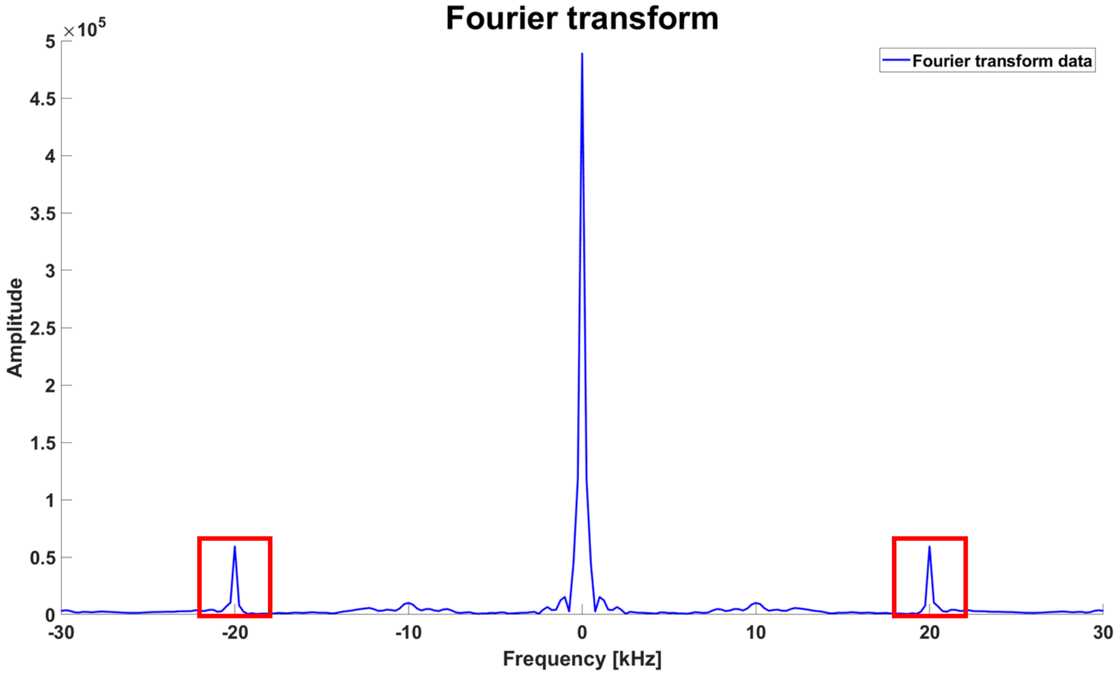

Figure 5.14: The data of current from the plasma (frequency domain).

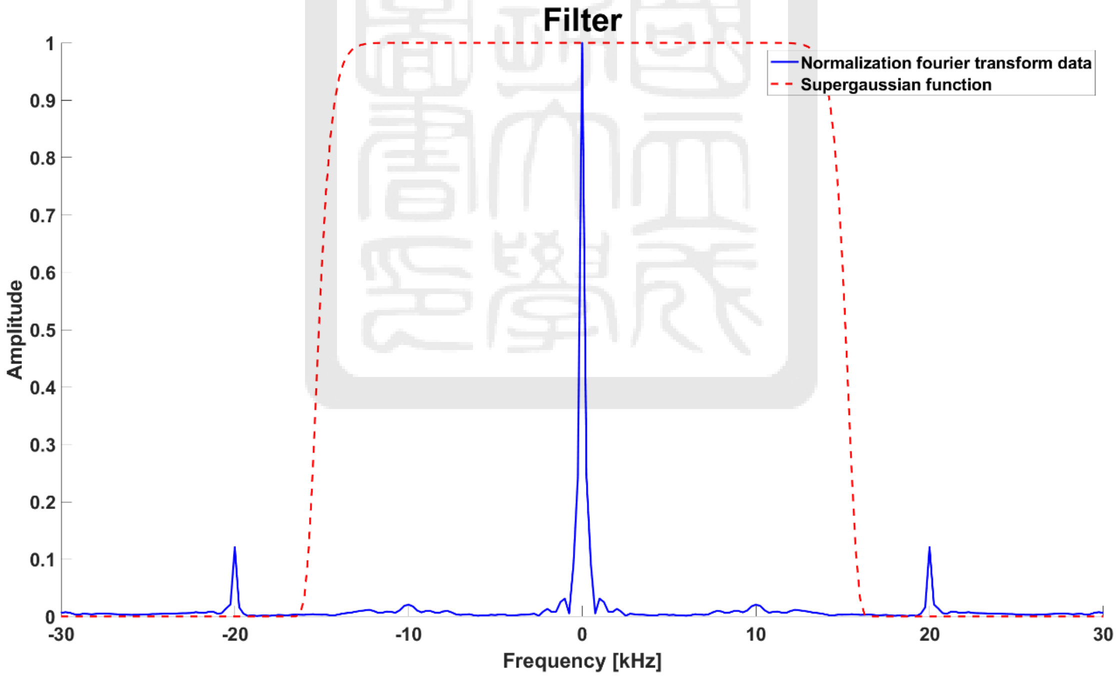

Figure 5.15: The normalization data and filter (frequency domain).

$$F(f) = \exp[-(\frac{f}{2*15000})^{30}] \ . \tag{5-9}$$

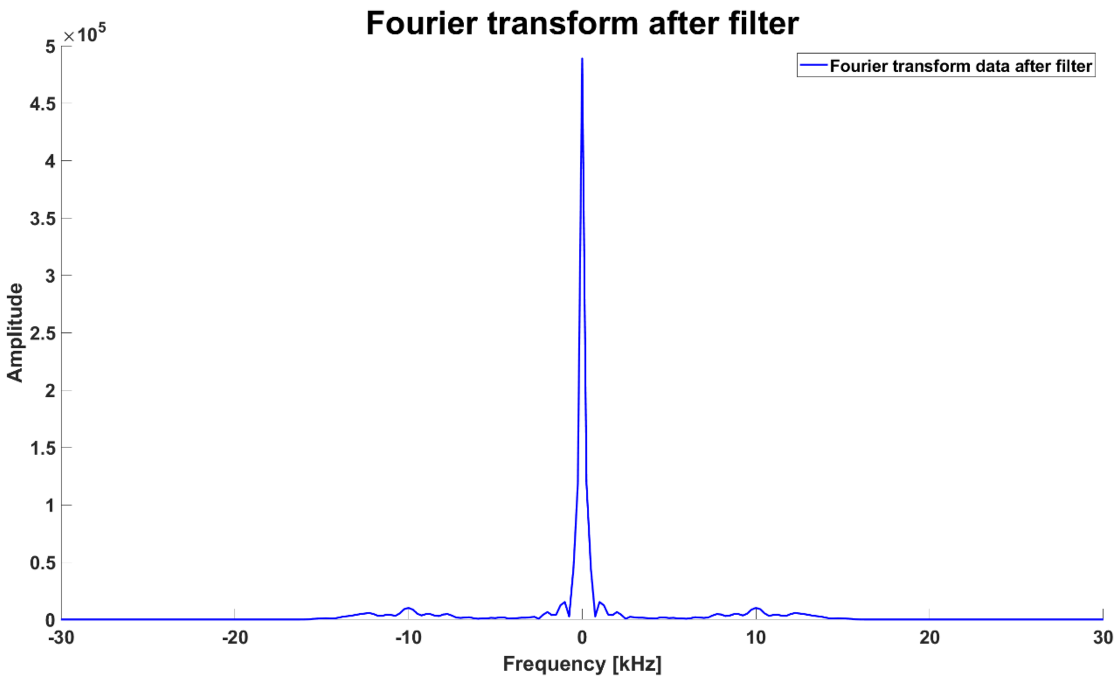

Figure 5.16: The filtered data (frequency domain).

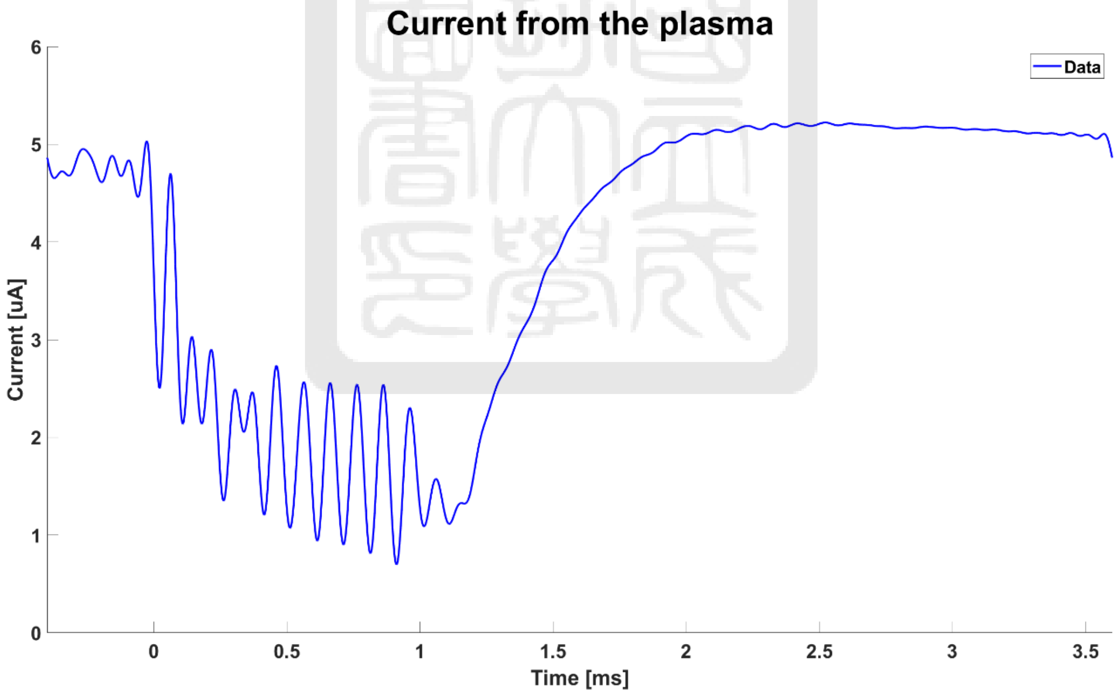

Figure 5.17: The filtered data (time domain).

In Figure 5.17, we found that the current from the plasma decreased for ~ 1 ms where a toroidal magnetic field was provided. Therefore, we need to get the averaged current from the plasma to the Langmuir probe in that period of time. Figure

5.18 is the data analysis of the current from the plasma for V_{battery} = 0 V as an example. A supergaussion function $-c * \exp[-\text{abs}[\frac{(t-d)^e}{(2*f^e)}]]$ is used to capture the current change due to the magnetic field. On the other hand, a tilted straight line $a + b * t$ is used to capture the background variation. Therefore, Eq (5-10) is used to fit to this data. Parameters "a", "b", "c", "d", "e", and "f ", are fitting coefficients. The parameter "c" represents the averaged current from the plasma. On the other hand, the FWHM can also be obtained by solving intersection points between Eq (5-10) and half of the peak current. The detail process is given in Appendix A 5.2. The averaged currents and FWHMs of currents from the plasma with different V_{battery} are shown in Table 5.3.

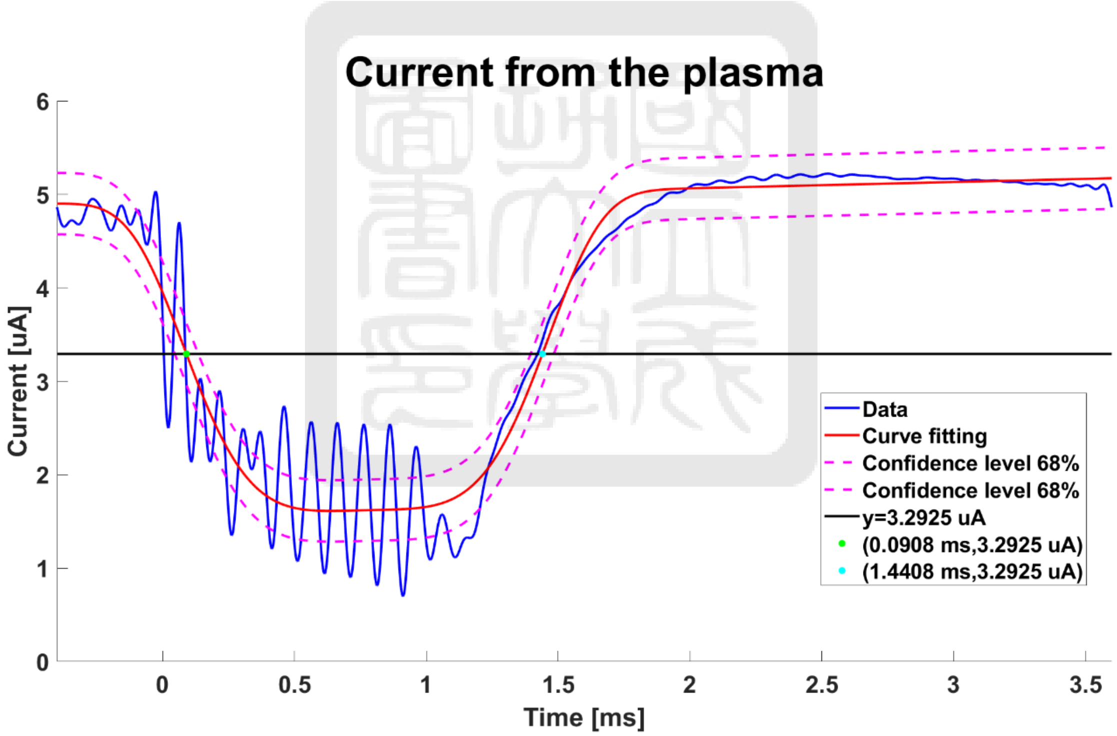

Figure 5.18: The analysis data of current from the plasma.

$$f(t) = (a+b * t)\text{-}c * \exp[\text{-abs}[\frac{(t-d)^e}{(2*f^e)}]] \,. \tag{5-10}$$

Table 5.3: The averaged current and FWHM of current from the plasma of four-stage PFN.

Battery voltage	0V	3V	6V	10V	15V	20V	25V	30V	35V	40V	45V	50V	Avg	Std
Current	3.3619 ±0.0073 uA	3.5951 ± 0.0065 uA	3.3829 ± 0.0065 uA	3.4650 ± 0.0072 uA	3.4805 ± 0.0079 uA	3.0427 ± 0.0065 uA	3.5045 ±0.0073 uA	3.5616 ±0.0065 uA	3.5959 ± 0.0104 uA	3.3034 ± 0.0086 uA	3.5246 ± 0.0067 uA	3.8283 ± 0.0091 uA	3.4705 uA	± 0.0075 uA

Battery voltage	0V	3V	6V	10V	15V	20V	25V	30V	35V	40V	45V	50V	Avg	Std
FWHM (ms)	1.3500	1.3059	1.3277	1.2982	1.3102	1.3632	1.3098	1.3417	1.3828	1.4062	1.2949	1.3129	1.3336	0.0341

5.3.2 The I-V curve of the Langmuir probe

From section 5.3.1, we have obtained information of the toroidal magnetic field and the current from the plasma to the Langmuir probe with different bias voltage. Therefore, we can get the I-V curve of the Langmuir probe at different magnetic field. Shown in Figure 5.19 is direct comparison of the toroidal magnetic field and the current from the plasma for V_{battery} = 0 V as an example. Data for different V_{battery} is given in Appendix A 5.3. When discharge current of the four-stage PFN is provided, the toroidal magnetic field is generated. Then, we can see the current from the plasma is reduced. It means more electrons hit the single Langumir probe causing the current to reduce. In other words, electrons are confined when magnetic field is generated.

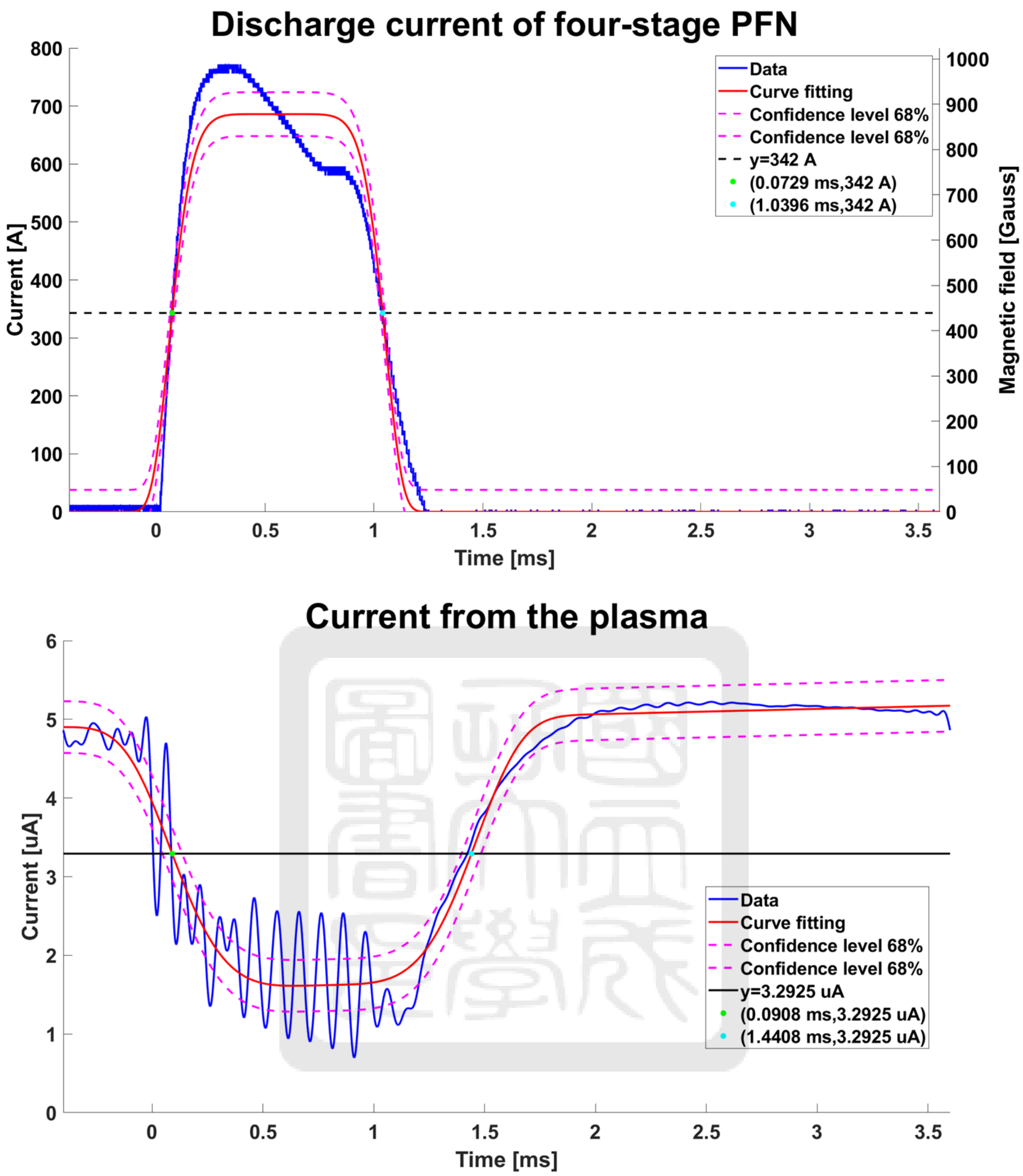

Figure 5.19: The plasma confine by a toroidal magnetic field.

Finally, we try to get the I-V curve of the single Langmuir probe at t= -0.3 ms and 0.7 ms. Notice that $V_{\text{bias}} = V_{\text{battery}} + IR_{\text{scope}}$. Eq (5-6) is used to calculate V_{bias}. At t = -0.3 ms, no magnetic field is generated. It's the background condition. At t=0.7 ms, it's the condition with the toroidal magnetic field.

Firstly, we look at the data without the toroidal magnetic field. Figure 5.20 is the the current from the plasma at -0.3 ms, with a V_{battery} of 0 V~50 V. At this point, the toroidal magnetic field has not been generated so that the plasma is not. The current from the plasma is 4.25 μA~ 4.89 μA.

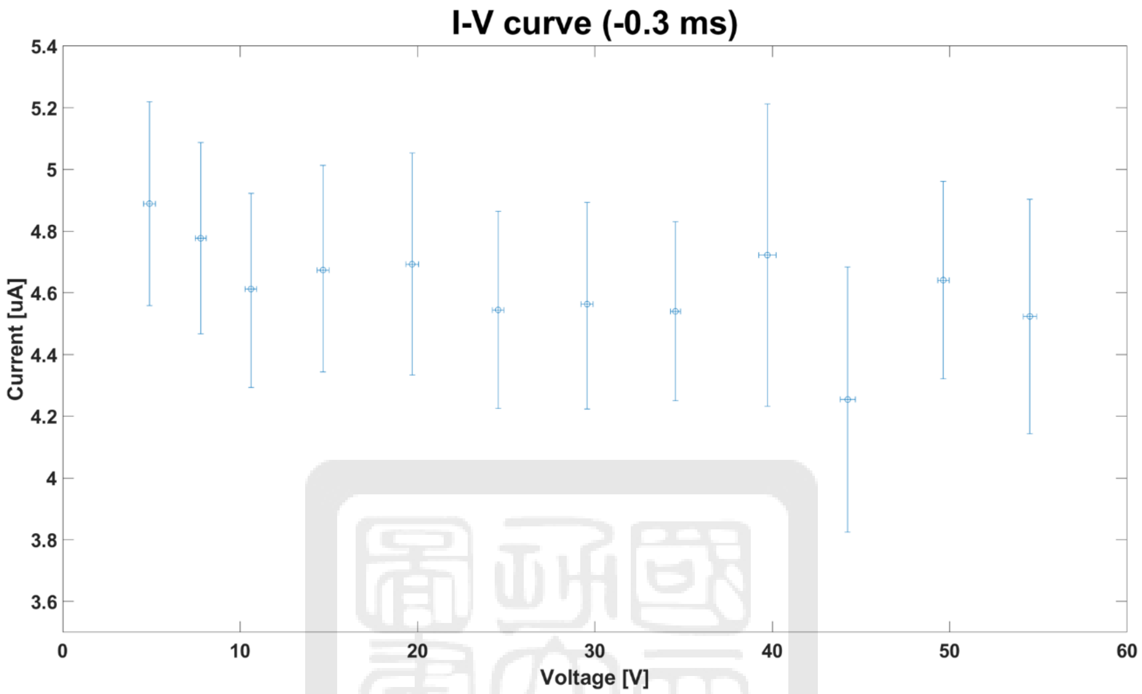

Figure 5.20: I-V curve at -0.3 ms.

Secondly, we look at the data with the toroidal magnetic field. Figure 5.21 is the current from the plasma at 0.7 ms, with V_{battery} of 0 V~50 V. With the toroidal magnetic field, electron density increases so that more electrons hit the single Langmuir probe. As a result, the current from the plasma is 0.93 μA~ 1.61 μA. They are lower than those in Figure 5.20. Therefore, we verify the electrons are confined by the magnetic field.

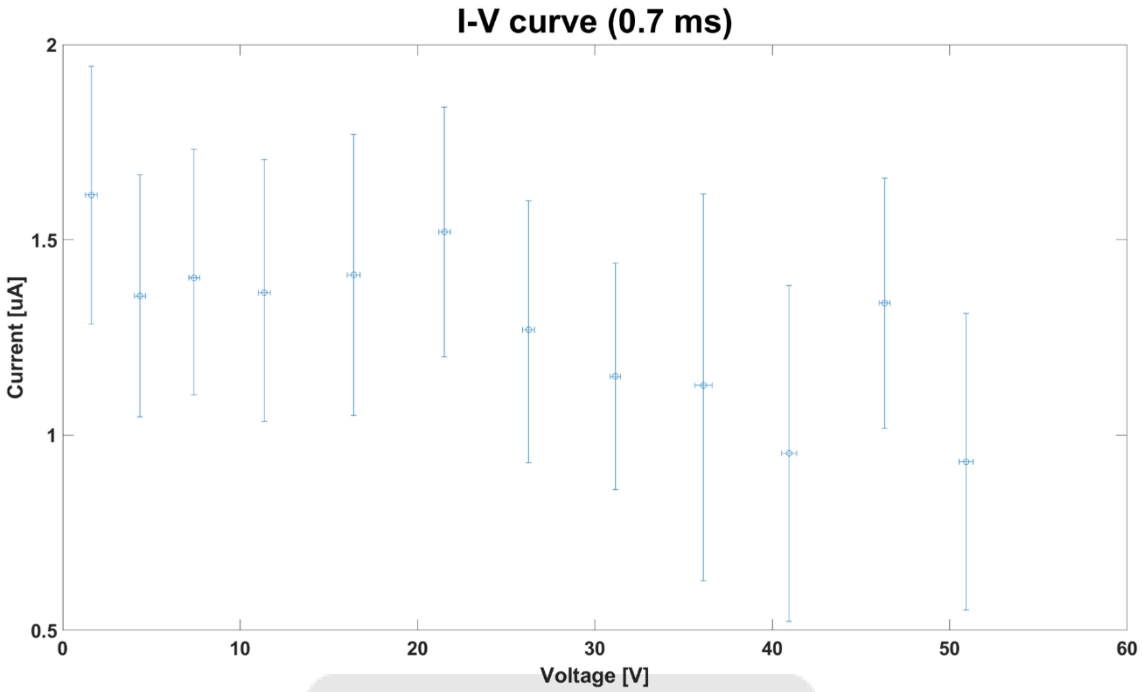

Figure 5.21: I-V curve at 0.7 ms.

5.4 Summary

When the discharged current of the four-stage PFN was provided, toroidal magnetic field was generated. At this time, the current from the plasma was reduced from 4.25 μA~ 4.89 μA to 0.93 μA~ 1.61 μA. It indicated that plasma was confined and more electrons hit the single Langmuir probe.

6. Future works

We have built some subsystems of the tokamak. They include the vacuum system, the plasma generator, the Pulse-forming-network system, the toroidal magnetic field system. To complete the mini-Tokamak, we need to finish other subsystems given in the following list in the future.

1. Increasing the charged voltage the Pulse-forming network

Although the Pulse-forming network was built, the charging voltage was only 500 V. It was only a half of the designed value. In the future, we will build a 1-kV power supply to charge the Pulse-forming network. Therefore, the expected toroidal field will be 876 G at r ≈ 2.5 cm.

2. Vertical field coils

We only have toroidal magnetic field to confine plasma in the toroidal direction. However, we have no control of the plasma shape in the poloidal direction yet. Therefore, a set of vertical field coils will be built to control the plasma shape.

3. The plasma heating system

In the future, we will build the microwave system. The microwave is used to heat the plasma. The principle using is electron-cyclotron-resonance heating (ECH). The cyclotron frequency of electrons gyro around the magnetic field is 2.45 Ghz when the

$$f = \frac{w}{2\pi} = \frac{qB}{2\pi m_e} \; . \qquad (6\text{-}1)$$

magnetic field is 876 G, the cyclotron frequency equals to the microwave frequency 2.45 GHz. Under this condition, the electron is resonance with the microwave and get the energy from microwave efficiently. In our design, when the PFN is charged to 1 kV, the ECH will happen at r ≈ 2.5 cm where r is the distance from the center of the tokamak.

4. Central solenoid

In the future, we will build the central solenoid. The central solenoid is used to induce the plasma current. And the plasma current to generate the poloidal magnetic field. Finally, the poloidal magnetic field is used to confine the plasma.

5. Plasma diagnostics

We have built a single Langmuir probe and verify that the plasma is confined. We will build a double Langmuir probe or a triple Langmuir probe to measure the plasma density and temperature. Therefore, we can verify the confinement quantitatively.

7. Summary

The goal this thesis is to build the toroidal field coil of a mini Tokamak and verify the plasma is confined by the toroidal coil.

We first built the cylindrical vacuum chamber. The diameter of the chamber was 30 cm and the height was 45 cm. At the center of the chamber, a KF 40 tube was installed. It was used for toroidal field coils. The chamber was filled with Ar and pumped down to 10^{-1} Torr. Then, the plasma was generated using an AC discharge. The voltage was ~1 kV and the frequency were 20 kHz. The AC voltage was delivered into the chamber through an electrode inserted into the chamber. Afterward, a set of toroidal coils made by AWG 8 wires was built. Eight turns in total went through the KF 40 tube at the center of the chamber. Two turns were bundled together so that there were four sets of toroidal field coils. To drive the toroidal field coils, a pulsed-forming network (PFN) was built. The total capacitance of the PFN was 645 uF. The PFN was charged to 500 V storing an energy of 80 J. PFN system included the spark-gap switch, the trigger box, the pulse generator, and the four-stage PFN. The trigger box was used to trigger the pulse generator. Then, the pulse generator generated the pulse voltage with a peak voltage of -8.0±0.4 kV triggering the spark-gap switch. Finally, the spark-gap switch was activated, and the current was generated by the four-stage PFN. The average current delivered by the PFN system was 760±80 kA with a width of 0.9218± 0.0004 ms. The generated magnetic field was 448±5 Gauss at r = 2.5 cm. In the future, the PFN will be charged to 1 kV, an expected magnetic field of 876 G at r ≈ 2.5 cm can be generated. Therefore, ECH can be used to heat the plasma efficiently. Finally, we used a single Langmuir probe to measure the current flowing from the plasma to the probe. The Langmuir probe was made of a wire with a diameter of 1.5 mm and a length of 10 mm. We found that the current from the plasma was 4.25 uA ~ 4.89 uA when there was no toroidal magnetic field. When the toroidal magnetic field was provided, the current dropped to 0.93 uA ~ 1.6 uA. It indicated that electrons were confined so that electron density increase. With more electrons hitting the Langmuir probe, the current flowing into the probe decreased. However, we only qualitatively verified that electrons were confined. In the future, we will build a triple Langmuir probe to measure the plasma density with temporal resolution. Therefore, we can verify the confinement quantitively. In addition, we will build the Increasing the charged voltage the Pulse-forming network, Vertical field coils, The plasma heating system, Central solenoid, Plasma diagnostics so that we will have a mini Tokamak with all subsystems.

References

[1] https://en.wikipedia.org/wiki/Sun.

[2] https://commons.wikimedia.org/wiki/File:D-t-fusion.png.

[3] https://zh.wikipedia.org/wiki/%E6%A0%B8%E8%81%9A%E5%8F%98.

[4] Fusion: An Introduction to the Physics and Technology of Magnetic Confinement Fusion - Second, Weston M. Stacey.

[5] Integrated Tokamak modeling: When physics informs engineering and research planning. Physics of Plasmas 25, 055602 (2018); https://doi.org/10.1063/1.5021489.

[6] https://en.wikipedia.org/wiki/Inertial_confinement_fusion.

[7] https://www.tokamakenergy.co.uk/technology/st40/

[8] Mei-Ferg Huang. Rust Remover Using Small Pulsed-Power System. 2017.

[9] Po-Yu Chang , Chih-Jui Hsieh , Mei-Feng Huang ,Ming-Cheng Jheng ,Yen-Cheng Lin,Jia-Kai Liu,and Sheng-Hua Yang. Rail-gap switch with a multistep high-voltage triggering system. 2020.

Appendix

A 2.1 The component of spherical tokamak

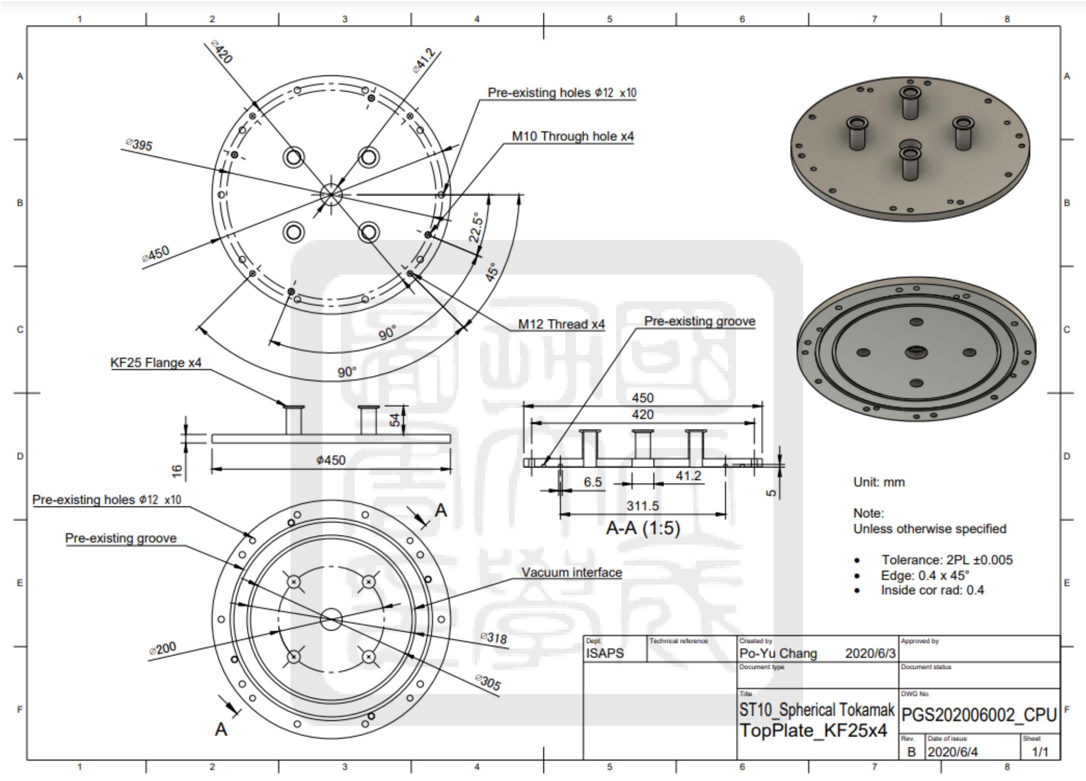

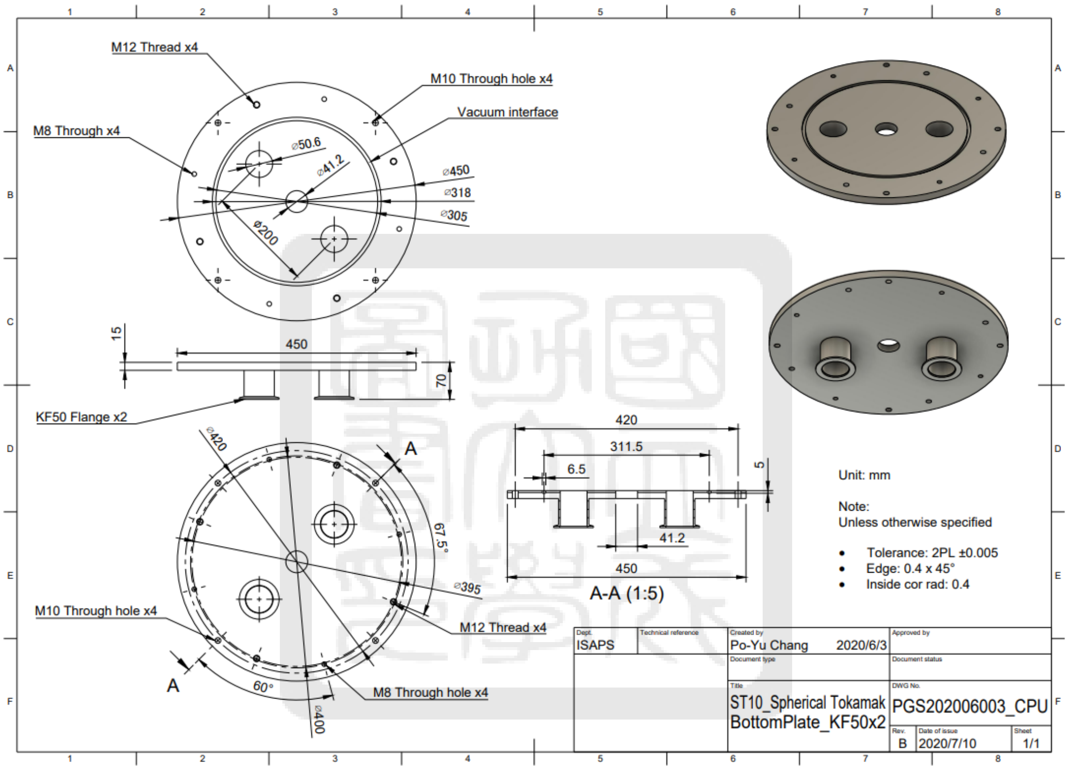
M12 Thread x4
M10 Through hole x4
Vacuum interface
M8 Through x4
⌀50.6
⌀41.2
⌀450
⌀318
⌀305
⌀200
15
450
70
KF50 Flange x2
⌀420
A
67.5°
⌀395
M10 Through hole x4
M12 Thread x4
A
60°
⌀400
M8 Through hole x4
420
311.5
6.5
5
41.2
450
A-A (1:5)
Unit: mm
Note:
Unless otherwise specified
Tolerance: 2PL ±0.005
Edge: 0.4 x 45°
Inside cor rad: 0.4
Dept.
ISAPS
Technical reference
Created by
Po-Yu Chang
2020/6/3
Approved by
Document type
Document status
Title
ST10_Spherical Tokamak BottomPlate_KF50x2
DWG No.
PGS202006003_CPU
Rev.
B
Date of issue
2020/7/10
Sheet
1/1

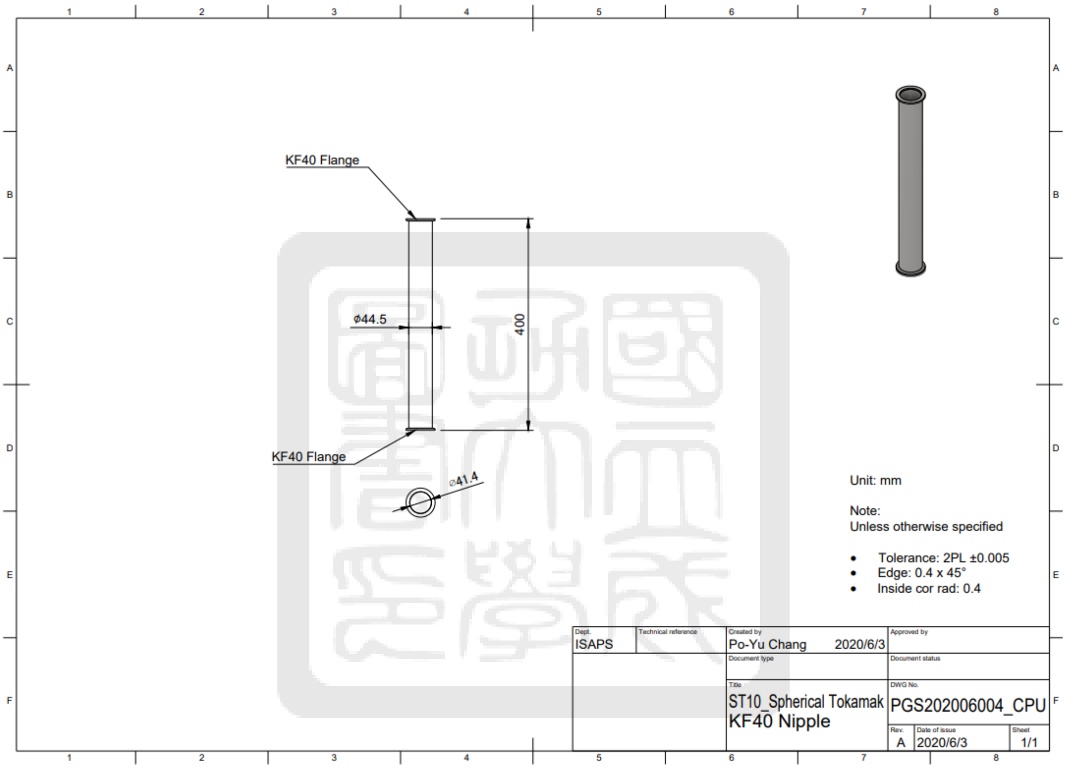
KF40 Flange
ø44.5
400
KF40 Flange
ø41.4
Unit: mm
Note:
Unless otherwise specified
• Tolerance: 2PL ±0.005
• Edge: 0.4 x 45°
• Inside cor rad: 0.4
Dept.
ISAPS
Technical reference
Created by
Po-Yu Chang 2020/6/3
Approved by
Document type
Document status
Title
ST10_Spherical Tokamak
KF40 Nipple
DWG No.
PGS202006004_CPU
Rev.
A
Date of issue
2020/6/3
Sheet
1/1

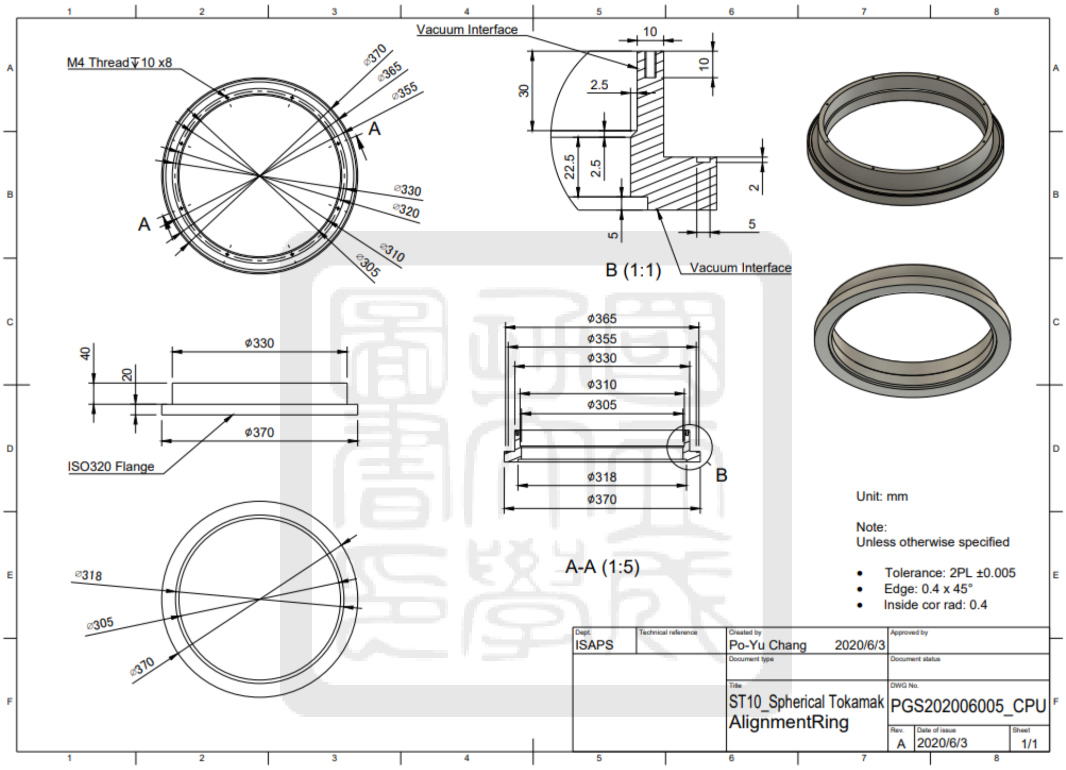
M4 Thread ↧10 x8
⌀370
⌀365
⌀355
⌀330
⌀320
⌀310
⌀305
A
Vacuum Interface
10
30
2.5
22.5
2.5
5
2
5
B (1:1)
⌀330
40
20
⌀370
ISO320 Flange
⌀365
⌀355
⌀330
⌀310
⌀305
⌀318
⌀370
B
A-A (1:5)
⌀318
⌀305
⌀370
Unit: mm
Note:
Unless otherwise specified
Tolerance: 2PL ±0.005
Edge: 0.4 x 45°
Inside cor rad: 0.4
Dept.
ISAPS
Technical reference
Created by
Po-Yu Chang 2020/6/3
Approved by
Document type
Document status
Title
ST10_Spherical Tokamak
AlignmentRing
DWG No.
PGS202006005_CPU
Rev.
A
Date of issue
2020/6/3
Sheet
1/1

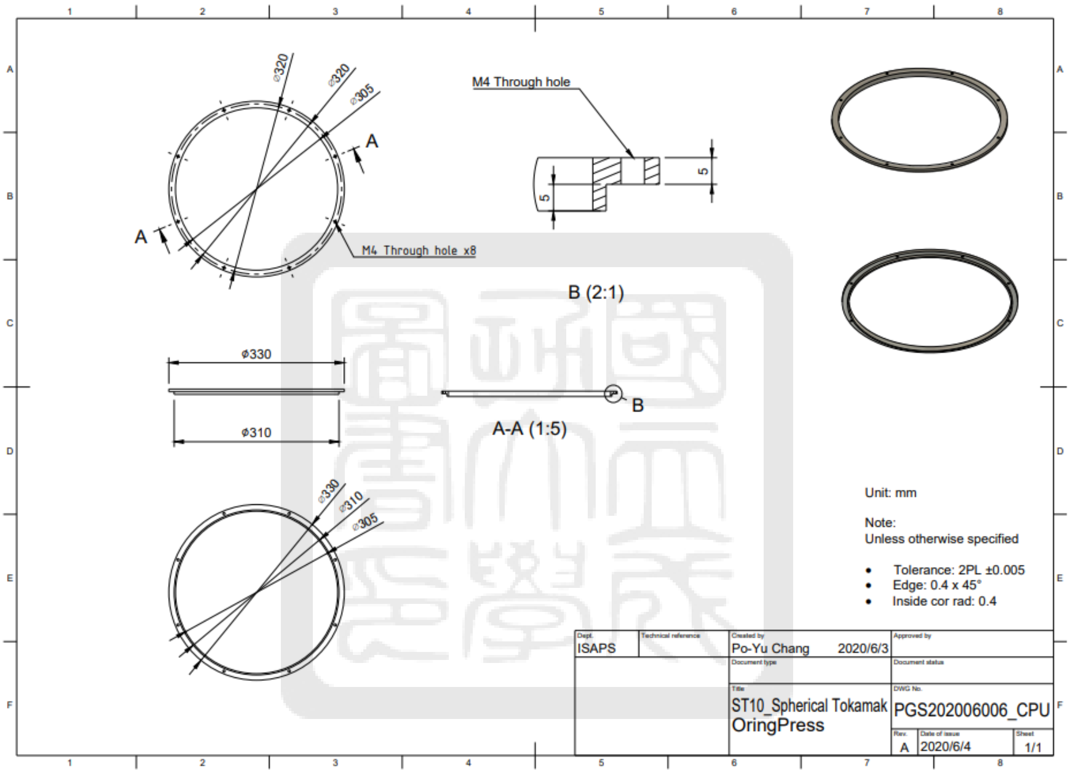
M4 Through hole
M4 Through hole x8
B (2:1)
A-A (1:5)
ϕ330
ϕ310
ϕ320
ϕ305
Unit: mm
Note:
Unless otherwise specified
Tolerance: 2PL ±0.005
Edge: 0.4 x 45°
Inside cor rad: 0.4
ISAPS
Po-Yu Chang 2020/6/3
ST10_Spherical Tokamak OringPress
PGS202006006_CPU
A 2020/6/4 1/1

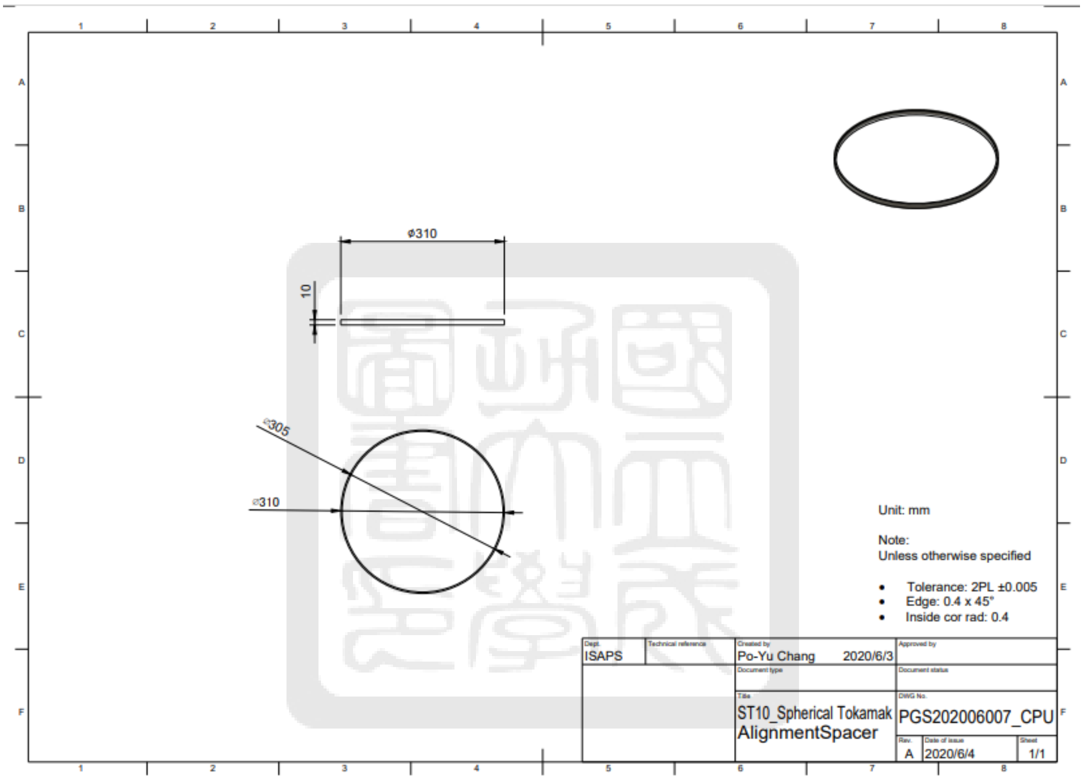

ϕ310
10
⌀305
⌀310
Unit: mm
Note:
Unless otherwise specified
• Tolerance: 2PL ±0.005
• Edge: 0.4 x 45°
• Inside cor rad: 0.4
Dept.
ISAPS
Technical reference
Created by
Po-Yu Chang 2020/6/3
Approved by
Document type
Document status
Title
ST10_Spherical Tokamak
AlignmentSpacer
DWG No.
PGS202006007_CPU
Rev.
A
Date of issue
2020/6/4
Sheet
1/1

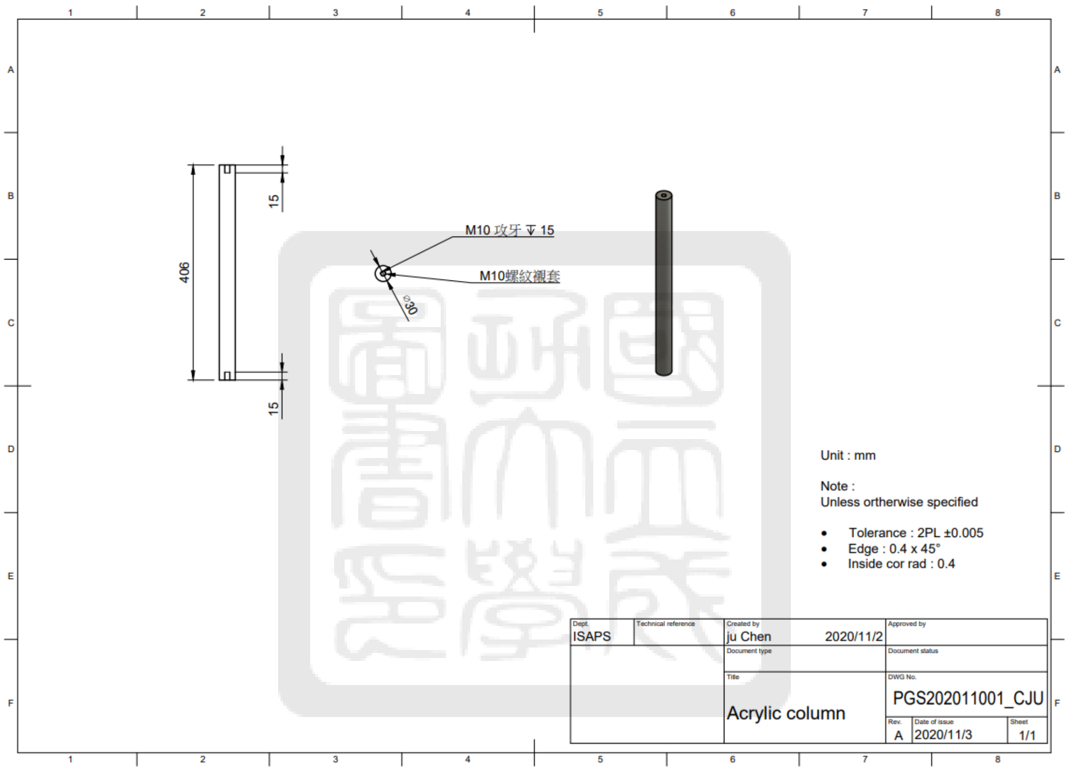
406
15
15
M10 攻牙 ↧ 15
M10螺紋襯套
⌀30
Unit : mm
Note :
Unless ortherwise specified
• Tolerance : 2PL ±0.005
• Edge : 0.4 x 45°
• Inside cor rad : 0.4
Dept.
ISAPS
Technical reference
Created by
ju Chen 2020/11/2
Approved by
Document type
Document status
Title
Acrylic column
DWG No.
PGS202011001_CJU
Rev.
A
Date of issue
2020/11/3
Sheet
1/1

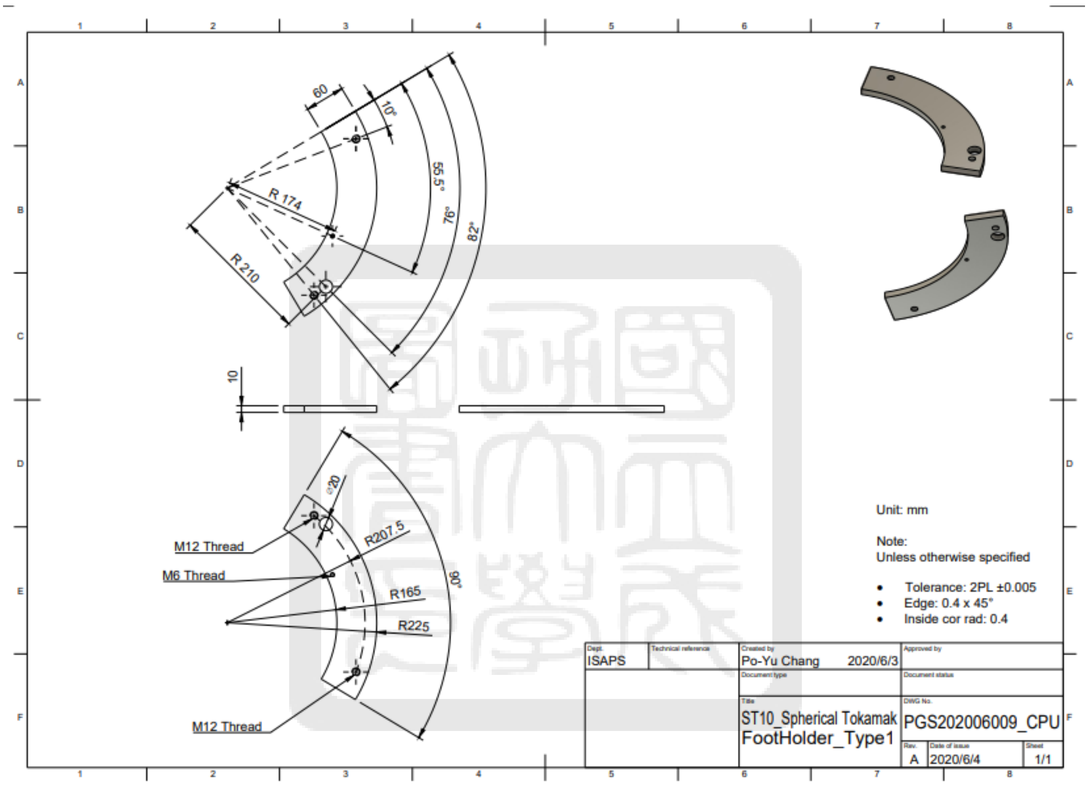
60
10°
55.5°
76°
82°
R 174
R 210
10
ø20
R207.5
R165
R225
90°
M12 Thread
M6 Thread
M12 Thread
Unit: mm
Note:
Unless otherwise specified
Tolerance: 2PL ±0.005
Edge: 0.4 x 45°
Inside cor rad: 0.4
Dept.
ISAPS
Technical reference
Created by
Po-Yu Chang 2020/6/3
Approved by
Document type
Document status
Title
ST10_Spherical Tokamak
FootHolder_Type1
DWG No.
PGS202006009_CPU
Rev.
A
Date of issue
2020/6/4
Sheet
1/1

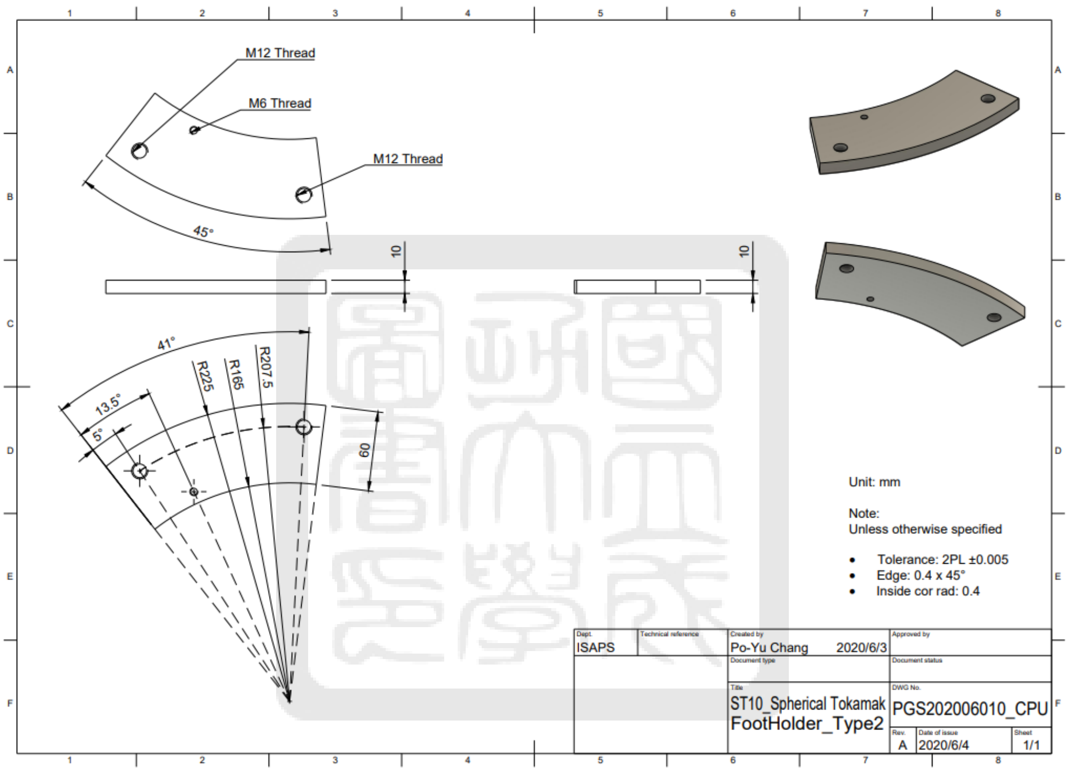
M12 Thread
M6 Thread
M12 Thread
45°
10
10
41°
13.5°
5°
R225
R165
R207.5
60
Unit: mm
Note:
Unless otherwise specified
Tolerance: 2PL ±0.005
Edge: 0.4 x 45°
Inside cor rad: 0.4
Dept.
ISAPS
Technical reference
Created by
Po-Yu Chang 2020/6/3
Approved by
Document type
Document status
Title
ST10_Spherical Tokamak
FootHolder_Type2
DWG No.
PGS202006010_CPU
Rev.
A
Date of issue
2020/6/4
Sheet
1/1

A 2.2 The process of gas injection

The process of gas injection.

(1) Close the Needle valve.

(2) Close Relief valve 1.

(3) Close Relief valve 2.

(4) Turn on the vacuum Pump.

(5) Open the Gate valve.

(6) Wait the chamber pressure reaching 10^{-3} torr.

(7) Close the Gate valve.

(8) Open the gas cylinder to 1 atm.

(9) Open the Needle valve.

(10) Wait the chamber pressure until the 10^{-1} torr.

(11) Close the Needle valve.

(12) The gas injection is done.

The process of stopping the experiment and vent the vacuum chamber.

(1) Close the gate value slowly open the Relif valve 1 until the pressure of chamber return to atmospheric pressure.

(2) Open Relief valve 2.

(3) Turn off the pump.

(4) Close Relief valve 2.

The process of stopping the experiment while keeping the chamber in vacuum.

(1) Close the gate value.

(2) Open Relief valve 2.

(3) Turn off the pump.

(4) Close Relief valve 2.

A 3.1 The layout of signal generator

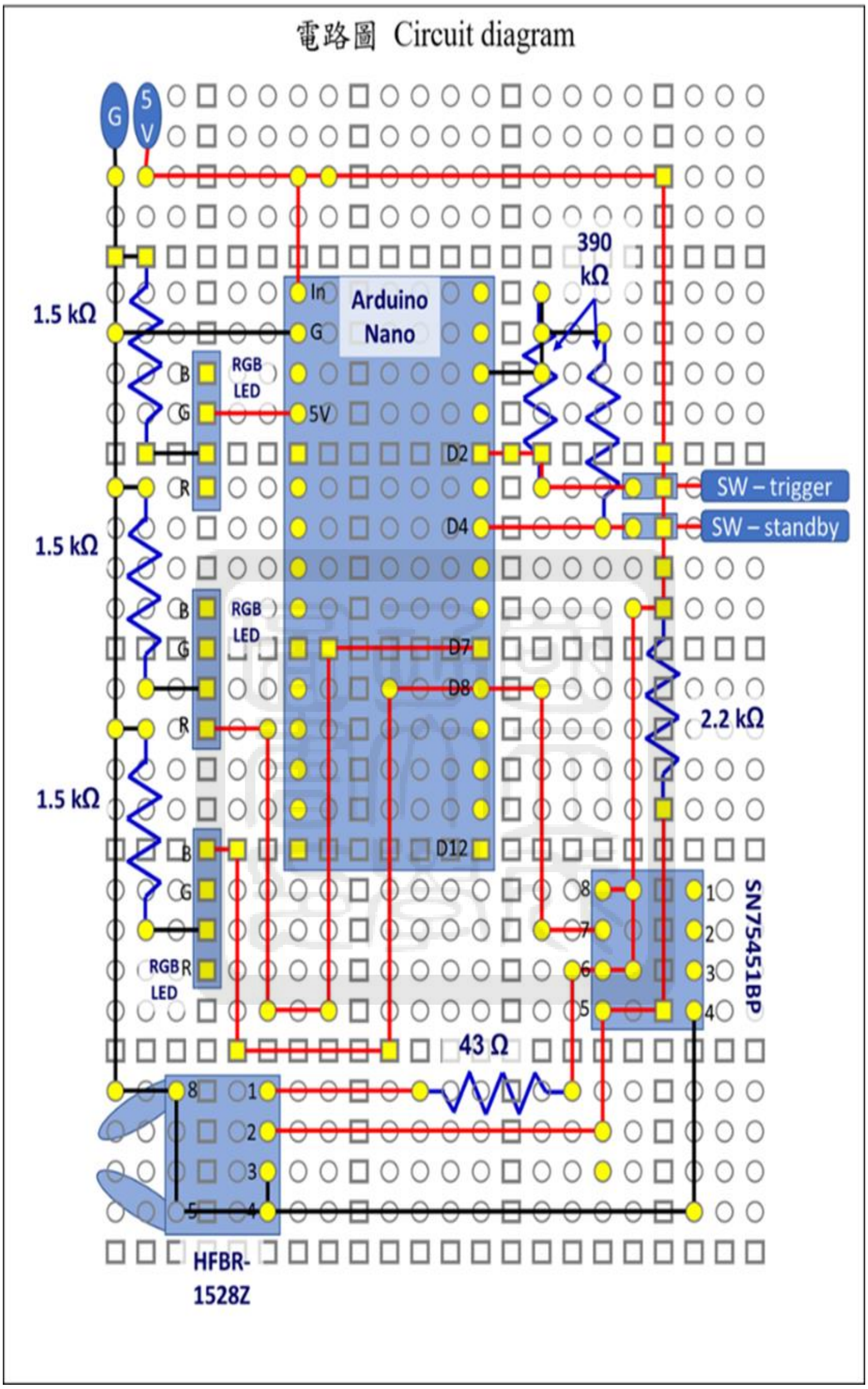

The code of signal generator

```
int TLED = 8;                         Trigger LED 的腳位
int SLED = 7;                         Stand by LED 的腳位
int t0 = 0;                           Trigger LED 腳位的初始值
int s0 = 0;                           Stand by LED 腳位的初始值
int t1 = 0;                           Trigger 前一個時間的值
int s1 = 1;                           Stand by 前一個時間的值
int t2;                               Trigger 當前時間的值
int s2;                               Stand by 當前時間的值
int triggerpin = 2;                   Trigger 腳位
int standbypin = 4;                   Stand by 腳位
int st;                               s2-s1
int tt;                               t2-t1

void setup()                          系統設定
{
  pinMode(TLED, OUTPUT);              Trigger LED 腳位設定
  pinMode(SLED, OUTPUT);              Stand by LED 腳位設定
  pinMode(triggerpin, INPUT);         Trigger 讀取腳位設定
  pinMode(standbypin, INPUT);         Stand by 讀取腳位設定
  Serial.begin(9600);
}

void loop()                           主迴圈
```

```
{
 t2 = digitalRead(triggerpin);                    讀取開關狀態(斷路為 0,通路為 1)
 s2 = digitalRead(standbypin);
 st = s2-s1;                                      判斷是否有撥動開關或按下按鈕
 tt = t2-t1;
 if (s0==0)                                       s0=1 才能送訊號
 {
  if(st==1)                                       表示開關撥桿從 off 到 on
  {
    s0 = 1;                                       唯一有機會將 s0 變為 1
    s1 = s2;                                      將 Stand by 前一個時間值=當前時間的值
    digitalWrite(SLED,s0);                        Stand by LED 亮
  }
  else
  {
    s1 = s2;                                      將 Stand by 前一個時間值=當前時間的值
  }
 }
 else
 {
  if (st==-1)                                     此判斷式表示開關撥桿從 on 到 of
  {
    s0=0;
    digitalWrite(SLED,s0);                        Stand by LED 暗
    s1 = s2;                                      將 Stand by 前一個時間值=當前時間的值
```

```
   }
   else if (tt==1)                                        此判斷式表示觸發按鈕按下
   {
     t0=1;
     digitalWrite(TLED,t0);                               Trigger LED 亮
     delayMicroseconds(300);                              亮 0.3ms
     digitalWrite(TLED,0);                                Trigger LED 暗
     t1 = t2;
     s0 = 0;
     digitalWrite(SLED,s0);
   }
   else
   {
     t1 = t2;                        將 Trigger 前一個時間值=當前時間的值

   }
  }
}
```

A 3.2 The data of the 1st PFN stage

Data 1

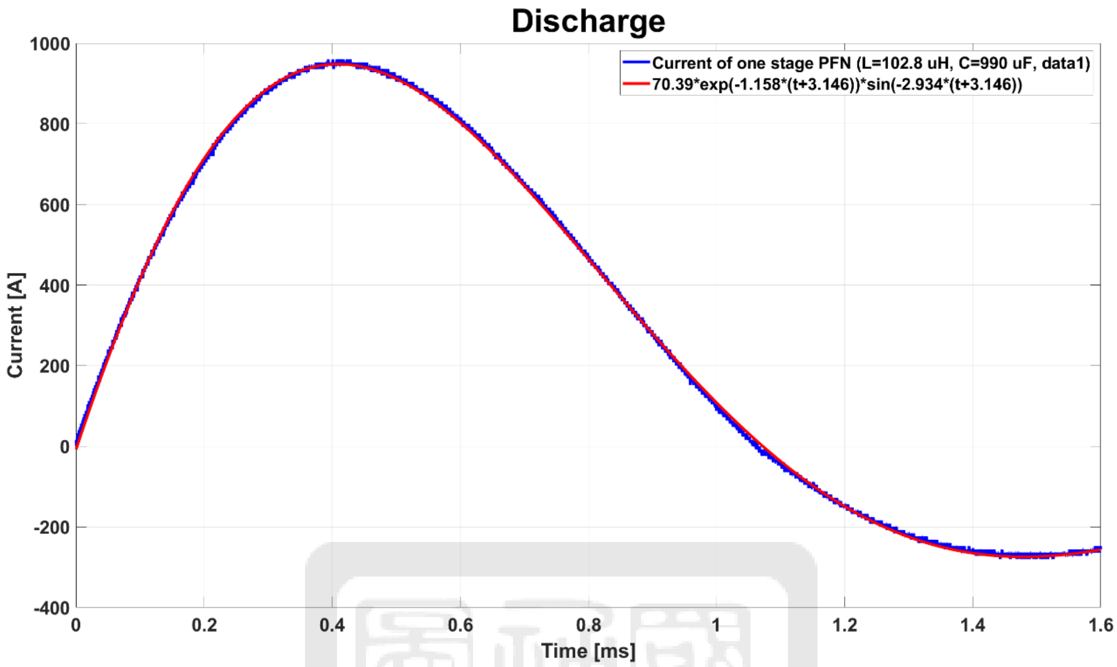

Data 2

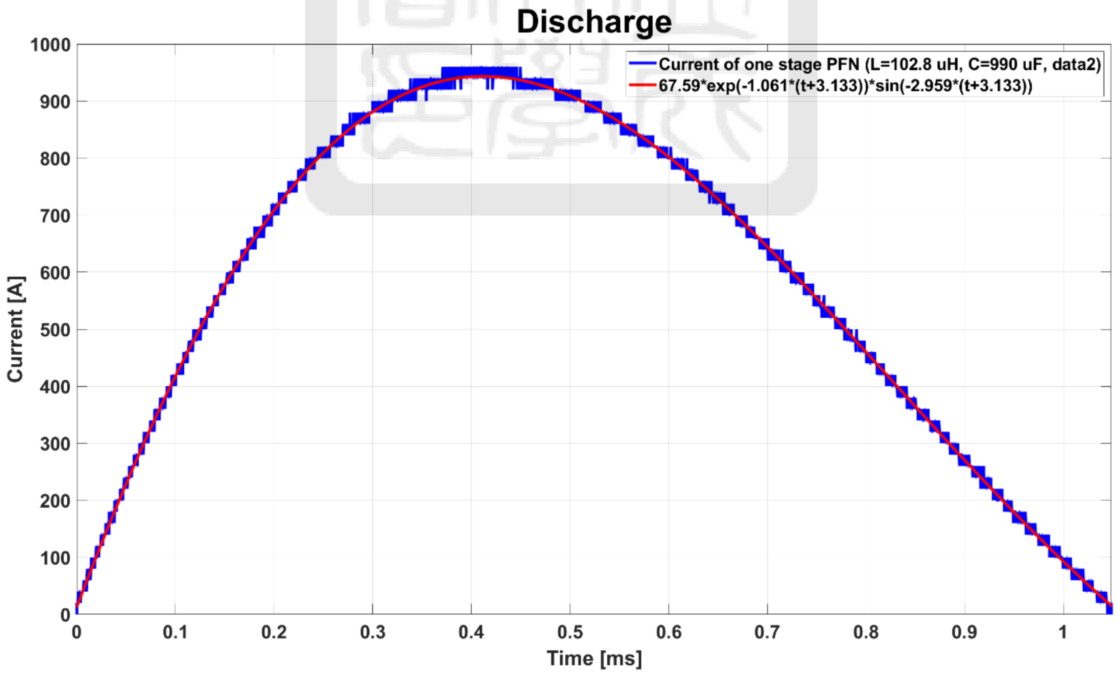

Data 3

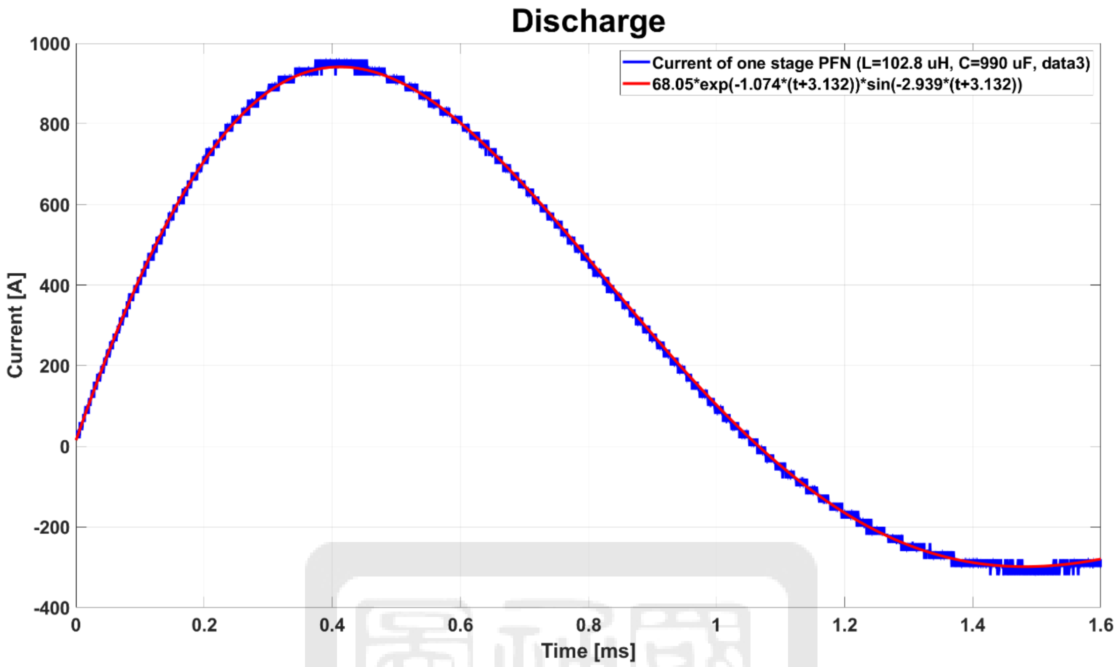
Discharge
Current of one stage PFN (L=102.8 uH, C=990 uF, data3)
68.05*exp(-1.074*(t+3.132))*sin(-2.939*(t+3.132))
Current [A]
Time [ms]

Data 4

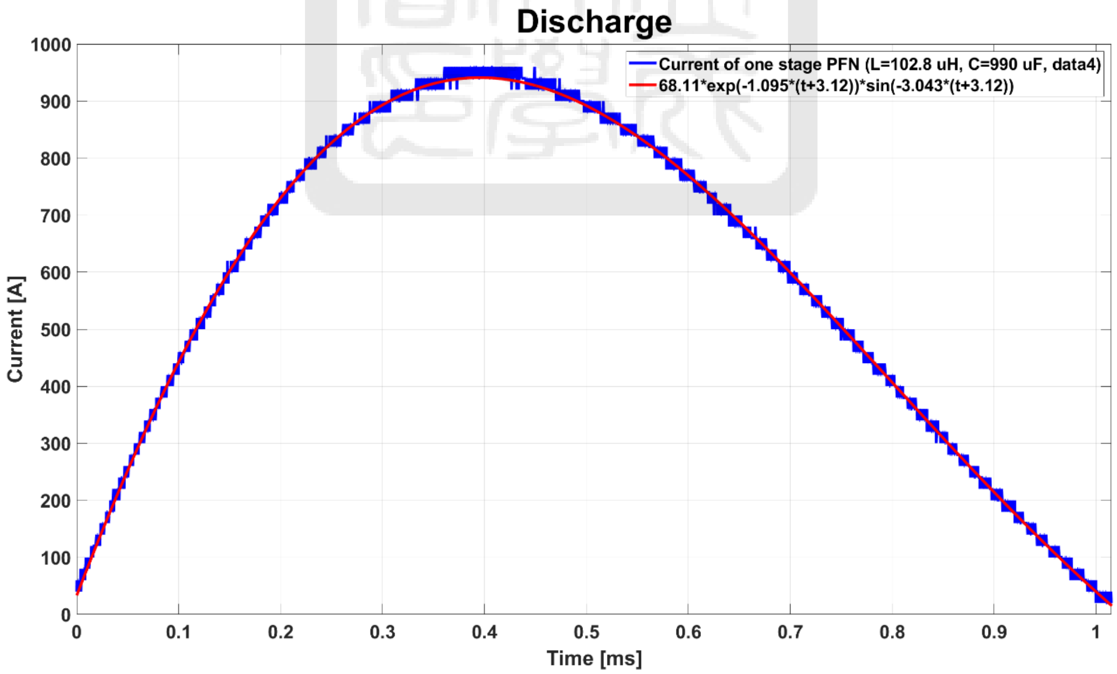
Discharge
Current of one stage PFN (L=102.8 uH, C=990 uF, data4)
68.11*exp(-1.095*(t+3.12))*sin(-3.043*(t+3.12))
Current [A]
Time [ms]

Data 5

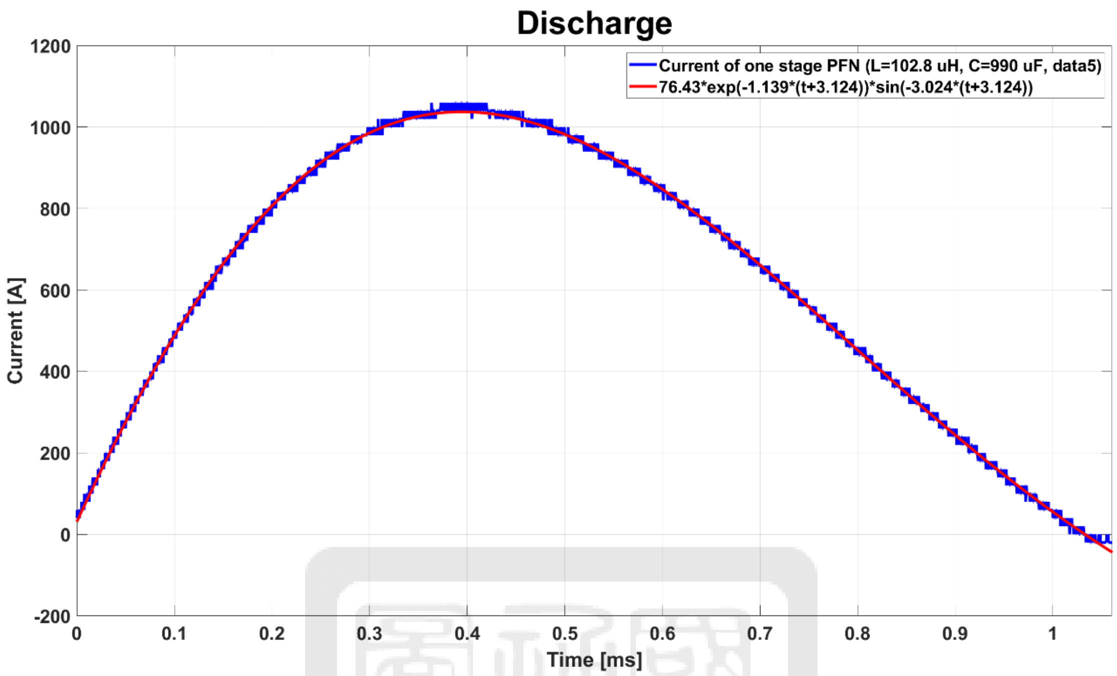
Discharge
Current of one stage PFN (L=102.8 uH, C=990 uF, data5)
76.43*exp(-1.139*(t+3.124))*sin(-3.024*(t+3.124))
Current [A]
Time [ms]
1200
1000
800
600
400
200
0
-200
0
0.1
0.2
0.3
0.4
0.5
0.6
0.7
0.8
0.9
1

Data 6

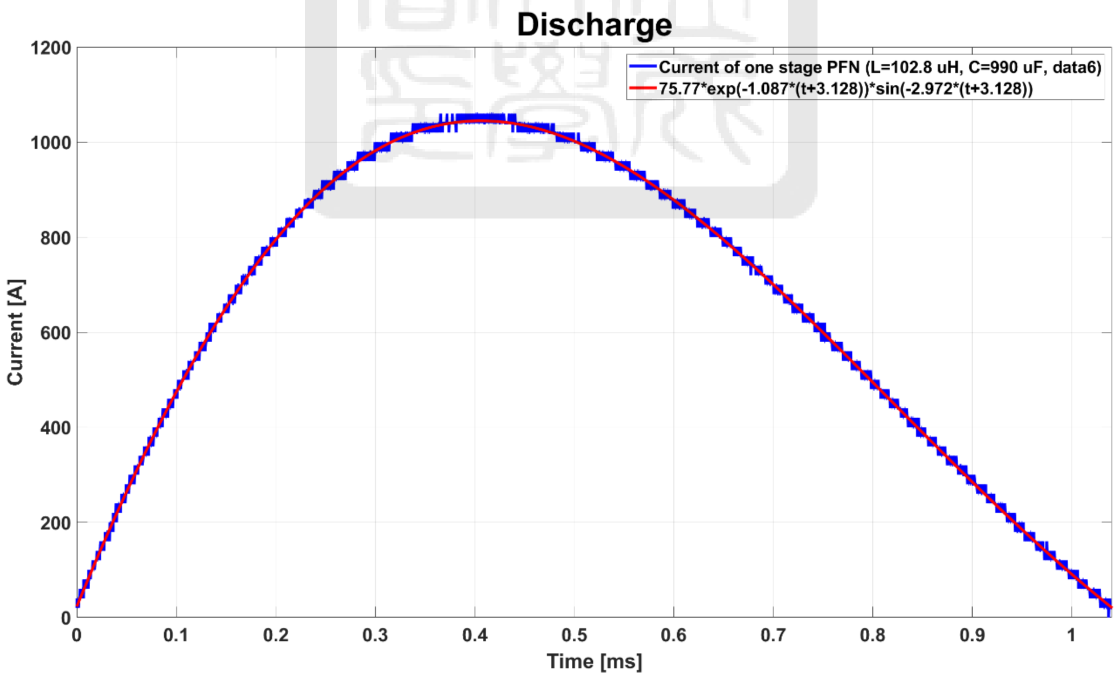
Discharge
Current of one stage PFN (L=102.8 uH, C=990 uF, data6)
75.77*exp(-1.087*(t+3.128))*sin(-2.972*(t+3.128))
Current [A]
Time [ms]
1200
1000
800
600
400
200
0
0
0.1
0.2
0.3
0.4
0.5
0.6
0.7
0.8
0.9
1

Data 7

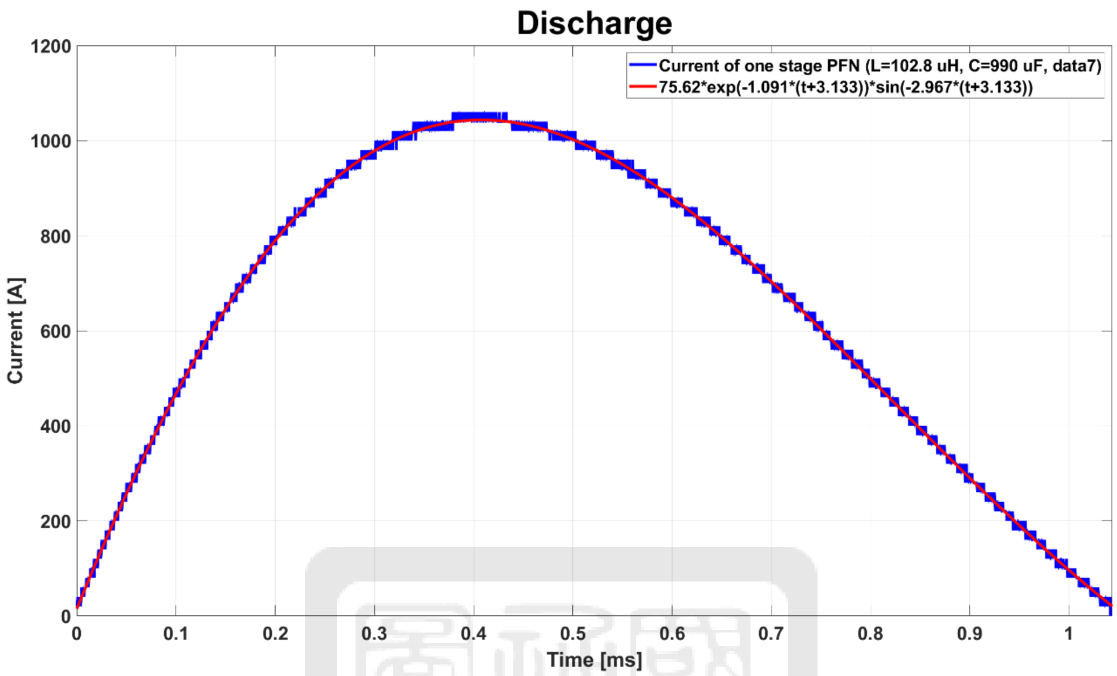
Discharge
Current of one stage PFN (L=102.8 uH, C=990 uF, data7)
75.62*exp(-1.091*(t+3.133))*sin(-2.967*(t+3.133))
Current [A]
Time [ms]

Data 8

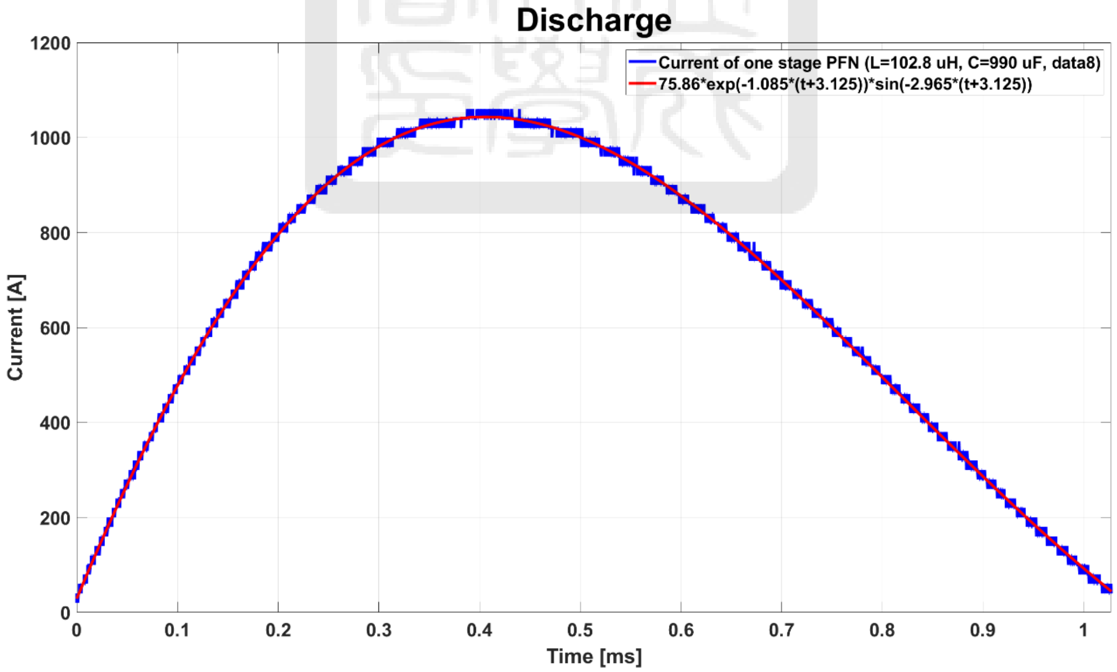
Discharge
Current of one stage PFN (L=102.8 uH, C=990 uF, data8)
75.86*exp(-1.085*(t+3.125))*sin(-2.965*(t+3.125))
Current [A]
Time [ms]

Data 9

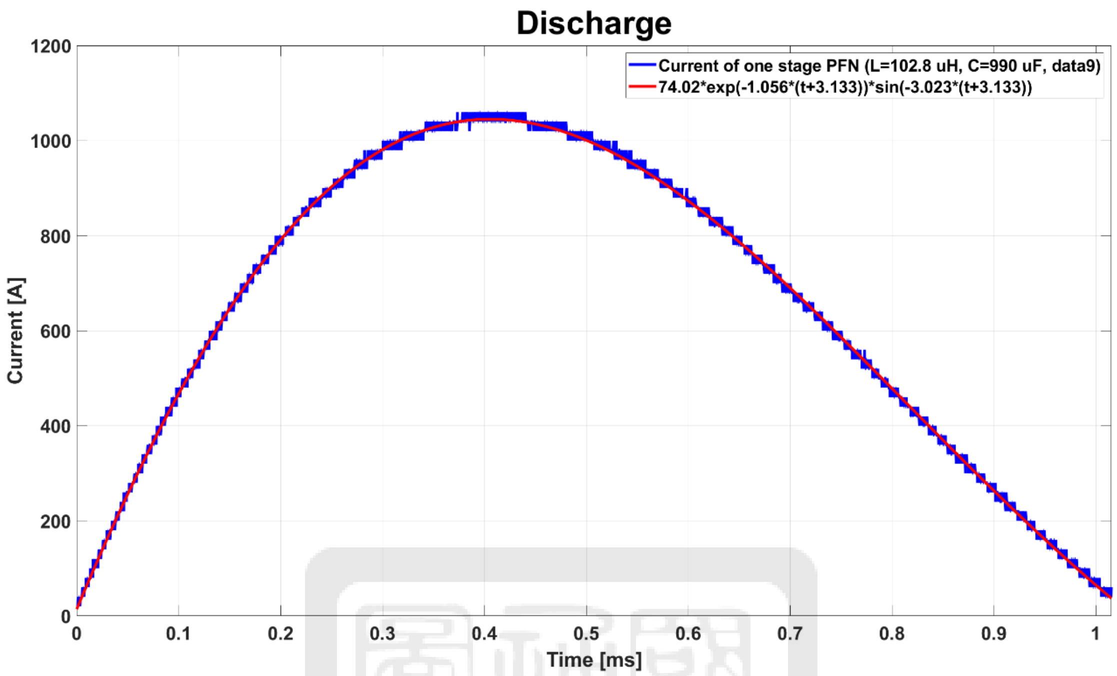

Data 10

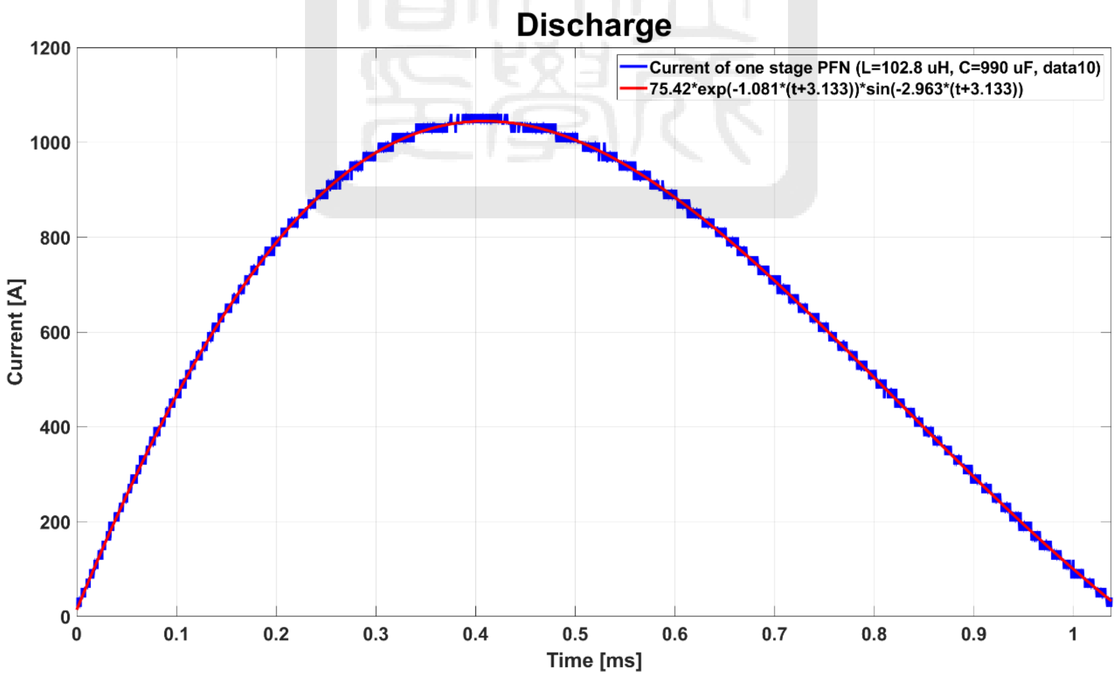

A 3.3 The data of the 2nd PFN stage

Data 1

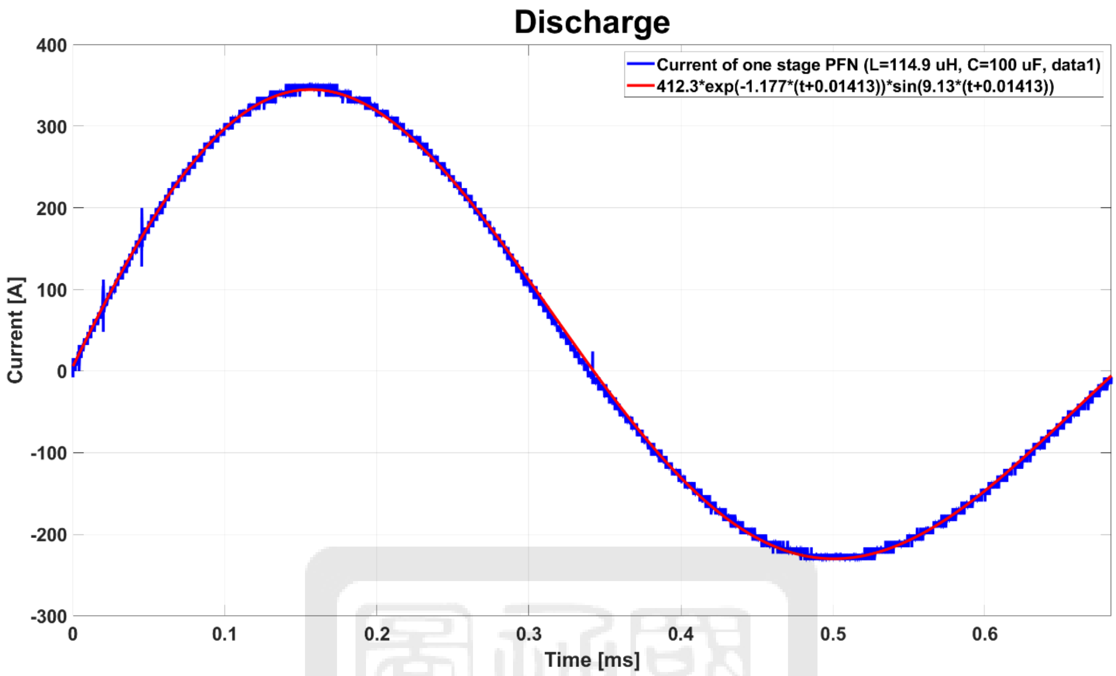

Data 2

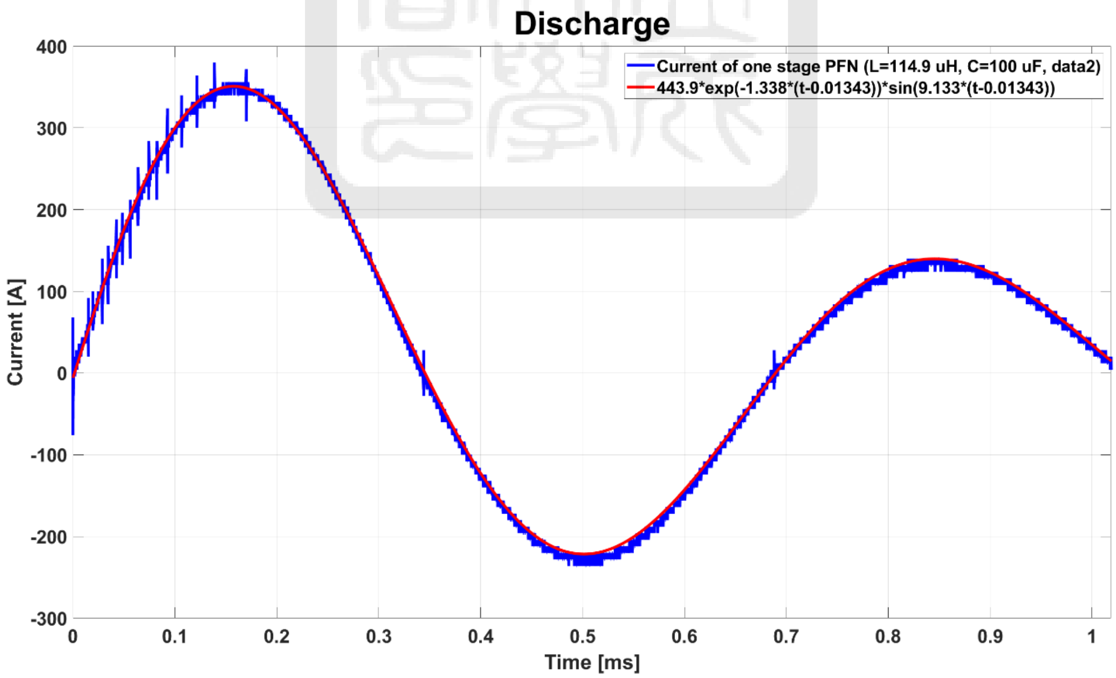

Data 3

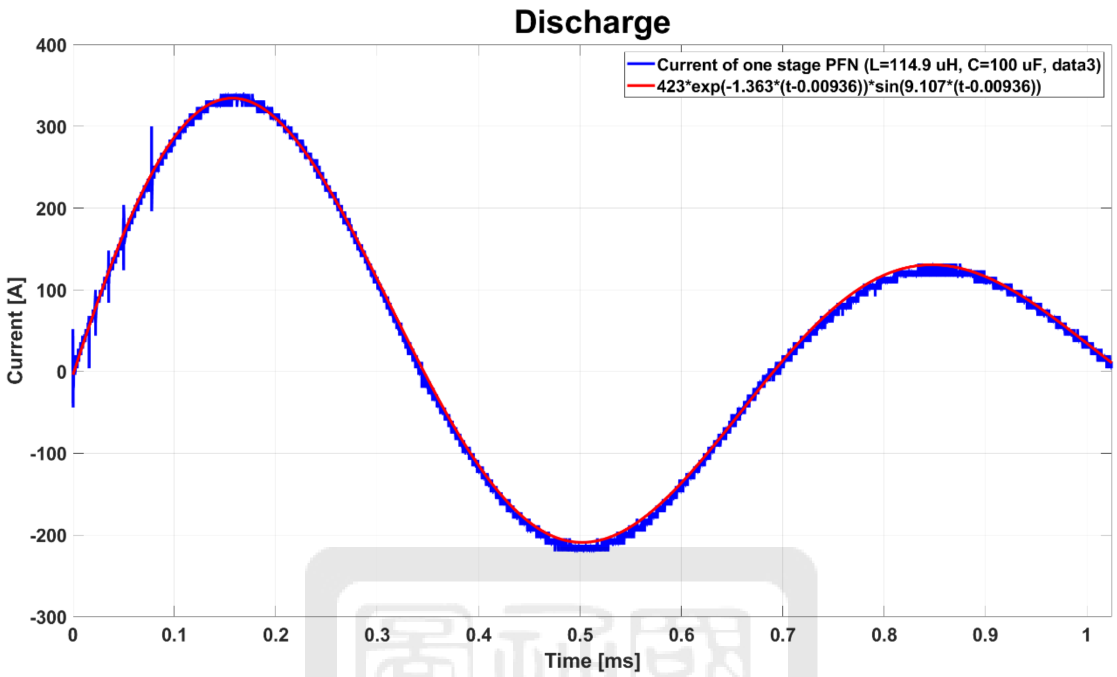
Discharge
Current of one stage PFN (L=114.9 uH, C=100 uF, data3)
423*exp(-1.363*(t-0.00936))*sin(9.107*(t-0.00936))
Current [A]
Time [ms]
400
300
200
100
0
-100
-200
-300
0
0.1
0.2
0.3
0.4
0.5
0.6
0.7
0.8
0.9
1

Data 4

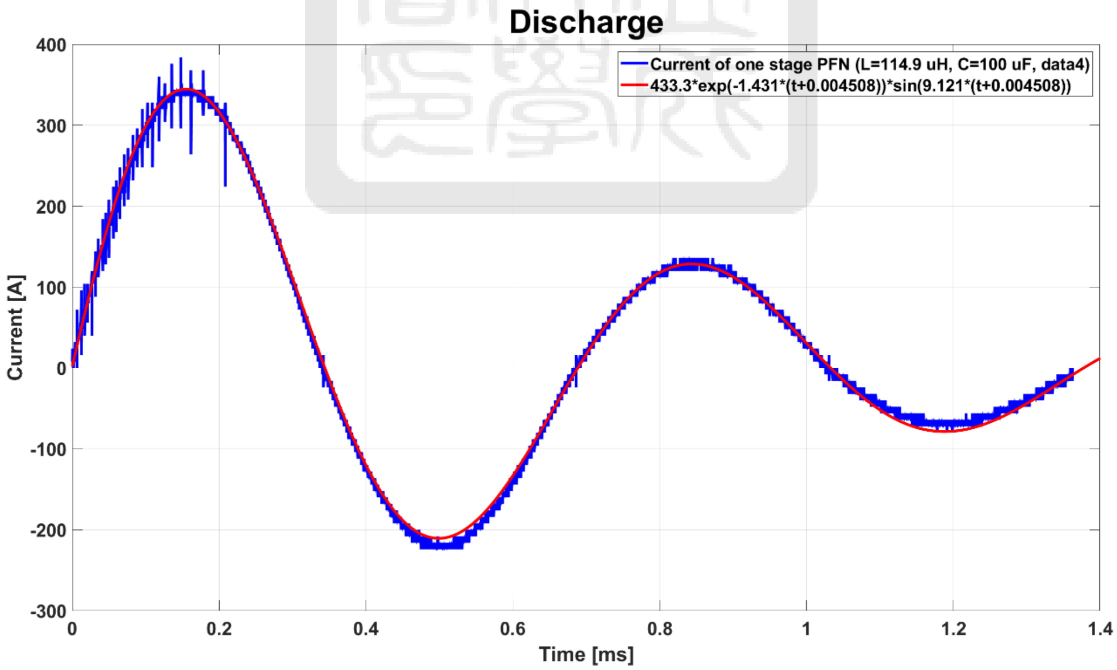
Discharge
Current of one stage PFN (L=114.9 uH, C=100 uF, data4)
433.3*exp(-1.431*(t+0.004508))*sin(9.121*(t+0.004508))
Current [A]
Time [ms]
400
300
200
100
0
-100
-200
-300
0
0.2
0.4
0.6
0.8
1
1.2
1.4

Data 5

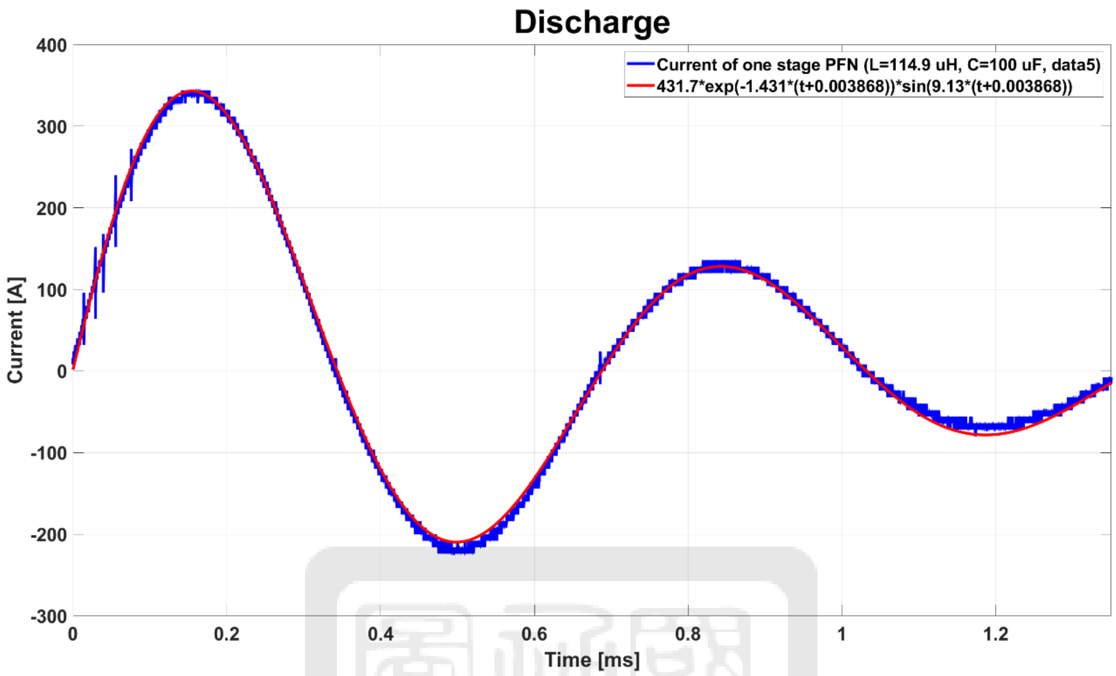
Discharge
Current of one stage PFN (L=114.9 uH, C=100 uF, data5)
431.7*exp(-1.431*(t+0.003868))*sin(9.13*(t+0.003868))
Current [A]
Time [ms]
400
300
200
100
0
-100
-200
-300
0
0.2
0.4
0.6
0.8
1
1.2

Data 6

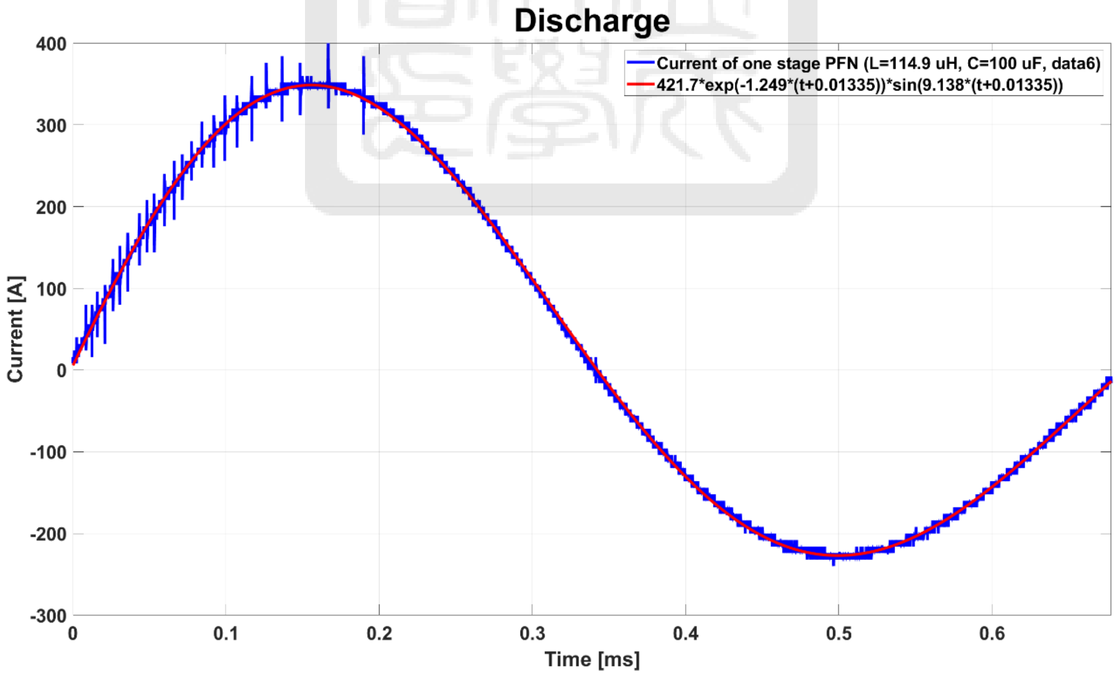
Discharge
Current of one stage PFN (L=114.9 uH, C=100 uF, data6)
421.7*exp(-1.249*(t+0.01335))*sin(9.138*(t+0.01335))
Current [A]
Time [ms]
400
300
200
100
0
-100
-200
-300
0
0.1
0.2
0.3
0.4
0.5
0.6

Data 7

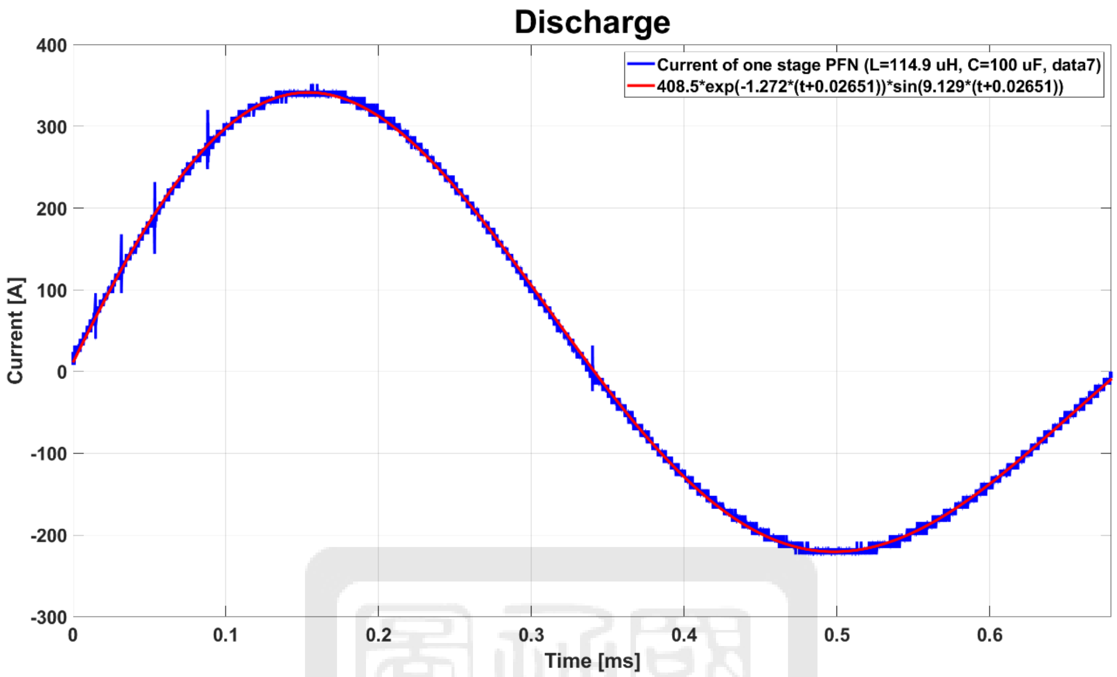

Discharge
Current of one stage PFN (L=114.9 uH, C=100 uF, data7)
408.5*exp(-1.272*(t+0.02651))*sin(9.129*(t+0.02651))
Current [A]
Time [ms]
400
300
200
100
0
-100
-200
-300
0
0.1
0.2
0.3
0.4
0.5
0.6

Data 8

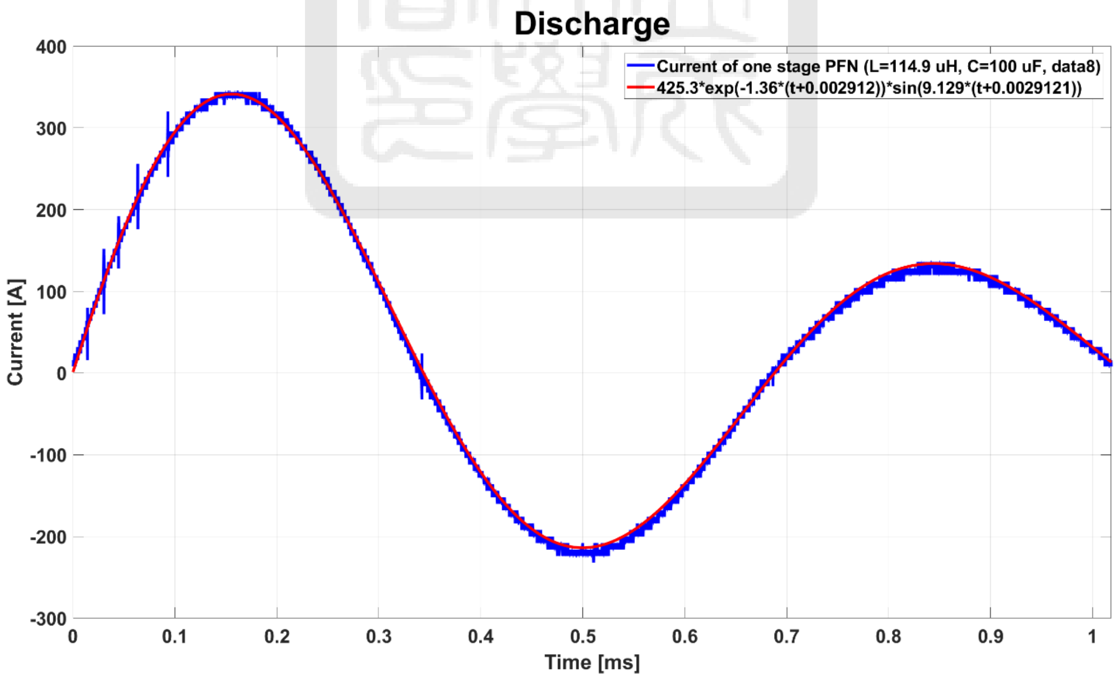

Discharge
Current of one stage PFN (L=114.9 uH, C=100 uF, data8)
425.3*exp(-1.36*(t+0.002912))*sin(9.129*(t+0.0029121))
Current [A]
Time [ms]
400
300
200
100
0
-100
-200
-300
0
0.1
0.2
0.3
0.4
0.5
0.6
0.7
0.8
0.9
1

Data 9

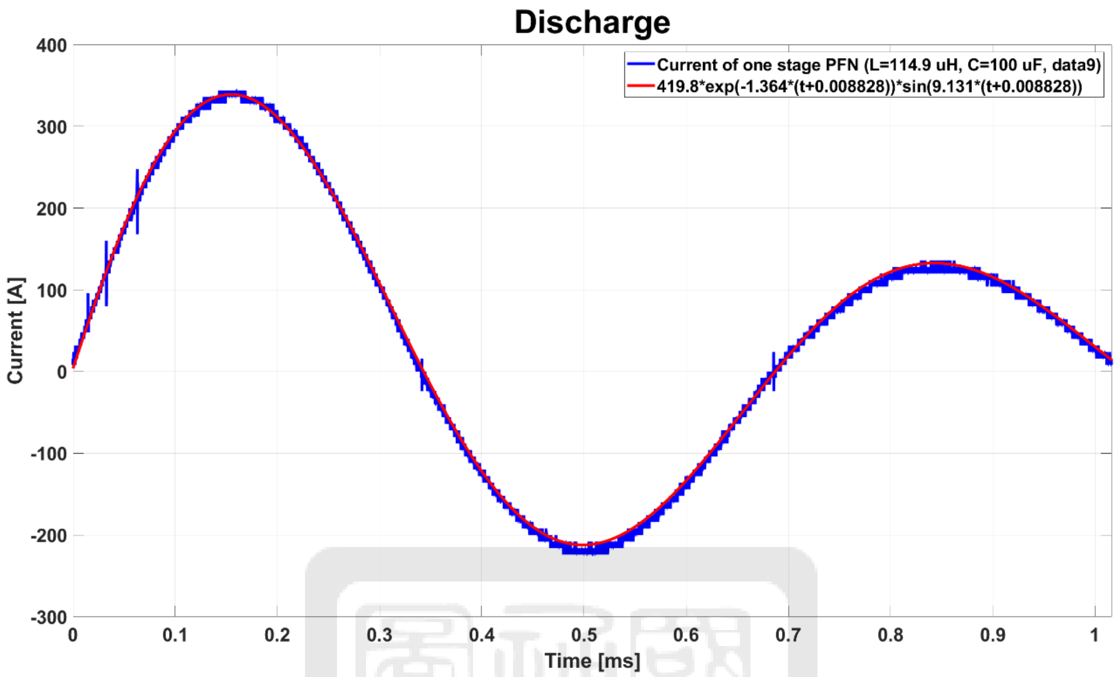

Data 10

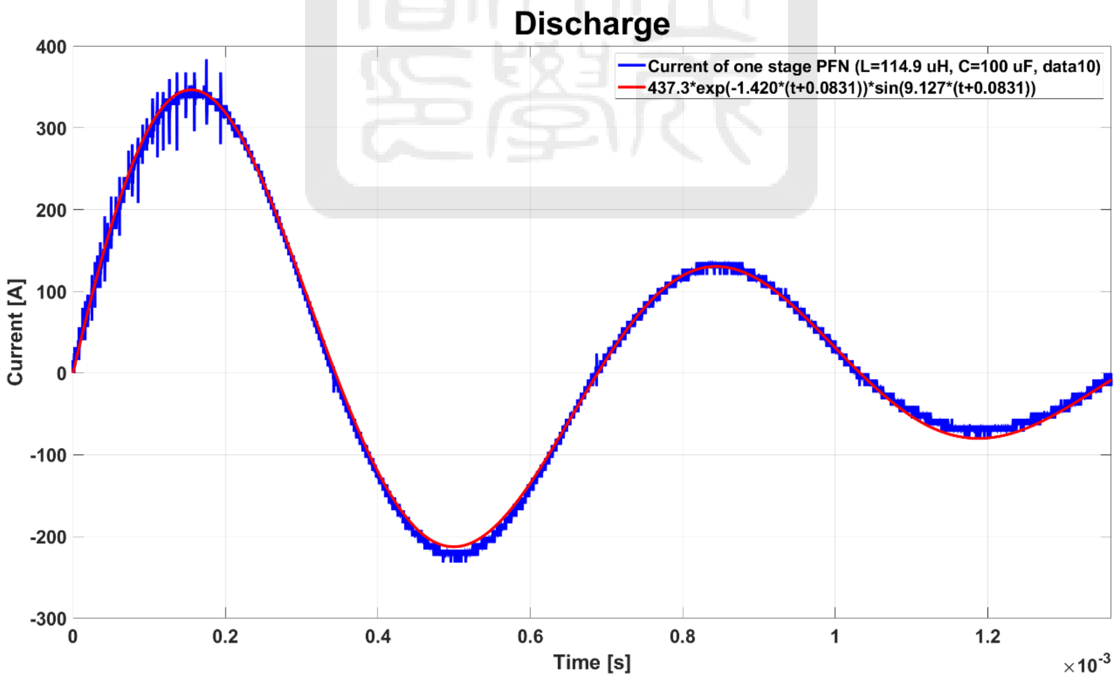

A 3.4 The data of the 3rd PFN stage

Data 1

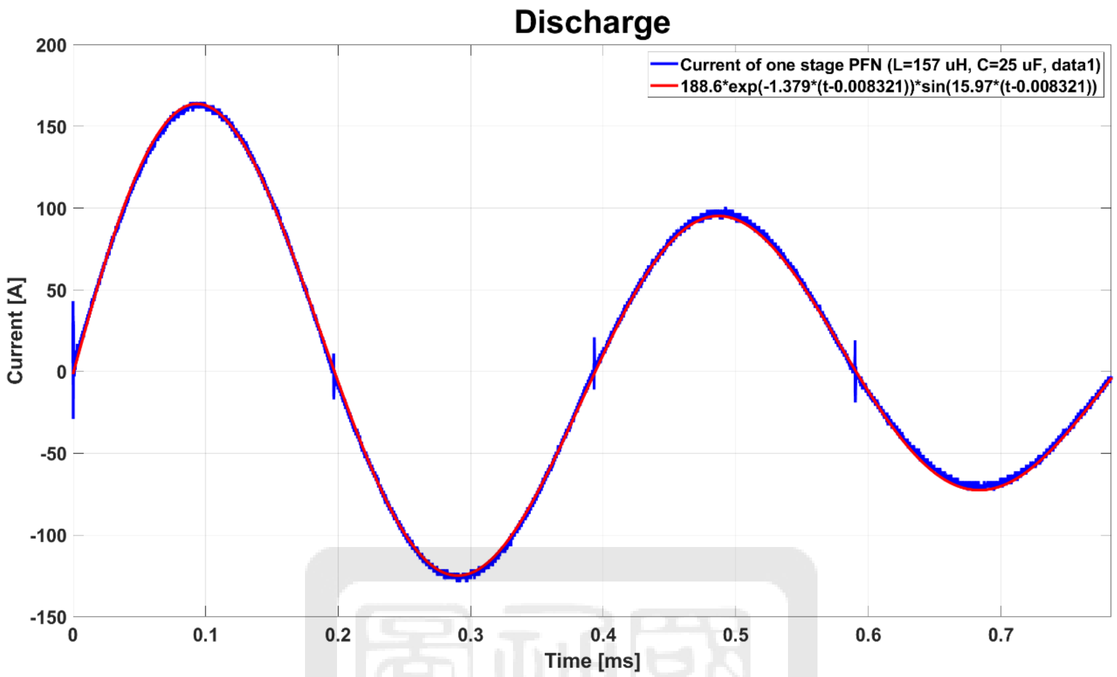

Data 2

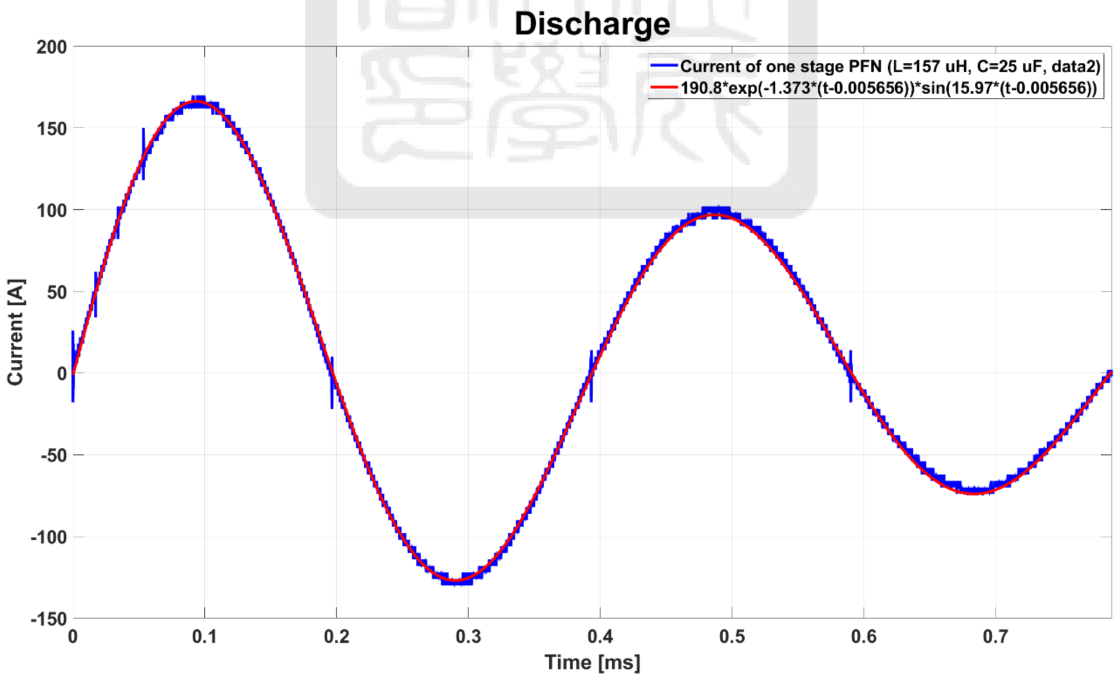

Data 3

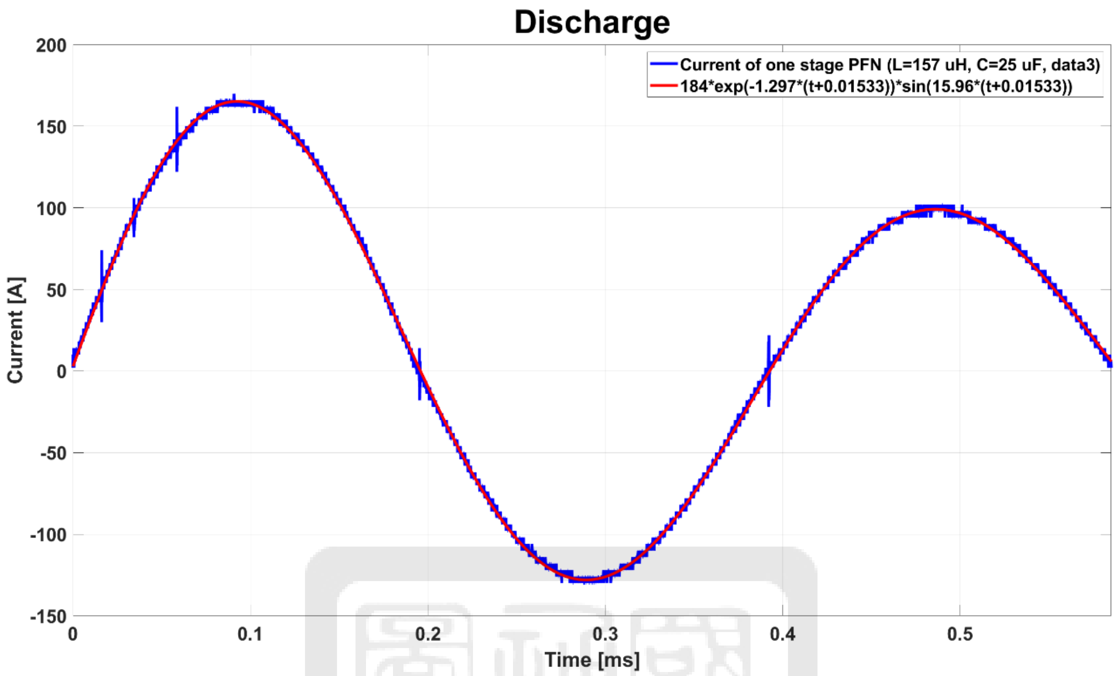
Discharge
Current of one stage PFN (L=157 uH, C=25 uF, data3)
184*exp(-1.297*(t+0.01533))*sin(15.96*(t+0.01533))
Current [A]
Time [ms]

Data 4

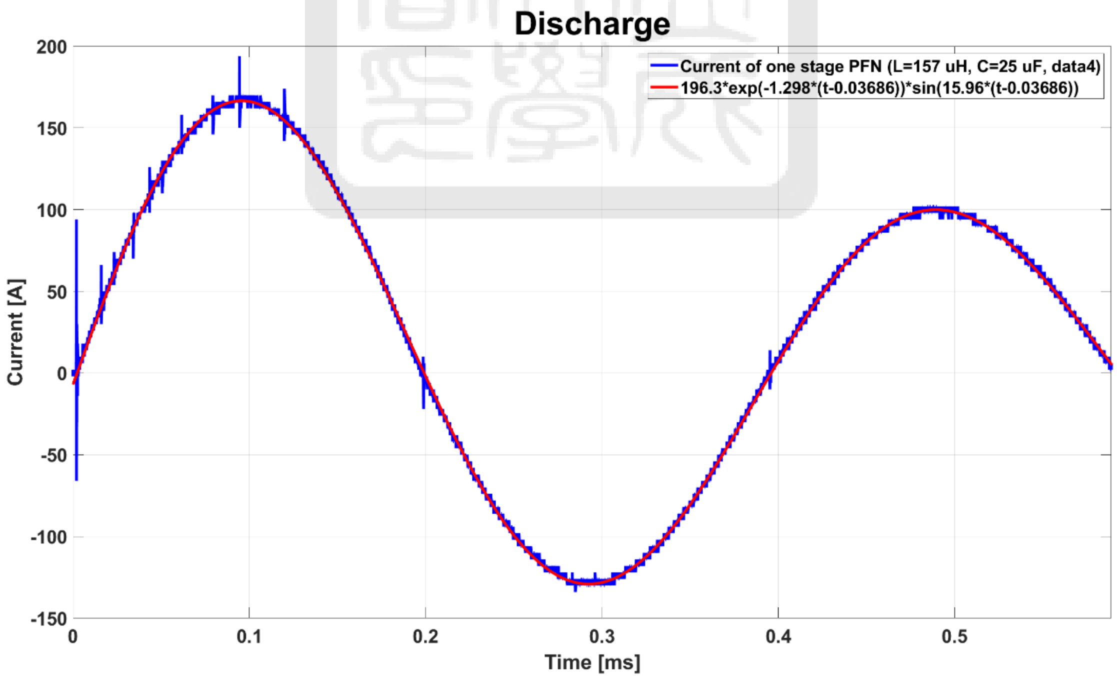
Discharge
Current of one stage PFN (L=157 uH, C=25 uF, data4)
196.3*exp(-1.298*(t-0.03686))*sin(15.96*(t-0.03686))
Current [A]
Time [ms]

Data 5

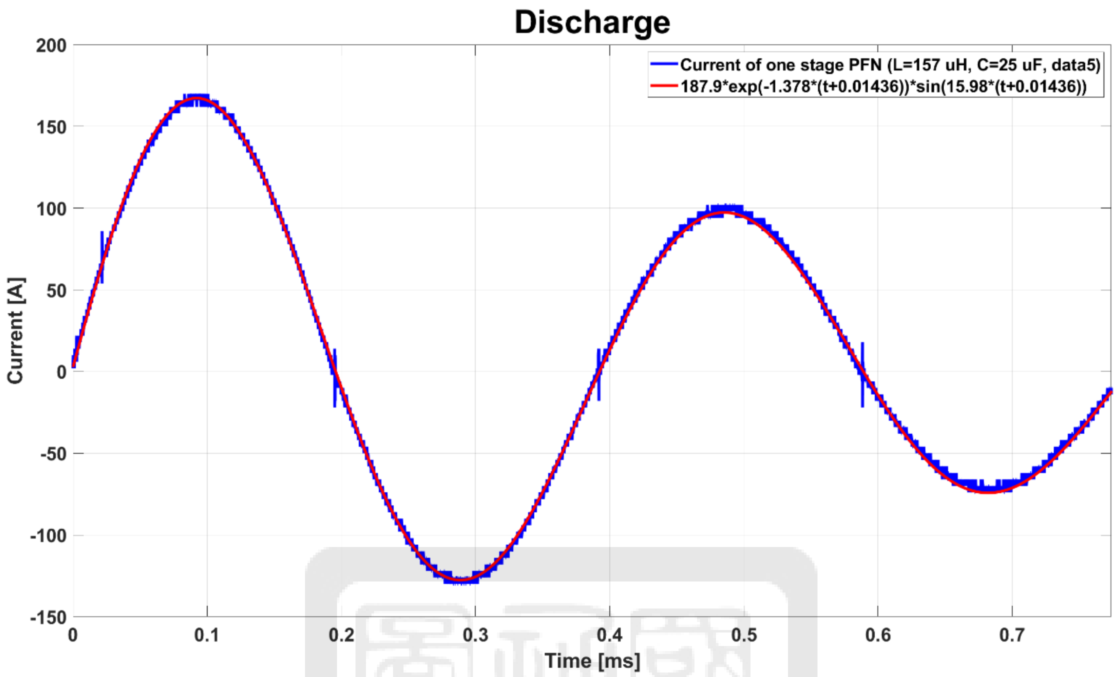

Discharge
Current of one stage PFN (L=157 uH, C=25 uF, data5)
187.9*exp(-1.378*(t+0.01436))*sin(15.98*(t+0.01436))
Current [A]
Time [ms]

Data 6

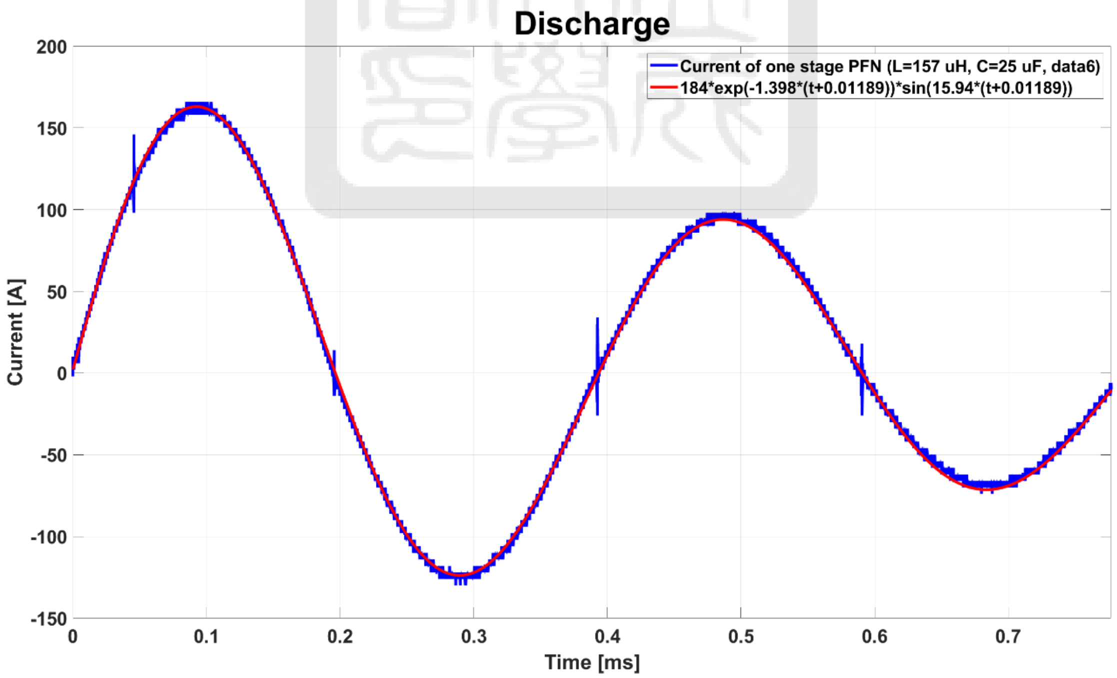

Discharge
Current of one stage PFN (L=157 uH, C=25 uF, data6)
184*exp(-1.398*(t+0.01189))*sin(15.94*(t+0.01189))
Current [A]
Time [ms]

Data 7

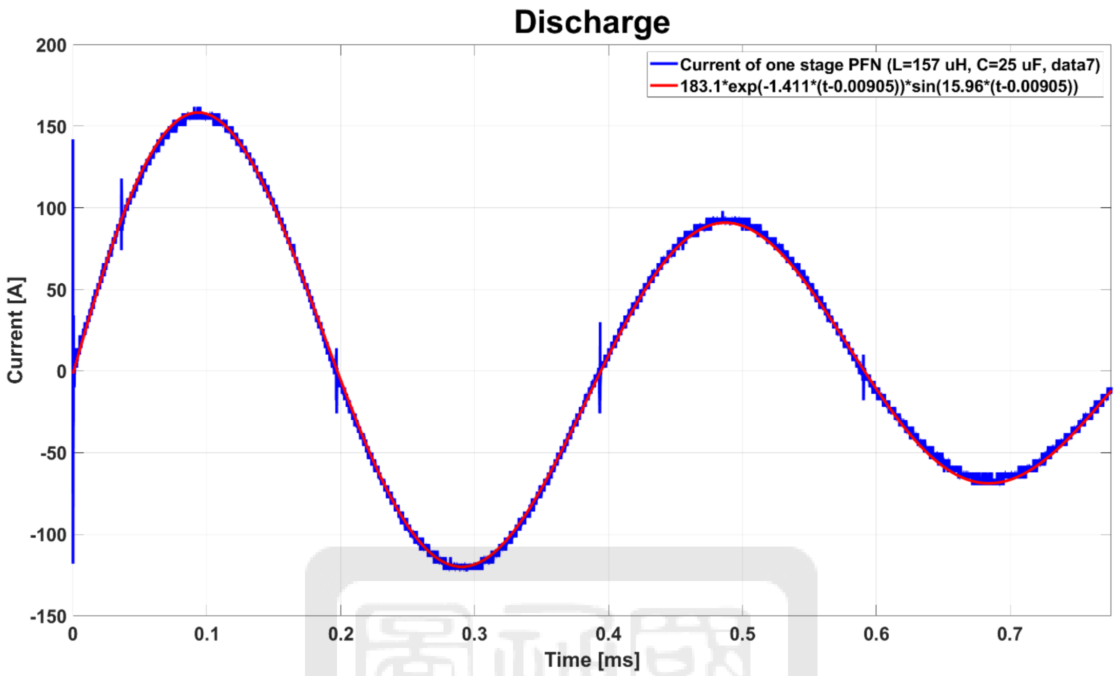
Discharge
Current of one stage PFN (L=157 uH, C=25 uF, data7)
183.1*exp(-1.411*(t-0.00905))*sin(15.96*(t-0.00905))
Current [A]
Time [ms]
200
150
100
50
0
-50
-100
-150
0
0.1
0.2
0.3
0.4
0.5
0.6
0.7

Data 8

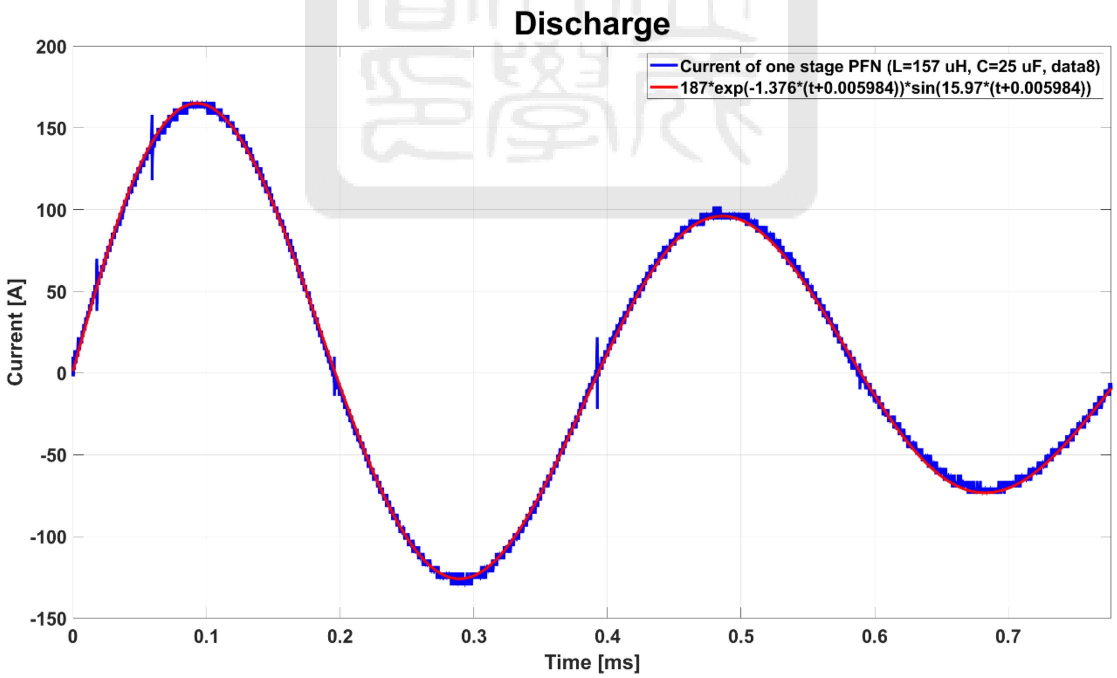
Discharge
Current of one stage PFN (L=157 uH, C=25 uF, data8)
187*exp(-1.376*(t+0.005984))*sin(15.97*(t+0.005984))
Current [A]
Time [ms]
200
150
100
50
0
-50
-100
-150
0
0.1
0.2
0.3
0.4
0.5
0.6
0.7

Data 9

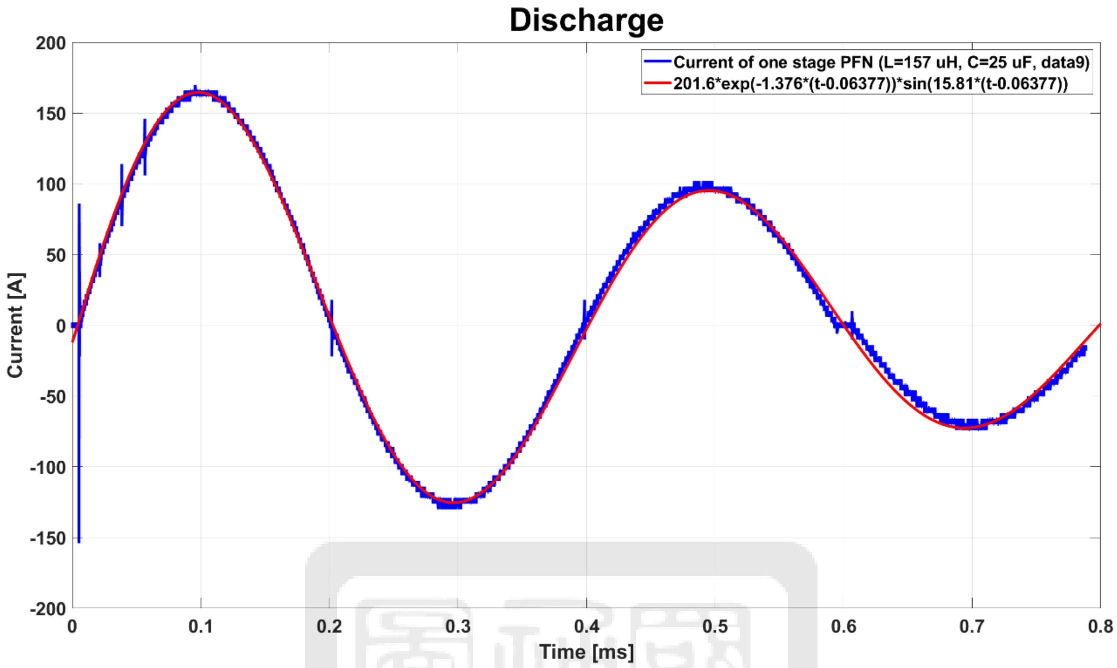

Data 10

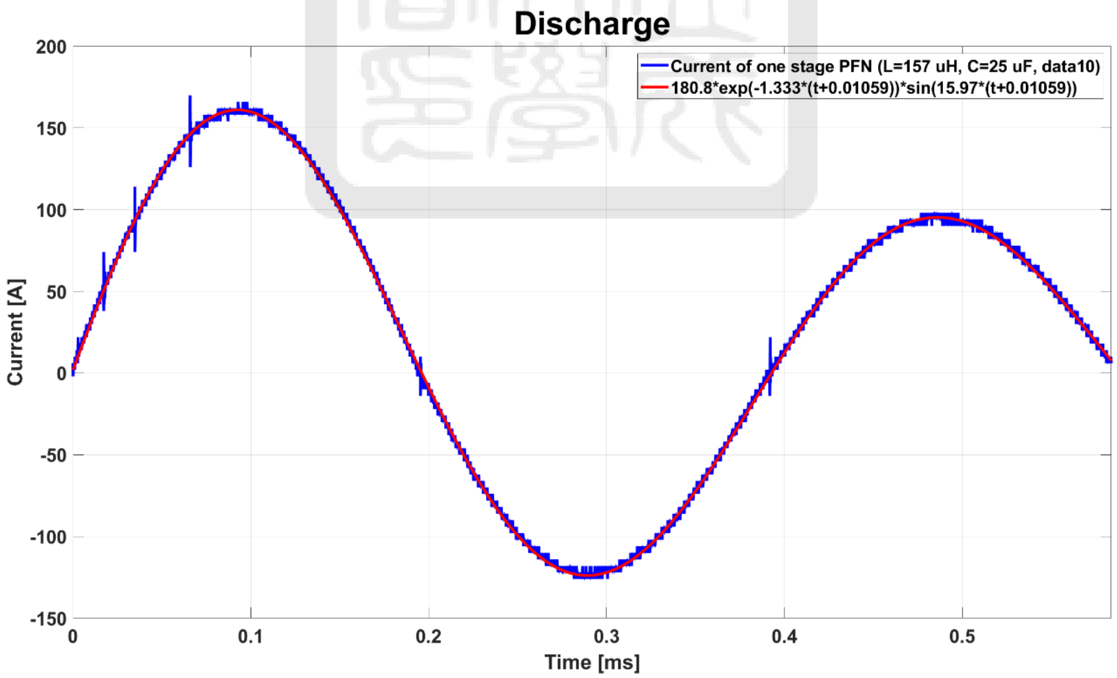

A 3.5 The data of the 4th PFN stage

Data 1

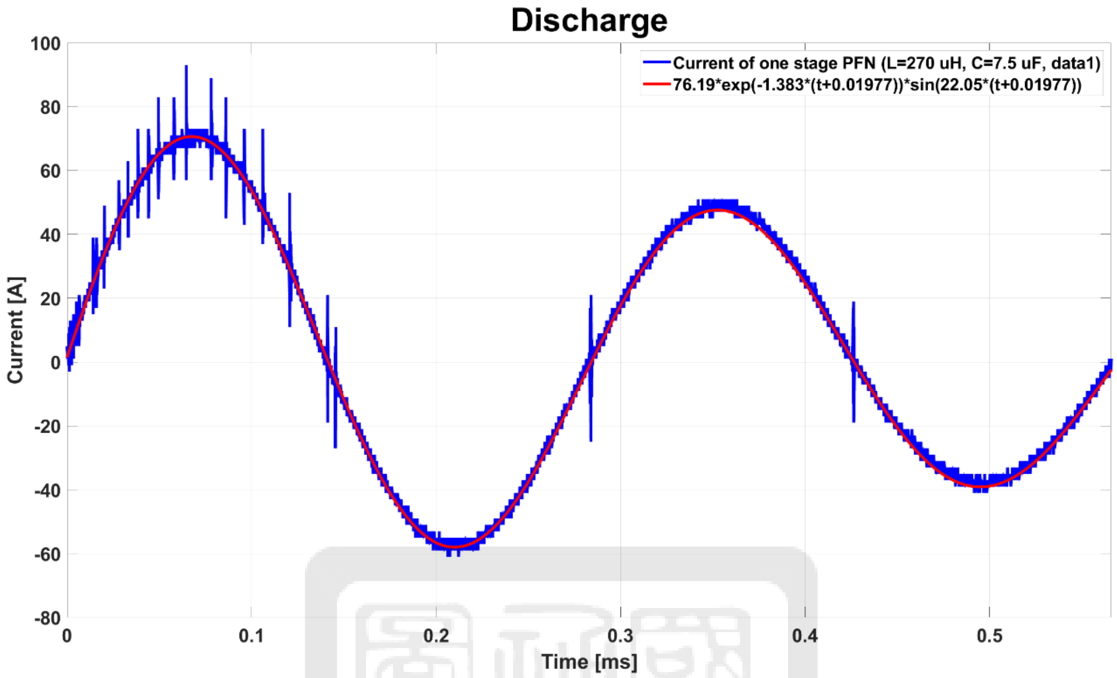

Data 2

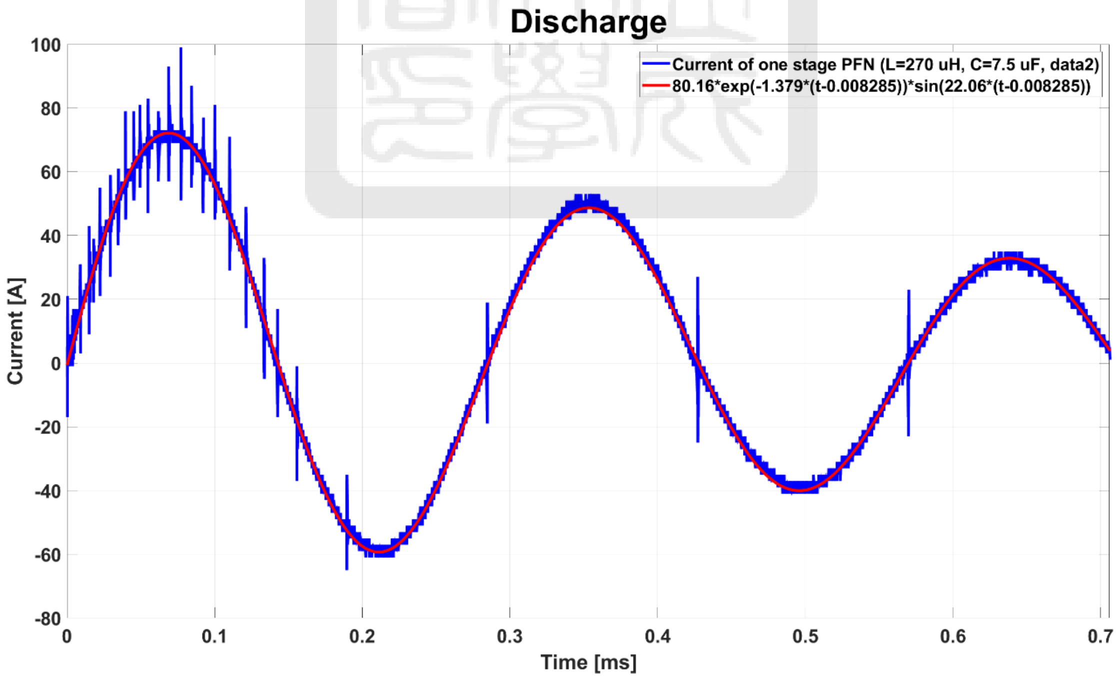

Data 3

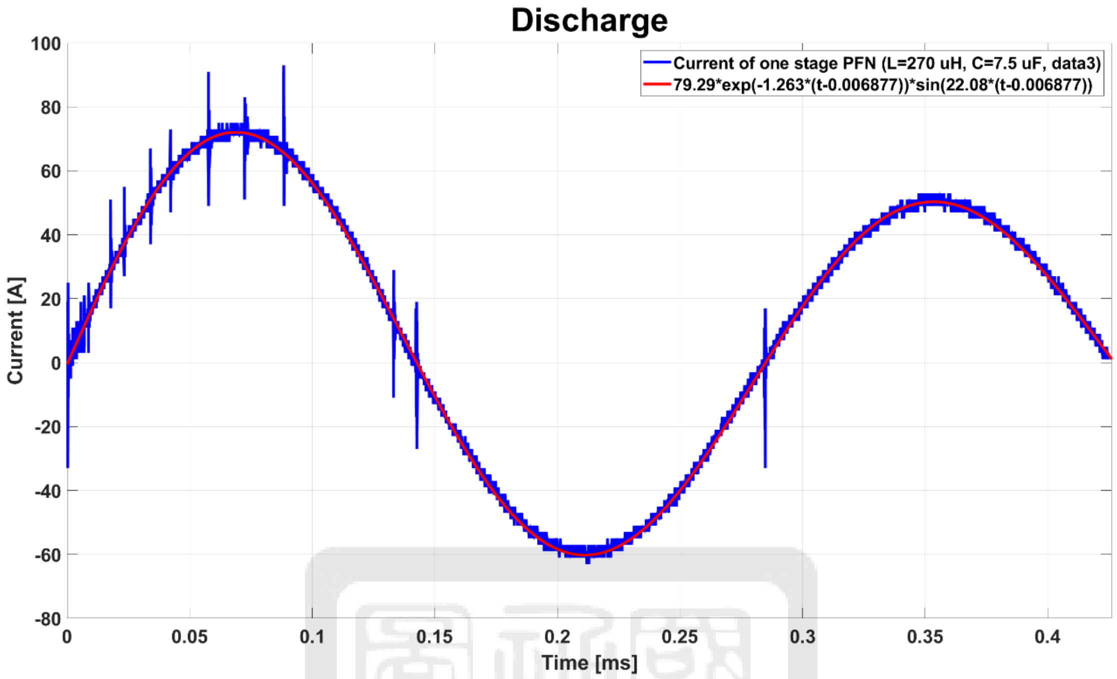
Discharge
Current of one stage PFN (L=270 uH, C=7.5 uF, data3)
79.29*exp(-1.263*(t-0.006877))*sin(22.08*(t-0.006877))
Current [A]
Time [ms]
100
80
60
40
20
0
-20
-40
-60
-80
0
0.05
0.1
0.15
0.2
0.25
0.3
0.35
0.4

Data 4

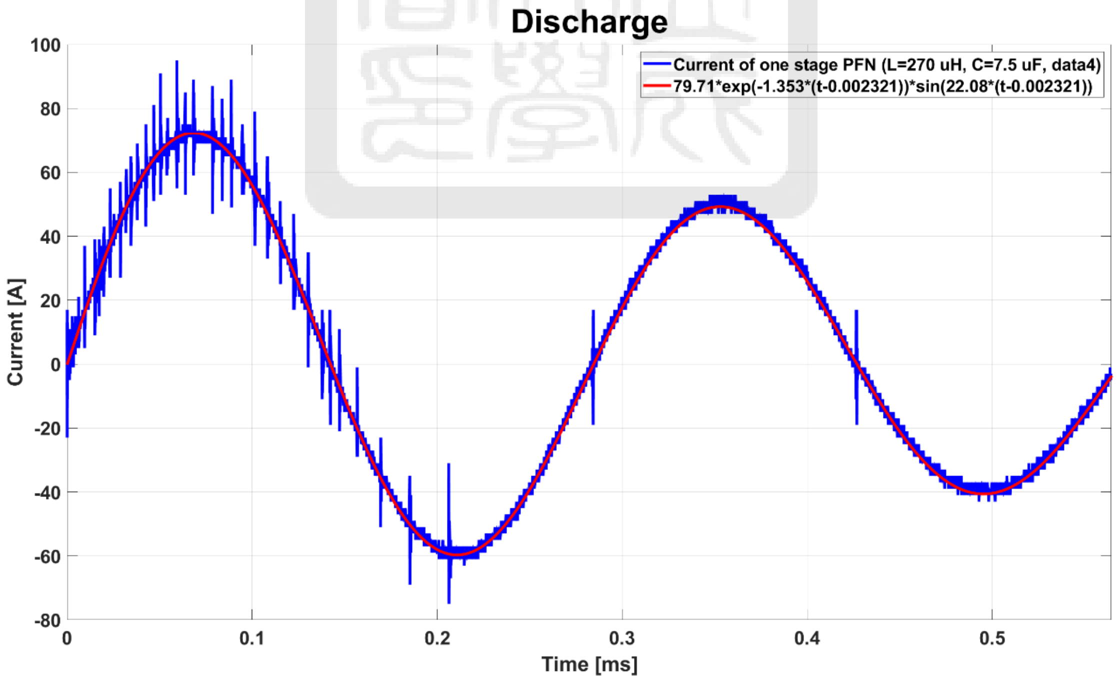
Discharge
Current of one stage PFN (L=270 uH, C=7.5 uF, data4)
79.71*exp(-1.353*(t-0.002321))*sin(22.08*(t-0.002321))
Current [A]
Time [ms]
100
80
60
40
20
0
-20
-40
-60
-80
0
0.1
0.2
0.3
0.4
0.5

Data 5

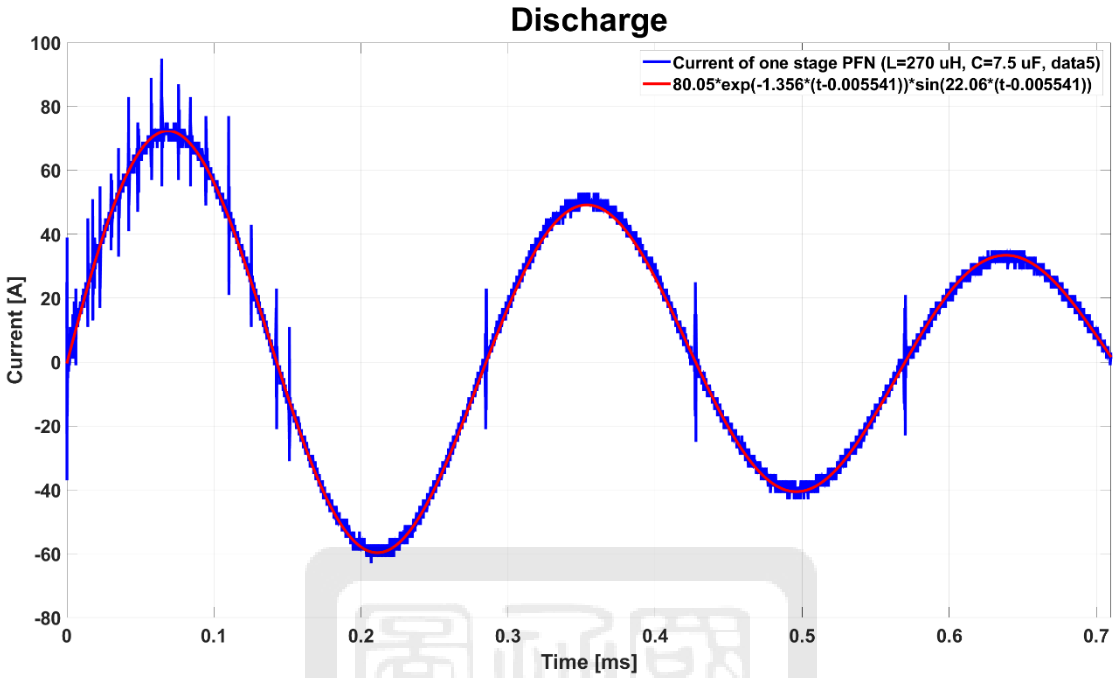
Discharge
Current of one stage PFN (L=270 uH, C=7.5 uF, data5)
80.05*exp(-1.356*(t-0.005541))*sin(22.06*(t-0.005541))
Current [A]
Time [ms]
100
80
60
40
20
0
-20
-40
-60
-80
0
0.1
0.2
0.3
0.4
0.5
0.6
0.7

Data 6

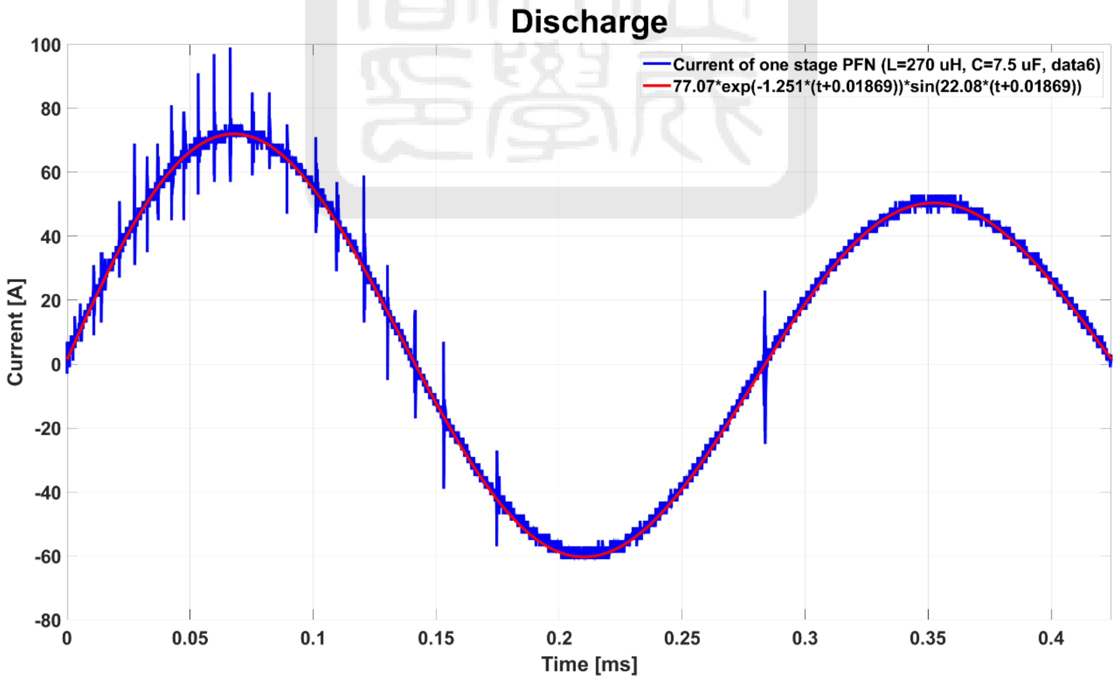
Discharge
Current of one stage PFN (L=270 uH, C=7.5 uF, data6)
77.07*exp(-1.251*(t+0.01869))*sin(22.08*(t+0.01869))
Current [A]
Time [ms]
100
80
60
40
20
0
-20
-40
-60
-80
0
0.05
0.1
0.15
0.2
0.25
0.3
0.35
0.4

Data 7

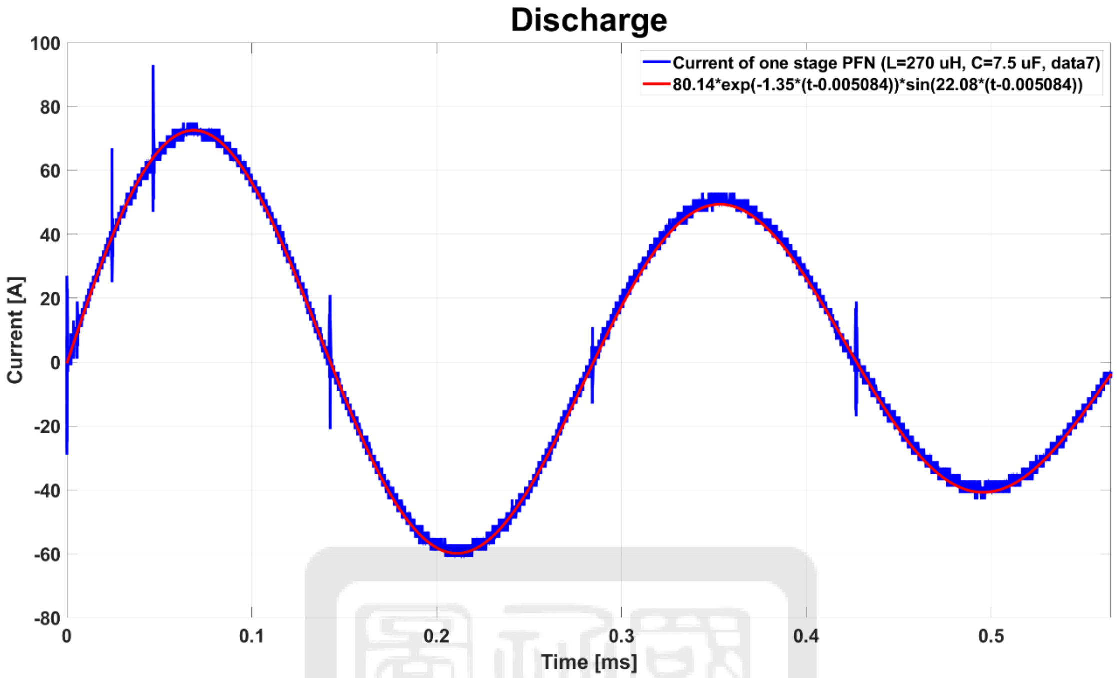

Discharge
Current of one stage PFN (L=270 uH, C=7.5 uF, data7)
80.14*exp(-1.35*(t-0.005084))*sin(22.08*(t-0.005084))
Current [A]
Time [ms]
100
80
60
40
20
0
-20
-40
-60
-80
0
0.1
0.2
0.3
0.4
0.5

Data 8

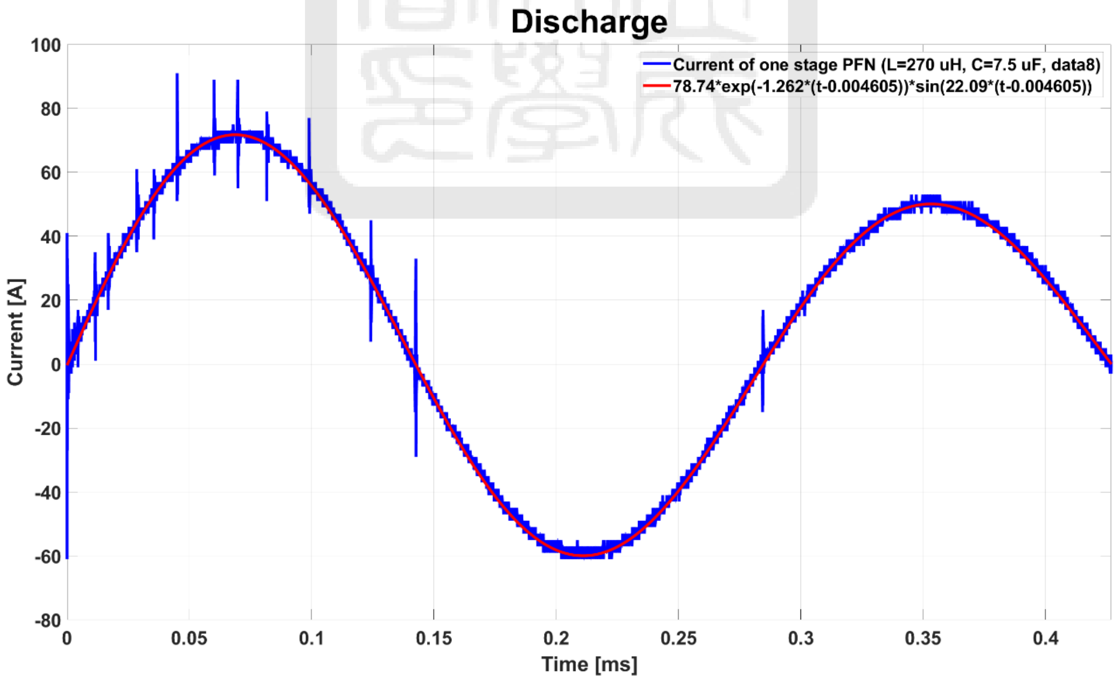

Discharge
Current of one stage PFN (L=270 uH, C=7.5 uF, data8)
78.74*exp(-1.262*(t-0.004605))*sin(22.09*(t-0.004605))
Current [A]
Time [ms]
100
80
60
40
20
0
-20
-40
-60
-80
0
0.05
0.1
0.15
0.2
0.25
0.3
0.35
0.4

Data 9

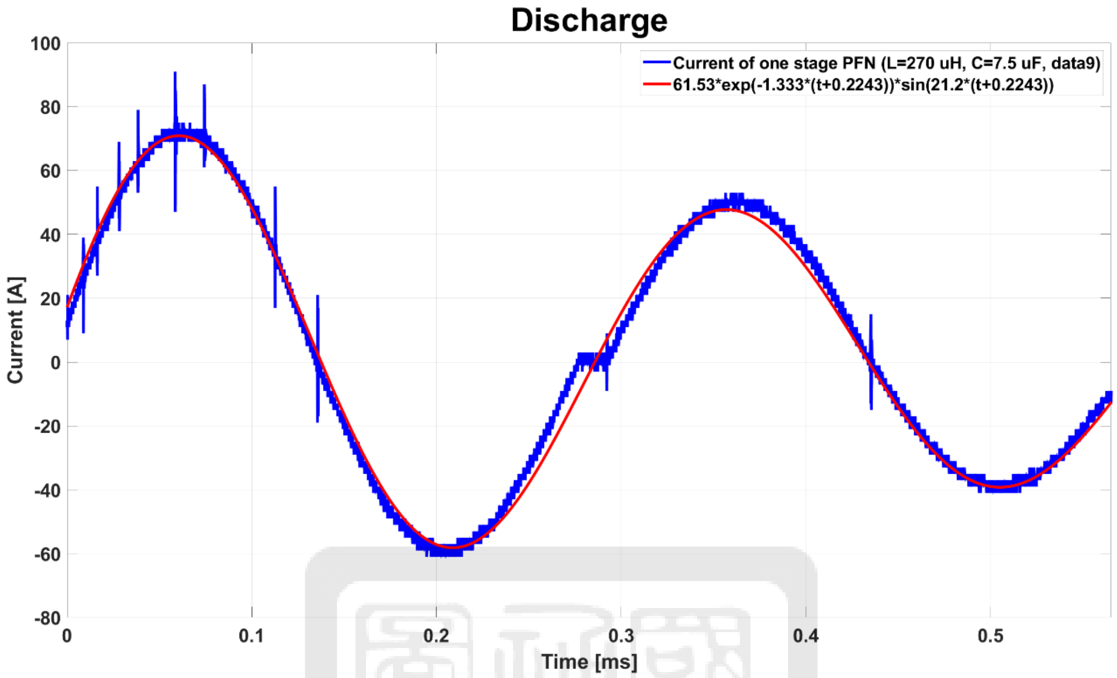

Data 10

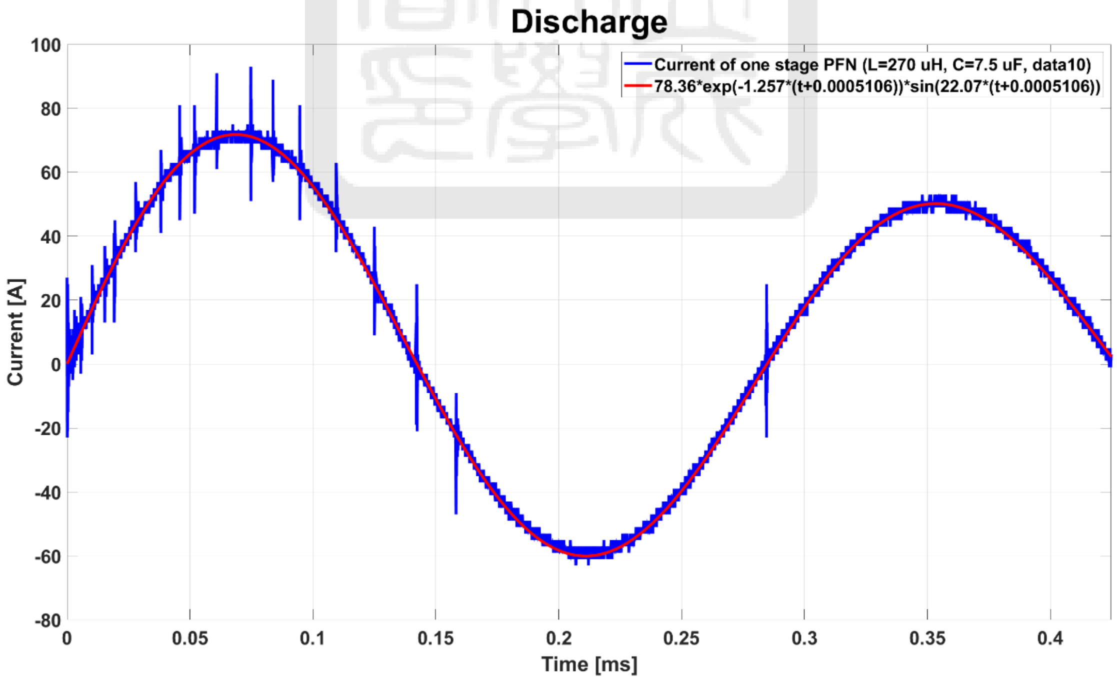

A 3.6 The result of PFN discharge test

Data 1

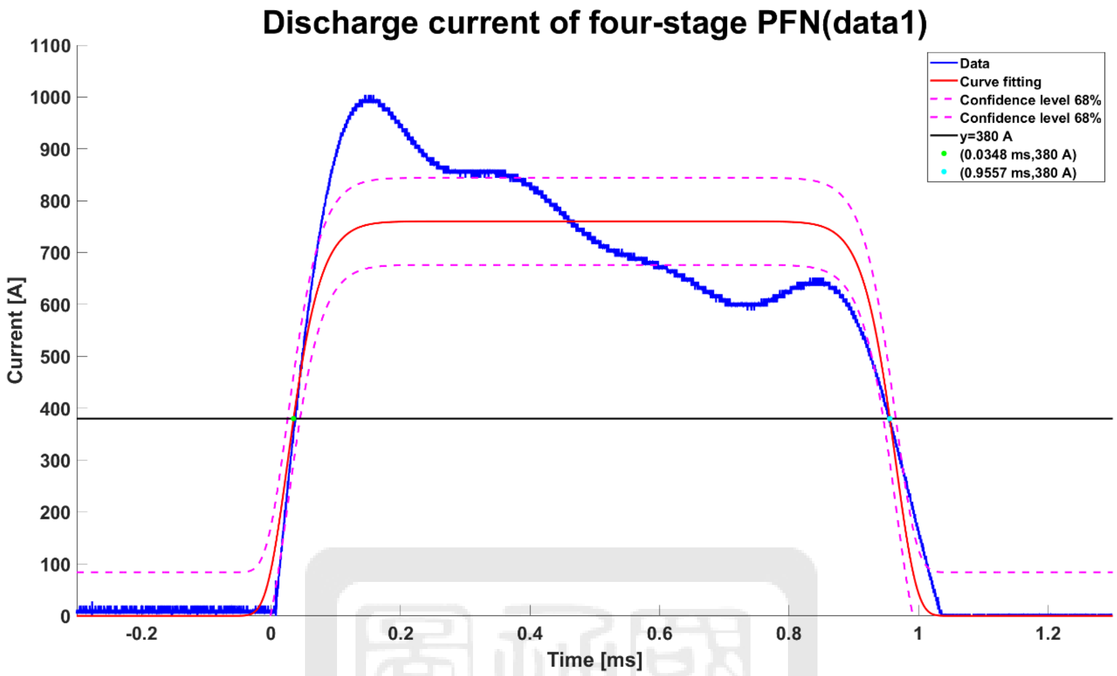

Data 2

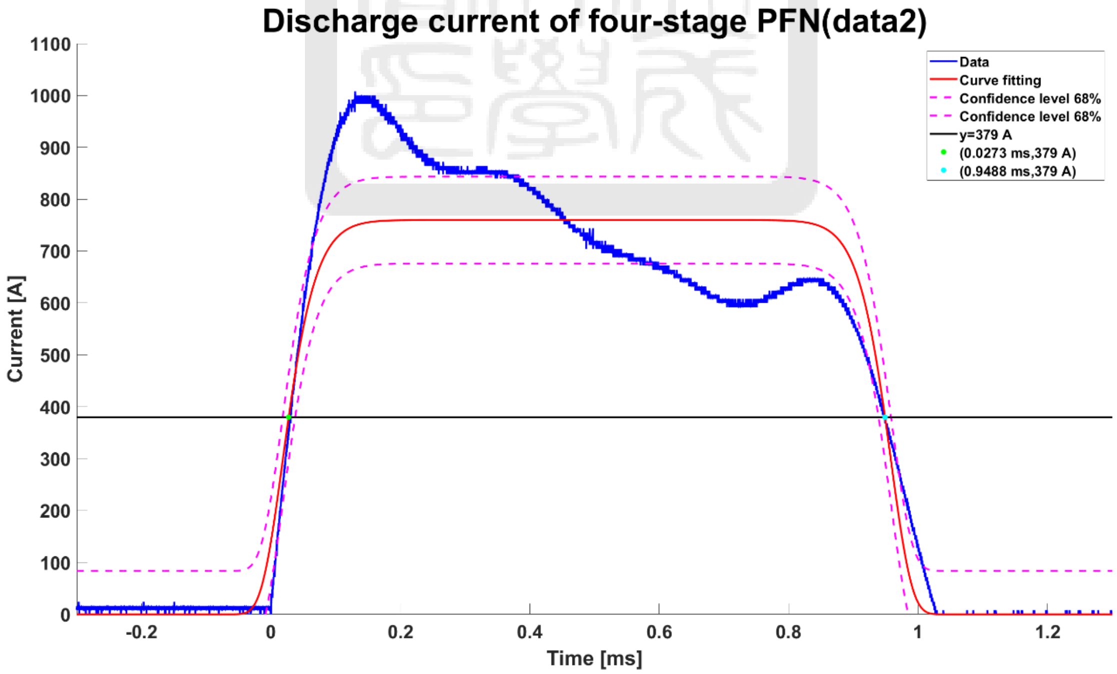

Data 3

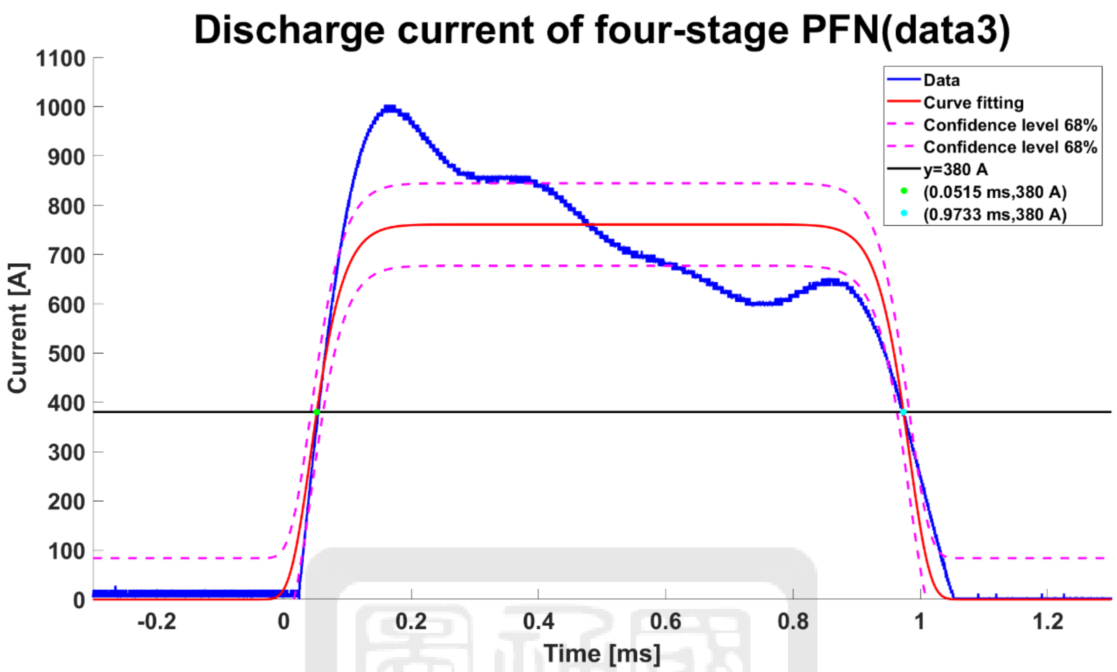

Discharge current of four-stage PFN(data3)
Data
Curve fitting
Confidence level 68%
Confidence level 68%
y=380 A
(0.0515 ms,380 A)
(0.9733 ms,380 A)
Current [A]
Time [ms]
1100
1000
900
800
700
600
500
400
300
200
100
0
-0.2
0
0.2
0.4
0.6
0.8
1
1.2

Data 4

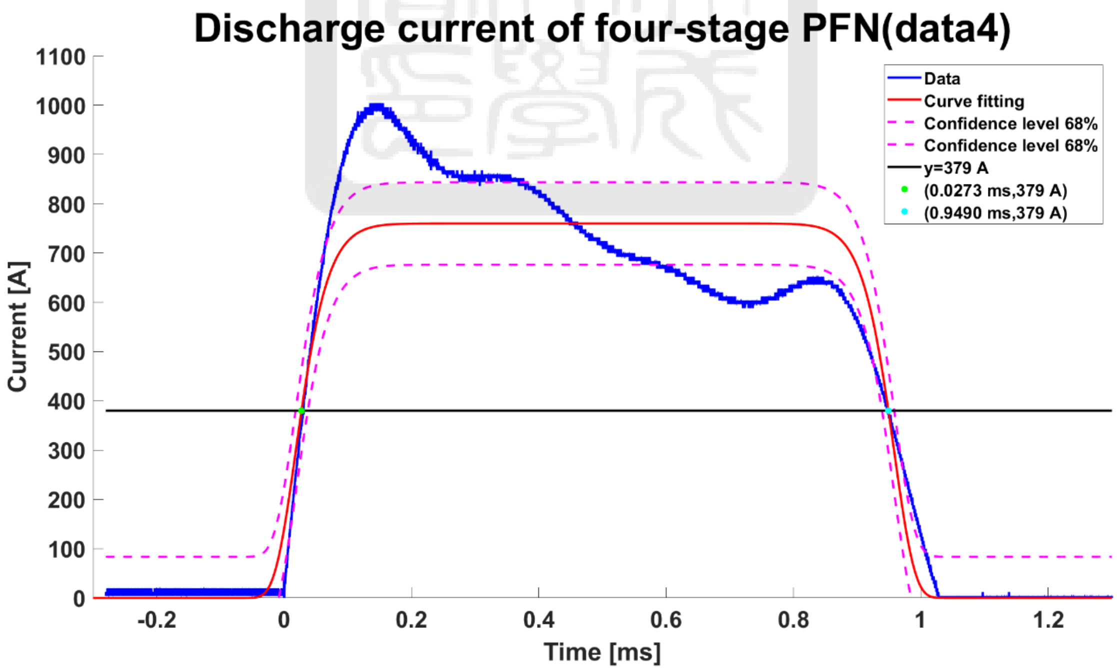

Discharge current of four-stage PFN(data4)
Data
Curve fitting
Confidence level 68%
Confidence level 68%
y=379 A
(0.0273 ms,379 A)
(0.9490 ms,379 A)
Current [A]
Time [ms]
1100
1000
900
800
700
600
500
400
300
200
100
0
-0.2
0
0.2
0.4
0.6
0.8
1
1.2

Data 5

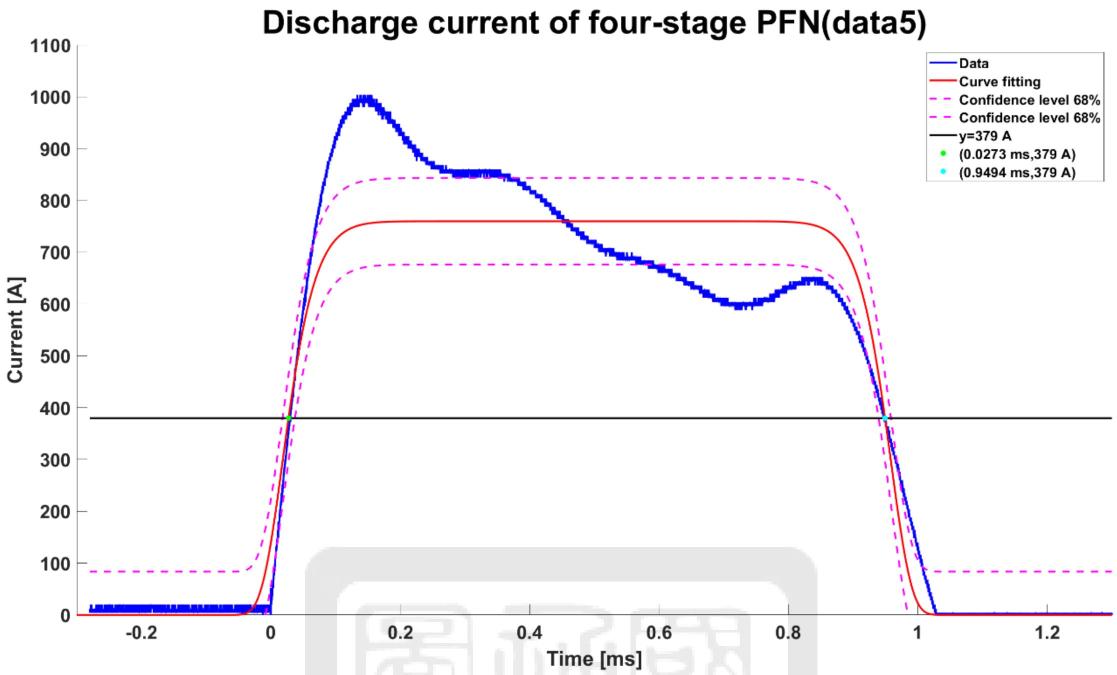
Discharge current of four-stage PFN(data5)
Current [A]
Time [ms]
Data
Curve fitting
Confidence level 68%
Confidence level 68%
y=379 A
(0.0273 ms,379 A)
(0.9494 ms,379 A)
0
100
200
300
400
500
600
700
800
900
1000
1100
-0.2
0
0.2
0.4
0.6
0.8
1
1.2

Data 6

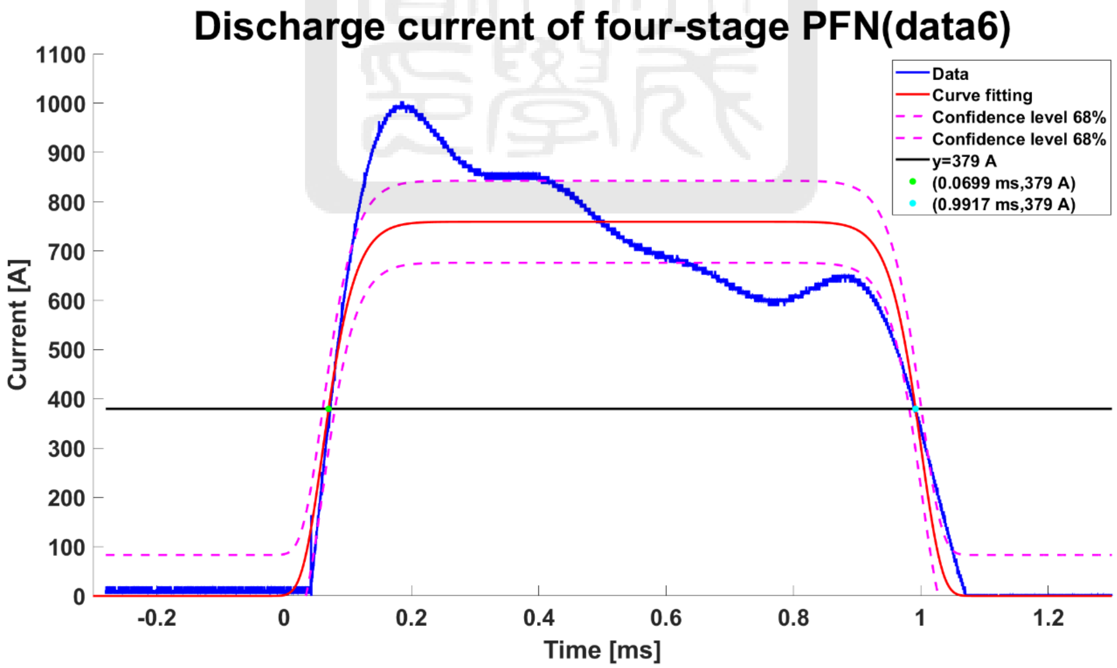
Discharge current of four-stage PFN(data6)
Current [A]
Time [ms]
Data
Curve fitting
Confidence level 68%
Confidence level 68%
y=379 A
(0.0699 ms,379 A)
(0.9917 ms,379 A)
0
100
200
300
400
500
600
700
800
900
1000
1100
-0.2
0
0.2
0.4
0.6
0.8
1
1.2

Data 7

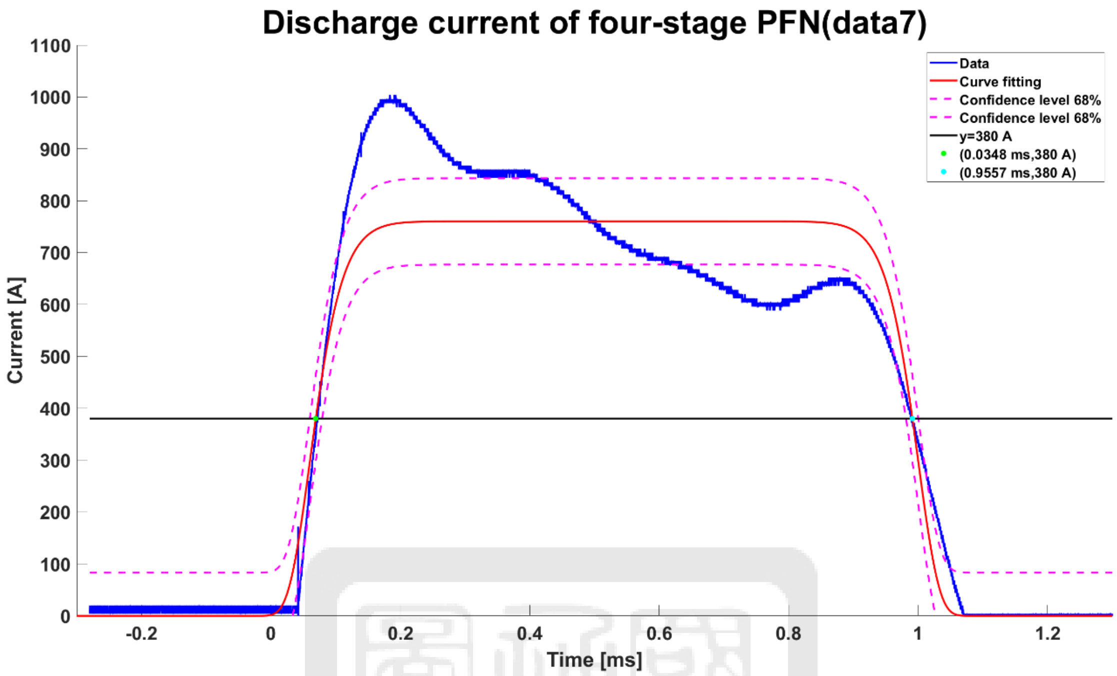

Discharge current of four-stage PFN(data7)
Data
Curve fitting
Confidence level 68%
Confidence level 68%
y=380 A
(0.0348 ms,380 A)
(0.9557 ms,380 A)
Current [A]
Time [ms]

Data 8

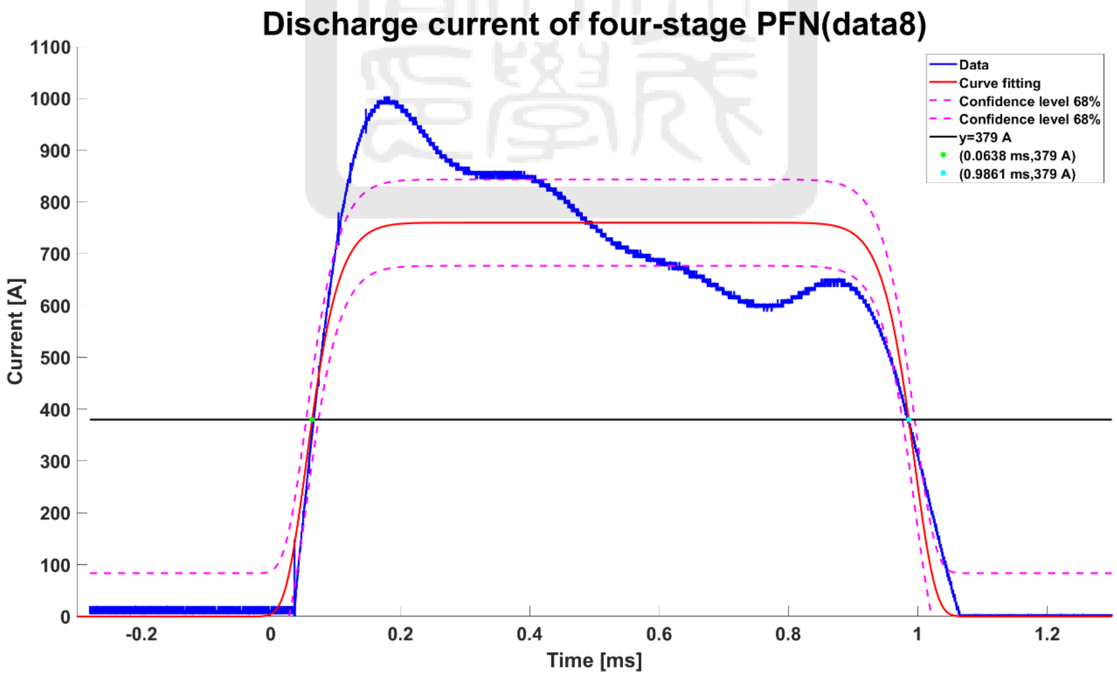

Discharge current of four-stage PFN(data8)
Data
Curve fitting
Confidence level 68%
Confidence level 68%
y=379 A
(0.0638 ms,379 A)
(0.9861 ms,379 A)
Current [A]
Time [ms]

Data 9

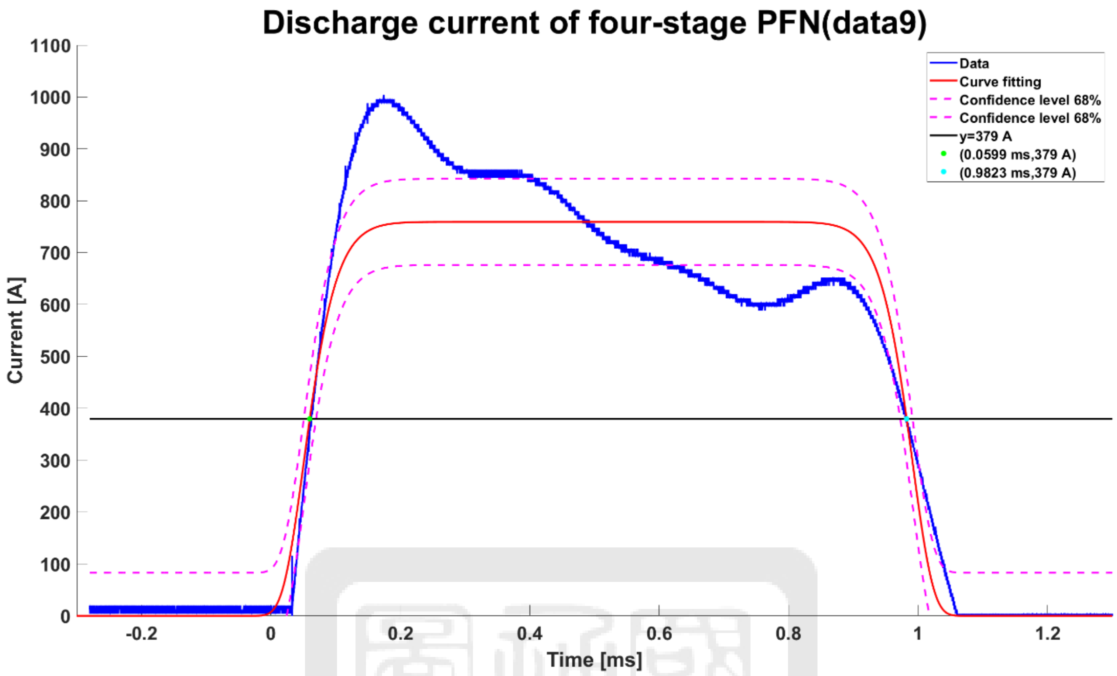

Data 10

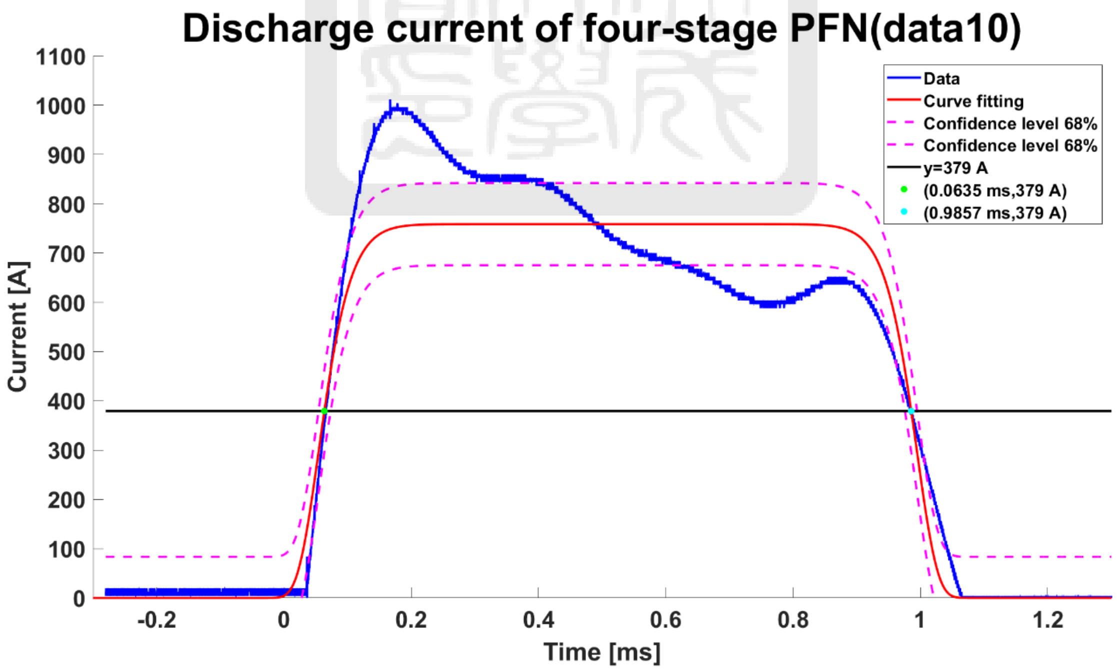

A 4.1 The drawing of the supports of toroidal magnetic field coils

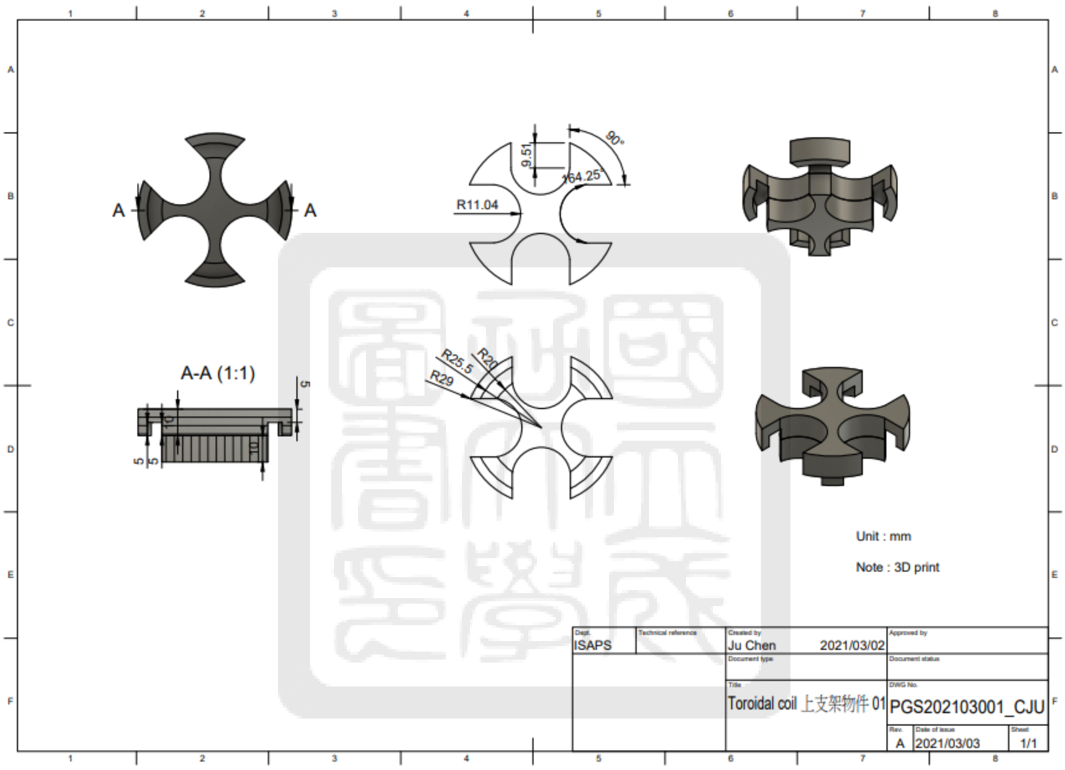

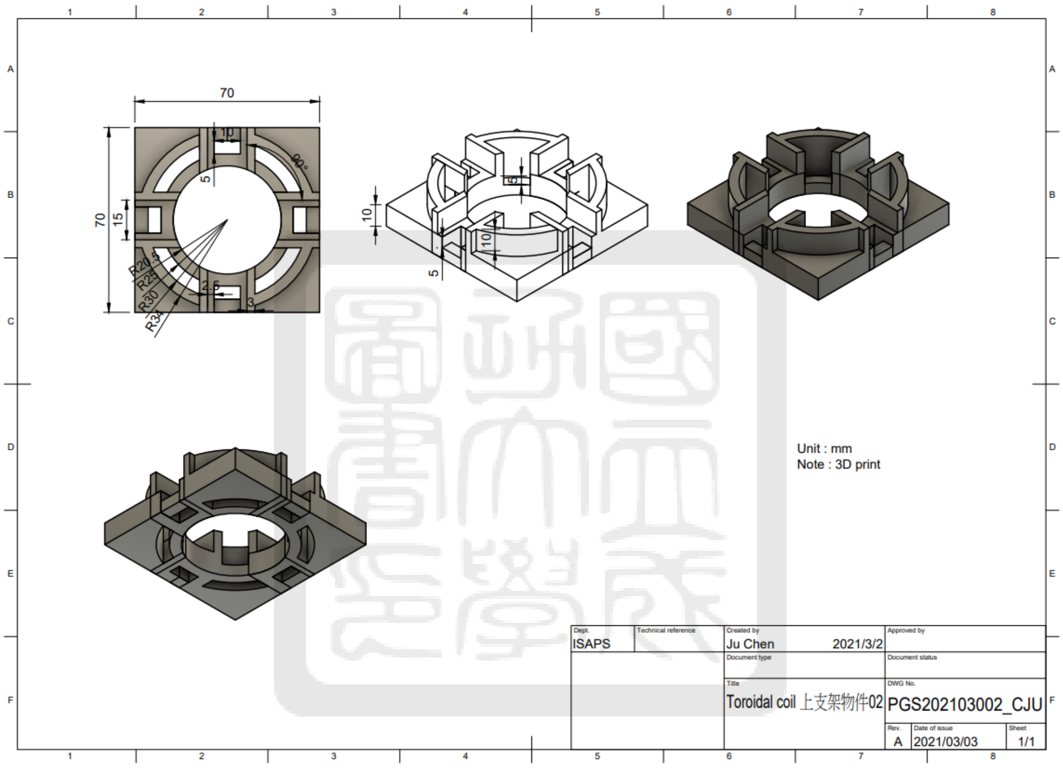
70
70
15
10
5
90°
R20.5
R25
R30
R34
2.5
3
10
5
10
10
Unit : mm
Note : 3D print
Dept.
ISAPS
Technical reference
Created by
Ju Chen
2021/3/2
Approved by
Document type
Document status
Title
Toroidal coil 上支架物件02
DWG No.
PGS202103002_CJU
Rev.
A
Date of issue
2021/03/03
Sheet
1/1

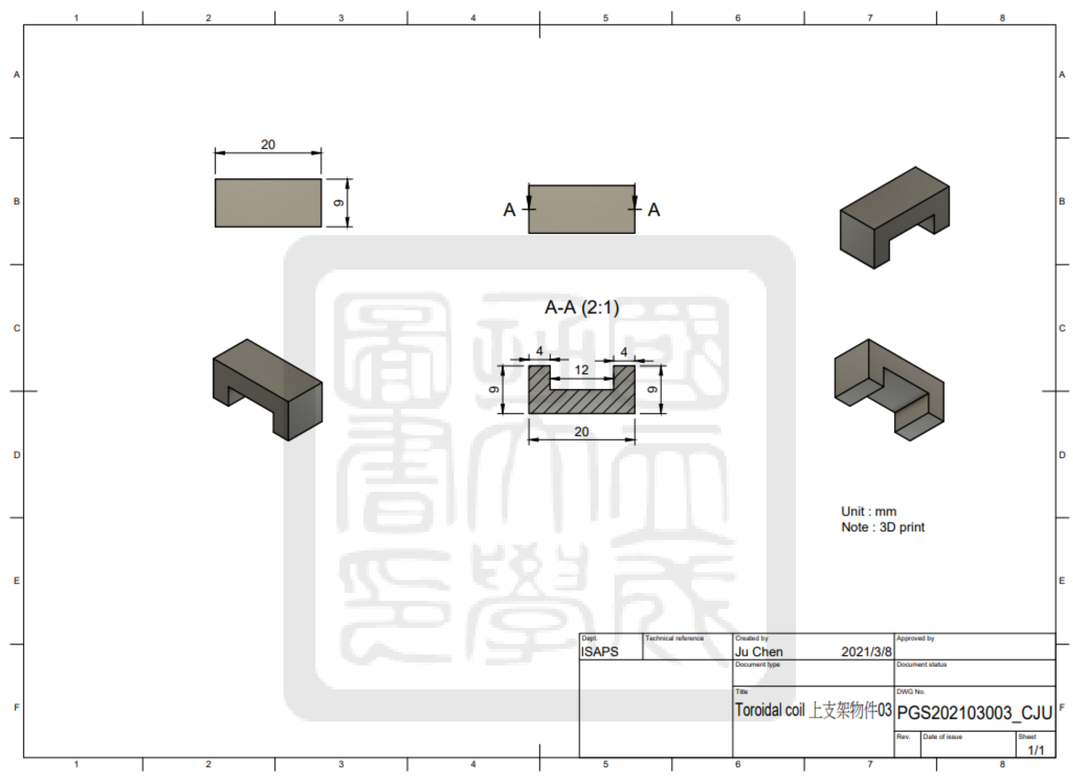
20
9
A
A
A-A (2:1)
4
12
4
9
9
20
Unit : mm
Note : 3D print
Dept.
ISAPS
Technical reference
Created by
Ju Chen
2021/3/8
Approved by
Document type
Document status
Title
Toroidal coil 上支架物件03
DWG No.
PGS202103003_CJU
Rev.
Date of issue
Sheet
1/1

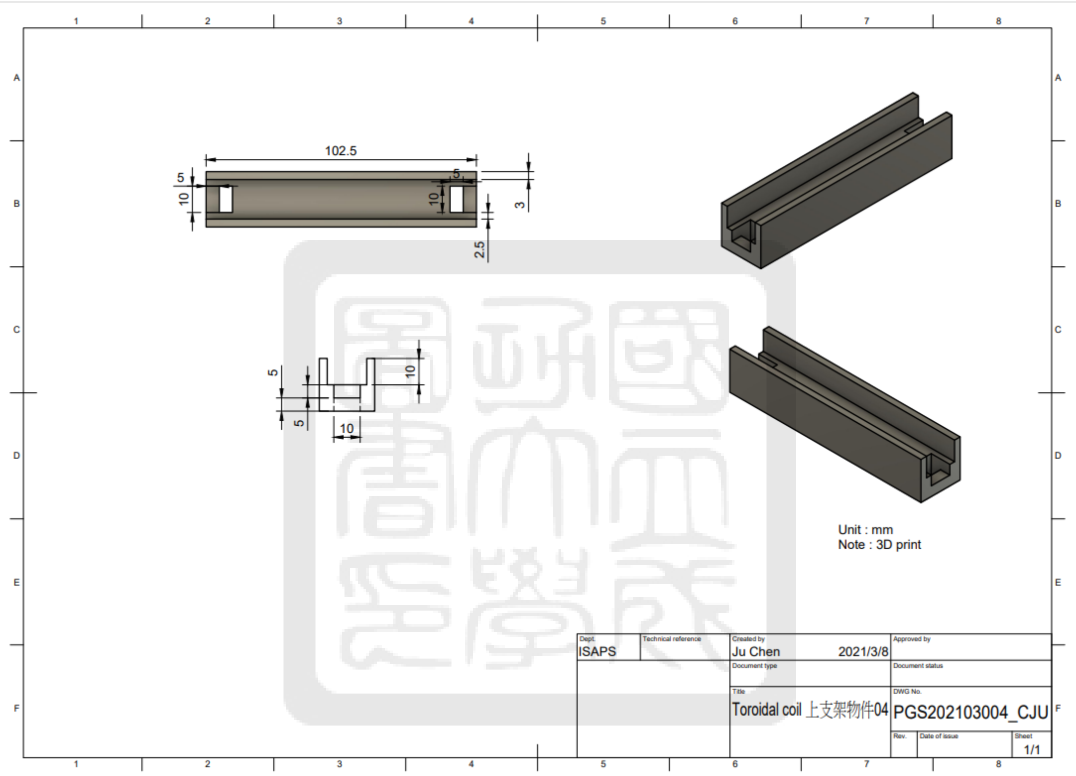
102.5
5
10
3
2.5
10
Unit : mm
Note : 3D print
Dept.
ISAPS
Technical reference
Created by
Ju Chen
2021/3/8
Approved by
Document type
Document status
Title
Toroidal coil 上支架物件04
DWG No.
PGS202103004_CJU
Rev.
Date of issue
Sheet
1/1

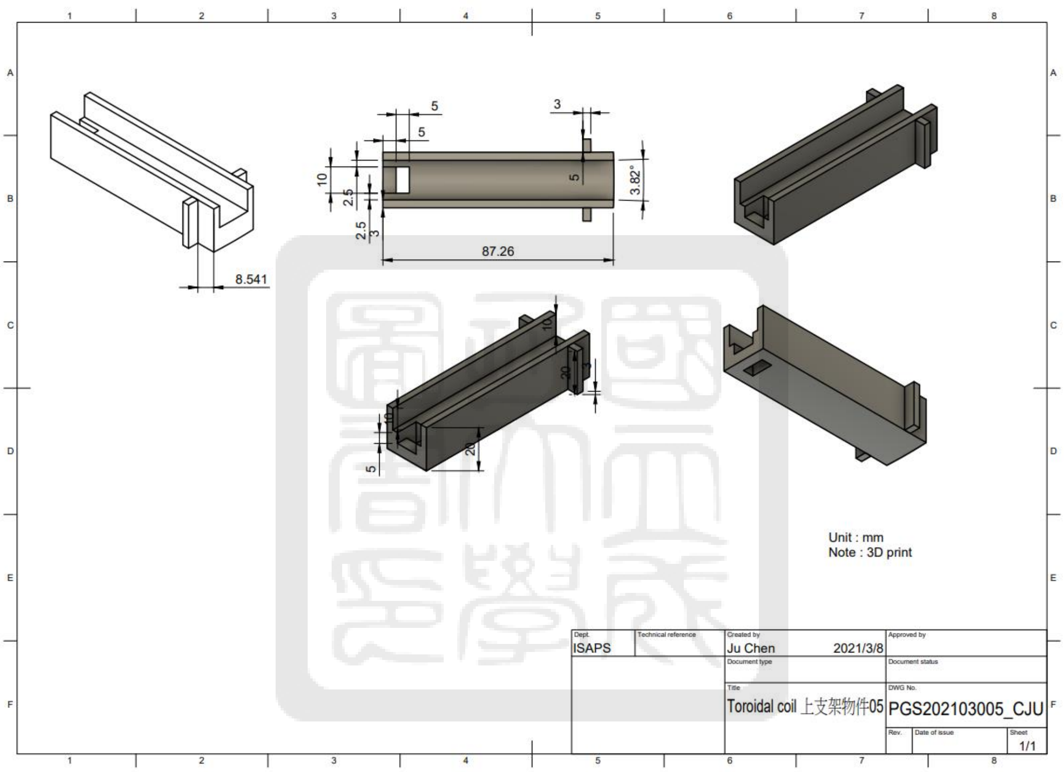

5
5
3
10
2.5
2.5
3
5
3.82°
87.26
8.541
10
20
20
10
5
Unit : mm
Note : 3D print
Dept.
ISAPS
Technical reference
Created by
Ju Chen
2021/3/8
Approved by
Document type
Document status
Title
Toroidal coil 上支架物件05
DWG No.
PGS202103005_CJU
Rev.
Date of issue
Sheet
1/1

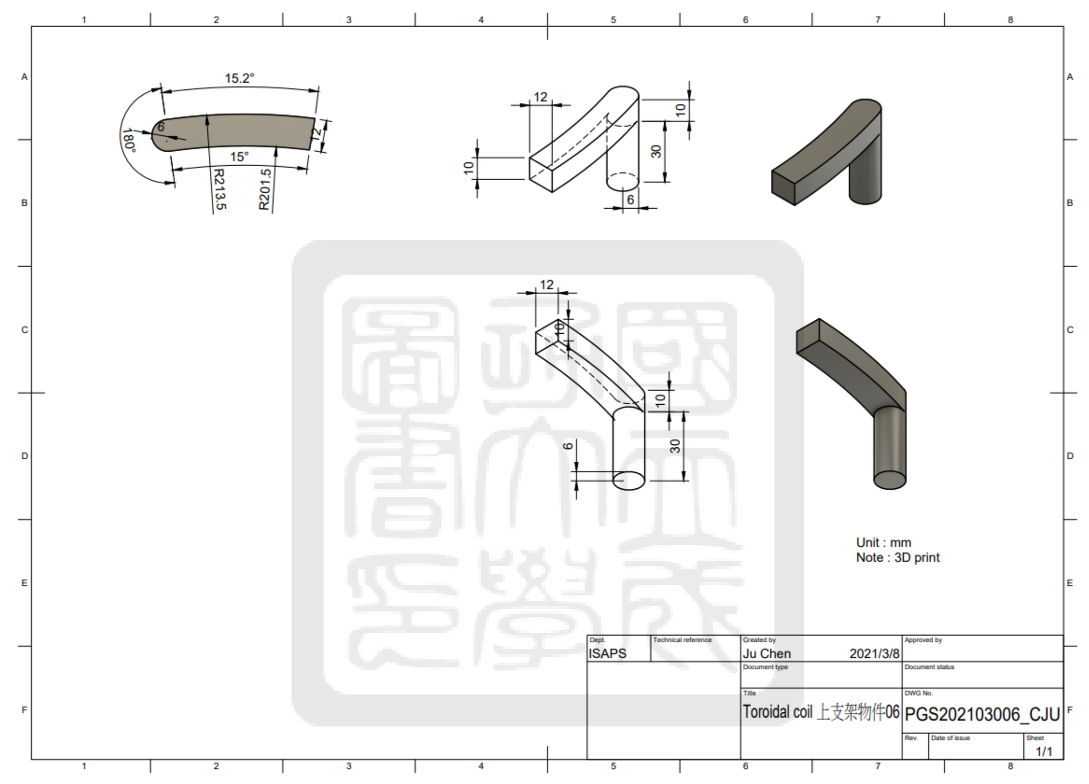
15.2°
180°
6
12
15°
R213.5
R201.5
12
10
10
30
6
12
10
10
6
30
Unit : mm
Note : 3D print
Dept.
ISAPS
Technical reference
Created by
Ju Chen
2021/3/8
Approved by
Document type
Document status
Title
Toroidal coil 上支架物件06
DWG No.
PGS202103006_CJU
Rev.
Date of issue
Sheet
1/1

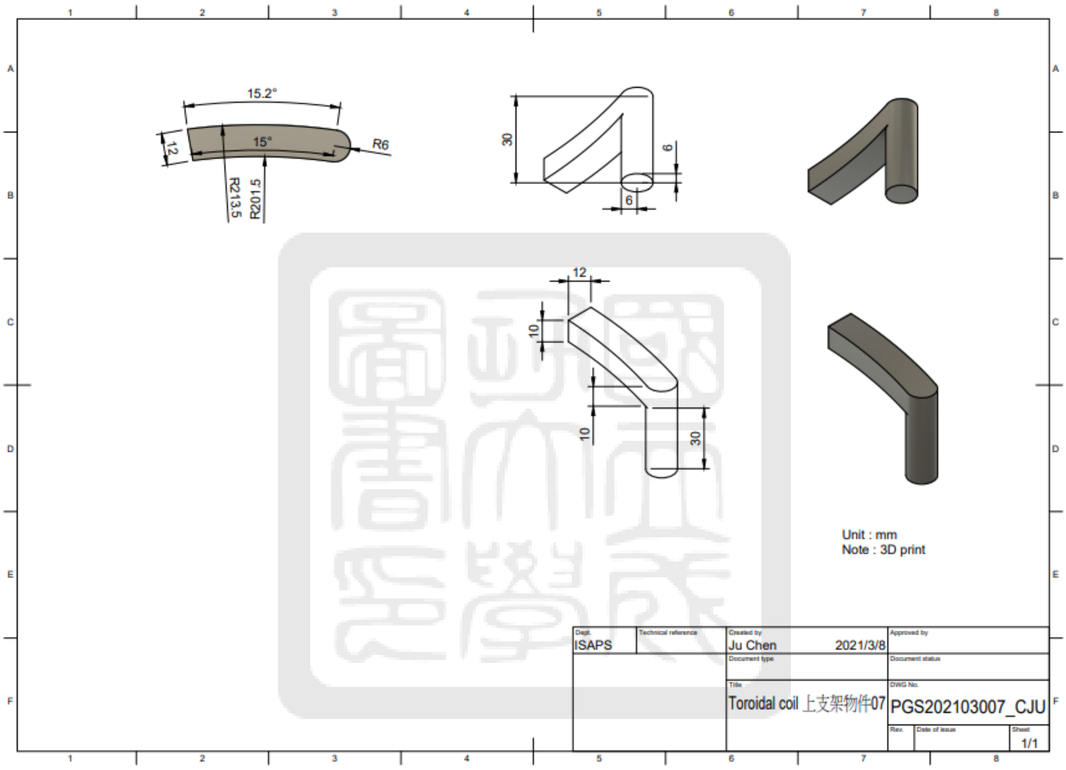
15.2°
15°
12
R6
R213.5
R201.5
30
6
6
12
10
10
30
Unit : mm
Note : 3D print
Dept.
ISAPS
Technical reference
Created by
Ju Chen
2021/3/8
Approved by
Document type
Document status
Title
Toroidal coil 上支架物件07
DWG No.
PGS202103007_CJU
Rev.
Date of issue
Sheet
1/1

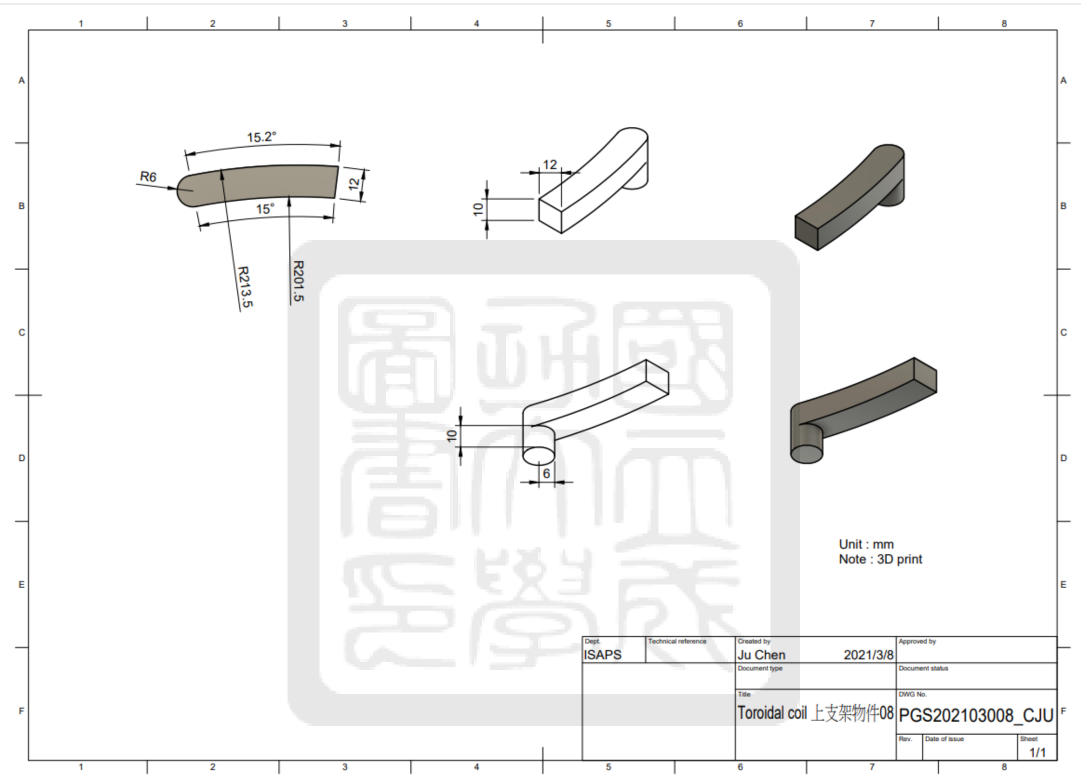
15.2°
R6
12
15°
R213.5
R201.5
12
10
10
6
Unit : mm
Note : 3D print
Dept.
ISAPS
Technical reference
Created by
Ju Chen
2021/3/8
Approved by
Document type
Document status
Title
Toroidal coil 上支架物件08
DWG No.
PGS202103008_CJU
Rev.
Date of issue
Sheet
1/1

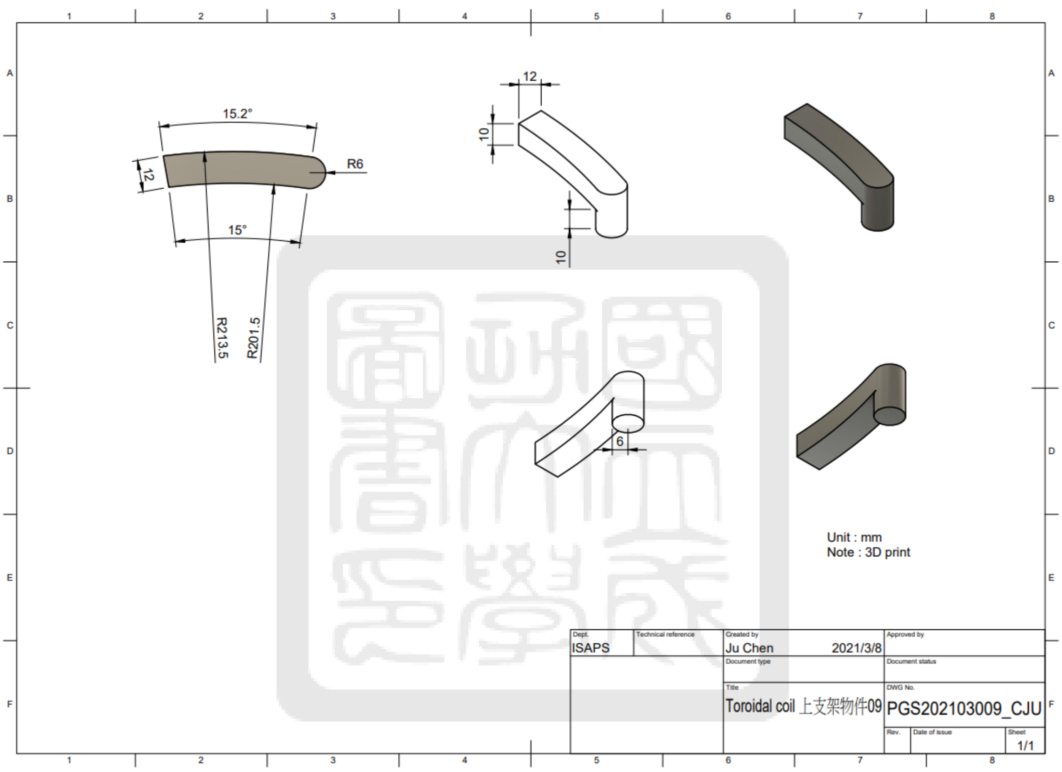
15.2°
12
R6
15°
R213.5
R201.5
12
10
10
6
Unit : mm
Note : 3D print
Dept.
ISAPS
Technical reference
Created by
Ju Chen
2021/3/8
Approved by
Document type
Document status
Title
Toroidal coil 上支架物件09
DWG No.
PGS202103009_CJU
Rev.
Date of issue
Sheet
1/1

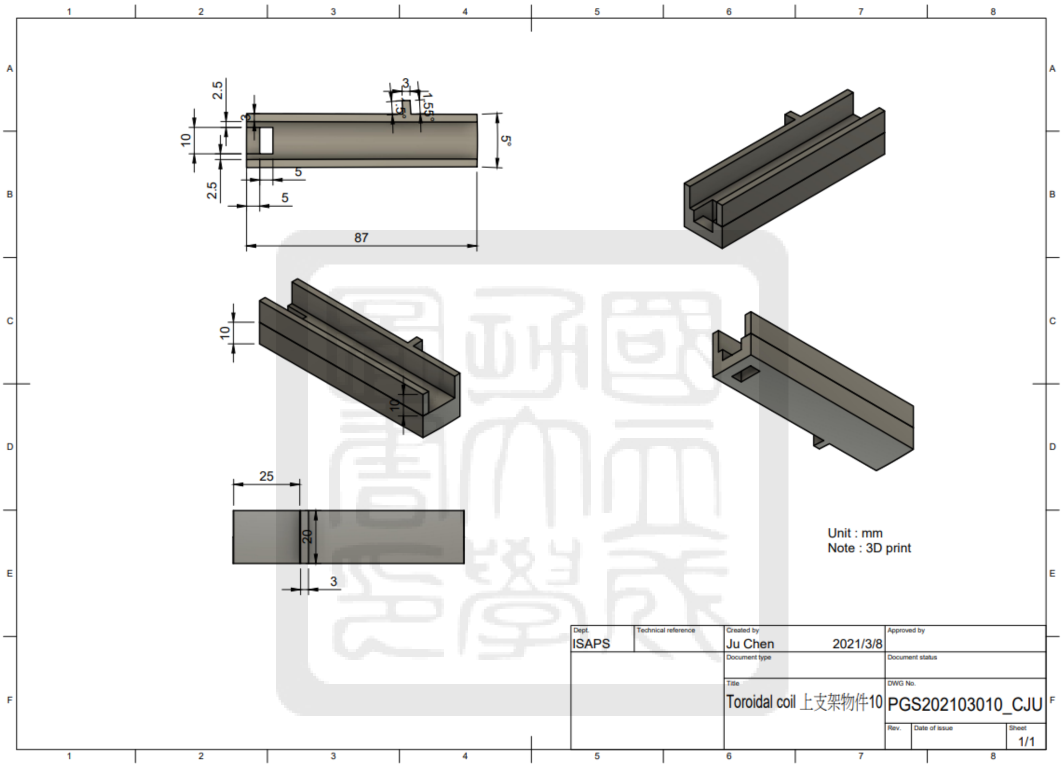
2.5
10
2.5
5
5
87
3
1.55
5°
10
10
25
20
3
Unit : mm
Note : 3D print
Dept.
ISAPS
Technical reference
Created by
Ju Chen
2021/3/8
Approved by
Document type
Document status
Title
Toroidal coil 上支架物件10
DWG No.
PGS202103010_CJU
Rev.
Date of issue
Sheet
1/1

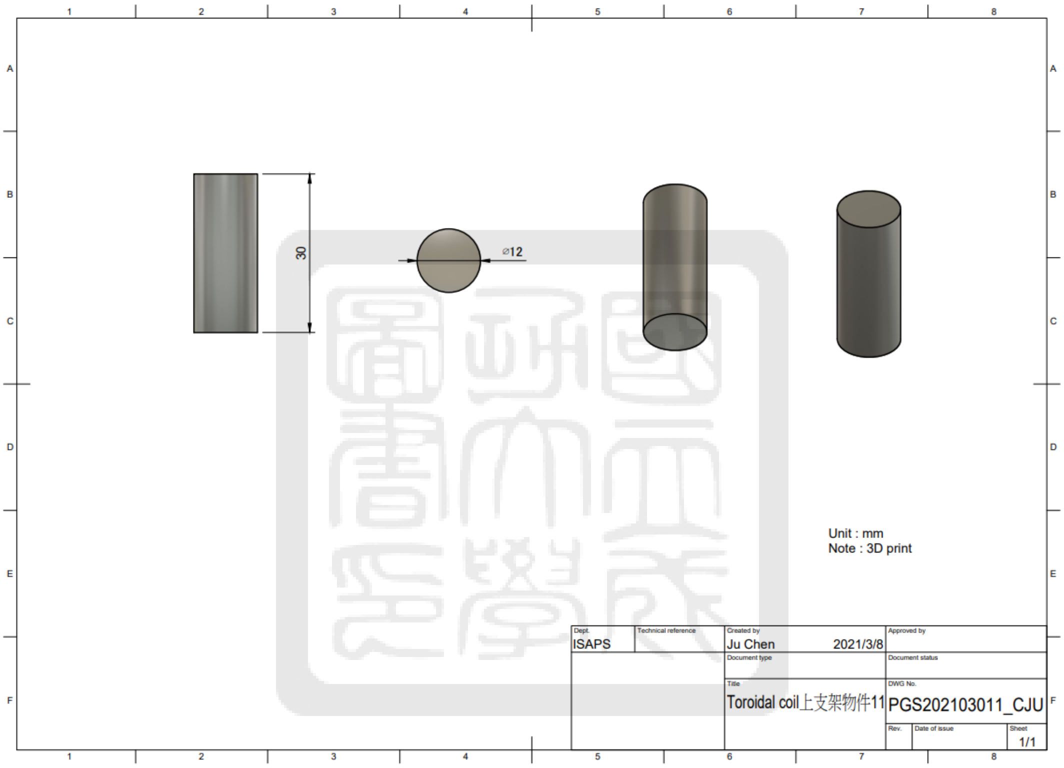

30
⌀12
Unit : mm
Note : 3D print
Dept.
ISAPS
Technical reference
Created by
Ju Chen
2021/3/8
Approved by
Document type
Document status
Title
Toroidal coil上支架物件11
DWG No.
PGS202103011_CJU
Rev.
Date of issue
Sheet
1/1

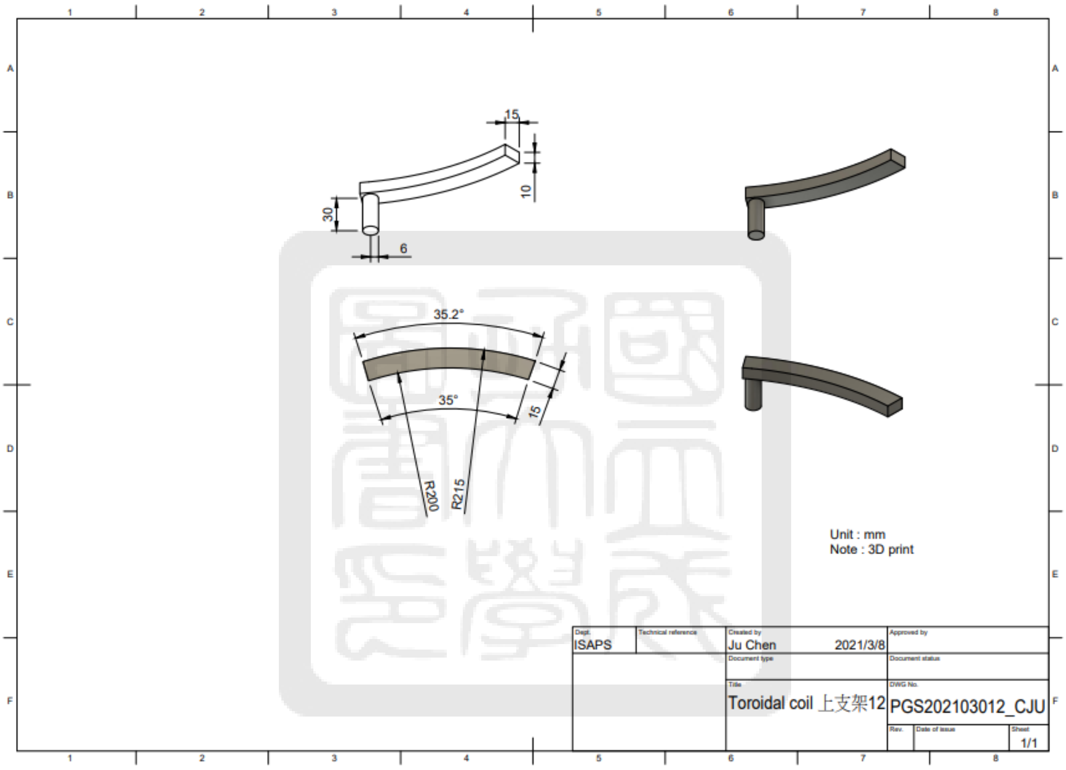
15
10
30
6
35.2°
35°
15
R200
R215
Unit : mm
Note : 3D print
Dept.
ISAPS
Technical reference
Created by
Ju Chen
2021/3/8
Approved by
Document type
Document status
Title
Toroidal coil 上支架12
DWG No.
PGS202103012_CJU
Rev.
Date of issue
Sheet
1/1

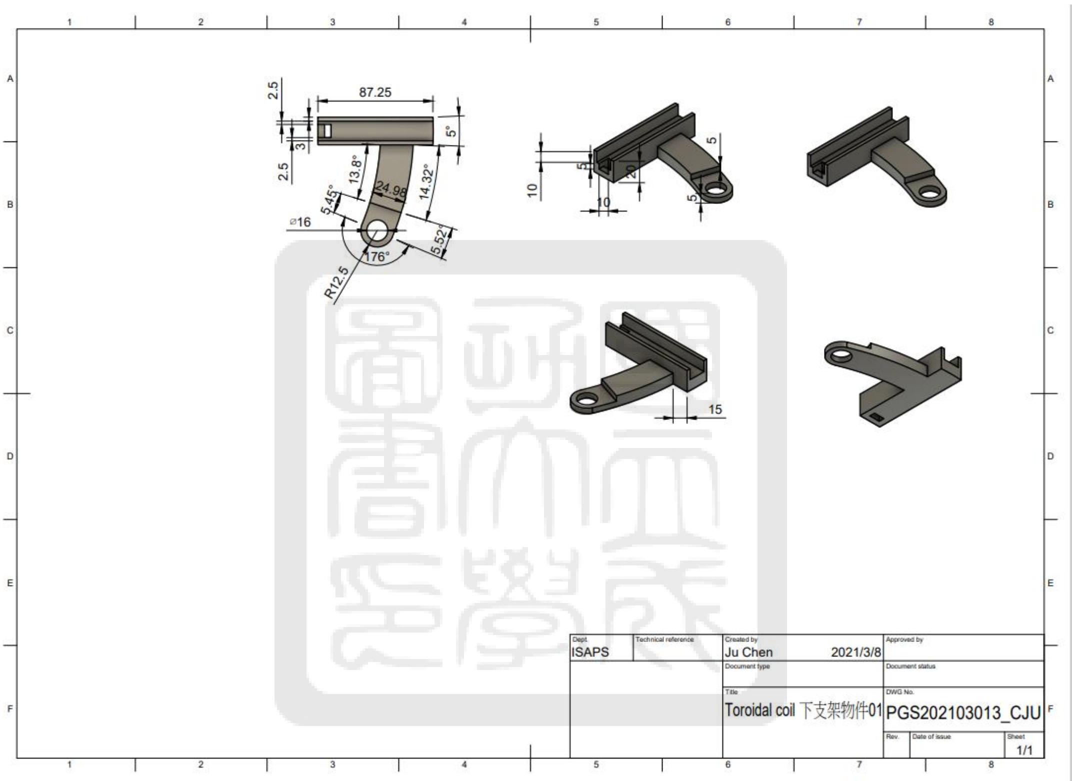

87.25
2.5
3
2.5
5°
13.8°
14.32°
5.45°
24.98
⌀16
5.52°
176°
R12.5
10
5
20
10
5
5
15
Dept.
ISAPS
Technical reference
Created by
Ju Chen
2021/3/8
Approved by
Document type
Document status
Title
Toroidal coil 下支架物件01
DWG No.
PGS202103013_CJU
Rev.
Date of issue
Sheet
1/1

A 4.2 The process to use the 3D printer

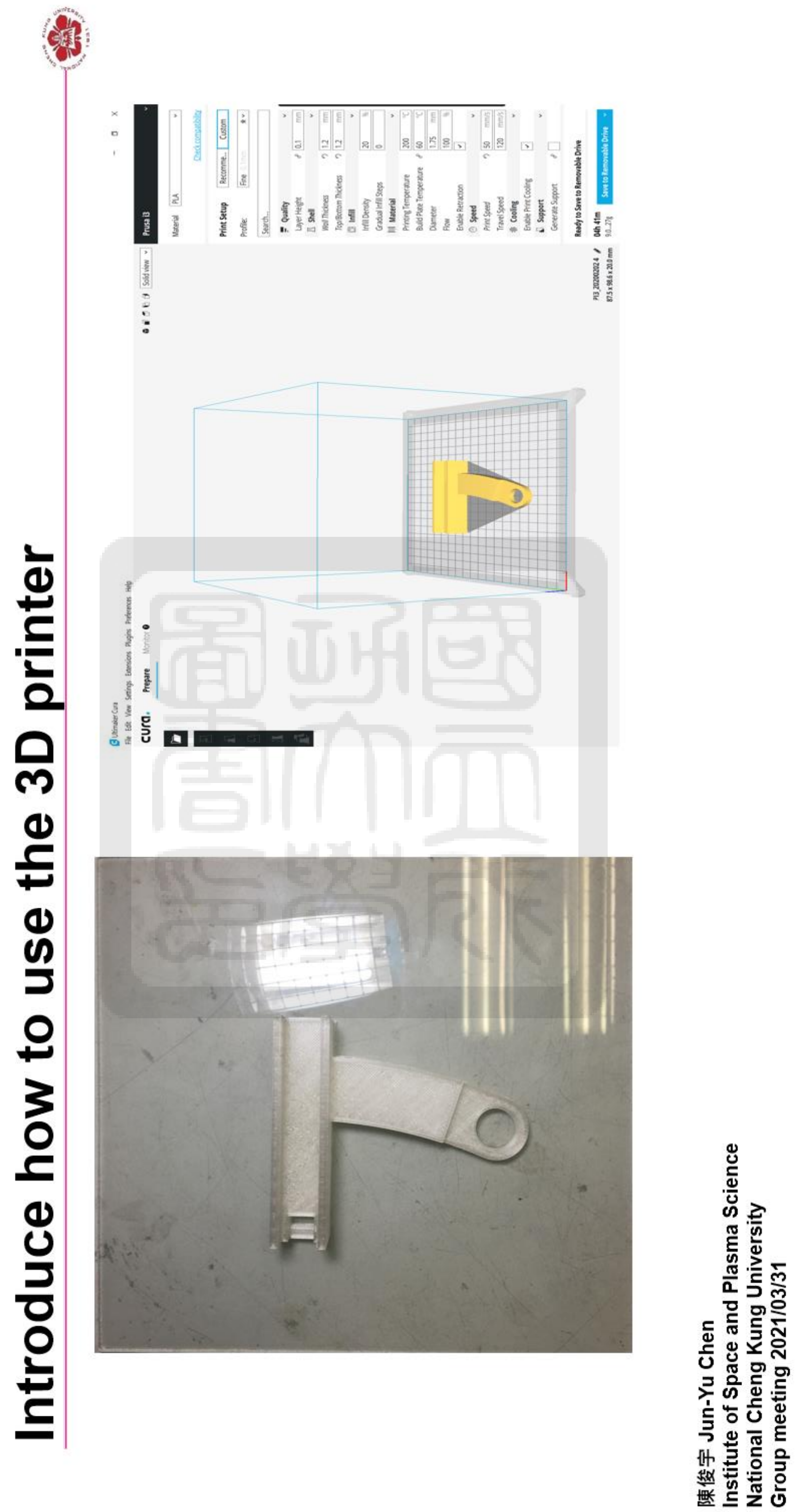

Process of printing

Software (Cura)

Click cura
↓
Select 3D printer model
↓
Choose material APL
↓
Adjust printing parameters
↓
Open 3D object file (stl file)
↓
Insert SD card
↓
Output the file

Hardware (3D printer)

Insert SD card
↓
Place the appropriate weight of material APL
↓
Warm up the 3D printer
↓
Select the file of print
↓
Print

Software interface introduction (Software)

1. Click on ultimaker cura

2. The file of 3D printed

3. Move the print object

4. The table of put the 3D printed object

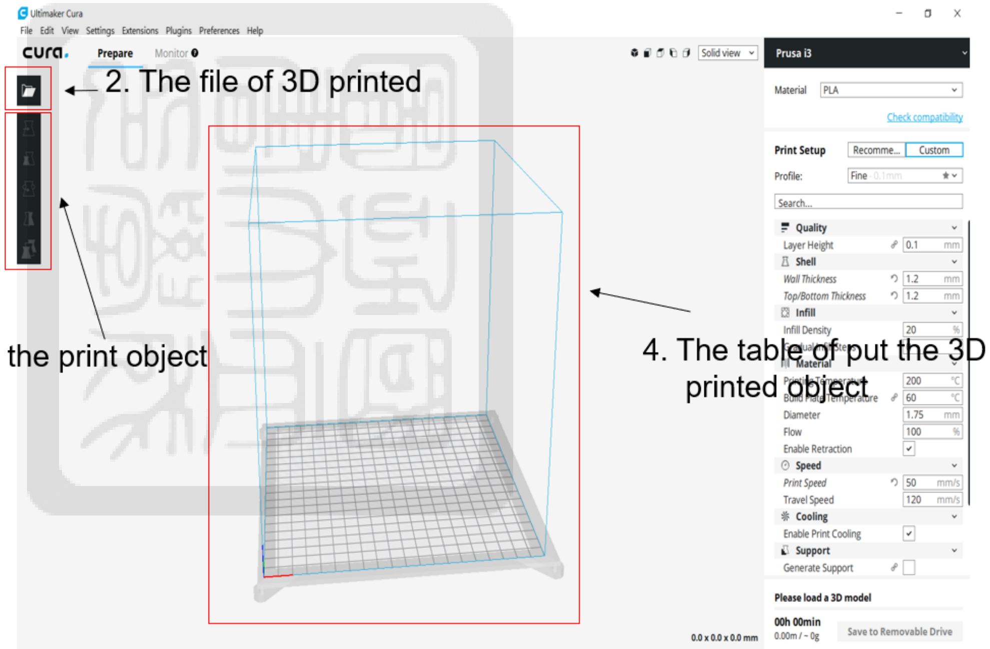

Software interface introduction

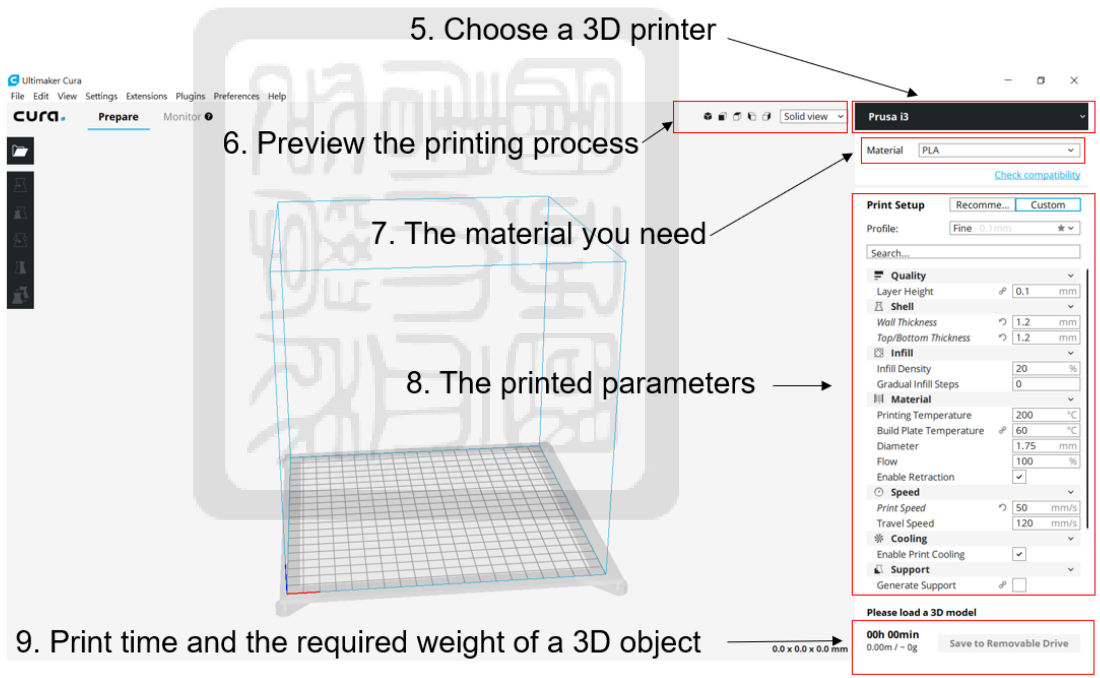

Select object of print

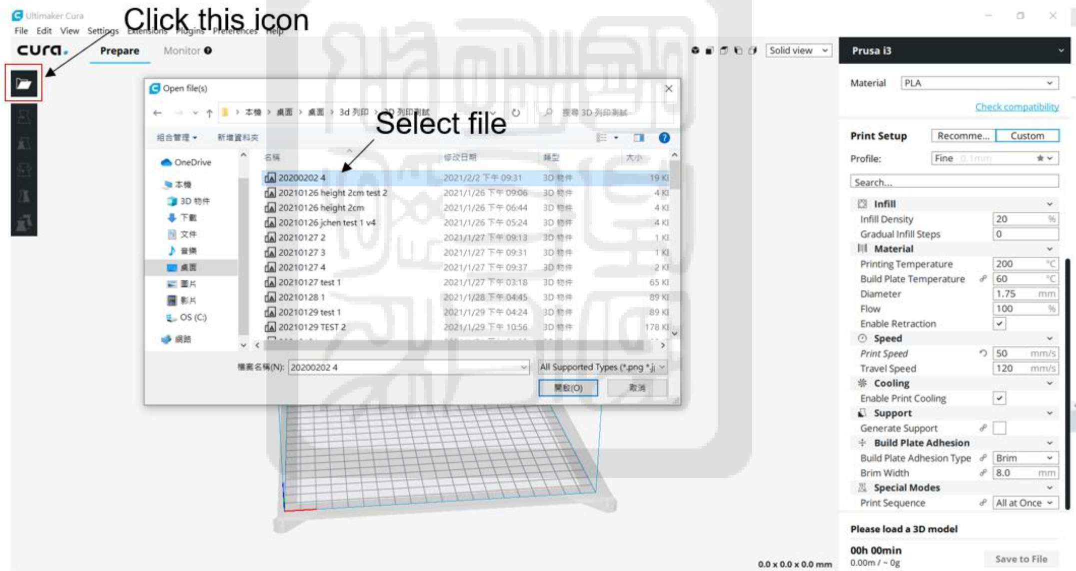

Confirm that the file can be printed

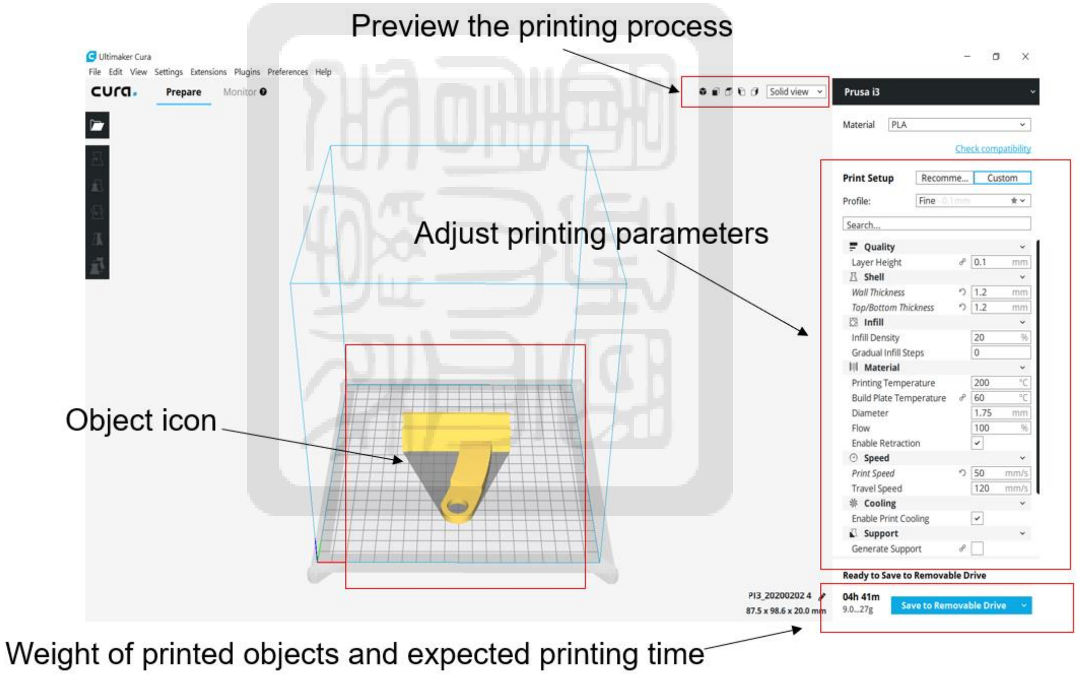

Insert card reader

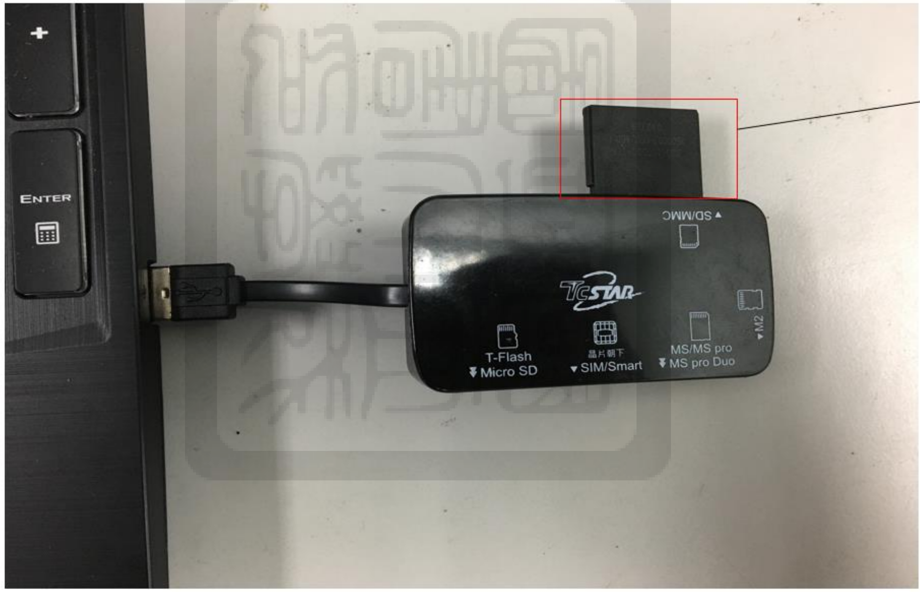

SD card

Output file

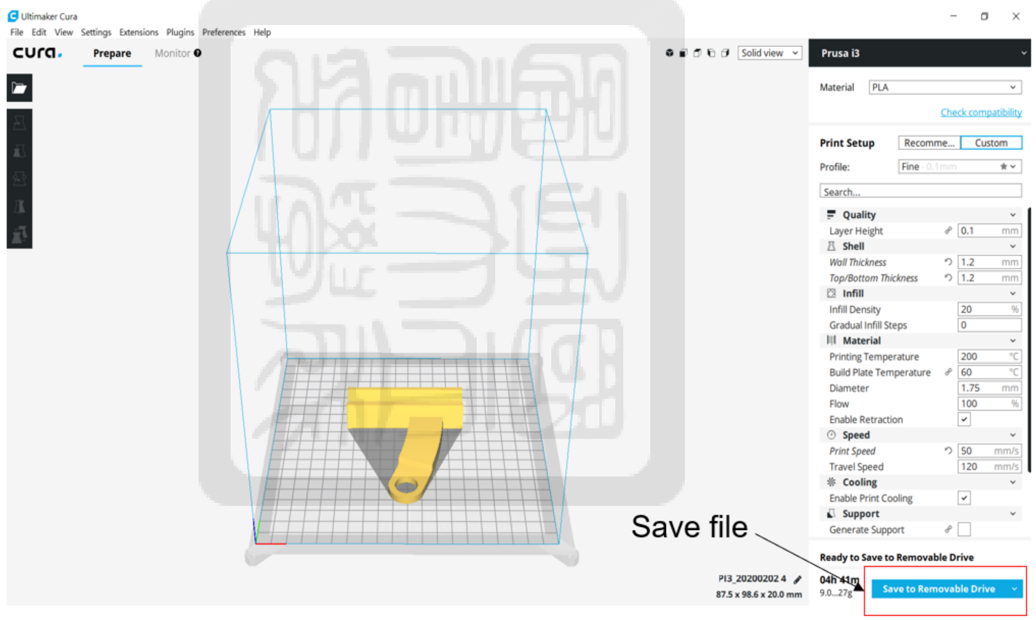

Ultimaker Cura
File Edit View Settings Extensions Plugins Preferences Help
cura.
Prepare
Monitor
Solid view
Prusa i3
Material
PLA
Check compatibility
Print Setup
Recomme...
Custom
Profile:
Fine
Search...
Quality
Layer Height
0.1
mm
Shell
Wall Thickness
1.2
Top/Bottom Thickness
1.2
Infill
Infill Density
20
%
Gradual Infill Steps
0
Material
Printing Temperature
200
Build Plate Temperature
60
Diameter
1.75
Flow
100
Enable Retraction
Speed
Print Speed
50
mm/s
Travel Speed
120
Cooling
Enable Print Cooling
Support
Generate Support
Ready to Save to Removable Drive
Save to Removable Drive
PI3_20200202 4
87.5 x 98.6 x 20.0 mm
04h 41m
9.0...27g
Save file

3D printer (Hardware)

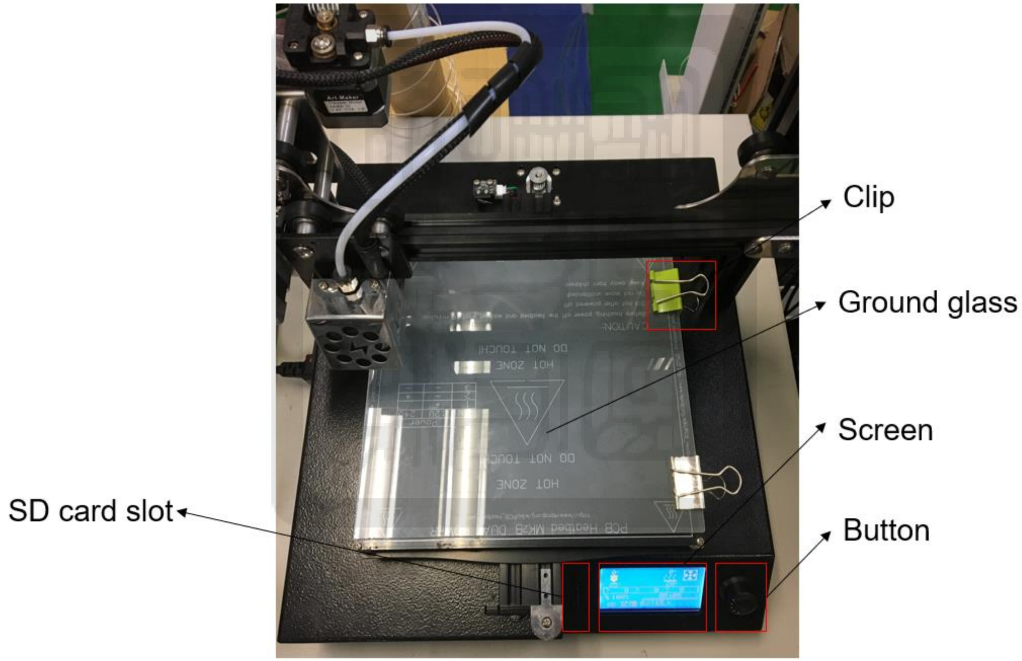

Measure the appropriate weight APL material

APL

Weight

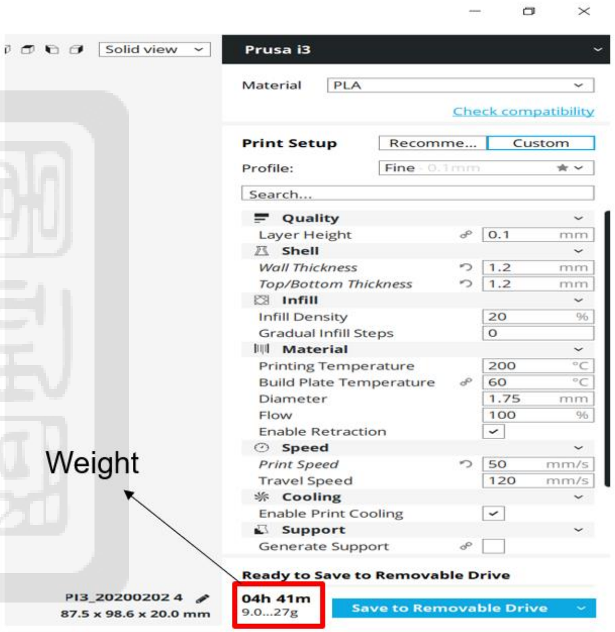

Put APL on the support

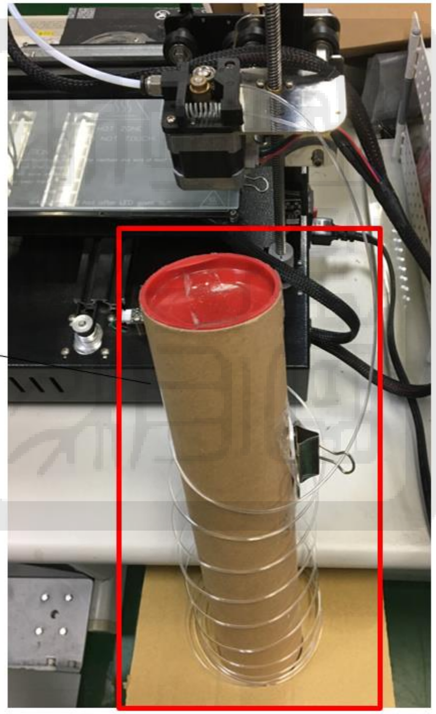

3D printing initial screen

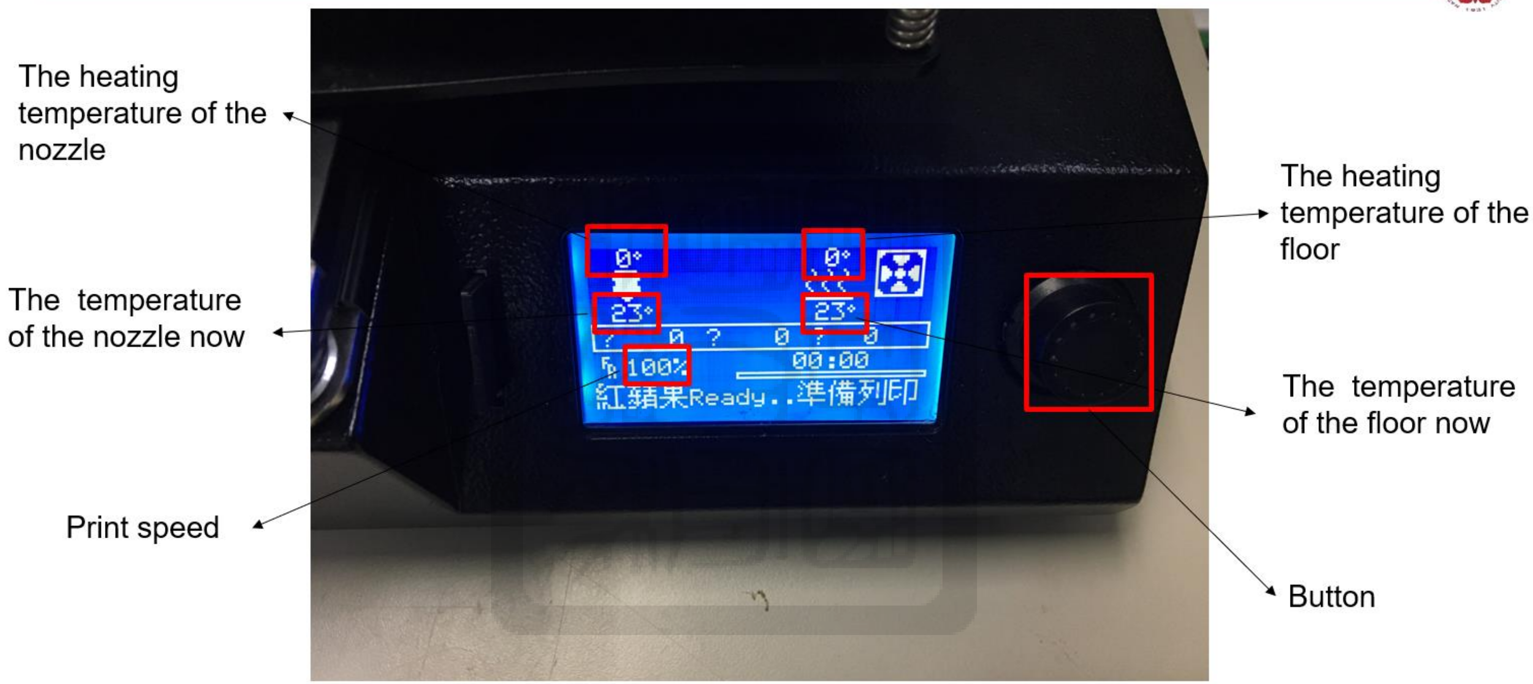

Warm up the 3D printer

Select print file

Print completed

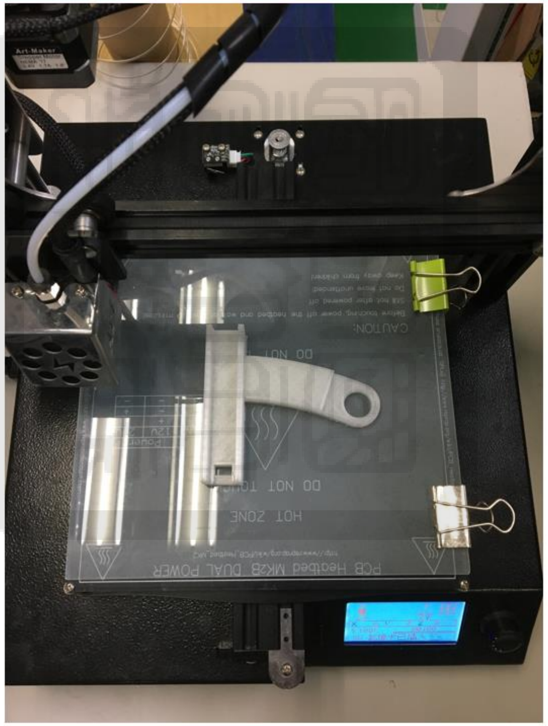

A 4.3 The data of discharge current (toroidal magnetic field coils)

Data 1

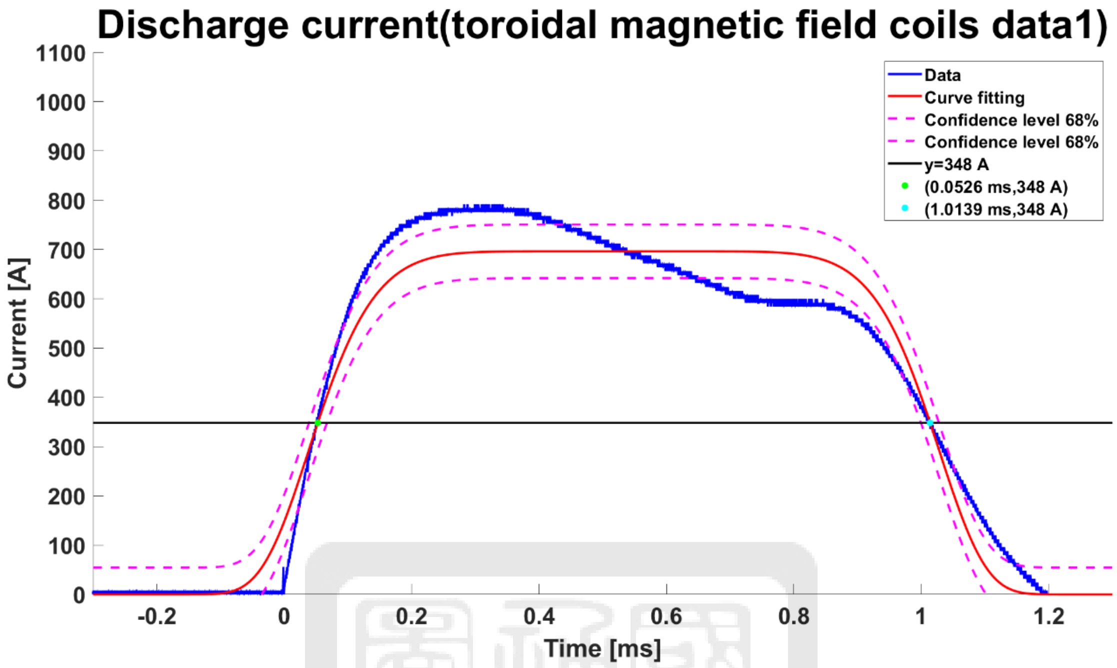

Data 2

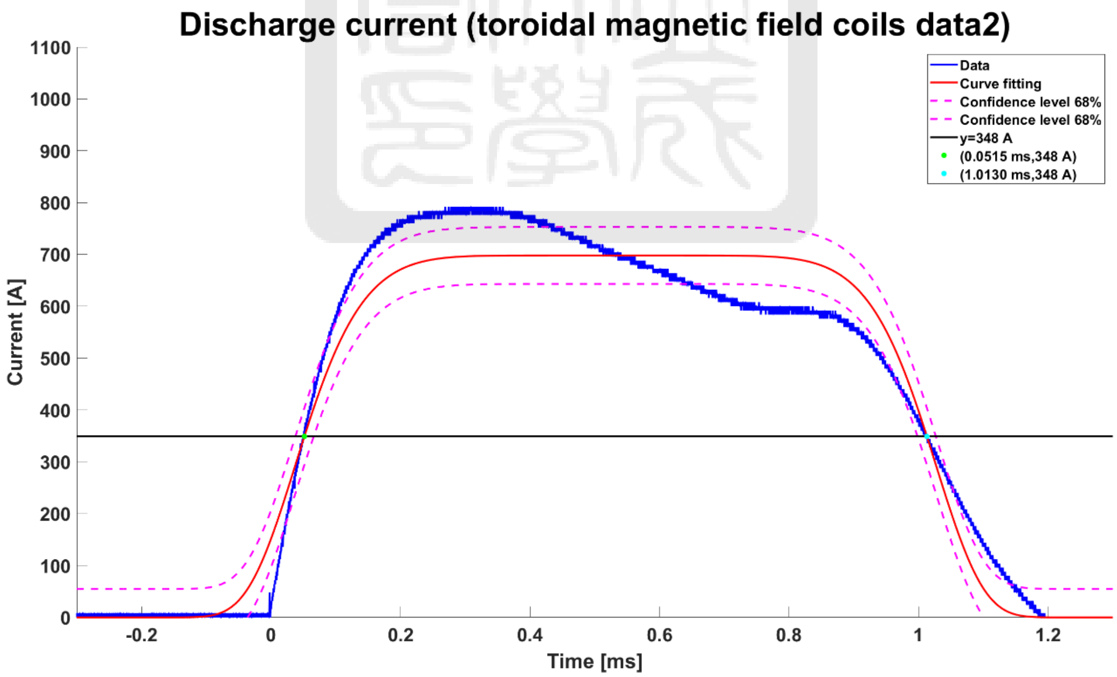

Data 3

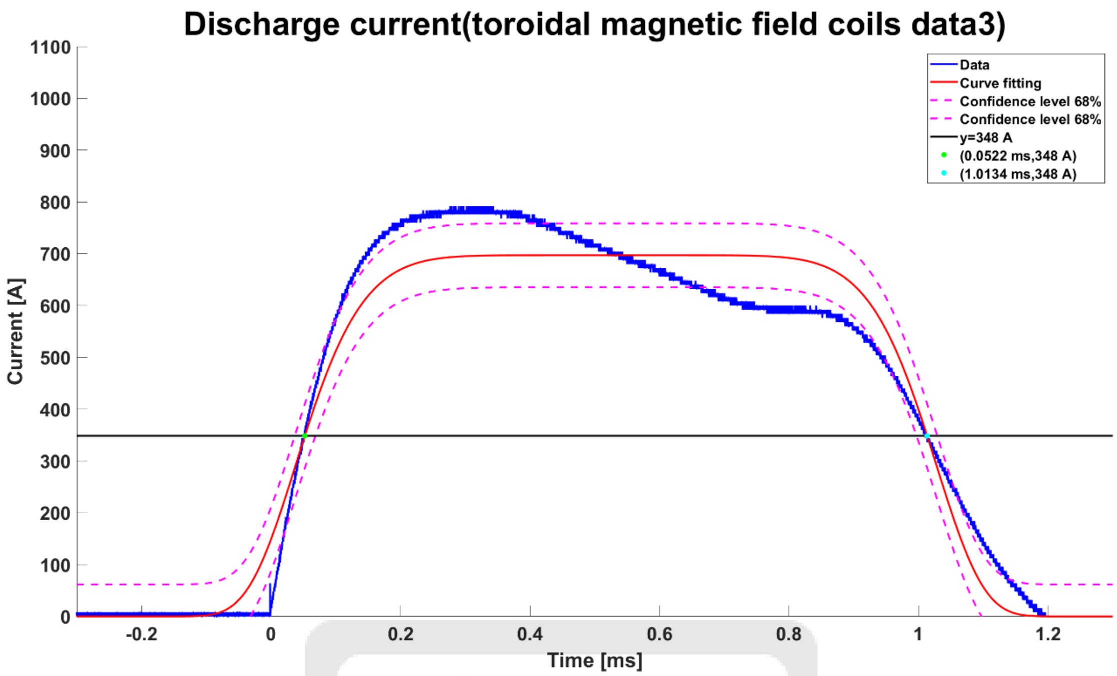

Discharge current(toroidal magnetic field coils data3)
Data
Curve fitting
Confidence level 68%
Confidence level 68%
y=348 A
(0.0522 ms,348 A)
(1.0134 ms,348 A)
Current [A]
Time [ms]

Data 4

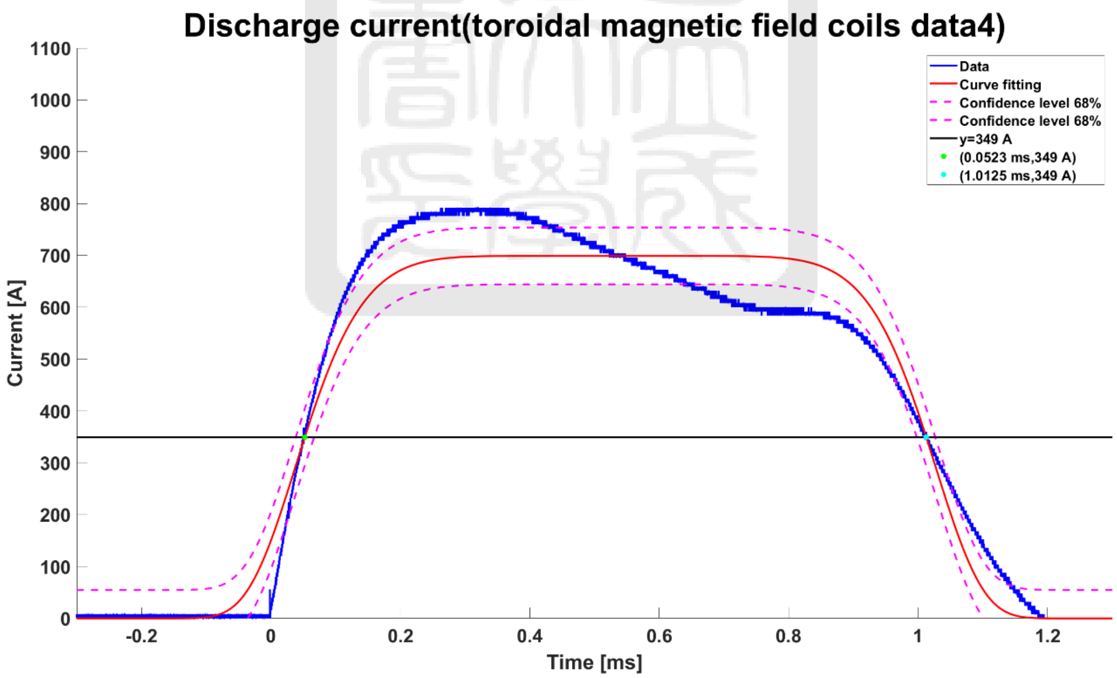

Discharge current(toroidal magnetic field coils data4)
Data
Curve fitting
Confidence level 68%
Confidence level 68%
y=349 A
(0.0523 ms,349 A)
(1.0125 ms,349 A)
Current [A]
Time [ms]

Data 5

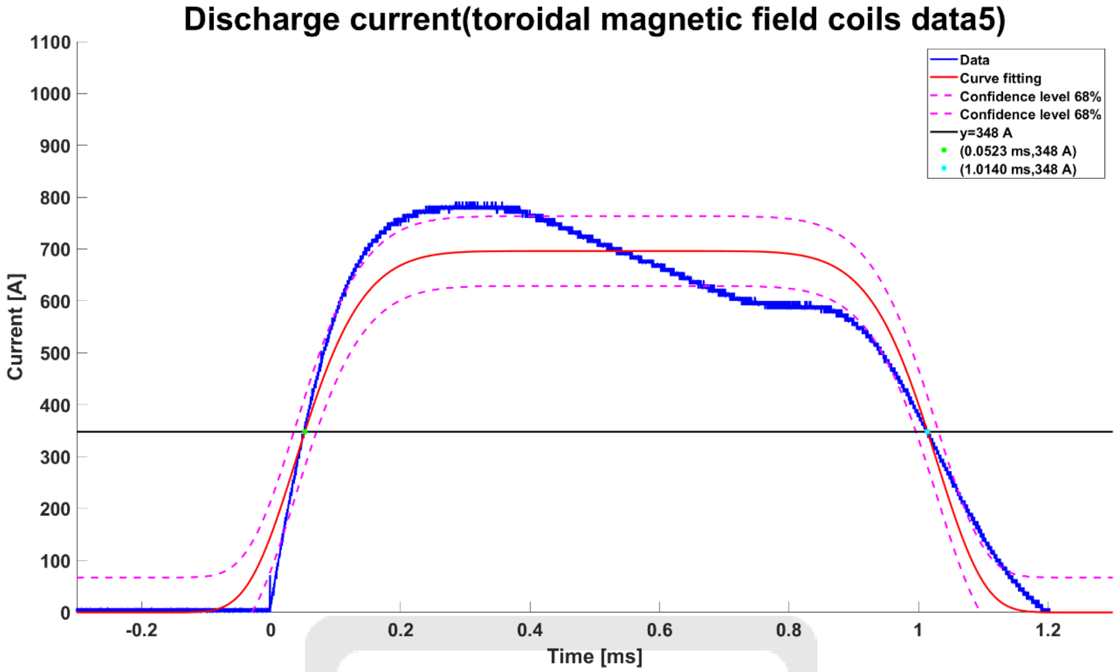
Discharge current(toroidal magnetic field coils data5)
Data
Curve fitting
Confidence level 68%
Confidence level 68%
y=348 A
(0.0523 ms,348 A)
(1.0140 ms,348 A)
Current [A]
Time [ms]

Data 6

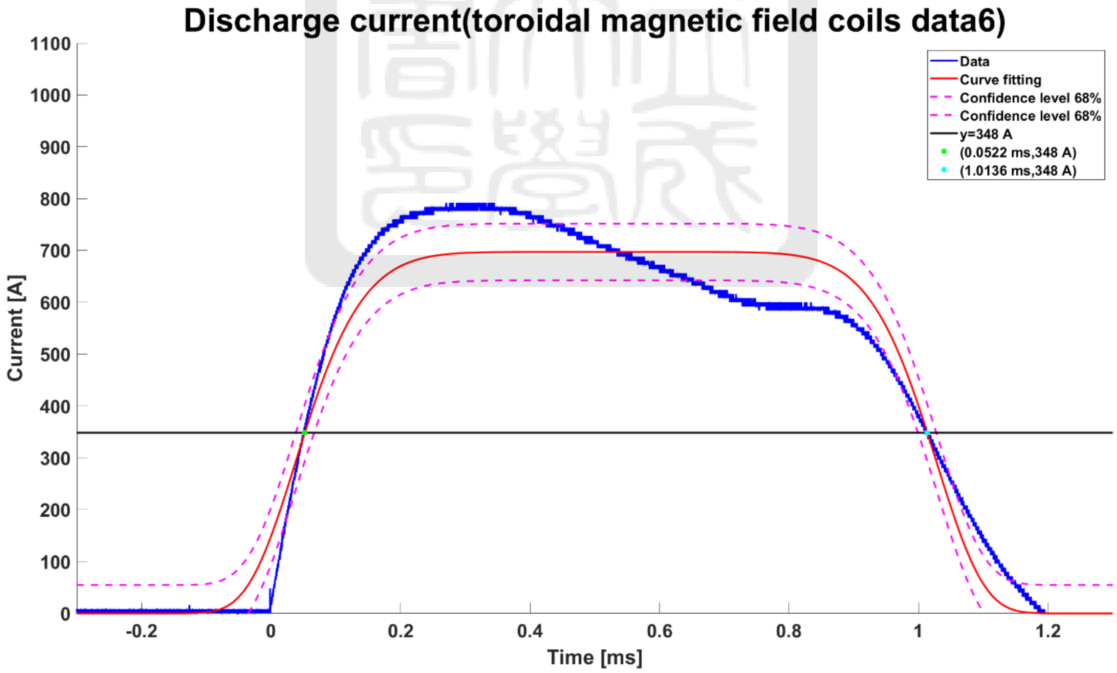
Discharge current(toroidal magnetic field coils data6)
Data
Curve fitting
Confidence level 68%
Confidence level 68%
y=348 A
(0.0522 ms,348 A)
(1.0136 ms,348 A)
Current [A]
Time [ms]

Data 7

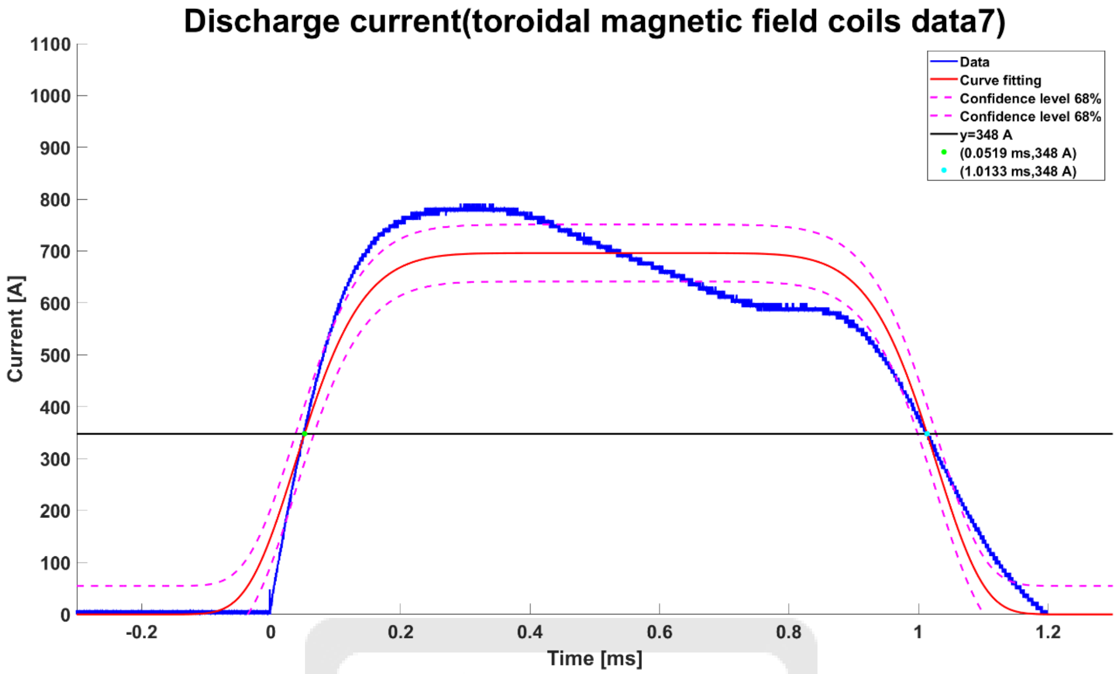
Discharge current(toroidal magnetic field coils data7)
Data
Curve fitting
Confidence level 68%
Confidence level 68%
y=348 A
(0.0519 ms,348 A)
(1.0133 ms,348 A)
Current [A]
Time [ms]

Data 8

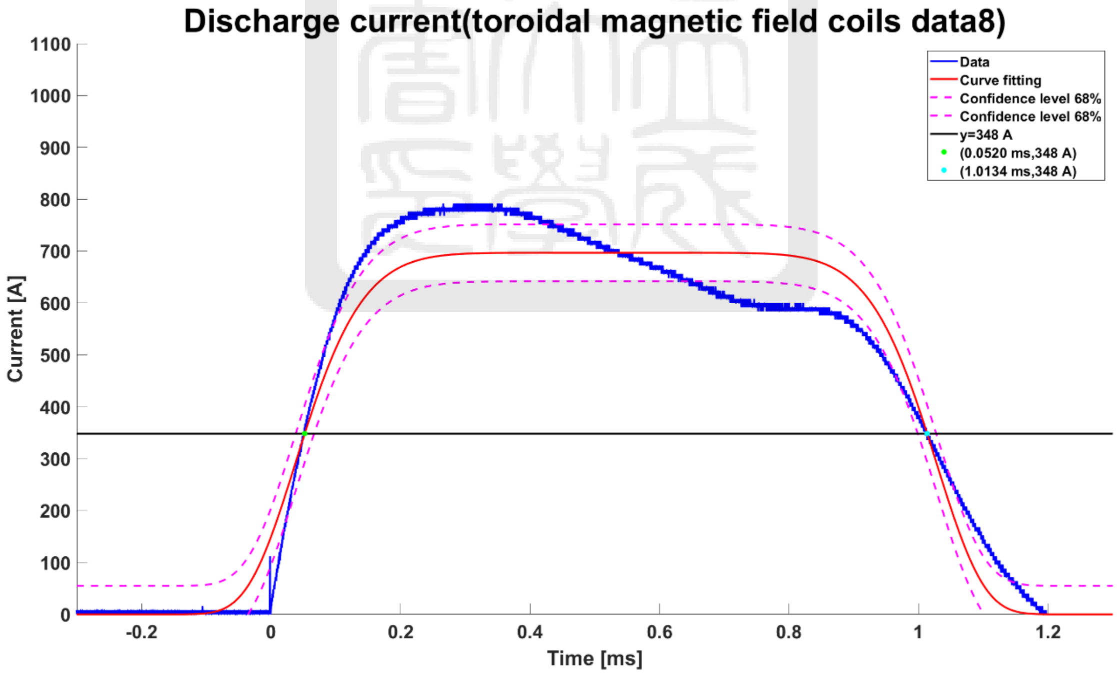
Discharge current(toroidal magnetic field coils data8)
Data
Curve fitting
Confidence level 68%
Confidence level 68%
y=348 A
(0.0520 ms,348 A)
(1.0134 ms,348 A)
Current [A]
Time [ms]

Data 9

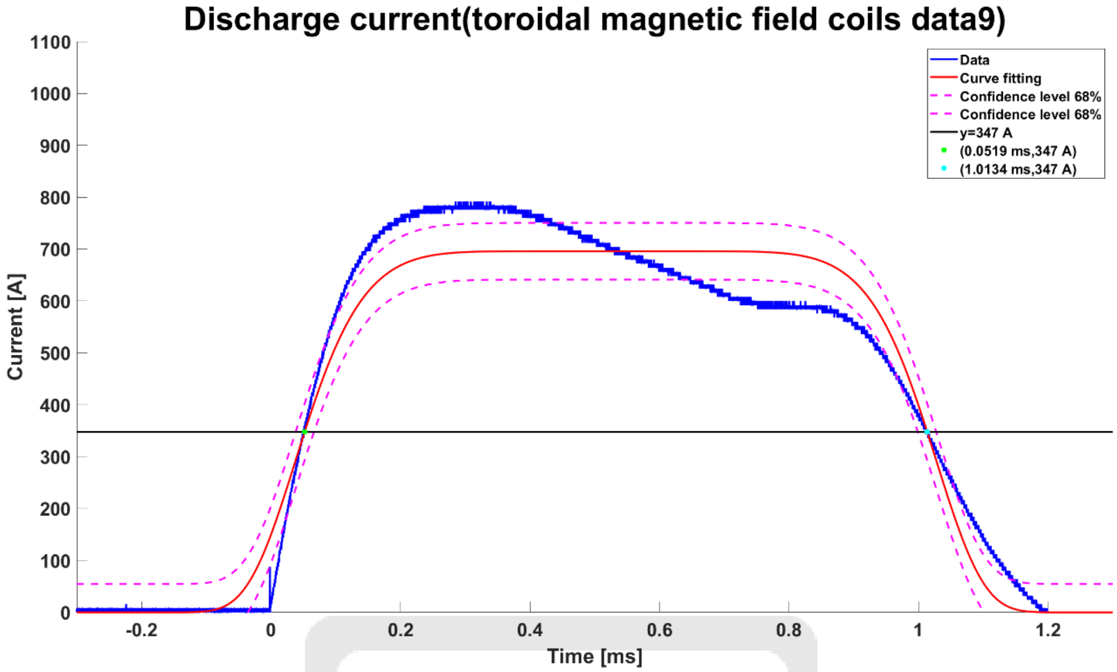

Data 10

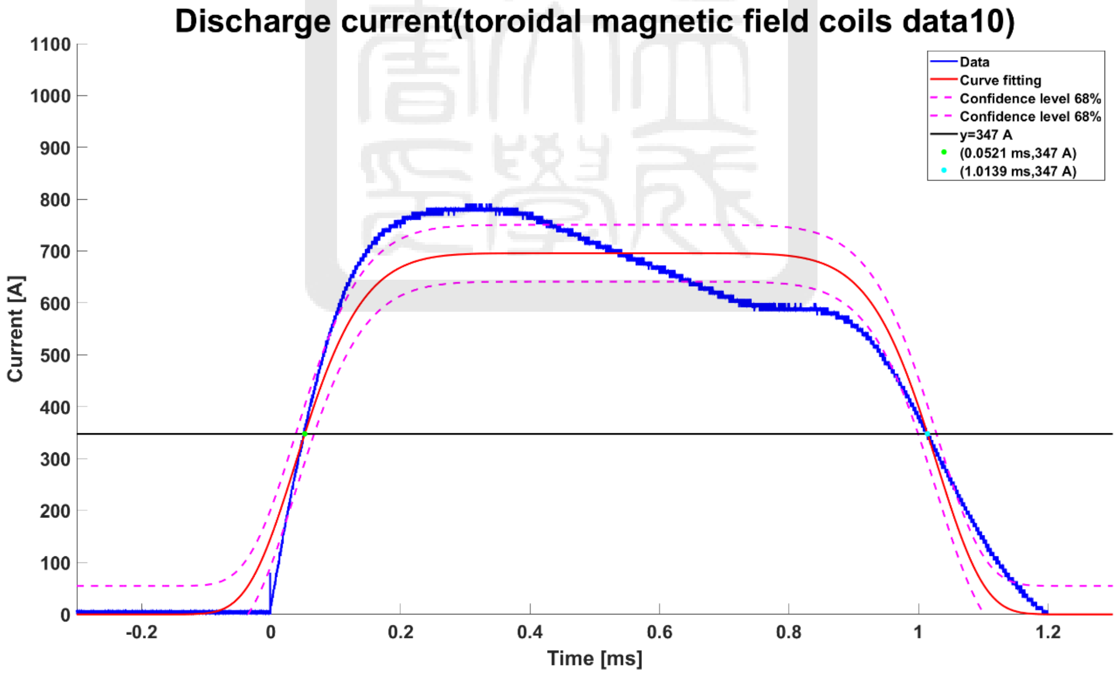

A 5.1 The detailed process of determining the FWHM in Figure 5.11

The detailed process of determining the FWHM in Figure 11 is the following:

(1) Step 1: Find the max value of Eq (8).

(2) Step 2: Find the half value of step 1.

(3) Step 3: Plot the straight line.

(4) Step 4: Plot the curve using Eq (8).

(5) Step 5: Find the intersection between two lines plotted in step 3 and step 4.

(6) Step 6: Find the difference between two points obtained in step 5.

Step 1: To find the max value of f(t)

$$\text{Max}\,[f(t)] = \text{Max}\,[a*\exp(\frac{-|t-b|^c}{2d^c})]$$

Step 2: To find the half value of max[f(t)]

$$\frac{\text{Max}\,[f(t)]}{2}$$

Step 3: To plot the straight line of step 2

$$y_1 = \frac{\text{Max}\,[f(t)]}{2}$$

Step 4: To plot the line of f(t)= a*exp($\frac{-|t-b|^c}{2d^c}$)

$$y_2 = f(t) = a*\exp(\frac{-|t-b|^c}{2d^c})$$

Step 5: We used the line of step 3 and step 4 to find the intersection and got the two points

Point one: (0.0729,342)

Point two: (1.0396,342)

Step 6: Finally, we used the step 5 two points to find the FWHM

Δ t = 1.0396-0.0729 = 0.9667 (ms)

A 5.2 The detailed process of determining the FWHM in Figure 5.18

The detailed process of determining the FWHM in Figure 18.

Step 1: Find min value of Eq (10).

Step 2: Get the minimum point (t_{min}, Min [f(t)]).

Step 3: To replace the time value t of a tilted straight line (a+bt).

Step 4: Get the point (t_{min}, a+b t_{min}).

Step 5: Obtain the differernce between step 2 point and step 3 point.

Step 6: Find the half value of step 5.

Step 7: Plot the straight line.

Step 8: Plot Eq (10).

Step 9: We use the line of step 7 and step 8 to find the intersections and got two point.

Step 10: The difference in time of two points in step 9 is the FWHM.

Step 1: To find the min value of f(t)

$$\mathrm{Min}[f(t)] = \mathrm{Min}[(a+bt)\text{-}c\exp\left[-\left|\frac{(t-d)^e}{(2f^e)}\right|\right]]$$

Step 2: To find the min point of f(t) of step 1

$$(t_{min}, \mathrm{Min}[f(t)])$$

Step 3: To replace the time value t of a tilted straight line (a+bt) that time value t from the step 2

$$(\boxed{t_{min}}, \mathrm{Min}[f(t)],) \Rightarrow (a+b\boxed{t})$$

Step 4: To obtain the point of (t, (a+b * t)) from the step 3

$$(t_{min}, (a+b\,t_{min}))$$

Step 5: To obtain difference between step 2 point and step 3 point

$$(a+b\,t_{min})-\mathrm{Min}[f(t)]$$

Step 6: To find the half value of step 5

$$\frac{(a+b\,t_{min})-\mathrm{Min}[f(t)]}{2}$$

Step 7: To plot the straight line of step 6

$$y_1 = \frac{\mathrm{Min}[f(t)]-(a+b\,t_{min})}{2}$$

Step 8: To plot the line of supergaussion function

$$y_2 = a+bt - c\exp[-\left|\frac{(t-d)^e}{(2f^e)}\right|]$$

Step 9: We used the line of step 7 and step 8 to find the intersection and got the two points

The point one (0.0908 , 3.2925)

The point two (1.4408 , 3.2925)

Step 10: Finally, we used the step 9 two points to find the FWHM

The point two - The point one = 1.4408 – 0.0908 = 1.3500 (ms)

A 5.3 Each data analyze of different battery voltage of single Langmuir probe

0V

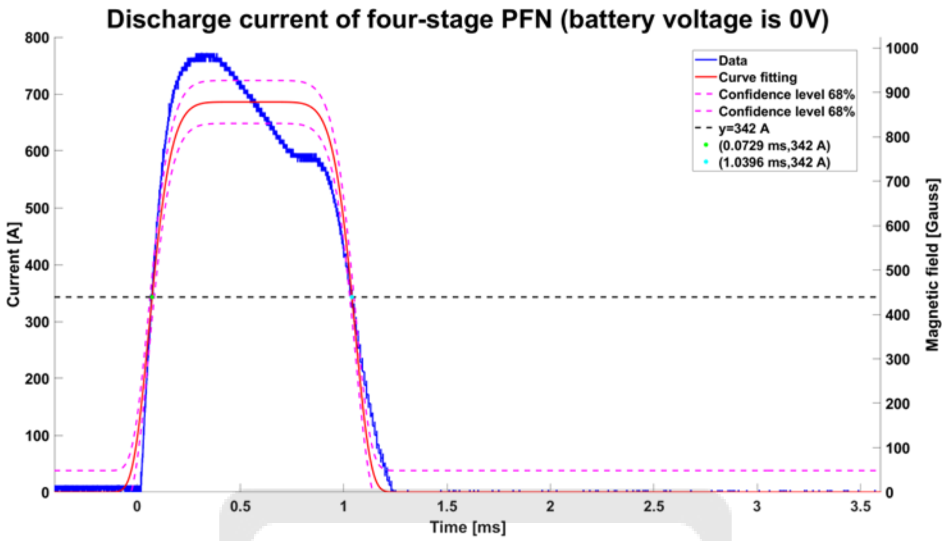

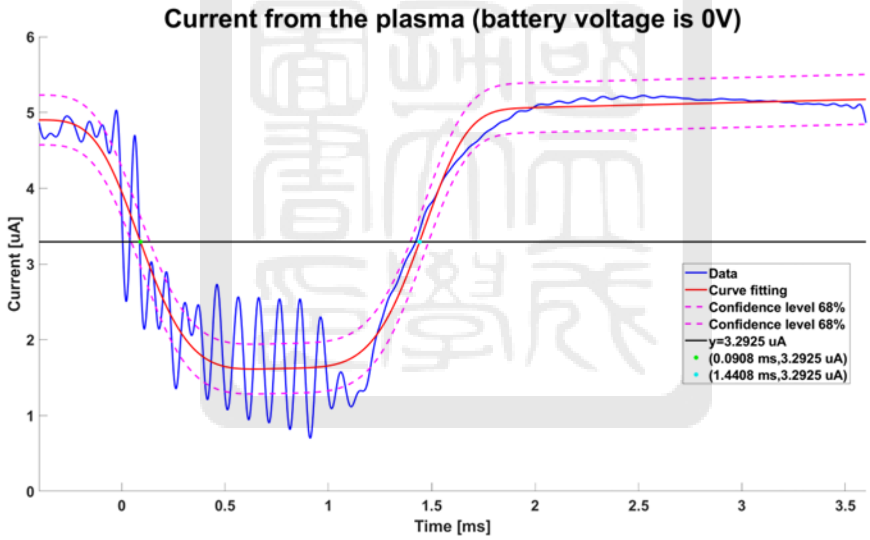

3V

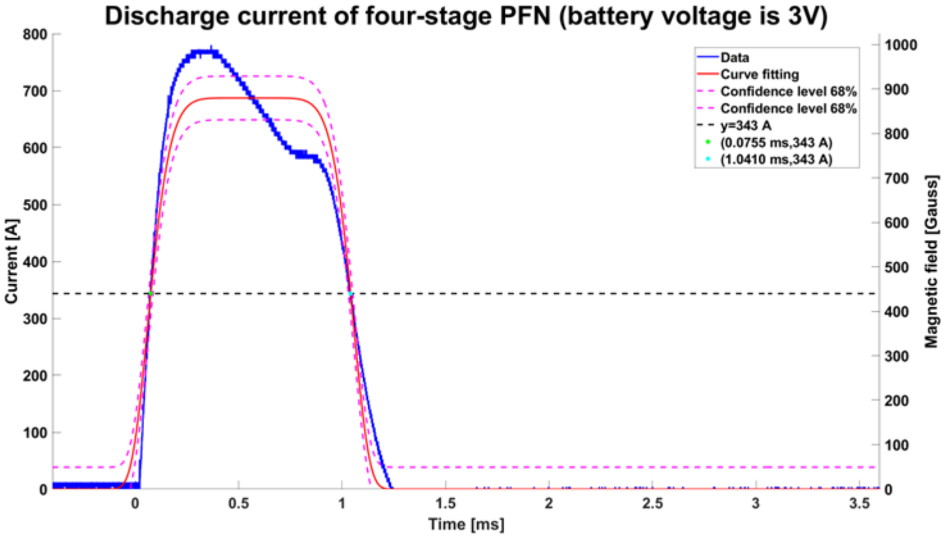
Discharge current of four-stage PFN (battery voltage is 3V)
Current [A]
Magnetic field [Gauss]
Time [ms]
Data
Curve fitting
Confidence level 68%
Confidence level 68%
y=343 A
(0.0755 ms,343 A)
(1.0410 ms,343 A)

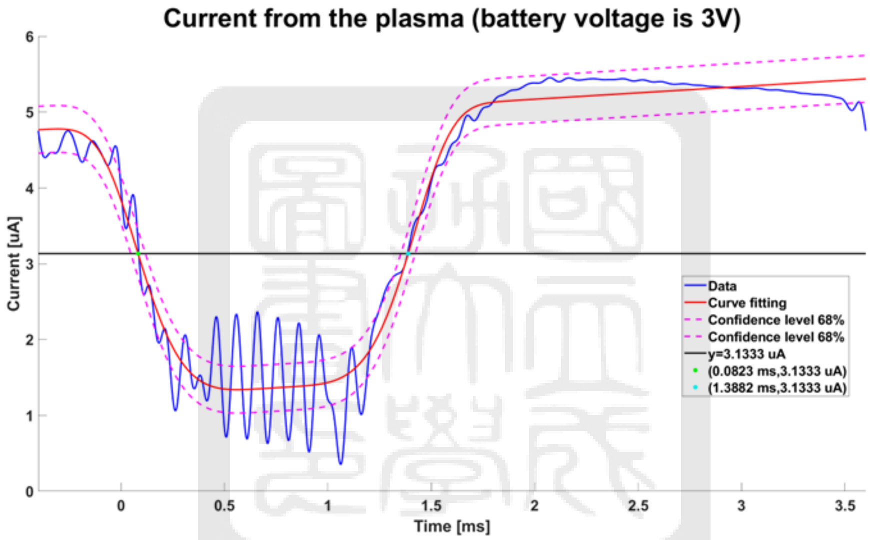
Current from the plasma (battery voltage is 3V)
Current [uA]
Time [ms]
Data
Curve fitting
Confidence level 68%
Confidence level 68%
y=3.1333 uA
(0.0823 ms,3.1333 uA)
(1.3882 ms,3.1333 uA)

6V

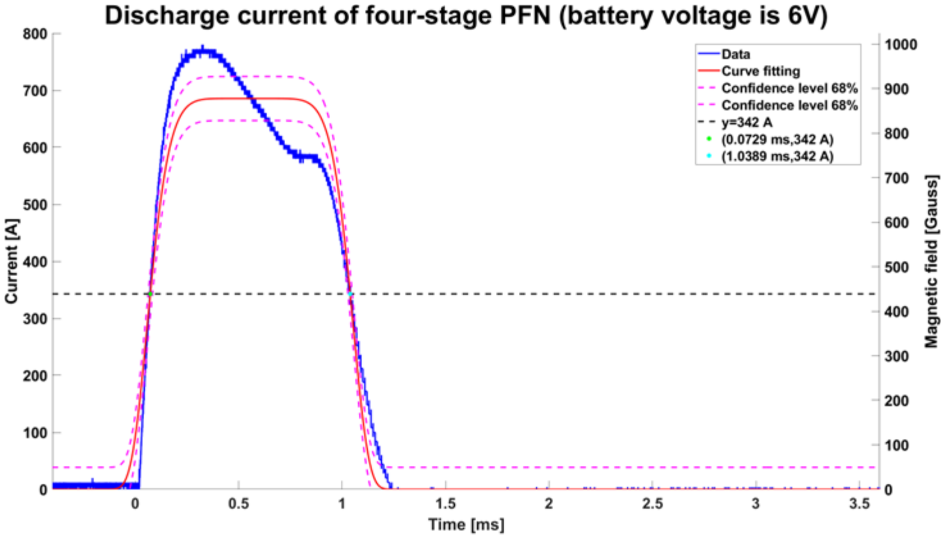

Discharge current of four-stage PFN (battery voltage is 6V)
Data
Curve fitting
Confidence level 68%
Confidence level 68%
y=342 A
(0.0729 ms,342 A)
(1.0389 ms,342 A)
Current [A]
Magnetic field [Gauss]
Time [ms]

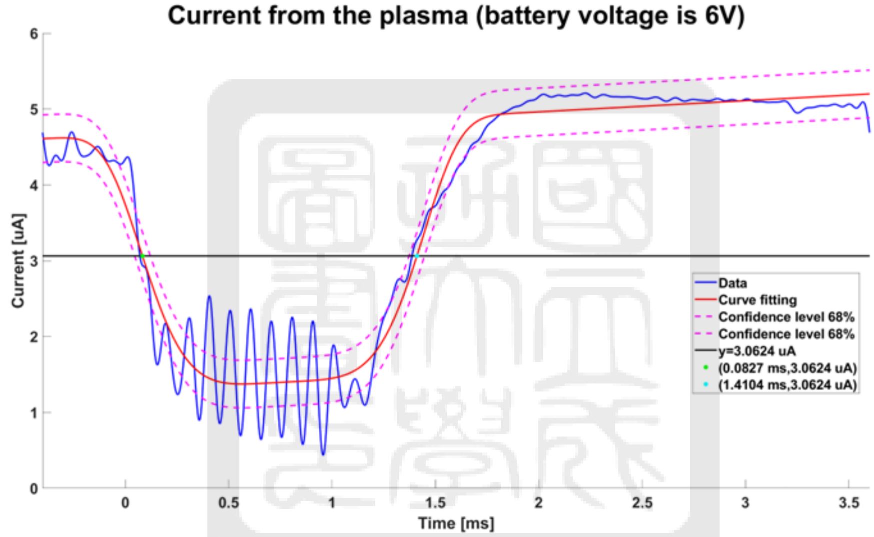

Current from the plasma (battery voltage is 6V)
Data
Curve fitting
Confidence level 68%
Confidence level 68%
y=3.0624 uA
(0.0827 ms,3.0624 uA)
(1.4104 ms,3.0624 uA)
Current [uA]
Time [ms]

10V

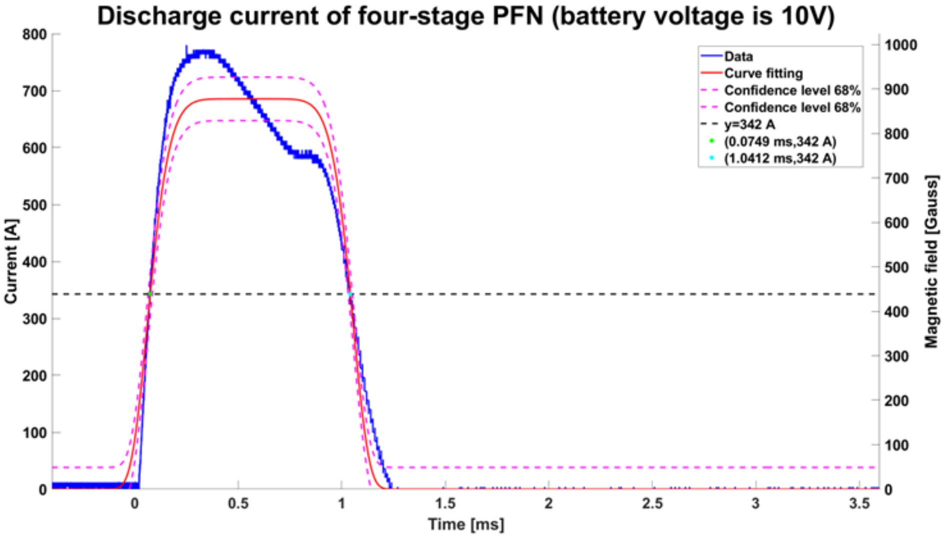

Discharge current of four-stage PFN (battery voltage is 10V)
Data
Curve fitting
Confidence level 68%
Confidence level 68%
y=342 A
(0.0749 ms,342 A)
(1.0412 ms,342 A)
Current [A]
Magnetic field [Gauss]
Time [ms]

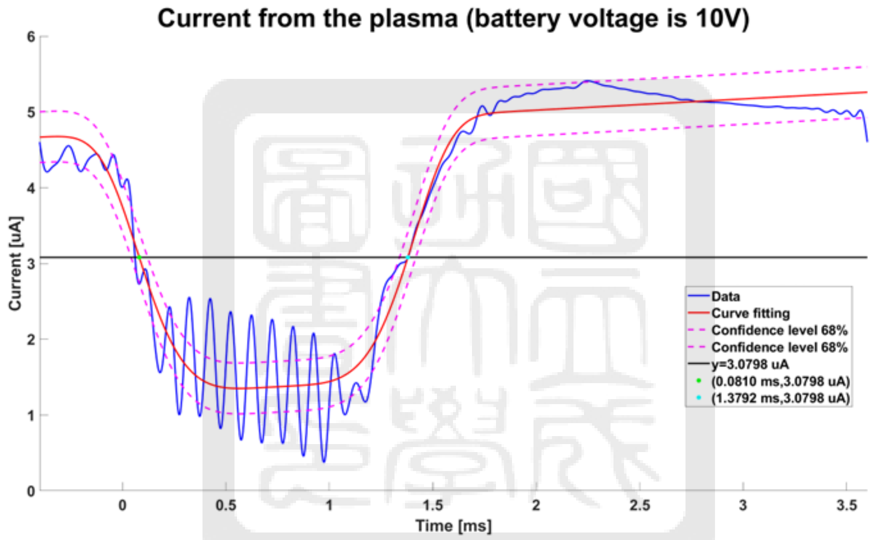

Current from the plasma (battery voltage is 10V)
Data
Curve fitting
Confidence level 68%
Confidence level 68%
y=3.0798 uA
(0.0810 ms,3.0798 uA)
(1.3792 ms,3.0798 uA)
Current [uA]
Time [ms]

15V

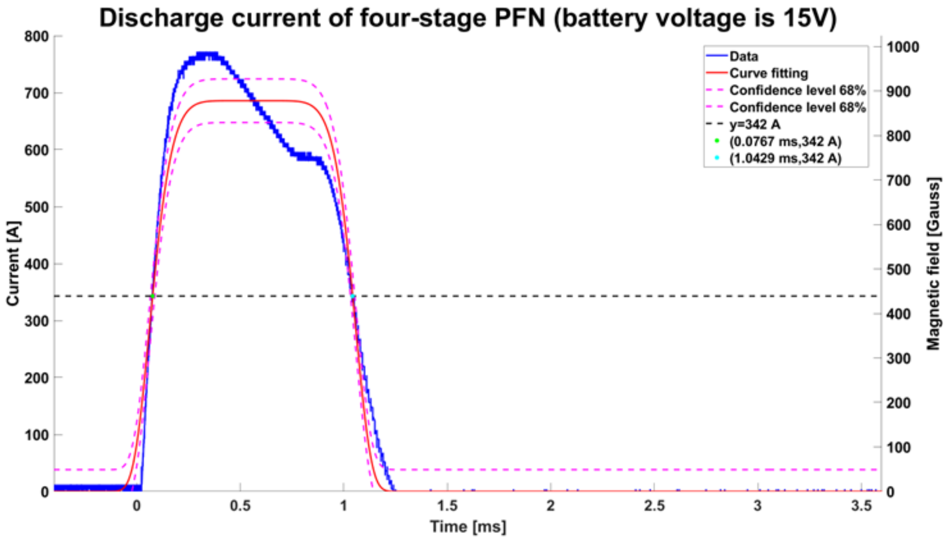
Discharge current of four-stage PFN (battery voltage is 15V)
Current [A]
Magnetic field [Gauss]
Time [ms]
Data
Curve fitting
Confidence level 68%
Confidence level 68%
y=342 A
(0.0767 ms,342 A)
(1.0429 ms,342 A)

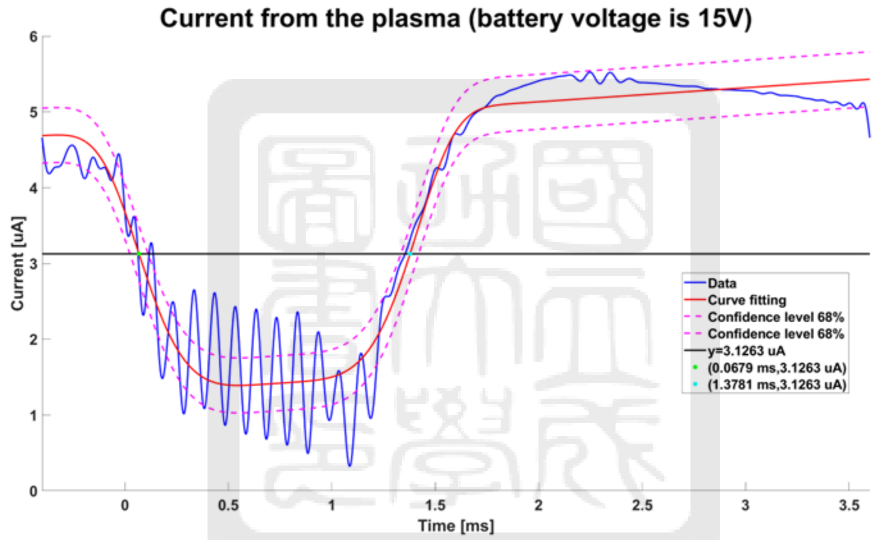
Current from the plasma (battery voltage is 15V)
Current [uA]
Time [ms]
Data
Curve fitting
Confidence level 68%
Confidence level 68%
y=3.1263 uA
(0.0679 ms,3.1263 uA)
(1.3781 ms,3.1263 uA)

20V

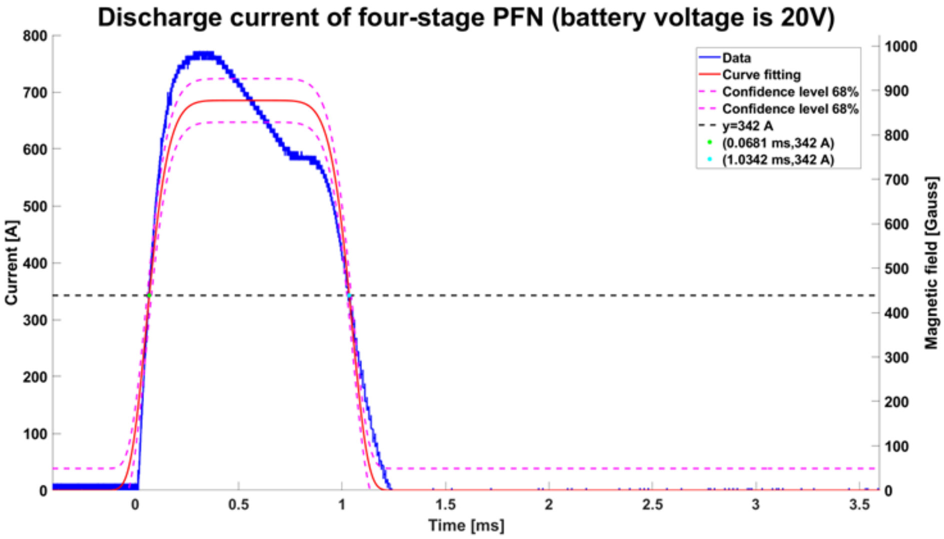

Discharge current of four-stage PFN (battery voltage is 20V)
Current [A]
Magnetic field [Gauss]
Time [ms]
Data
Curve fitting
Confidence level 68%
Confidence level 68%
y=342 A
(0.0681 ms,342 A)
(1.0342 ms,342 A)

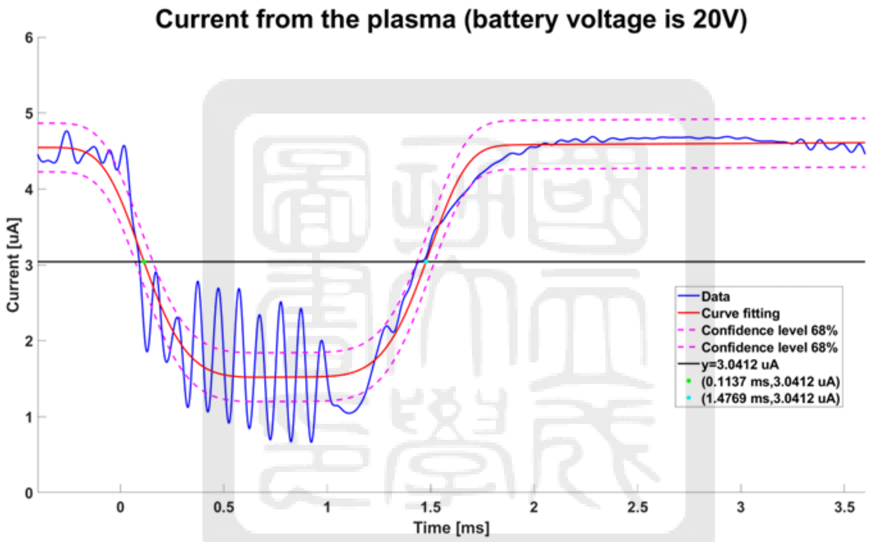

Current from the plasma (battery voltage is 20V)
Current [uA]
Time [ms]
Data
Curve fitting
Confidence level 68%
Confidence level 68%
y=3.0412 uA
(0.1137 ms,3.0412 uA)
(1.4769 ms,3.0412 uA)

25V

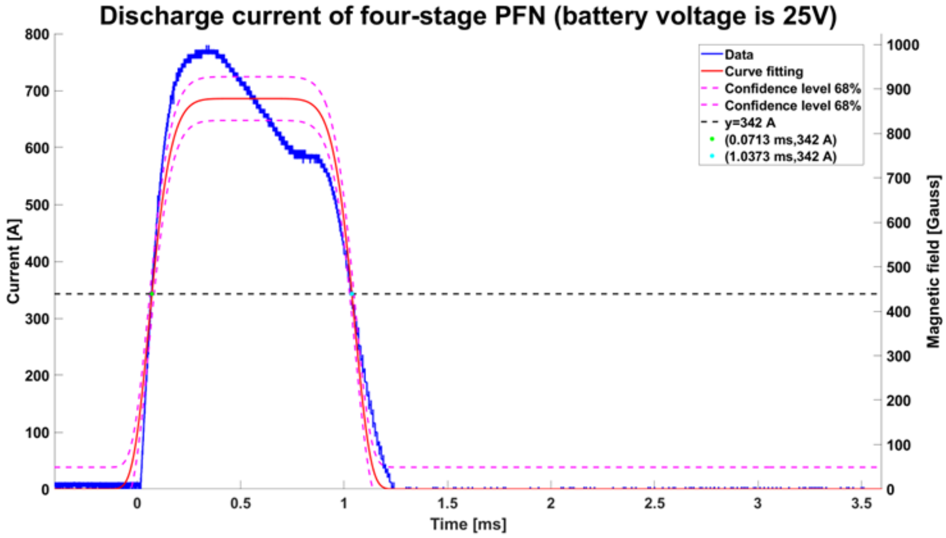
Discharge current of four-stage PFN (battery voltage is 25V)
Current [A]
Magnetic field [Gauss]
Time [ms]
Data
Curve fitting
Confidence level 68%
Confidence level 68%
y=342 A
(0.0713 ms,342 A)
(1.0373 ms,342 A)

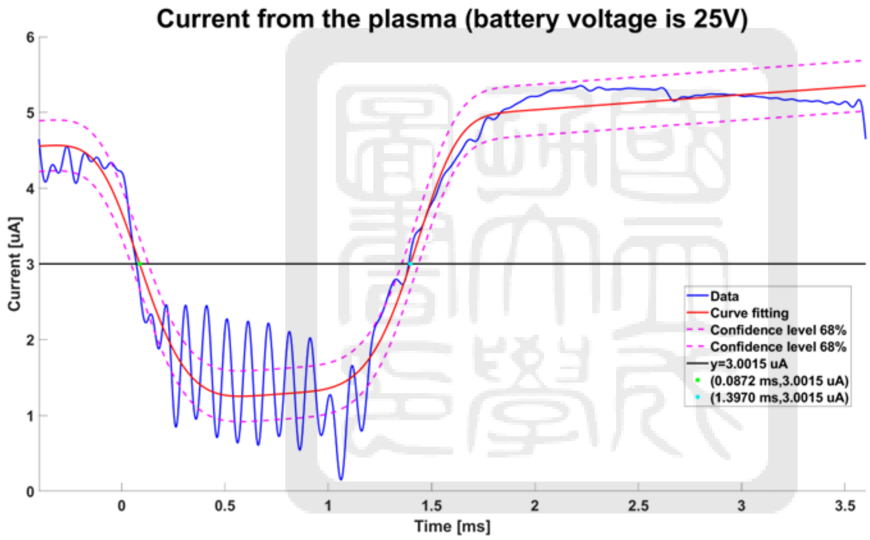
Current from the plasma (battery voltage is 25V)
Current [uA]
Time [ms]
Data
Curve fitting
Confidence level 68%
Confidence level 68%
y=3.0015 uA
(0.0872 ms,3.0015 uA)
(1.3970 ms,3.0015 uA)

30V

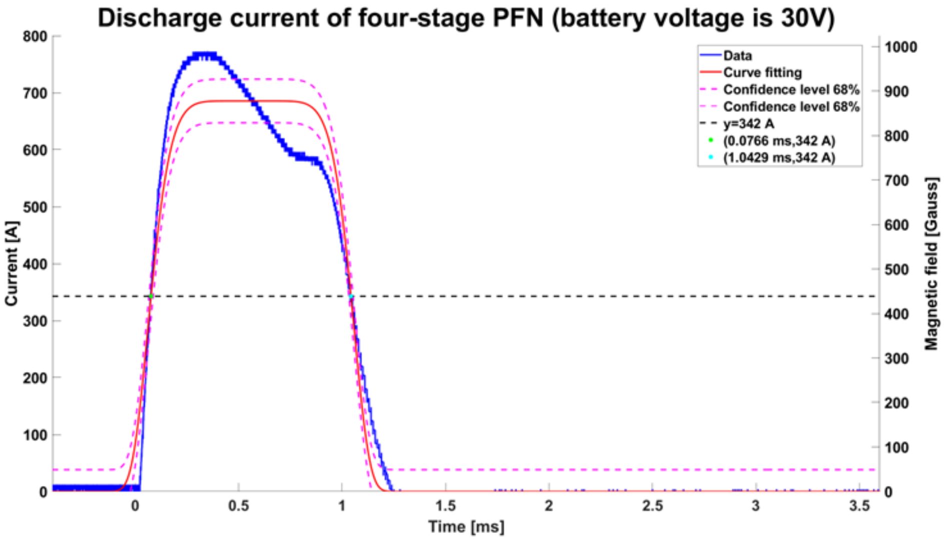
Discharge current of four-stage PFN (battery voltage is 30V)
Current [A]
Magnetic field [Gauss]
Time [ms]
0
100
200
300
400
500
600
700
800
900
1000
0.5
1
1.5
2
2.5
3
3.5
Data
Curve fitting
Confidence level 68%
Confidence level 68%
y=342 A
(0.0766 ms,342 A)
(1.0429 ms,342 A)

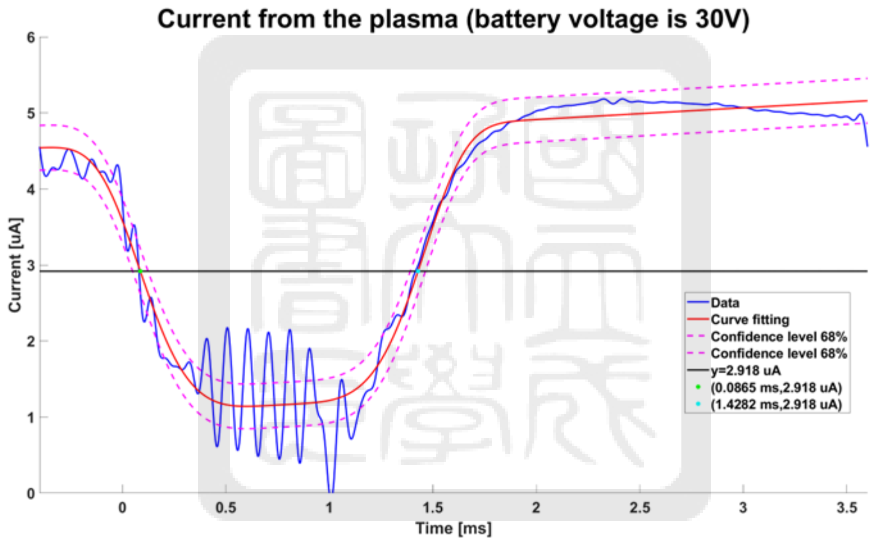
Current from the plasma (battery voltage is 30V)
Current [uA]
Time [ms]
0
1
2
3
4
5
6
0.5
1.5
2.5
3.5
Data
Curve fitting
Confidence level 68%
Confidence level 68%
y=2.918 uA
(0.0865 ms,2.918 uA)
(1.4282 ms,2.918 uA)

35V

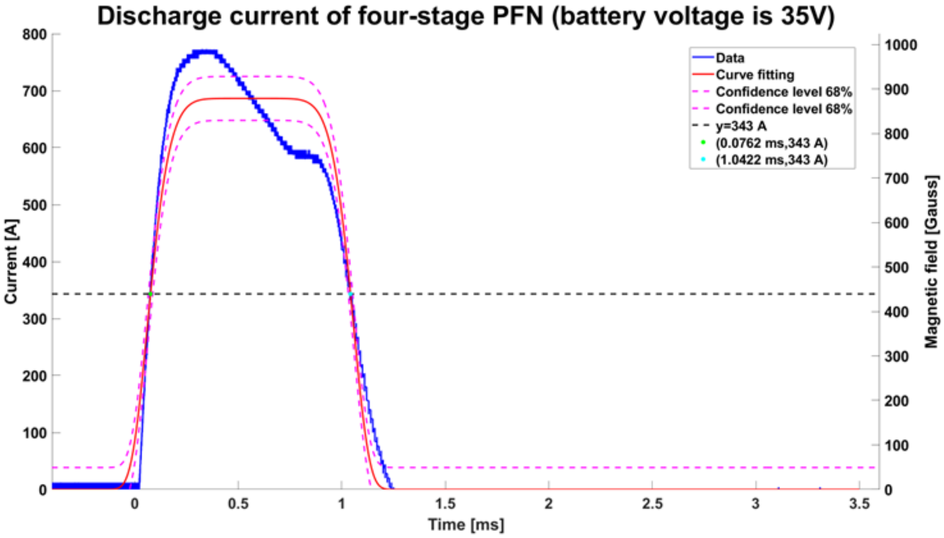

Discharge current of four-stage PFN (battery voltage is 35V)
Current [A]
Magnetic field [Gauss]
Time [ms]
Data
Curve fitting
Confidence level 68%
Confidence level 68%
y=343 A
(0.0762 ms,343 A)
(1.0422 ms,343 A)

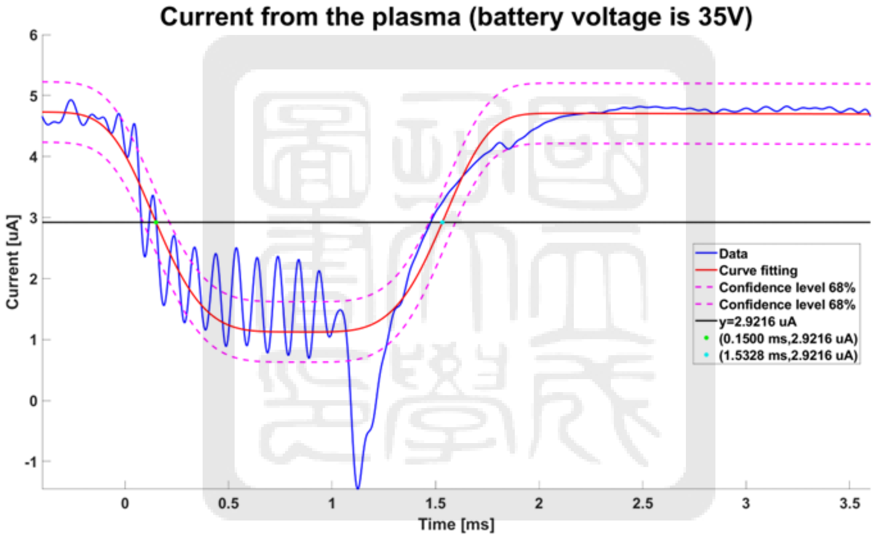

Current from the plasma (battery voltage is 35V)
Current [uA]
Time [ms]
Data
Curve fitting
Confidence level 68%
Confidence level 68%
y=2.9216 uA
(0.1500 ms,2.9216 uA)
(1.5328 ms,2.9216 uA)

40V

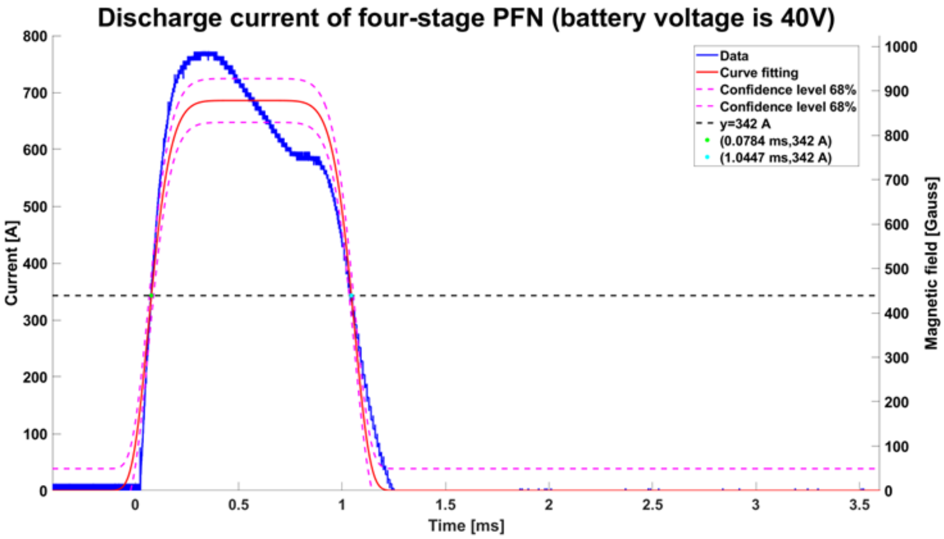

Discharge current of four-stage PFN (battery voltage is 40V)
Current [A]
Magnetic field [Gauss]
Time [ms]
Data
Curve fitting
Confidence level 68%
Confidence level 68%
y=342 A
(0.0784 ms,342 A)
(1.0447 ms,342 A)

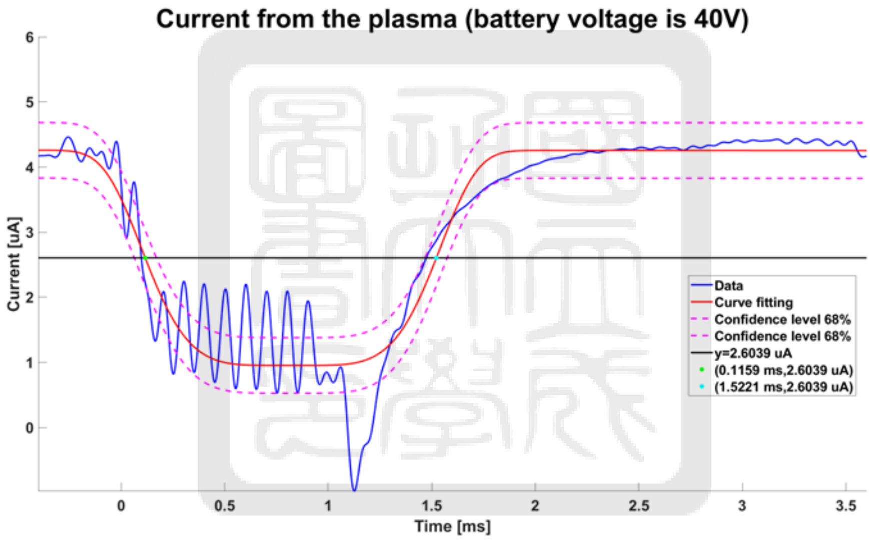

Current from the plasma (battery voltage is 40V)
Current [uA]
Time [ms]
Data
Curve fitting
Confidence level 68%
Confidence level 68%
y=2.6039 uA
(0.1159 ms,2.6039 uA)
(1.5221 ms,2.6039 uA)

45V

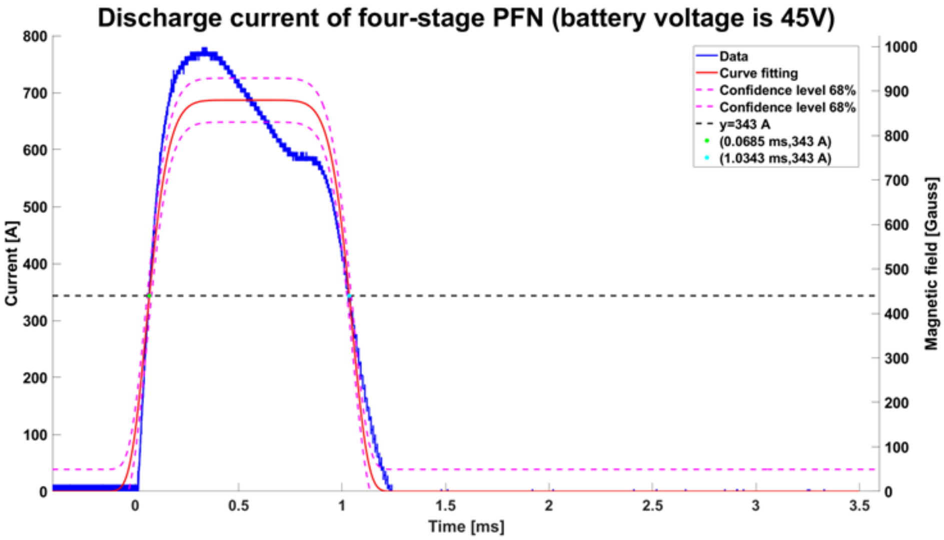
Discharge current of four-stage PFN (battery voltage is 45V)
Current [A]
Magnetic field [Gauss]
Time [ms]
Data
Curve fitting
Confidence level 68%
Confidence level 68%
y=343 A
(0.0685 ms,343 A)
(1.0343 ms,343 A)

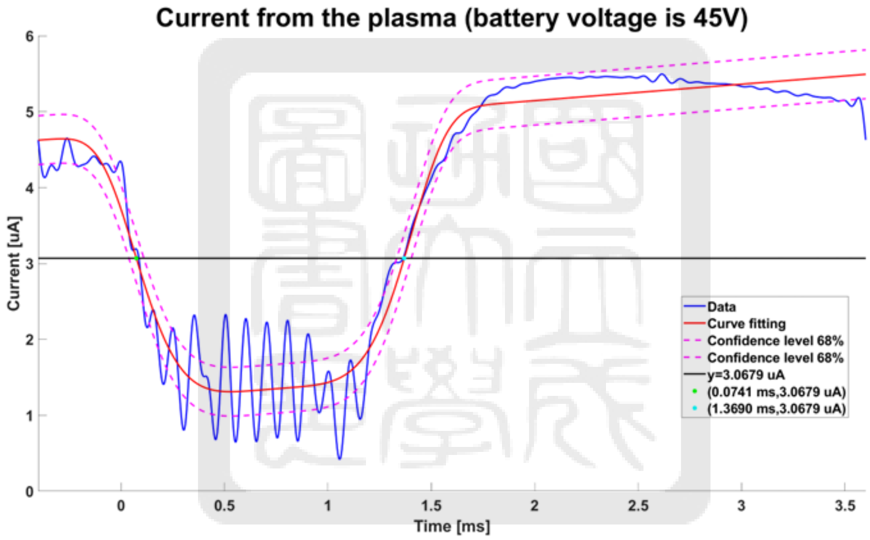
Current from the plasma (battery voltage is 45V)
Current [uA]
Time [ms]
Data
Curve fitting
Confidence level 68%
Confidence level 68%
y=3.0679 uA
(0.0741 ms,3.0679 uA)
(1.3690 ms,3.0679 uA)

50V

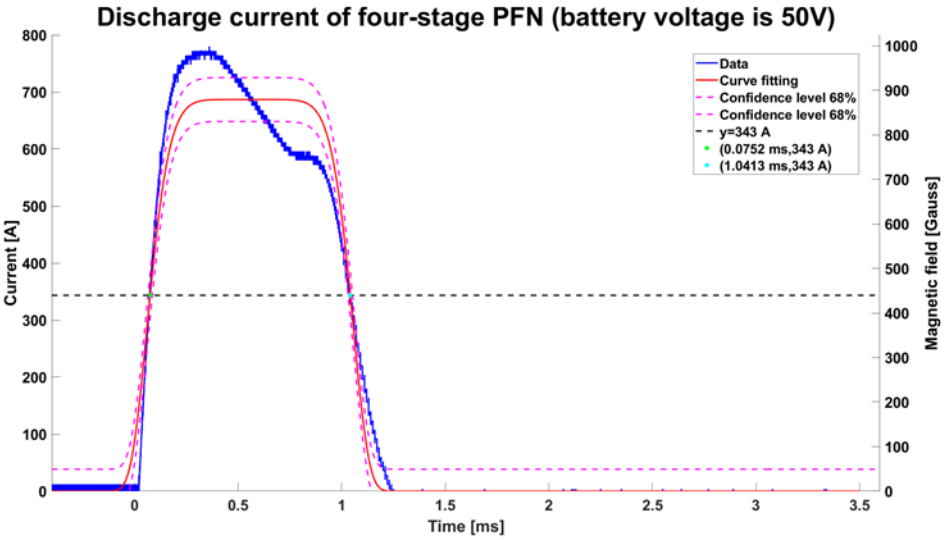

Discharge current of four-stage PFN (battery voltage is 50V)
Data
Curve fitting
Confidence level 68%
Confidence level 68%
y=343 A
(0.0752 ms,343 A)
(1.0413 ms,343 A)
Current [A]
Magnetic field [Gauss]
Time [ms]

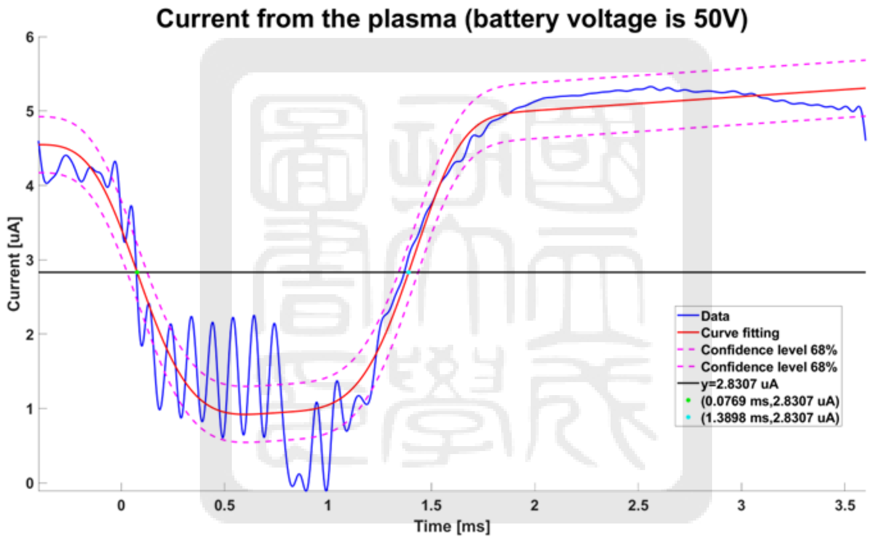

Current from the plasma (battery voltage is 50V)
Data
Curve fitting
Confidence level 68%
Confidence level 68%
y=2.8307 uA
(0.0769 ms,2.8307 uA)
(1.3898 ms,2.8307 uA)
Current [uA]
Time [ms]

A8 The venders of all components

Component	Vender	Note
鋁擠型	金全通	711台南市歸仁區和順路一段296號
3D列印機耗材	紅蘋果	台南市東區東門路與崇學路交叉口
維修3D列印機	紅蘋果	台南市東區東門路與崇學路交叉口
電子材料	南一電子	700台南市中西區民族路二段95號
氣體管路元件	南台南	台南市安南區郡安路4段135號
氣體管路元件	雲山行	704台南市北區公園北路175號
1/8 X 6 mm 氣管快拆接頭	三通行	704台南市北區西門路三段146號
水管	成利水電材料行	704台南市北區公園路377巷2-3號
鋁板	三川金屬	710永康區中正南路70號
Paschen’s curve separator	大漢美術用品社	701台南市東區青年路258號
金手指	露天	
YUASA SMF 55B24L 電池	成功電池行	700台南市中西區成功路315號

A9 Folder of data

The experimental data is located in / Experiments / 2022_jchen / 2022.5.26 thesis experiment data.

- I ever analyzed all the data. In folder/2022.05.26 數據處理.
- The data of the thesis in chapter 3. In folder/2022.5.26 chapter 3 data.
- The data of the thesis in chapter 4. In folder/2022.5.26 chapter 4 data.
- The data of the thesis in chapter 5. In folder/2022.5.26 chapter 5 data.